# STUDIES ON NATURAL GUM-BASED INJECTABLE HYDROGEL FOR WOUND HEALING APPLICATIONS

A Thesis Submitted for the Degree of

## **DOCTOR OF PHILOSOPHY**

in

**Chemistry** 

by

Jitendra Kumar

(2K20/PhD/AC/05)

Under the Supervision of

Prof. Roli Purwar

**Department of Applied Chemistry** 

**Delhi Technological University** 



To the

Department of Applied Chemistry
DELHI TECHNOLOGICAL UNIVERSITY

(Formerly Delhi College of Engineering)

Shahbad Daulatpur, Main Bawana Road, Delhi-110042, India.

October, 2025

Dedicated

To my parents

Shri Shiv Murti and Smt. Sona Devi

To my siblings

Mrs. Poonam, Mrs. Neelam, and Mr. Hishay Kumar

To my Nephew

Sourav and Ritesh

To my lovely niece

Mishita

Thanks for your endless encouragement, support, love, and prayers.

### **ACKNOWLEDGEMENTS**

The journey of a Ph.D., full of challenges, ups & downs, and excitement, is different for each. Still, it can only be completed when every individual and institution's support, guidance, and motivation are added. I am deeply grateful to my supervisor, Prof. Roli **Purwar**, for her invaluable guidance, expertise, and support throughout this journey. My heartfelt thanks go to my parents for their unwavering love and patience. I am extremely grateful to Honourable Prof. Yogesh Singh, former Vice-Chancellor, and Honourable **Prof. Prateek Sharma**, Vice-Chancellor of DTU, for allowing me to pursue my Ph.D. Also, my gratitude extends to Prof. D. Kumar, former DRC chairman, Department of Applied Chemistry; **Prof. Ram Singh**, DRC chairman, Department of Applied Chemistry; **Prof. Sudhir G. Warkar,** former Head of the Department of Applied Chemistry, and **Prof.** Anil Kumar, Head of the Department of Applied Chemistry, for providing the necessary facilities. I wish to express my sincere thanks to all faculty members of the Department of Applied Chemistry, DTU, for their help and support during this research work. I would like to thank SRC and DRC members and other faculty members of the Department of Applied Chemistry, Delhi Technological University, for their expertise and constructive feedback, which immensely contributed to the quality of this thesis. I am obliged to thank all the non-teaching and technical staff of the department for their endless help and resource management whenever required. Lastly, I acknowledge DTU for funding my research.

Jitendra Kumar

### **DELHI TECHNOLOGICAL UNIVERSITY**



Formerly Delhi College of Engineering Shahbad Daulatpur, Main Bawana Road, Delhi – 110042

### **CANDIDATE'S DECLARATION**

I, **Jitendra Kumar**, hereby certify that the work being presented in the thesis entitled "Studies on Natural Gum-based Injectable Hydrogel for Wound Healing Applications" of the requirements for the award of the Degree of Doctor of Philosophy, submitted in the Department of Applied Chemistry, Delhi Technological University is an authentic record of my work carried out during period from 26.08.2020 to 05.05.2025 under the supervision of Prof. Roli Purwar.

The matter presented in the thesis has not been submitted by me for the award of any degree from this or any other institute.

Jitendra Kumar

This is to certify that the student has incorporated all the corrections suggested by the examiners in the thesis and the statement by the candidate is correct to the best of our knowledge.

**Signature of Supervisor** 

**Signature of External Examiner** 

**DELHI TECHNOLOGICAL UNIVERSITY** 

Formerly Delhi College of Engineering

Shahbad Daulatpur, Main Bawana Road, Delhi – 110042

**CERTIFICATE BY THE SUPERVISOR** 

This is to certify that Mr. Jitendra Kumar (Roll No.: 2K20/PHD/AC/05) has carried

out the research work presented in this thesis entitled "Studies on Natural Gum-based

Injectable Hydrogel for Wound Healing Applications" for the award of Doctor of

Philosophy from the Department of Applied Chemistry, Delhi Technological University,

Delhi, under my supervision. The thesis embodies the result of original work, and studies

are carried out by the student himself, and the contents of the thesis do not form the basis

for the award of any other degree to the candidate or anybody else from this or any other

University/Institute.

Prof. Roli Purwar

(Supervisor)

(Department of Applied Chemistry, DTU)

Date: 08.10.2025

### **ABSTRACT**

This thesis describes the fabrication and characterization of novel injectable hydrogels using functionalized natural gums (Moringa oleifera gum, mesquite gum, neem gum, and okra gum) with multi-aldehyde groups and carboxymethyl chitosan crosslinked through a Schiff base mechanism at 37°C. The optimal concentration of an oxidizing agent is determined to maximize aldehyde content in each gum, which in turn affects the gelation time and physical properties such as syringeability, porosity, self-healing ability, and gel content. Structural characterization is performed using Fourier-transform infrared and nuclear magnetic resonance spectroscopy, while surface morphology and rheological properties are analyzed by scanning electron microscopy and rheometry, respectively. The swelling ratio was assessed for dry and gel form in phosphate buffer saline at pH 5.5, 7.4, and 8.5 at 37°C, indicating pH-responsive behavior. Ciprofloxacin HCl is loaded as a model drug, and its release behavior is studied under different pH conditions (5.5, 7.4, and 8.5) for dry and gel form, revealing a pH-dependent release profile. The Korsemeyer-Peppas model evaluates drug release mechanisms. In vitro cytotoxicity using L-929 fibroblast cells confirms the biocompatibility of the injectable hydrogels, with varied cell viability depending upon the gum used. Hemolysis assays are also carried out to ensure the biocompatibility of the injectable hydrogels. Additionally, antibacterial activity is assessed against Gram-positive and Gram-negative bacteria, and hydrolytic degradation of the injectable hydrogels is evaluated in PBS at pH 7.4.

### TABLE OF CONTENTS

ACKNOWLEDGEMENTS	iii
CANDIDATE'S DECLARATION	iv
CERTIFICATE BY THE SUPERVISOR	V
ABSTRACT	vi
TABLE OF CONTENTS	vii
LIST OF TABLES	xiii
LIST OF FIGURES	XV
LIST OF ABBREVIATIONS	xviii
LIST OF SCHEMES	xix
CHAPTER 1	1-8
INTRODUCTION	1
1.1 General	1
1.2 Research Gap and Hypothesis	8
1.3 Objective	8
CHAPTER 2	9-96
LITERATURE SURVEY	9
2.1 Hydrogels and their application in the biomedical field	9
2.2 Injectable hydrogels and their application in the biomedical field	38
2.3 Biomedical applications of natural gum-based hydrogels and inject crosslinks through Schiff-based bonds	
2.4 Chitosan	73
2.4.1 Alkali treatment	74
2.4.2 Acylation	74
2.4.3 Carboxylation	75
2.4.4 Quaternization	75

2.4.5 Esterification	75
2.4.6 Etherification	75
2.5 Moringa oleifera gum	87
2.6 Mesquite gum	90
2.7 Neem Gum.	91
2.8 Okra Gum	96
CHAPTER 3	99-116
MATERIALS AND METHODS	99
3.1 Materials	99
3.2 Methods	99
3.2.1 Oxidation of gum	99
3.2.1.1. Oxidation of MOG	99
3.2.1.2. Oxidation of MG	101
3.2.1.3. Oxidation of NG	102
3.2.1.4. Oxidation of OG	103
3.2.2 Derivatization of Chitosan	104
3.2.3 Synthesis of IHs	105
3.2.3.1 MOG-based IH	105
3.2.3.2 MG-based IH	105
3.2.3.3 NG-based IH	105
3.2.3.4 OG-based IH	106
3.3 Characterization	106
3.3.1 Tube Inversion Test	106
3.3.2 Gel content	107
3.3.3 Porosity	107
3.3.4 Load-bearing capacity and structural integrity	107
3.3.5 Syringeability and injectability evaluation	108
3.3.6 Self-healing evaluation	108
3.3.7 Rheological properties of synthesized injectable hydrogel	109

3.3.8 Swelling ratio	110
3.3.8.1 Swelling study from dry form (Method 1)	110
3.3.8.2 Swelling study from gel form (Method 2)	110
3.3.9 Drug loading and release kinetics	112
3.3.9.1. Drug release from dry form of IHs (Method 1)	112
3.3.9.2. Drug release from gel form of IHs (Method 2)	113
3.3.10 Cytotoxicity evaluation	113
3.3.11 Hemolysis assay	114
3.3.12 Antibacterial assay	114
3.3.13 Hydrolytic degradation	115
CHAPTER 4	117-140
SYNTHESIS AND CHARACTERIZATION OF INJECTAE BASED ON MULTIALDEHYDE <i>MORINGA OLEIFERA</i> GUN WITH CARBOXYMETHYL CHITOSAN VIA SCHIFF BASE N	M CROSSLINKED
4.1 Introduction	117
4.2 Effect of Concentration of NaIO <sub>4</sub> on Gelation time	118
4.3 Effect of Concentration of Oxidized Moringa Oleifera Gum on	Gelation time119
4.4 Physical properties of injectable hydrogel	121
4.5 Structural Properties	125
4.6 Rheological Properties	128
4.7 Morphological Evaluation	130
4.8 Swelling Study	131
4.8.1 Swelling Study from Dry Form of IH-3-7 (Method 1)	131
4.8.2 Swelling Study from Gel Form of IH-3-7 (Method 2)	131
4.9 Drug Release Study	132
4.9.1 Drug Release from Dry Form of IH-3-7 (Method 1)	133
4.9.2 Drug Release from Gel Form of IH-3-7 (Method 2)	133
4.10 Cytotoxicity Evaluation	135
4.11 Hemolysis assay	137

4.12 Hydrolytic Degradation Studies	. 138
4.13 Conclusion	. 139
CHAPTER 5141	-168
SYNTHESIS AND CHARACTERIZATION OF INJECTABLE HYDIBASED ON MULTIALDEHYDE MESQUITE GUM CROSSLINKED CARBOXYMETHYL CHITOSAN VIA SCHIFF BASE MECHANISM	WITH
5.1 Introduction	. 141
5.2 Effect of concentration of NaIO <sub>4</sub> on gelation time	. 142
5.3 Effect of concentration of oxidized MG on gelation time	. 144
5.4 Physical properties of IHs	. 145
5.5 Structural properties	. 148
5.6 Rheological properties	. 151
5.7 Morphological evaluation	. 154
5.8 Swelling study of IHs	. 156
5.8.1 Swelling study from dry form of IHs (Method 1)	. 156
5.8.2 Swelling study from gel form of IHs (Method 2)	. 156
5.9 Drug release behavior	. 158
5.9.1 Drug release from dry form of IHs (Method 1)	. 158
5.9.2 Drug release from gel form of IHs (Method 2)	. 159
5.10 In vitro cytotoxicity assay	. 163
5.11 Hemolysis assay	. 164
5.12 Antibacterial assay	. 165
5.13 Hydrolytic degradation	. 166
5.14 Conclusions	. 167
CHAPTER 6	-198
SYNTHESIS AND CHARACTERIZATION OF INJECTABLE HYDI	ROGEL
BASED ON MULTIALDEHYDE NEEM GUM CROSSLINKED	WITH
CARBOXYMETHYL CHITOSAN VIA SCHIFF BASE MECHANISM	
6.1 Introduction	
6.2 Effect of concentration of NaIO <sub>4</sub> on gelation time	170

6.3 Effect of concentration of oxidized NG on gelation time	172
6.4 Physical properties of IHs	173
6.5 Structural properties	176
6.6 Rheological properties	179
6.7 Morphological Evaluation	183
6.8 Swelling study of IHs	184
6.8.1 Swelling study from dry form of IHs (Method 1)	184
6.8.2 Swelling study from gel form of IHs (Method 2)	185
6.9 Drug release behavior	187
6.9.1 Drug release study from dry form of IHs (Method 1)	188
6.9.2 Drug release study from gel form of IHs (Method 2)	188
6.10 In vitro cytotoxicity evaluation	192
6.11 Hemolysis assay	193
6.12 Antibacterial assay	194
6.13 Hydrolytic degradation	195
6.14 Conclusion	197
CHAPTER 7	199-220
SYNTHESIS AND CHARACTERIZATION OF INJECTABLE I BASED ON MULTIALDEHYDE OKRA GUM CROSSLINE CARBOXYMETHYL CHITOSAN VIA SCHIFF BASE MECHANISM	KED WITH
7.1 Introduction	199
7.2 Gelation time	199
7.3 Physical properties of OG2C1	201
7.4 Structural properties	205
7.5 Rheological study	207
7.6 Morphological evaluation	210
7.7 Swelling study	210
7.7.1 Swelling study from dry form of OG2C1 (Method 1)	211
7.7.2 Swelling study from gel form of OG2C1 (Method 2)	211

7.8 Drug release study	212
7.8.1 Drug release study from dry form of OG2C1 (Method 1)	212
7.8.2 Drug release study from gel form of OG2C1 (Method 2)	213
7.9 In vitro cytotoxicity assay	215
7.10 Hemolytic activity	216
7.11 Antibacterial assay	217
7.12 <i>In vitro</i> degradation	218
7.13 Conclusion	219
CHAPTER 8	221-226
OVERALL CONCLUSION, FUTURE SCOPE, AND SOCIAL I	MPACT221
8.1 Overall Conclusion	221
8.2 Future Scope	225
8.3 Social Impact	225
REFERENCES	227-282
LIST OF PUBLICATIONS, INTERNATIONAL CONFERENCE	
PROOFS	283-290
PLAGIARISM VERIFICATION WITH PROOF	291-293
CURRICULUM VITAE	294-299

### LIST OF TABLES

Table 2.1 Natural gum-based hydrogel using chemical crosslinks    22
Table 2.2 Natural gum-based hydrogel using physical crosslinks    33
Table 2.3 Natural gum-based hydrogel using hybrid crosslinks    37
Table 2.4 Natural gum-based injectable hydrogel using chemical crosslinks for
biomedical applications
Table 2.5 Natural gum-based injectable hydrogel using physical crosslinks for
biomedical applications
Table 2.6 Natural gum-based injectable hydrogel using hybrid crosslinks for
biomedical application
<b>Table 2.7</b> Natural gum-based hydrogel using Schiff base crosslinks for biomedical
applications
Table 2.8 Natural gum-based injectable hydrogel using Schiff base crosslinks for
biomedical applications
Table 2.9 Biomedical application of derivatized chitosan as an injectable hydrogel.83
Table 2.10 Various applications of MOG-based hydrogel    89
Table 2.11 Various applications of neem gum-based hydrogel    95
Table 2.12 Various applications of okra gum-based hydrogel    97
Table 4.1 Effect of concentration of NaIO4 on gelation time of injectable hydrogels
Table 4.2 Effect of concentration of oxidized Moringa oleifera gum (MOG-CHO-3)
on gelation time
Table 4.3 Physical properties of IH-3-7   124
Table 4.4 K-P kinetic model parameters for IH-3-7
Table 5.1 Effect of concentration of NaIO4 on gelation time of injectable
hydrogel143
Table 5.2 Effect of concentration of oxidized MG (MOG-CHO-2) on gelation time.144
Table 5.3 Physical Properties of IHs   148
Table 5.4 K-P kinetic model parameters for IH-MG-1, IH-MG-3, and IH-MG-5 in dry
and gel form in PBS at pH 5.5, 7.4, and 8.5
<b>Table 6.1</b> Effect of concentration of NaIO <sub>4</sub> on gelation time of IHs171
<b>Table 6.2</b> Effect of concentration of oxidized NG (NG-CHO-0.5) on gelation time172
<b>Table 6.3</b> Physical Properties of IHs

Table 6.4 K-P kinetic model parameters for IH-0.5-1, IH-0.5-3, and IH-	0.5-5 in dry
and gel form in PBS at pH 5.5, 7.4, and 8.5	191
Table 7.1 The concentration of precursors for the synthesis of IHs	201
Table 7.2 Physical properties of OG2C1	204
Table 7. 3 K-P kinetic model parameters for OG2C1 in dry and gel for	m in PBS at
pH 5.5, 7.4, and 8.5	215
Table 8. 1 Comparison of optimized IHs with literature data on swelling,	drug release,
and degradation	222

### LIST OF FIGURES

Fig. 2.1 Pictorial representation of natural gum-based hydrogel for biomedical
application
Fig. 2.2 Pictorial representation of natural gum-based injectable hydrogel for
biomedical applications
Fig. 2.3 Pictorial representation of natural gum-based hydrogel using SB crosslinks
for biomedical applications
Fig. 2.4 Pictorial representation of natural gum-based injectable hydrogel using SB
crosslinks for biomedical applications
Fig. 4.1 (a) Oxidation of Moringa oleifera gum (MOG-CHO-3), (b) Derivatization of
chitosan (CMCh), (c) Synthesis of injectable hydrogel (IH-3-7)118
Fig. 4.2 Physical properties of injectable hydrogel (a) Load bearing capacity (b)
structural integrity (c) injectability
Fig. 4.3 (a) IH-3-7 cut into two halves, (b) Gels were joined together manually, (c)
Filled and extruded through an 18 G needle, and (d) button-shaped self-healed IH-3-
7
Fig. 4.4 FT-IR spectra of (a) MOG, MOG-CHO-3 (b) chitosan, CMCh and (c) MOG-
CHO-3, CMCh, IH-3-7
<b>Fig. 4.5</b> <sup>1</sup> H-NMR spectra of (a) MOG (b) MOG-CHO-3
Fig. 4. 6 (a) Flow sweep test (b) Amplitude sweep test (c) frequency sweep test (d)
step-strain analysis
Fig. 4.7 SEM micrograph of IH-3-7 (a) before gel content (b) after gel content 130
Fig. 4.8 The swelling ratio of IH-3-7 in PBS at 5.5 and pH 7.4 (a) dry form (b) gel
form
Fig. 4.9 Drug release behavior of IH-3-7 in PBS 5.5 and PBS 7.4 (a) Dry form (b) Gel
form
Fig. 4.10 (a) Cell viability of IH-3-7 and cipro-loaded IH-3-7. Inverted phase
microscopic images of (b) control. IH-3-7 treated L-929 cell line at (c1) 1µg mL <sup>-1</sup> (c2)
$50~\mu g~mL^{-1}$ . Cipro loaded IH-3-7 treated L-929 cell line at (d1)1 $\mu g~mL^{-1}$ (d2) $500~\mu g$
$mL^{-1}$
<b>Fig. 4. 11</b> Hemolysis ratio of IH-3-7
Fig. 4. 12 Hydrolytic degradation behavior of IH-3-7 in PBS at pH 7.4 at 37°C 139
Fig. 5. 1 (a) Oxidation of mesquite gum (MG-CHO) (b) Derivatization of chitosan
(CMCh) (c) Fabrication of IH

Fig. 5. 2 Pictorial representation of self-healing behavior of injectable hydrogel 146
Fig. 5. 3 Pictorial representation of injectability of IH through 21G needle 147
Fig. 5. 4 FT-IR spectra of (a) MG, MG-CHO-2 (b) chitosan, CMCh and (c) MG-CHO-
2, CMCh, IH-MG-5149
Fig. 5. 5 <sup>1</sup> H-NMR spectra of (a) MG (b) MG-CHO-2 (c) chitosan (d) CMCh 150
Fig. 5. 6 (a) Isothermal time sweep study (b) flow sweep behavior (c) Amplitude
sweep study (d) Frequency sweep study IH-MG-1, IH-MG-3, and IH-MG-5. Step-
strain measurement of (e1) IH-MG-1 (e2) IH-MG-3 (e3) IH-MG-5153
Fig. 5. 7 SEM images at 1300X (a1) IH-MG-1 (b1) IH-MG-3 (c1) IH-MG-5 and
1800X (a2) IH-MG-1 (b2) IH-MG-3 (c2) IH-MG-5
Fig. 5. 8 Swelling behavior of IHs in PBS in dry form at (a) pH 5.5 (b) pH 7.4 (c) pH
8.5 and in gel form at (d) pH 5.5 (e) pH 7.4 (f) pH 8.5
Fig. 5. 9 Drug release behavior of IHs in PBS in dry form (a) at pH 5.5 (b) pH 7.4 (c)
pH 8.5 and in gel form (d) at pH 5.5 (e) at pH 7.4 (f) at pH 8.5161
Fig. 5. 10 (a) Cytotoxicity of injectable hydrogels. Inverted phase microscopic images
of (b) control. IH-0.5-1 treated L-929 cell line at (c1) $1\mu g\ mL^{1}$ (c2) $500\ \mu g\ mL^{1}.$ IH-
0.5-3 treated L-929 cell line at (d1)1 $\mu$ g mL <sup>-1</sup> (d2) 500 $\mu$ g mL <sup>-1</sup> . IH-0.5-5 treated L-
929 cell line at (e1) 1 $\mu$ g mL <sup>-1</sup> (e2) 500 $\mu$ g mL <sup>-1</sup>
Fig. 5. 11 Statistical representation of hemolysis ratio of IHs
Fig. 5. 12 Antibacterial activity of (a) IH-MG-1 (b) IH-MG-3 (c) IH-MG-5165
Fig. 5. 13 Hydrolytic degradation behavior of IHs in PBS at pH 7.4 (a) dry form (b)
gel form
Fig. 6. 1 (a) Oxidation of neem gum (NG-CHO) (b) Derivatization of chitosan
(CMCh) (c) Fabrication of IH
Fig. 6. 2 Pictorial representation of macroscopically self-healing of injectable
hydrogel
Fig. 6. 3 Injectability evaluation of synthesized injectable hydrogel
Fig. 6. 4 FT-IR spectra of (a) NG, NG-CHO-0.5 (b) chitosan, CMCh and (c) NG-
CHO-0.5, CMCh, IH-0.5-5
Fig. 6. 5 <sup>1</sup> H-NMR spectra of (a) NG (b) NG-CHO-0.5 (c) chitosan (d) CMCh 178
Fig. 6. 6 (a) Isothermal time sweep study (b) G'G" v/s shear strain showing LVE
region and crossover point (c) G'G" v/s angular frequency showing stiff and elastic
nature (d) Viscosity v/s shear rate showing shear-thinning behavior. Oscillatory step-
strain measurements of (e1) IH-0.5-1 (e2) IH-0.5-3 (e3) IH-0.5-5
Fig. 6. 7 FESEM images at different magnifications of (a) IH-0.5-1, (b) IH-0.5-3, (c)
IH-0.5-5

Fig. 6. 8 Swelling behavior of IH in PBS in dry form (a) at pH 5.5 (b) pH 7.4 (c) pH
8.5 and in gel form (d) at pH 5.5 (e) at pH 7.4 (f) at pH 8.5 (g) mechanism of swelling.
Fig. 6. 9 Drug release behavior of IHs in PBS in dry form at (a) pH 5.5 (b) pH 7.4 (c)
pH 8.5 and in gel form at (d) pH 5.5 (e) pH 7.4 (f) pH 8.5
Fig. 6. 10 (a) Cytotoxicity of injectable hydrogels. Inverted phase microscopic images
of (b) control. IH-0.5-1 treated L-929 cell line at (c1) 1μg mL <sup>-1</sup> (c2) 500 μg mL <sup>-1</sup> . IH-
0.5-3 treated L-929 cell line at (d1)1 $\mu$ g mL <sup>-1</sup> (d2) 500 $\mu$ g mL <sup>-1</sup> IH-0.5-5 treated L-929
cell line at (e1) 1µg mL <sup>-1</sup> (e2) 500 µg mL <sup>-1</sup> 192
Fig. 6. 11 Hemolysis assay for IHs
<b>Fig. 6. 12</b> The antibacterial activity of (a) IH-0.5-1(b) IH-0.5-3 (c) IH-0.5-5
<b>Fig. 6. 13</b> Hydrolytic degradation behavior of IHs in PBS at pH 7.4 (a) dry form (b)
gel form
Fig. 7. 1 (a) Tube inversion test. Time sweep study of (b) OG1C2 (c) OG1C1 (d)
OG2C1
Fig. 7. 2 Injectability evaluation of OG2C1 using 26 G needle
Fig. 7. 3 Pictorial representation of Self-healing of OG2C1
Fig. 7. 4 FT-IR spectra of (a1) OG, OG-CHO (b1) OG-CHO, CMCh, OG2C1.
Reaction Scheme (a2) oxidation of OG (b2) synthesis of OG2C1206
Fig. 7. 5 <sup>1</sup> H-NMR spectra of (a) chitosan (b) CMCh (c) OG (d) OG-CHO (e) reaction
scheme of derivatization of chitosan
Fig. 7. 6 (a) Flow sweep study (b) Amplitude sweep study (c) Frequency sweep study
(d) Step-strain analysis
<b>Fig. 7. 7</b> SEM images of OG2C1 at 5000X
Fig. 7. 8 Swelling study of OG2C1 in PBS at pH 5.5, 7.4, and 8.5 (a) dry form (b) gel
form
Fig. 7. 9 Drug release study of OG2C1 in PBS at pH 5.5, 7.4, and 8.5 (a) dry form (b)
gel form
<b>Fig. 7. 10</b> <i>In vitro</i> cytotoxicity assessment of OG2C1
Fig. 7. 11 Hemolysis evaluation of OG2C1216
Fig. 7. 12 (a) Antibacterial assessment bar diagram of OG2C1. Antibacterial
evaluation of OG2C1 against (b) E. coli. (b) S. aureus
Fig. 7. 13 Hydrolytic degradation of OG2C1 in dry and gel form

### LIST OF ABBREVIATIONS

Full Name	Abbreviation used
MOG	Moringa oleifera gum
MG	Mesquite gum
NG	Neem gum
OG	Okra gum
IH	Injectable hydrogel
CMCh	Carboxymethyl chitosan
G	Gauze
EDC	(1-ethyl-3-(3-dimethylaminopropyl)carbodiimide)
NHS	(N-hydroxysuccinimide)
NNMBA	N, N'-methylene bisacrylamide
FRP	free-radical polymerization
GP	graft copolymerization
PEGDA	polyethylene glycol diacrylate
CaCl <sub>2</sub>	Calcium chloride
DMEM	Dulbecco's Modified Eagle Medium
FBS	Fetal Bovine Serum
DMSO	Dimethyl sulfoxide

### LIST OF SCHEMES

Scheme No.	Name of Scheme	Page No.
3.1	Reaction of MOG with hydroxylamine hydrochloride	100
3.2	Reaction of hydrochloric acid with sodium hydroxide	100
3.3	Reaction of MG with hydroxylamine hydrochloride	101
3.4	Reaction of hydrochloric acid with sodium hydroxide	101
3.5	Reaction of NG with hydroxylamine hydrochloride	102
3.6	Reaction of hydrochloric acid with sodium hydroxide	102
3.7	Reaction of OG with hydroxylamine hydrochloride	103
3.8	Reaction of hydrochloric acid with sodium hydroxide	103

#### CHAPTER 1

#### INTRODUCTION

#### 1.1 General

Hydrogels consist of three-dimensional viscoelastic crosslinked structures formed from hydrophilic polymers. They can retain significant amounts of water within their network without altering their initial structure and garner considerable interest as effective carriers for drug delivery in wound healing [1]. Their distinctive attributes include customizable physical properties, substantial water content, and manageable degradability. Injectable hydrogels (IHs) constitute a specialized subset of hydrogels engineered to be administered in liquid form and later transformed into solid hydrogel matrices upon introduction into the body [2]. This kind of liquid administration reduces the number of surgical procedures and is highly suitable for irregularly shaped sites. It can be tailored to possess adjustable properties, including viscosity, mechanical strength, and degradation rate, enhancing its versatility for diverse medical applications. It can be responsive to external stimuli such as temperature, pH, light, and magnetic fields, facilitating targeted drug release and tissue regeneration. It can function as a carrier for therapeutic agents like drugs, cells, proteins, and bioactive molecules, enabling the treatment of various conditions. Further, it can emulate the extracellular matrix environment, supporting cell growth and migration while fostering tissue repair. Polysaccharide-based IHs serve as versatile drug delivery systems and offer a minimally invasive alternative to surgical procedures, capable of filling and conforming to spaces of any shape [3]. With abundant hydroxyl and amine groups, polysaccharides facilitate drug conjugation and various chemical modifications essential for drug delivery applications [4]. The porous architecture of IHs provides an ideal matrix for drug loading, shielding drugs from harsh environmental conditions while enabling controlled release [5]. The release kinetics, primarily governed by molecule diffusion, ensure optimal drug delivery over time [3]. Polysaccharides present several advantages, including biocompatibility, biodegradability, non-toxic nature, and the ability to be sourced from renewable natural origins. These qualities make them well-suited for incorporation into IHs, catering to various biomedical applications. Some examples of polysaccharides used in the formation of IHs are chitosan [6], hyaluronic acid [7], gellan gum[8], gum arabic [9], and guar gum [10]. Natural gum-based IHs can be prepared through various methods, including chemical and physical crosslinking. Covalent bonds are formed between polymeric chains in chemical crosslinking, often through reactions such as Michael-type addition. On the other hand, physical crosslinking involves the formation of non-covalent bonds, such as hydrogen bonding, between polymer chains [11]. Zang and colleagues developed a self-healed polysaccharide-based IH via physical crosslinks [12]. This system is based on chitosan and sodium alginate networks cross-linked by reversible imine bonds formed from a Schiff base reaction of the amino groups on chitosan with aldehyde groups on oxidized sodium alginate. Similarly, an "all-sugar" hydrogel dressing is developed based on a dynamic borate bonding network between the hydroxyl groups of okra polysaccharide and xyloglucan [13].

Schiff base reactions represent a class of condensation reactions linking an aldehyde or ketone with a primary amine to produce an imine or Schiff base. Mechanistically, the amine first attacks the carbonyl carbon of the aldehyde to form a carbinolamine intermediate. This intermediate then undergoes dehydration, resulting in the formation of the Schiff base reaction. These reactions find application across diverse sectors, such as the paint industry, polymer technology, pharmaceuticals, and medicine, due to the functional groups inherent in their structures [14]. Due to numerous inherent advantages, Schiff-based reactions play a pivotal role in developing IHs, particularly those derived from polysaccharides. These IHs offer simplicity in fabrication, injectability, and self-healing under physiological conditions [15]. IHs can be customized for specific drug delivery applications and wound healing cell therapy by establishing Schiff base linkages between amine and aldehyde groups. Employing Schiff base chemistry provides several distinct benefits over traditional crosslinking techniques. Firstly, it enables the rapid formation of IHs without requiring additional crosslinkers, thereby mitigating potential cytotoxicity concerns of crosslinking agents [16]. Secondly, the reversible nature of the imine bond confers degradation properties to the IHs, making them suitable for controlled drug release and biodegradable implants [17]. Thirdly, their self-healing attribute facilitates the restoration of structural integrity upon damage, thereby enhancing the durability and functionality of the IHs [18] [19]. Overall, leveraging Schiff base reactions in constructing IHs represents a valuable strategy for addressing drug delivery and regenerative medicine challenges in wound healing applications. A pH-responsive, injectable, and selfhealing chitosan-coumarin hydrogel was synthesized based on Schiff base and hydrogen bonds [20]. An IH was prepared using pectin aldehyde and DL-lysine via the

Schiff base mechanism used for drug delivery application [21]. The IHs were prepared using nanoparticle-crosslinked xyloglucan/ε-poly-l-lysine composite with hemostatic, antimicrobial, and angiogenic properties for infected wound healing applications [22]. Chitosan, a linear polysaccharide, is derived from the deacetylation process of chitin. Chitin is sourced mainly from crustacean shells like shrimp and crabs and from the cell walls of fungi such as reishi mushrooms. Chitosan exhibits various properties and finds applications in different fields, including agriculture, food science, materials science, and the biomedical industry [23]. Despite its numerous advantages, chitosan encounters several limitations in biomedical applications. Careful consideration of chitosan's insolubility in water and most common organic solvents [24], limited mechanical strength in some chitosan-based materials [25], uncontrolled biodegradation leading to variability in degradation rates [26], and the potential for bioaccumulation of degradation products is necessary to ensure safety and effectiveness in applications [27]. Introducing carboxymethyl groups into chitosan exhibits improved solubility, biodegradability, and biocompatibility, thus broadening its utility in drug delivery, tissue engineering, and wound healing. Carboxymethyl chitosan IHs possess favorable attributes like non-toxicity, moisture retention, and pH responsiveness, making them suitable for injectable applications. Moreover, these IHs can be customized through chemical modifications to adjust properties such as drug release kinetics, mechanical strength, and degradation rates [28].

Moringa oleifera gum (MOG) is derived from the stem exudate of the Moringa oleifera tree in native parts of Africa and Asia, which possesses hydrophilic properties.

The Africans used to call it "Never Die" or "Miracle Tree" for its ability to treat more

than 300 diseases and was honored as "Botanical of the Year – 2007" by the National Institute of Health (NIH) [29]. The chemical constituents include glucose, rhamnose, galactose, glycolic acid, and arabinose. The prospective uses of MOG in the food, cosmetics, and pharmaceutical industries have drawn interest [30]. Hydrogels can be made from MOG using different crosslinking techniques, such as chemical and physical crosslinking [31]. Studies have highlighted the versatile utility of MOG hydrogel across various fields, including drug delivery systems and wound care [32]. MOG has been integrated with other polymers or modified to create functionalized nanogels, which demonstrate pH responsiveness and exhibit potential in delivering anticancer drugs such as doxorubicin [33]. Furthermore, blending MOG with poly(vinyl alcohol), superabsorbent hydrogels with favorable swelling ratios, reswelling capabilities, and water retention properties have been formulated [34]. These hydrogels are promising for wound dressing applications owing to their healing, anti-inflammatory, and antimicrobial attributes. Compared to conventional synthetic alternatives, MOG-based hydrogels offer enhanced biocompatibility, biodegradability, and reduced environmental impact.

Mesquite gum (MG), also known as mesquite gum Arabic, was collected from mesquite trees, notably from species like *Prosopis juliflora* and *Prosopis glandulosa*. Indigenous communities have historically utilized this gum for diverse applications, including as a food enhancer, a binding agent, and in traditional remedies [35]. Mesquite gum is an intricate polysaccharide composed primarily of arabinose, galactose, rhamnose, and glucuronic acid residues [36]. This water-soluble gum creates viscous solutions and has excellent emulsifying, stabilizing, thickening, biodegradable, and non-toxic properties. In the pharmaceuticals sector, mesquite gum

is used as a carrier in drug delivery systems; it acts as a binder in tablets and for controlled drug release. Mesquite gum can also be modified chemically; oxidation, grafting, or crosslinking can improve its properties regarding hydrogel formation in biomedical applications. Its versatility and eco-friendly nature make it a valued natural polymer in various sectors. Furthermore, researchers have investigated its use in developing hydrogels, such as mesquite gum/chitosan insoluble complexes, which exhibit intriguing viscoelastic characteristics [37].

Azadirachta indica, referred to as neem gum (NG), Indian gum, or Indian gum arabic, is sourced from the bark of the neem tree. Chemical constituents of NG include Larabinose, L-fucose, D-galactose, D-glucuronic acid, D-xylose, glucose, and mannose. Neem gum is water-soluble and creates viscous solutions with stabilizing and emulsifying properties. It is biodegradable, non-toxic, and environmentally friendly, so it can be used in several industries. Its adhesive, emulsifying, and thickening qualities render it valuable in various sectors such as pharmaceuticals, food, and cosmetics [38]. Neem gum has been employed to create pH-responsive hydrogel matrices for drug delivery. One study aimed to fabricate a neem gum-based localized drug delivery system for sustained methotrexate release under diverse pH conditions. The hydrogel matrix exhibited promising attributes, including high drug encapsulation capacity, non-Fickian drug release kinetics, and compatibility with various blood types [39]. Another investigation explored the efficacy of a hydrogel comprising neem and silk fibroin biomaterials for wound healing. The neem-silk fibroin hydrogel formulation demonstrated expedited wound healing compared to control groups [40]. These results underscore the potential of neem gum-based hydrogels in pharmaceutical and biomedical arenas.

Okra gum (OG) is extracted from the pods of the okra plant (Abelmoschus esculentus) [41]. The primary components of okra gum are polysaccharides, including rhamnose, galactose, glucose, galacturonic acid, and glucuronic acid [42]. These components contribute to its unique properties, such as high viscosity at low concentrations and biodegradability. It possesses bioactive compounds that exhibit anti-inflammatory, antibacterial, and antifungal activities, enhancing its appeal in health-related applications. This gum is soluble in cold water and exhibits mucoadhesive properties, making it suitable for various applications [43]. OG is used as a thickening and emulsifying agent in sauces, dressings, and dairy products. It enhances texture and stability in food formulations. It acts as a binder in tablet formulations, improving the physical characteristics of tablets, such as hardness and disintegration time [44]. Studies have shown that okra gum can sustain the release of drugs, making it valuable for controlled-release formulations [45]. It is employed in creams and lotions for its thickening and stabilizing properties, contributing to product consistency and performance. Packaging industries also use OG for its potential use in biodegradable packaging materials, offering an eco-friendly alternative to conventional plastics [46]. Basharat et al. reported a research article based on acrylic acid grafted Abelmoschus esculentus hydrogel via free radical polymerization to release Pantoprazole Sodium drug [47]. Okunlola et al. synthesize microspheres using okra gum with sodium alginate via an ionic emulsification method to release ambroxol hydrochloride [48]. A similar study was published by Ghumman et al., which designed microspheres using alginate and OG through an inotropic gelation technique for sustained release of Oxcarbazepine [49]. Maryam et al. designed a pH-sensitive okra gum and gelatinbased polymeric blend through an aqueous polymerization method to release

Cytarabine [50]. Patra *et al.* synthesized a hydrogel using carboxymethylated okra gum with polymethacrylamide copolymer via the free-radical initiation method and microwave radiation application. Ceric ammonium nitrate was used as a free-radical-initiator to release Diclofenac Sodium [51].

### 1.2 Research Gap and Hypothesis

Based on the literature survey, it has been noted that no IH was synthesized based on the combination of carboxymethyl chitosan and natural gum such as *Moringa oleifera* gum, mesquite gum, neem gum, and okra gum with Schiff base crosslinks. Thus, it was hypothesized that the combination of multi-aldehyde natural gum (*Moringa oleifera* gum, mesquite gum, neem gum, and okra gum) and carboxymethyl chitosan would form an IH through dynamic Schiff base chemistry at physiological temperature (37°C), exhibiting desirable properties such as easy syringeability, injectability, and self-healing capabilities without additional crosslinkers. This IH will demonstrate favorable surface morphology, controlled swelling behavior, and sustained drug release kinetics. Furthermore, the IH will show excellent biocompatibility, low cytotoxicity, minimal hemolysis, and controlled hydrolytic degradation, making it a promising candidate for biomedical applications.

### 1.3 Objective

The objective of the thesis is to synthesize and characterize self-healing IHs based on multi-aldehyde natural gum, i.e., *Moringa oleifera* gum, mesquite gum, neem gum, and okra gum with carboxymethyl chitosan using Schiff base crosslink at physiological temperature.

#### **CHAPTER 2**

#### LITERATURE SURVEY

### 2.1 Hydrogels and their application in the biomedical field

Hydrogels, a class of polymeric materials, have gathered significant consideration due to their distinctive attributes and the broad spectrum of applications. Hydrogels consist of three-dimensional networks of hydrophilic polymers, enabling them to absorb and retain substantial amounts of water or biological fluids while preserving their structural integrity (Figure 2.1). With their high water content, hydrogels resemble natural living tissues, capable of retaining water up to thousands of times their dry weight, making them ideal for moisture retention applications. Hydrogels exhibit diverse structures, ranging from linear to cross-linked networks. The cross-linking among polymer chains is pivotal for upholding the hydrogel's integrity and mechanical strength. Various methods are employed to synthesize hydrogels, including chemical cross-linking of monomers and physical entanglement of polymers or a hybrid approach. The synthesis technique significantly influences properties such as swelling behavior, mechanical strength, and biocompatibility. Hydrogels swell upon exposure to water or biological fluids due to hydrophilic groups within the polymer network. The mechanical properties of hydrogels vary based on cross-linking density and polymer composition, ranging from soft and elastic to stiff and durable. Hydrogels exhibit a degree of flexibility remarkably similar to natural tissue due to their high water content. Many hydrogels are biocompatible, making them suitable for biomedical applications such as drug delivery, tissue engineering, wound healing, and contact lenses. Certain hydrogels exhibit responsiveness to external stimuli like pH, temperature, light, or electric fields, enabling the controlled release of drugs or molecules in response to specific environmental cues. Hydrogels are utilized in diapers, sanitary napkins, and wound dressings due to their absorbent properties. Despite their advantages, hydrogels encounter challenges such as inadequate mechanical strength, limited stability, and potential biocompatibility concerns, contingent upon application and composition specifics. They are biocompatible, biodegradable, and can be administered via injection. Entrapping microbial cells within hydrogel beads offers the advantage of low toxicity. They enable the timed release of growth factors and other nutrients, promoting proper tissue growth. Hydrogels possess good transport properties. They are non-adherent and may require secondary dressing for securement. Sensations similar to those caused by the movement of maggots may be experienced [52].

Hydrogels have gained significant attention in wound healing applications due to their unique properties and versatility. These biomaterials offer advantages such as a moist environment that promotes tissue regeneration, granulation, and re-epithelialization [53]. Hydrogel dressings can be tailored to deliver specific mediators like antiseptics, antibiotics, anti-inflammatories, and antioxidants to address critical issues in chronic wounds [54]. They can also incorporate bioactive molecules to accelerate wound healing by promoting angiogenesis, re-epithelialization, and extracellular matrix production. Chronic wounds, affecting a significant portion of the population, can benefit from hydrogel dressings with properties like biodegradability, adhesivity, and

antimicrobial, anti-inflammatory, and pre-angiogenic bioactivities [55]. These functional hydrogels can accelerate healing by providing a conducive wound repair and regeneration environment. Additionally, hydrogel dressings can be modified to include cells, growth factors, and other biomolecules to enhance wound contraction and healing [56]. Due to the ability to form a "viscous solution" or "gel," a set of naturally occurring polysaccharides is referred to as "gum." These polysaccharide gums are among the abundant essential ingredients that come from plants [57]. Their biodegradable, biocompatible, and sustainable qualities are the main reasons they are being researched. These polysaccharides' molecular makeup and chemical composition are frequently influenced by their extraction and processing techniques and their place of origin. Complex polysaccharides and carbohydrate polymers make up plant gums. The alginate unit, hyaluronan, and sugar monomers-starch and cellulose, for example—can be used to determine the chemical makeup. Additionally, this can be produced from several monosaccharides [58]. These polysaccharide gums are also known as "hydrocolloids" at times. Natural gums are one of the less expensive hydrocolloids used in the food business. They bind water, prevent ice crystals in emulsifiers and frozen items, and serve as moisturizers, stabilizers, thickeners, and food additives. They also pose no risk to human health. One of their standard features is their ability to create viscous dispersions and gels in water. Therefore, gel formation, or the formation of these hydrogels as a byproduct of hydrocolloids or gums, is a phenomenon wherein polysaccharide units associate or crosslink to form a threedimensional network that traps or immobilizes water within to take the form of a stiff structure that is resistant to flow [59]. Numerous investigations on different plantbased gums, particularly seed gums and plant exudates, have led to the discovery of critical natural sources of complex polysaccharides that encourage the intended application because of their suitable textures and stabilities. Their molecular architectures and chemical compositions determine their functional, physical, and chemical characteristics. Clarifying the connection between molecular structure, chemical composition, and corresponding physical properties has attracted much attention lately. A gum's structure determines whether it is suitable as a renewable resource and whether it may be used for different purposes. One type of polysaccharide that can increase a solution's viscosity even at deficient concentrations is natural gum. Gums are typically formed from the woody portions of plants or trees or can be found in seed coats. They are then further categorized based on their type. They can also be classified as charged, ionic, uncharged polymers, or polyelectrolytes. Natural gums can originate from various terra firma and marine sources. While pectin, guar, and locust bean gums are derived from land plants, some gums found in seaweeds, such as carrageenan and alginates, are excellent sources of food gums because they are either derived from the cell walls of different algae or are deposited in intracellular regions as reserve food materials. Seed gums are extracted from the seed kernels, while exudate gums are produced via gummosis, which involves the fragmentation of plant cellulose. Animal tissue is the source of gelatin, while microbial fermentation produces xanthan gum. Gums are naturally occurring polysaccharides with an organic origin, regardless of their source [60].

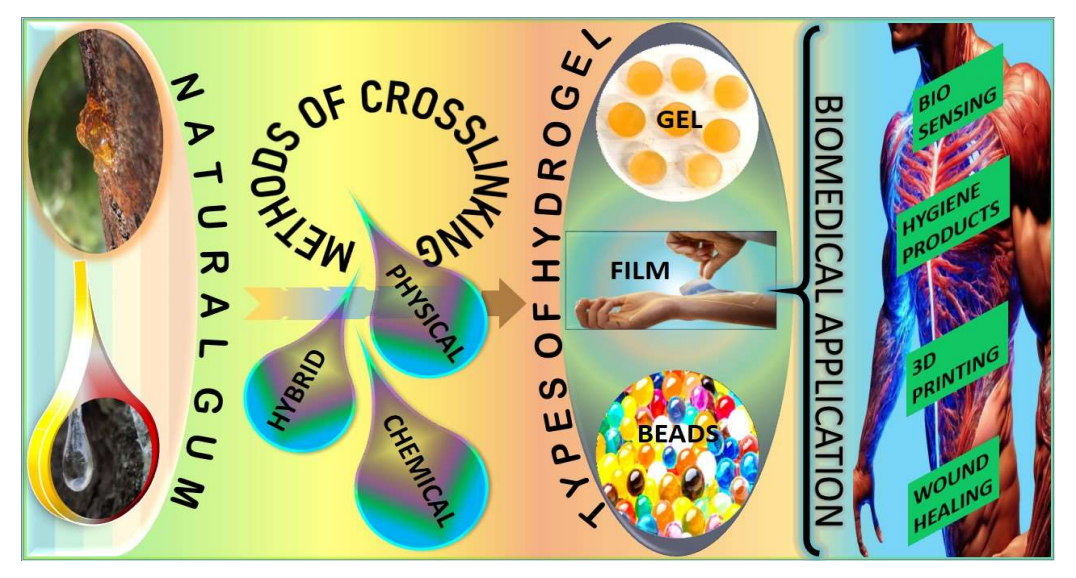


Fig. 2.1 Pictorial representation of natural gum-based hydrogel for biomedical application.

Natural gum polysaccharides from plants, trees, and seaweeds showcase numerous characteristics that render them valuable across industrial, pharmaceutical, and food sectors. Natural gum polysaccharides tend to be hydrophilic, displaying an affinity for water [61]. This quality benefits applications requiring moisture retention, like food, cosmetics, and pharmaceutical formulations. Many natural gum polysaccharides exhibit high viscosity when dissolved. This feature finds utility in stabilizing emulsions, suspending particles, and thickening solutions in food and pharmaceutical industries. Specific natural gum polysaccharides can form films upon drying their solutions. These films often possess barrier properties, proving advantageous in food packaging and coating endeavors. Natural gum polysaccharides are typically biodegradable, offering eco-friendly alternatives to synthetic polymers in various applications. Specific natural gums, such as agar, alginate, and carrageenan, demonstrate gel-forming properties in creating textured structures in food, pharmaceuticals, and other industries [62]. Natural gum polysaccharides blend well with other common formulation ingredients, including proteins, sugars, and synthetic

polymers. Many natural gum polysaccharides boast non-toxic and biocompatible attributes, making them suitable for pharmaceuticals, cosmetics, and biomedical applications [63]. Natural gum polysaccharides exhibit diverse rheological behaviors, such as shear-thinning or shear-thickening, and are adaptable to specific applications. Some natural gum polysaccharides possess emulsifying and stabilizing properties, which are beneficial in formulating emulsions and suspensions within food, pharmaceuticals, and cosmetics [64]. Specific natural gum polysaccharides from seaweeds and plants offer potential health benefits such as dietary fiber and prebiotic effects [65].

An antioxidant, antibacterial, and biodegradable hydrogel film was synthesized from carboxymethyl tragacanth gum and clove extract via the solution casting method used for wound dressing [66]. Koneru et al. synthesized cellulose-based nanocomposite hydrogel films of sodium carboxymethyl cellulose and grapefruit seed extract nanoparticles for wound healing applications [67]. A zinc oxide nanoparticles and allantoin incorporated chia seed mucilage-based antimicrobial hydrogel scaffold was developed via solvent casting to accelerate wound healing [68]. Babaluei et al. synthesized conductive hydrogels based on tragacanth and silk fibroin containing dopamine-functionalized carboxyl-capped aniline pentamer for burn wound healing application [69]. An aloe vera-sterculia gum-based copolymeric hydrogel dressing was prepared through graft copolymerization (GP) for drug delivery application [70]. Li et al. synthesized a guar gum-based supramolecular hydrogel via sol-gel transition, which may be utilized for biomedical applications [71]. Guar gum graft polymer-based silver nanocomposite hydrogels were developed through GP and used for effective anticancer drug release applications [72]. Baljit Singh and Abhishek Dhiman reported

a research article in which a hydrogel dressing was synthesized using acacia gum crosslinked with polyvinyl imidazole to release antibiotic/anesthetic drugs [73]. A hydrogel was synthesized using sulfated zwitterionic poly sulfobetaine methacrylate and K-Carrageenan network via physical crosslinks to promote wound healing applications [74]. A chemically modified gellan gum hydrogel was developed by incorporating methacrylate through three polymerization methods: step growth through thiol-ene photoclick chemistry and chain growth via photopolymerization for tissue engineering scaffolds [75]. A blend hydrogel of tyramine conjugated gum tragacanth and poly (vinyl alcohol) was developed by electron beam irradiation and proposed for biomedical application [76]. A new drug delivery platform was prepared by grafting sodium alginate with β-carboxyethyl acrylate and acrylamide via free radical polymerization (FRP) for wound healing application [77]. A hydrogel was fabricated using collagen, chitosan, N-acetyl cysteine, and ε-poly-lysine by EDC (1ethyl-3-(3-dimethylaminopropyl)carbodiimide) and NHS (N-hydroxysuccinimide) as a crosslinker for wound healing applications [78]. A photo-curable hydrogel in the form of chitosan inks was developed based on the simultaneous photocrosslinking of methacrylate chitosan with N, N'-methylene bisacrylamide (NNMBA), polyethylene glycol diacrylate (PEGDA), and acrylic acid to be applied in extrusion 3D printing for wound healing application [79]. A biopolymer alginate grafted to synthetic polyacrylic acid that has been chemically crosslinked using NNMBA to produce a pH-responsive hydrogel for biomedical applications by combining adhesive and conducting properties [80]. An acacia gum polysaccharide-based hydrogel wound dressing was synthesized via free radical graft polymerization using NNMBA as a crosslinker for drug delivery applications [81]. A poly(acrylamide-co-acrylamidoglycolic acid) and

guar gum-based hydrogel was fabricated using NNMBA as a crosslinked by a green protocol utilizing rhubarb stem-extract as bioreductant for drug delivery application [82]. A polyvinyl alcohol-guar gum-based smart hydrogel composite was designed using sodium borohydrate as a crosslinking agent for drug delivery application [83]. A dual-sensitive composite hydrogel network was synthesized from guar gum grafted polyacrylamide glycolic acid using sodium borohydride, crosslinker, utilized to explore sustained release of 5-fluorouracil [84]. Modified gum arabic cross-linked with gelatin scaffold used for hydrogel synthesis in biomedical applications [85]. A nonthermal plasma-assisted surface nano-textured hydrogel was designed using carboxymethyl guar gum and chitosan using tetraethyl orthosilicate as the crosslinker for their diverse applications in biomedicine [86]. The hydrogel was synthesized by semi-interpenetration of guar gum in a matrix of crosslinked collagen with a hydrophilic polyurethane-based crosslinker utilized for biomedicine as dressings in chronic wound healing [87]. A hydrogel was fabricated based on acacia gum and poly(2-arylamido-2-methylpropanesulfonic acid) via supra-molecular interactions for colon-specific drug delivery [88]. A biodegradable tragacanth gum biopolymer-based silver nanocomposite hydrogels were prepared with acrylamide as a monomer using a simple redox polymerization method crosslinked with NNMBA for use in wound healing as well as water purification applications [89]. A locust bean gum microgel capsule was readily prepared by divinyl sulfone crosslinking mechanism for drug delivery applications [90]. A hydrogel was developed based on gum tragacanth and acrylic acid using a glutaraldehyde crosslinker to control pantoprazole sodium [91]. A hydrogel was synthesized using poly(vinyl sulfonic acid) and sterculia gum by graft polymerization using an NNMBA crosslinker for colon-specific drug delivery

applications [92]. An Arabic gum-based hydrogel system was designed through a free radical polymerization reaction through NNMBA as a cross-linking agent and tetramethylethylenediamine as a catalyst for the cross-linking process for agriculture and biomedical applications [93]. Smart collagen and xanthan gum-based semi-IPN hydrogel with an antibacterial effect were fabricated using polyurethane as a crosslinking agent for drug release capacity and excellent performance in vitro bioactivity for wound healing application [94]. Mesoporous silica nanospheres and aldehyde-based methacrylated hyaluronic acid were combined with sulfhydrated guar gum to create a multi-network hydrogel through Schiff base reaction and photocrosslinking mechanism for biomedical applications [95]. Gelatin and polydopamine crosslinked with guar gum and cellulose nanocrystal via the borate didiol bond, intramolecular Schiff base reaction, and Michael addition for biomedical applications [96]. A hydrogel network composed of sterculia gum, carbopol, and graphene oxide was developed through a radiation-induced crosslinking mechanism for drug delivery mechanism [97]. Gum tragacanth-cl-poly (lactic acid-co-itaconic acid) hydrogel was prepared under microwave irradiation using an NNMBA crosslinker for biomedical applications [98]. A karaya gum-g-poly (acrylic acid) hydrogel was synthesized through an FRP using an NNMBA crosslinker for hydrophobic drug delivery [99]. An antimicrobial hydrogel composed of cellulose and arabic gum containing sulfadiazine is crosslinked by epichlorohydrin for drug delivery application [100]. A pH-sensitive, biodegradable ternary blended hydrogel film was developed using chitosan, guar gum, and polyvinyl pyrrolidone cross-linked via sodium tripolyphosphate by solution casting method for drug delivery application [101]. A low-cost crosslinked 3D printable hydrogel was fabricated based on biocompatible natural polymers such as gelatin and xanthan gum crosslinked by glutaraldehyde to grow human skin cells [102]. A radiation-induced graftcopolymerization technique was used to synthesize hydrogel composed of sterculia gum and polyvinyl alcohol used for drug delivery formulations [103]. An almond gumbased copolymeric hydrogel was fabricated by GP with polyvinyl alcohol and poly(2acrylamido-2-methylpropane sulphonic) acid for effectual colon-drug delivery [104]. A hydrogel was fabricated using gum acacia and tragacanth gum with polyacrylamide through GP reaction using an NNMBA crosslinker for drug delivery carrier [105]. A Butea monosperma gum-based hydrogel encapsulated with curcumin was fabricated with radiation-induced crosslinking and further employed for two diverse applications, i.e., drug delivery and anti-bacterial application [106]. An aloe vera, sterculia gum, and polyvinyl sulfonic acid-based hydrogel were developed by copolymerization reaction using an NNMBA crosslinker for wound dressing applications [107]. A pH-sensitive and self-healable hydrogel was fabricated using gum arabic aldehyde and polyvinyl alcohol through Schiff base crosslinks for drug delivery applications [108]. A biocompatible, mucoadhesive hydrogel was prepared based on natural polysaccharide sterculia gum and polyvinyl pyrrolidone through gamma radiation for drug delivery devices [109]. A bio nanocomposite scaffold was developed composed of acacia gum loaded with manganese sulfide nanorods in the presence of divinyl sulfone for tissue engineering applications [110]. A biomaterial hydrogel was synthesized using a combination of arabic gum, a natural polymer, and polyethylene glycol dimethacrylate, a synthetic polymer, by FRP using NNMBA crosslinker for hydrophobic drug release [111]. A hydrogel was developed composed of tragacanth gum, N-isopropyl acrylamide, and 2-(vinlyoxy) ethanol via simple redox polymerization using NNMBA

as a crosslinker and potassium persulfate as an initiator for the inactivation of multidrug-resistant bacteria [112]. A pH and salt-responsive hydrogel was designed based on guar gum as a renewable substrate using an NNMBA crosslinker for curcumin release [113]. A pH- and redox-responsive drug delivery system based on natural tragacanth gum was developed using an NNMBA crosslinker for targeted chemo/hyperthermia cancer treatment [114]. A pH and temperature-sensitive tamarind gum-based hydrogel was synthesized by FRP using a combination of acrylamide, Nisopropyl acrylamide, and ethylene glycol vinyl ether monomers with bis [2-(methacryloyloxy) ethyl] phosphate as a crosslinker for colon-specific anti-cancer drug delivery [115]. A hydrogel wound dressing was derived from polysaccharide tragacanth and alginate gum by radiation-induced copolymerization technique to manage the microbial infection and pain of the wounds simultaneously [116]. A hydrogel comprising carboxymethyl guar gum and polyvinyl alcohol was fabricated using tetraethyl orthosilicate as a crosslinker for wound healing applications [117]. Xanthan gum and polyvinyl pyrrolidone polymer were chemically cross-linked with acrylic acid monomer using ethylene glycol dimethacrylate and ammonium persulfate and sodium hydrogen sulfite as a cross-linker and initiator, respectively, to form a hydrogel for controlled drug delivery system [118]. The chemically oxidized gum arabic was prepared and used as a naturally derived nontoxic and pH-responsive crosslinker to develop smart polyvinyl alcohol-based hydrogel utilized for drug delivery applications [119]. A kappa-carrageenan, guar gum, and polyvinyl alcoholbased pH-sensitive hydrogels were prepared using silane as a crosslinker for oral drug delivery applications [120]. A pH-responsive protein hybrid crosslinked network hydrogel was formulated using sterculia gum and gelation, reinforced with Fe<sub>3</sub>O<sub>4</sub> nanoparticles through a Schiff base crosslinking mechanism for drug delivery application [121]. A blend of hydrogels composed of tyramine-conjugated gum tragacanth and polyvinyl alcohol was prepared by electron beam irradiation and used as a promising scaffold for tissue engineering [122]. A semi-IPN hydrogel composed of carboxymethyl guar gum and gelatin was synthesized using a glutaraldehyde crosslinker for sustained release of ciprofloxacin [123]. A bio-polymeric hydrogel scaffold of xanthan gum and dialdehyde alginate was synthesized using a tetraethyl orthosilicate crosslinker for tissue engineering applications [124]. Polysaccharide sterculia gum and psyllium-based hydrogel dressings were formulated using a gamma irradiation crosslinking mechanism for drug delivery applications [125]. A hydrogel was derived from copolymerizing tragacanth gum and gelatin using FRP and crosslinked through NNMBA for drug delivery [126]. Two borax-crosslinked carboxymethyl guar-based superabsorbents with bentonite and fumed silica particle reinforcement hydrogels were synthesized and used for disposable hygiene products [127]. Lidocaine and gentamicin-loaded gum acacia-carbopol-polyvinyl imidazolebased hydrogel was formulated via NNMBA crosslinker for wound dressings for better wound healing [128]. A graphene oxide incorporated sterculia gum-poly hydrogels were designed by encapsulating a vancomycin antibiotic drug and crosslinking through NNMBA for colon-specific drug delivery [129]. The sterculia gum and alginate polysaccharides were explored to form hydrogel dressing by radiation method for brain drug delivery [130]. A pH-sensitive hydrogel was formed composed of gum ghatti-clpoly(acrylic acid) using an NNMBA crosslinker for sodium diclofenac drug release [131]. A calcium-free phosphate approach was developed to enhance the formation of bone-like apatite within phosphate cross-linked guar gum-based hydrogels FRP of

acrylamide monomer and bis[2-methacryloyloxy] ethyl phosphate as a cross-linker for bone tissue engineering applications [132]. A hydrogel was fabricated based on biopolymers chitosan and guar gum using glutaraldehyde crosslinker for sustained release of a commonly used orally prescribed analgesic, paracetamol [133]. A gellan gum-based magnetic double network hydrogel nanocomposite was formulated using different crosslinkers Fe<sup>2+</sup>/Fe<sup>3+</sup> and an NNMBA for drug delivery applications [134]. A pH-responsive, semi-IPN polymer hydrogel was designed based on tamarind gumco-poly(acrylamidoglycolic acid) polymers that were synthesized using simple FRP in the presence of bis [2-(methacryloyloxy)ethyl] phosphate as a crosslinker and potassium persulphate as an initiator for drug delivery applications [135]. A guar gumg-poly(N-acryloyl-L-phenyl alanine) based pH responsive smart hydrogels were prepared using a single-step radical polymerization reaction using an NNMBA as a crosslinker and potassium persulphate as an initiator for in-vitro anticancer drug delivery [136]. Superabsorbent hybrid hydrogel compositions prepared from xanthan gum, sodium carboxymethylcellulose, and graphene oxide were synthesized by ebeam radiation crosslinking for biomedical engineering [137]. A water-soluble and photo-polymerizable hydrogel was designed using guar gum-methacrylate for tissue engineering [138]. Self-crosslinked chitosan with xanthan interpenetrated hypromellose hydrogels was developed through Schiff base crosslinking for the controlled delivery of ampicillin, minocycline, and rifampicin [139]. Tyramine conjugated tragacanth gum-based hydrogel was prepared by electron beam irradiation for biomedical application [140]. A pH-sensitive cationic guar gum/poly (acrylic acid) polyelectrolyte-based hydrogel was synthesized by photo-initiated FRP for drug delivery applications [141]. Polyethylene glycol and xanthan-gum-based

interpenetrating network hydrogel were designed via FRP using acrylic acid as a monomer in the presence of ammonium peroxy disulfate /sodium hydrogen sulfite as initiators and ethylene glycol dimethacrylate as a crosslinker for drug release applications [142]. A biodegradable hydrogel composite composed of gum ghatti-copoly(acrylic acid-aniline) was prepared through GP in the presence of an NNMBA and ammonium persulphate as a crosslinker-initiator system in aqueous solution for drug releases systems [143]. A tragacanth gum-based pH-responsive hydrogel was formulated using FRP and NNMBA crosslinker for drug delivery systems [144]. An NNMBA crosslinked hydrogel was synthesized using a karaya gum starch hybrid backbone and grafted with polyacrylic acid for drug delivery applications [145]. A hybrid dressing consisting of silk fibroin /polyvinyl alcohol nanofibers and sodium alginate /gum tragacanth hydrogel incorporating cardamom extract as an antibacterial agent was prepared using glutaraldehyde crosslinker for drug release systems [146]. A semi-IPN and IPN hydrogel were fabricated and composed of plant gum exudate of Boswellia serrate, polyacrylamide, and polyacrylic acid using γ-radiation or nanocomposite scaffolds [147]. A dual-function hydrogel system was designed based on a guar gum and sodium borohydride containing silver nanoparticles for biomedical applications [148].

Table 2.1 Natural gum-based hydrogel using chemical crosslinks

Srl.	Natural gum	Method/crosslinker	Application	Reference
No				
1	Tragacanth	Solvent casting/citric acid	Wound	[66]
	gum	crosslinker	dressing	
2	Carboxymethyl	Solvent casting/citric acid	Wound healing	[67]
	cellulose	crosslinker		
3	Chia seed	Solvent casting/glycerol	Wound healing	[68]
		plasticizer		

4	Tragacanth	Michael addition	Wound healing	[69]
	gum		8	[ [ ]
5	Sterculia gum	GP/NNMBA crosslinker	Moxifloxacin release	[70]
6	Guar gum	Borate/diol bond	Propose for biomedical	[71]
			application	
7	Guar gum	GP/NaBH <sub>4</sub> reducing agent	5-fluorouracil drug release	[72]
8	Acacia gum	GP/NNMBA crosslinker	Gentamicin release	[73]
9	Carageenan gum	FRP/NNMBA	Wound healing	[74]
10	Guar gum	Thiol-ene photo click chemistry and photopolymerization	Tissue scaffold	[75]
11	Tragacanth gum	Electron beam irradiation	Propose for biomedical application	[76]
12	Sodium alginate	FRP/NNMBA	Wound healing	[77]
13	Chitosan	FRP/EDC and NHS crosslinker	Wound healing	[78]
14	Chitosan	GP/NNMBA and PEGDA	Wound healing	[79]
15	Sodium alginate	FRP/NNMBA	Adhesive for biomedical	[80]
16	Acacia gum	FRP/NNMBA	Moxifloxacin release	[81]
17	Guar gum	FRP/NNMBA	5-fluorouracil release	[82]
18	Guar gum	FRP/NNMBA	Propose for biomedical application	[83]
19	Guar gum	FRP/NNMBA	5-fluorouracil release	[84]
20	Gum arabic	Schiff base	Wound healing	[85]
21	Guar gum and	Covalent	Diclofenac	[86]
22	chitosan	bond/Tetraethylorthosilicate	sodium release	F071
22	Guar gum	Semi IPN/Polyurethane based crosslinker	Wound dressing	[87]
23	Acacia gum`	GP/NNMBA	Levofloxacin release	[88]
24	Tragacanth gum	GP/NNMBA	Wound healing	[89]

25	Locust bean	Microemulsion	Sodium	[90]
	gum	technique/Divinyl sulfone	diclofenac	
		crosslinker	release	50.15
26	Tragacanth gum	FRP/Glutaraldehyde crosslinker	Wound healing	[91]
27	Sterculia gum	GP/NNMBA crosslinker	Vancomycin release	[92]
28	Gum arabic	GP/NNMBA	Propose for biomedical application	[93]
29	Xanthan	Semi IPN/Polyurethane crosslinker	Wound healing	[94]
30	Guar gum and hyaluronic acid	Schiff base and photocrosslinking	Propose for biomedical application	[95]
31	Guar gum	Schiff base, Michael addition, and borate didiol bonds	Propose for biomedical application	[96]
32	Sterculia gum	Radiation-induced crosslinking	Gemcitabine release	[97]
33	Tragacanth gum	GP/NNMBA	Wound healing	[98]
34	Karaya gum	GP/NNMBA	Quercitin release	[99]
35	Arabic gum	Covalent crosslink/Epichlorohydrin crosslinker	Sulfadiazine release	[100]
36	Guar gum	Solution casting/sodium tripolyphosphate crosslinker	Ciprofloxacin delivery	[101]
37	Xanthan gum	Covalent crosslinks/Glutaraldehyde	Human skin cells	[102]
38	Sterculia gum	Gamma radiation	Tetracycline hydrochloride release	[103]
39	Almond gum	GP/NNMBA	Hydrocortisone release	[104]
40	Gum Acacia, tragacanth gum	NNMBA	Ceftriaxone release	[105]
41	Butea monosperama gum	Radiation-induced crosslinking	Curcumin release	[106]
42	Sterculia gum	GP/NNMBA	Wound dressing	[107]

43	Gum arabic	Schiff base	Rivastigmine release	[108]
44	Sterculia gum	Gamma radiation	Ciprofloxacin delivery	[109]
45	Acacia Senegal gum	Divinyl sulphone	Tissue engineering	[110]
46	Gum arabic	GP/NNMBA	Quercitin release	[111]
47	Tragacanth gum	GP/NNMBA	5-fluorouracil release	[112]
48	Guar gum	GP/NNMBA	Curcumin release	[113]
49	Tragacanth gum	GP/NNMBA	Cancer treatment	[114]
50	Tamarind gum	Covalent crosslink/ethyl phosphate crosslinker	5-fluorouracil release	[115]
51	Tragacanth gum and alginate gum	Radiation-induced crosslinking	Wound healing	[116]
52	Guar gum	Covalent bond/Tetraethyl orthosilicate	Wound healing	[117]
53	Xanthan gum	IPN/Sodium hydrogen sulfite	5-fluorouracil release	[118]
54	Gum arabic	Covalent crosslinks/Oxidized gum arabic crosslinker	Folic acid release	[119]
55	Guar gum and kappa-carrageenan	Covalent bond/Silane crosslinker	Release of Cephradine	[120]
56	Sterculia gum	Schiff base	Doxorubicin and gentamicin release	[121]
57	Tragacanth gum	Electron beam irradiation	Tissue engineering	[122]
58	Guar gum	Covalent bond/Glutaraldehyde	Ciprofloxacin release	[123]
59	Xanthan gum	Covalent bond/Tetraethyl orthosilicate	Tissue engineering	[124]
60	Sterculia gum	Radiation-induced crosslinking	Moxifloxacin hydrochloride release	[125]
61	Tragacanth gum	GP/NNMBA	Moxifloxacin hydrochloride release	[126]

62	Guar gum	Covalent crosslinks/Borax	Disposable	[127]
		crosslinker	hygiene products	
(2	C	CD/NINIMD A		[120]
63	Gum acacia	GP/NNMBA	Wound dressing	[128]
64	Stanaulia aum	GP/NNMBA		[120]
04	Sterculia gum	GP/INININIDA	Vancomycin release	[129]
65	Sterculia gum	Gamma radiation	Citicoline	[130]
	and alginate gum		release	
66	Gum Ghatti	GP/NNMBA	Sodium	[131]
			Diclofenac	
			release	
67	Guar gum	FRP/BMEP	Tissue	[132]
			engineering	
68	Guar gum	Schiff base/Glutaraldehyde	Paracetamol	[133]
		crosslinker	release	
69	Gellan gum	GP/NNMBA	Metformin	[134]
			Hydrochloride	
			release	
70	Tamarind gum	Semi IPN/NNMBA	Doxorubicin	[135]
			hydrochloride	
			release	540.67
71	Guar gum	FRP/NNMBA	Imatinib	[136]
			mesylate	
70	37 .1	T1 ( 1 ' 1' ('	release	[127]
72	Xanthan gum	Electron beam irradiation	Propose for	[137]
			biomedical	
73	Cuanaum	Photocrosslinker	engineering Tissue	F1201
/3	Guar gum	Photocrossinker		[138]
74	Xanthan gum	Schiff base	engineering Propose for	[139]
/ <b>-</b>	Zianinan gum	Semin base	biomedical	[137]
			engineering	
75	Tragacanth	Electron beam irradiation	Propose for	[140]
, 5	gum		biomedical	[]
			engineering	
76	Alginate gum	Covalent	Bovine serum	[149]
		crosslink/Glutaraldehyde	albumin release	
		crosslinker		
77	Guar gum	Photoinitiator	Ketoprofen	[141]
			release	
78	Guar gum	Covalent	Ciprofloxacin	[150]
		crosslink/Glutaraldehyde	release	
		crosslinker		

79	Guar gum	IPN/Ethylene glycol dimethyl acrylate crosslinker	Venlafaxine release	[142]
80	Gum Ghatti	GP/NNMBA	Amoxicillin trihydrate release	[143]
81	Tragacanth gum	FRP/NNMBA	Amoxicillin release	[144]
82	Karaya gum	GP/NNMBA	Paracetamol and aspiri release	[145]
83	Sodium alginate and tragacanth gum	Glutaraldehyde crosslinker	Wound healing and tissue engineering	[146]
84	Boswellia serrate gum	Gamma radiation/NNMBA	Scaffolds	[147]
85	Guar gum	Covalent crosslinks/Sodium borohydrate crosslinker	Propose for biomedical applications	[148]

He *et al.* synthesized a biodegradable, antibacterial alginate/carboxymethyl chitosan/kangfuxin sponges via a green crosslinking method for promoting blood coagulation and full-thickness in wound healing application [151]. Gao *et al.* fabricated a hydrogen-bonded curdlan-chitosan/polyvinyl alcohol edible dual-functional hydrogel bandage that promotes wound healing [152]. Mohammadbagher Heydari and coworkers prepared a two-layer nanofibers-hydrogel using tragacanth gum lavender extract mupirocin through an electrospinning technique as a wound dressing [153]. A bio-inspired alginate gum with gum arabic hydrogel with micro-/nanoscale structures was synthesized via ionic interaction for controlled drug release in chronic wound healing [154]. Sharma *et al.* fabricated a polyvinyl alcohol/chitosan/pectin hydrogel loaded with green-synthesized nanometals via a physical crosslinking mechanism to release ciprofloxacin [155]. Jahan *et al.* fabricated a hybrid hydrogel using methacrylate gellan gum and gelatin crosslinked through UV

radiation for wound healing applications [156]. A bilayer wound dressing was synthesized, composed of asymmetric polycaprolactone membrane and chitosancarrageenan hydrogel to release storax balsam in wound healing applications [157]. electrospinning/3D printing drug-loaded antibacterial polycaprolactone An nanofibers/sodium alginate gelatin hydrogel bilayer scaffold was designed for skin wound repair [158]. A pH-sensitive super porous hydrogel was designed by blending two natural polysaccharides, opuntia mucilage, and carrageenan, using microwave irradiation for drug release and tissue scaffolds [159]. Marjan Ghorbani developed a honey-loaded ethyl cellulose/gum tragacanth nanofibers hydrogel through physical crosslinking for wound dressing material [160]. Li et al. synthesized a guar gum-based supramolecular hydrogel via sol-gel transition, which may be utilized for biomedical applications [71]. Islam M. Adel and colleagues fabricated a gellan gum-based bipolymeric hydrogel scaffold for rosuvastatin calcium release in wound healing applications [161]. A gellan gum-hyaluronic acid spongy-like hydrogel was synthesized for tissue engineering applications [162]. Shu et al. synthesized flexible hydrogels based on carboxymethyl guar gum and polyacrylic acid crosslinked via chemical, physical, and ionic interaction for ultra-highly sensitive and reliable strain and pressure sensors in biomedical applications [163]. A similar study was conducted by Qiankun Zeng and researchers in which a food gum hydrogel was synthesized using konjac glucomannan and xanthan gum for wound healing applications [164]. Davydova et al. developed a physically crosslinked hydrogel derived from alginate and pectin for wound healing applications [165]. A hydrogel of sodium alginate, gelatin, and silver nanoparticles crosslinked through electrostatic interaction and hydrogen bonding to heal cutaneous lesions [166]. Huang et al. fabricated a conductive hydrogel using sodium hyaluronate, tea tree oil, and wellan gum via sol-gel transition for wound dressing application [167]. Zhang et al. synthesized a hydrogel using gum arabic and pectin through ionic interaction for wound healing applications [168]. A hydrogel was synthesized using sulfated zwitterionic poly sulfobetaine methacrylate and κ-carrageenan network via physical crosslinks to promote wound healing applications [74]. Sun et al. developed an adhesive hydrogel comprised of sodium alginate, gum arabic, and calcium ions for wound healing applications [169]. A supramolecular chitin-based hydrogel with self-adapting properties was synthesized through host-guest interaction for wound healing [170]. Iqbal et al. fabricated a hydrogel using chitosan and guar gum-based ternary blends with polyvinyl alcohol for drug release application [171]. A thermo-reversible self-assembled gellan gum hydrogel was synthesized using green chemistry through physical crosslinks containing amino acid bio gelators for biomedical application [172]. An acrylamideco-butyl acrylate/xanthan gum-based hydrophobically associated conductive hydrogel was designed via a dual crosslinking mechanism for wound healing application [173]. Muktar et al. synthesized a hydrogel using gellan gum and virgin coconut oil through physical crosslinking for wound healing applications [174]. Alginate and gum arabicbased biomimetic hydrogel was synthesized through ionic interaction, which improves diabetic wound regeneration [175]. A dual cross-linked gellan gum and gelatin-based multifunctional nanocomposite hydrogel were developed via ionic and coupling reaction (1-ethyl-3-(3-dimethyl aminopropyl) carbodiimide and Nhydroxysulfosuccinimide) mechanism for wound healing application [176]. Mohammad Mahfuz Ali Khan Shawan and colleagues synthesized a hydrogel using xanthan gum and gelation via hydrogel bonding for wound healing applications [177].

A hydrogel based on low-methoxyl amidated citrus pectin and flaxseed gum formulated with tripeptide glycyl-L-histidyl-L-lysine using ionic interaction to improve wound healing [178]. Mahmood et al. synthesized hydrogel films using ofloxacin with tea tree or lavender oil in gellan gum by solvent casting ionotropic gelation method as wound dressing [179]. A composite polysaccharide hydrogel was synthesized from fenugreek gum and cellulose through hydrogen bonding for wound healing applications [180]. A group of researchers synthesized guar gum-based hydrogel wound patches with antibacterial silver nanoparticles and antioxidant epigallocatechin gallate through a coordination bond, showing fast wound closure with synergistic interaction without any inherent toxicity [181]. Deng et al. developed a composite hydrogel based on cellulose and flaxseed gum by hydrogen bonding for wound healing applications [182]. An interpenetrating network of hydrogel consisting of gellan gum and polyacrylamide was synthesized by chemical crosslinking and Mg<sup>2+</sup> ion immersion techniques for wound healing applications [183]. A xanthan gum and konjac glucomannan blend hydrogel was synthesized without using a chemical crosslinker; instead, temperature was used to crosslink for wound healing [184]. A catechol-functionalized hydrogel was developed based on multiple hydrogen bonds and  $\pi$ - $\pi$  stacking using dopamine-modified dialdehyde carboxymethyl cellulose and polyacrylic acid for wound healing applications [185]. An in-air microfluidics system was developed to generate hydrogel particles based on sodium alginate solution using calcium chloride (CaCl<sub>2</sub>) as a crosslinker and ethyl alcohol for wound healing applications [186]. A hydrogel was synthesized based on collagen, chitosan, and hyaluronic acid using 4% paraformaldehyde as a crosslinker to provide soft and flexible 3D networks mimicking the extracellular matrix of natural tissues [187]. A facile, green synthesis methodology was used to synthesize hydrogels combined with zinc oxide nanoparticles using three polysaccharide gums (acacia gum, guar gum, and xanthan gum) for wound healing applications [188]. An acacia gum nano compositebased hydrogels were synthesized via water-in-oil micro-emulsion polymerization technique for drug delivery applications [189]. A natural polymer-based hydrogel was fabricated by combining gellan gum and acacia gum using zinc chloride (ZnCl<sub>2</sub>) as a crosslinking agent for biomedical applications [190]. A gellan gum-hydroxyapatite composite spongy-like hydrogel was synthesized using a CaCl2 crosslinker for bone tissue engineering [191]. A natural sundew hydrogel was developed using sodium alginate and gum arabic with a calcium ion-mediated cross-linking mechanism for controlled drug release in chronic wound healing applications [192]. A physically crosslinked hydrogel was fabricated and characterized based on Persian gum loaded with gentamicin for drug delivery application [193]. A double network-based hydrogel was developed based on gellan gum and gelatin through electrostatic interaction for electronic devices in biomedical applications [194]. An ultra-stretchable and selfhealing crosslinked poly (ethylene oxide)-cationic guar gum hydrogel was developed through a borax crosslinker for tissue engineering, drug delivery, or food storage applications [195]. An interpenetrating network hydrogel composed of locust bean gum and cellulose microfibrils was designed using a CaCl<sub>2</sub> crosslinker as bio-inks for 3D printing applications [196]. A degradable and pH-responsive chitosan/guar gum/polyvinyl alcohol blended hydrogel was designed through a tetra ethoxy silane crosslinker for wound dressing applications [197]. A hydrogel fabricated by freeze/thaw technique composed of polyvinyl alcohol and xanthan gum for potential application in soft tissue engineering [198]. A hydrogel of N-trimethyl chitosan/sodium carboxymethyl xanthan gum was prepared using an ionic crosslinking mechanism for drug delivery application [199]. A magnetic nanocomposite natural hydrogel based on pectin, tragacanth gum, silk fibroin, and integrated graphitic carbon nitride was fabricated using CaCl<sub>2</sub> crosslinker to treat hyperthermia [200]. A physical crosslinked polyvinyl alcohol/acacia gum hydrogel hybrid film was developed with drug delivery ability in wound dressing applications [201]. A guar gum and carrageenan-based hydrogel was prepared using a borax crosslinker for biomedical applications [202]. A gellan gum and retrograded starch blend hydrogel were designed through a dual crosslinking mechanism for drug delivery applications [203]. A highstrength composite hydrogel was fabricated based on chitosan and basil seed gum with the assistance of gallic acid as a cross-linking agent for tissue engineering applications [204]. A κ-carrageenan/polyacrylamide hydrogel was developed through a dual physical-cross-linking strategy for biomedical applications [205]. A Bi<sub>2</sub>S<sub>3</sub>-embedded gellan gum hydrogel was developed through a one-pot synthesis method for localized tumor photothermal/antiangiogenic therapy [206]. The polymeric hydrogels were synthesized by employing FRP using graft copolymer, 2-acrylamido-2-methyl-1propanesulfonic acid, and 2-hydroxy ethyl acrylate from N-acryloyl-L-phenylalanine and guar gum for drug delivery applications [207]. A xanthan gum-based hydrogel was synthesized using sol-gel conversion by UV irradiation in the presence of sodium lactate via an ion-induced crosslinking mechanism for biomedical applications as sensors [208]. A carboxymethyl tamarind gum-polyvinyl alcohol-based hydrogel film was prepared using citric acid as a crosslinker by solvent casting technique for wound healing applications [209]. The hydrogels were formulated based on pectin and brea gum using the ionic crosslinking mechanism for drug release application [210].

Electroactive nanocomposite hydrogels were prepared by encapsulating green-synthesized polypyrrole colloids within bioamine-crosslinked gellan gum networks by an emulsion polymerization method via an ionotropic crosslinking mechanism for drug release applications [211]. An ionic crosslinking mechanism prepared a gellan gum, kappa-carrageenan, and alginate gum-based hydrogel for ocular safety and eye surface permanence determination [212]. A pH-sensitive microbead hydrogel was synthesized from sodium alginate and modified karaya gum by GP using 2-hydroxyethyl methacrylate through *in situ* FRP via simple ionotropic gelation technique for controlled release of D-penicillamine drug [213].

**Table 2.2** Natural gum-based hydrogel using physical crosslinks

Srl. No	Natural gum	Method	Application	Reference
1	Alginate and carboxymethyl chitosan	Electrostatic interaction and freeze-drying	Wound healing	[151]
2	Chitosan	Hydrogen bonding	Bandages	[152]
3	Tragacanth gum	Hydrogen bonding	Wound dressing	[153]
4	Alginate gum and gum arabic	Ionic interaction	Mitsugumin 53 release	[154]
5	Chitosan	Freeze-thaw	Ciprofloxacin release	[155]
6	Gellan gum	UV irradiation	Wound healing	[156]
7	Carrageenan	Ionic interaction	Storax release	[157]
8	Alginate and gellan gum	ionic interaction	Amoxicillin release	[158]
9	Kappa- carrageenan	H-bonding	Ciprofloxacin release	[159]
10	Tragacanth gum	Electrospinning/H-bonding	Nanofibers for wound dressing	[160]
11	Gellan gum	Hydrogel bonding, ionic interaction	Rosuvastatin calcium release	[161]

12	Gellan gum and	ionic cross-linking	Tissue	[162]
13	hyaluronic acid	coordination bonds,	engineering Strain sensors	[163]
13	Guar gum	hydrogen bonds, and	Strain sensors	[103]
		ionic interaction		
14	Chitosan	FRP and freeze-thawing	Wound dressing	[214]
15	Konjac	H-bonding	Wound healing	[164]
	glucomannan and			
16	xanthan gum Alginate	Hydrogen bonding	Wound healing	[165]
17		Electrostatic interaction	Wound healing	
	Sodium alginate			[166]
18	Sodium hyaluronatre and	Hydrogen-bonding	Wound dressing	[167]
	wellan gum			
19	Gum arabic	Ionic interaction	Wound healing	[168]
20	Sodium alginate,	Ionic interaction	Wound healing	[169]
21	gum arabic	II	XX7 11 1'	[170]
21	Chitin	Host-guest interaction	Wound healing	[170]
22	Guar gum and chitosan	Hydrogen-bonding	Wound healing	[171]
23	Gellan gum	Ionic interaction	Wound healing	[172]
24	Xanthan gum	Hydrogen bonding and	Wound healing	[173]
25	C 11	ionic interaction	XX7 11 1'	F1.7.43
25	Gellan gum	Hydrogen-bonding	Wound healing	[174]
26	Alginate gum and Gum arabic	Ionic interaction	Wound healing	[175]
27	Gellan gum	Ionic interaction	Wound healing	[176]
28	Xanthan gum	Hydrogen bonding	Wound healing	[177]
29	Flaxseed gum	Ionic interaction	Wound healing	[178]
30	Gellan gum	Solvent casting/CaCl <sub>2</sub> crosslinker	Ofloxacin release	[179]
31	Fenugreek gum	Hydrogen-bonding	Wound healing	[180]
32	Guar gum	Coordination bond	Wound patch	[181]
33	Flaxseed gum	Hydrogen bonding	Wound healing	[182]
34	Gellan gum	Ionic interaction	Wound healing	[183]
35	Xanthan gum and Konjac glucomannan	Temperature stimuli	Wound healing	[184]

36	Carboxymethyl chitosan	Hydrogen bonds $\pi$ – $\pi$ stacking	Wound healing	[185]
37	Sodium alginate	Ionic crosslinking/CaCl <sub>2</sub>	Wound healing	[186]
		crosslinker		
38	Chitosan, hyaluronic acid	Coordinate bond	Wound healing	[187]
39	Acacia gum, guar gum, xanthan gum	Hydrophobic interaction	Wound healing	[188]
40	Acacia gum	Hydrophobic interaction	Propose for biomedical application	[189]
41	Gellan gum and acacia gum	Ionic interaction/ZnCl <sub>2</sub> crosslinker	Tissue engineering	[190]
42	Gellan gum	Ionic interaction/CaCl <sub>2</sub> crosslinker	Wound healing	[191]
43	Sodium alginate and gum arabic	Ionic interaction	Wound healing	[192]
44	Persian gum	Physical crosslinking	Gentamicin release	[193]
45	Gellan gum	Electrostatic interaction	Electronic devices for biomedical	[194]
46	Guar gum	Ionic crosslinker/Borax crosslinker	Propose for biomedical application	[195]
47	Locust bean gum	Ionic crosslinking/CaCl <sub>2</sub>	Bio inks	[196]
48	Guar gum	Ionic crosslinking/CaCl <sub>2</sub>	Wound dressing	[197]
49	Xanthan gum	Freeze-thaw	Tissue engineering	[198]
50	Xanthan gum	Ionic crosslinking	Ciprofloxacin release	[199]
51	Tragacanth gum	CaCl <sub>2</sub> crosslinker	Used in magnetic hyperthermia	[200]
52	Acacia gum	Hydrogen-bonding	Erythromycin release	[201]
53	Guar gum and carrageenan	Ionic interaction/Borax crosslinker	Electronic sensors in biomedical	[202]
54	Gellan gum	Ionic crosslinking	Ketoprofen release	[203]
55	Basil seed gum and chitosan	H-bonding/Gallic acid crosslinker	Tissue engineering	[204]

56	Kappa carrageenan	Ionic interaction and hydrophobic interaction	Propose for biomedical engineering	[205]
57	Gellan gum	Ionic interaction	Tumor treatment	[206]
58	Guar gum	Electrostatic interaction/NNMBA	Wound healing	[207]
59	Xanthan gum	Ion induced crosslinking	Propose for biomedical engineering	[208]
60	Tamarind gum	Solvent casting/Citric acid crosslinker	Moxifloxacin release	[209]
61	Brea gum	Ionic crosslinking	Methoxyl Pectin release	[210]
62	Gellan gum	Ionic crosslinking	Ibuprofen release	[211]
63	Gellan gum, kappa carrageenan, and sodium alginate	Ionic crosslinking	Eye surface permanence determination	[212]
64	Karaya gum sodium alginate	Ionic crosslinking	D-penicillamine release	[213]

A conductive, self-healing, and tough hydrogel was constructed by synergistic multiple interactions among montmorillonite, poly (acrylamide-co-acrylonitrile), xanthan gum, and ferric ion used for flexible conductive devices in tissue engineering application [215]. Khalaji *et al.* synthesized a hydrogel comprising carboxymethyl chitosan and oxidized alginate grafted catechol on a hydrophobic electrospun layer through Schiff base and coordination bond utilized as a skin substitute for infected burned wound healing [216]. A group of researchers developed a polysaccharide-based bio-adhesive hydrogel tape consisting of dual crosslinking of allyl cellulose and carboxymethyl chitosan for wound healing applications [217]. A binary blended hydrogel film was prepared composed of vanillin crosslinked chitosan /locust bean gum and then synthesized its complexes with Fe<sup>3+</sup>, Zn<sup>2+</sup> & Cu<sup>2+</sup> metal ions by solution casting method via Schiff base and metal ion bonding for biomedical applications

[218]. A tough, anti-fatigue, and stimuli-responsive hydrogel was prepared composed of gellan gum reinforced by flexible nanoparticulate polyurethane based on a dual physical hydrogen bonding and chemical photo-cured methacrylate network through fast and green solution mixing and the following photo-curing for drug delivery applications [219]. A highly stretchable, sensitive, and multifunctional polysaccharide-based dual-network hydrogel sensor was constructed using dialdehyde carboxymethyl cellulose, chitosan, poly(acrylic acid), and aluminum ions crosslink through Schiff base bonds and metal coordination mechanism for intelligent sensors, particularly for applications in wet and underwater environments [220]. Fungal mushroom-derived carboxymethyl chitosan-polydopamine-based hydrogels were derived through dynamic Schiff base cross-linking and hydrogen bonds with multifunctionality utilized as a wound dressing material for infected wounds [221]. A hydrogel was fabricated by gallic acid grafted chitosan and oxidized *Bletilla striata* polysaccharide as the scaffold formed by two types of dynamic crosslinking, i.e., Schiff base and pyrogallol-Fe<sup>3+</sup> utilized for wound treatment purposes [222].

**Table 2.3** Natural gum-based hydrogel using hybrid crosslinks

Srl. No	Natural gum	Method	Application	Reference
1	Xanthan gum	Hydrogen bonding, covalent bonding, ionic interactions	Tissue engineering	[215]
2	Alginate gum and carboxymethyl chitosan	Schiff base and coordination bond	Burn Wound healing	[216]
3	Xanthan gum	GP/Glutaraldehyde crosslinker	Wound dressing	[223]
4	Carboxymethyl chitosan	Hydrogen-bonding and covalent crosslinks	Wound healing	[217]

5	Chitosan and locust	Schiff base and	Wound [218]
	bean gum	Coordination crosslinks	healing
6	Gellan gum	Photocrosslinking and hydrogen bonding	Soft tissue [219] engineering
7	Chitosan	Schiff base and coordination bond	Sensor for human movements
8	Chitosan	Schiff base and Hydrogen-bond	Wound [221] healing
9	Chitosan	Schiff base and ionic interaction	Wound [222] healing

## 2.2 Injectable hydrogels and their application in the biomedical field

IHs are a subclass of hydrogels and, *in vivo*, are prepared by extruding through a syringe to a specific site and, under the influence of stimuli (pH, temperature, enzymes, light), transformed into a gel [224]. IHs, especially those derived from natural gums, have emerged as promising wound healing materials due to their unique properties, such as notable biocompatibility and tailored injectability, making them promising for various biomedical applications [225]. IHs offer distinct advantages over traditional hydrogels, such as being easy to handle, being used to fill irregular shapes, and not requiring a secondary dressing. Therapeutic agents are mixed with the precursors before injection and later entrapped in the hydrogel network. Transformation takes place either due to physical crosslinking or chemical crosslinking (Figure 2.2). Physical crosslinking involves hydrogen bonding, electrostatic interactions, van der Wall forces,  $\pi$ - $\pi$ , hydrophobic, and host-guest interactions. Chemical crosslinks include Diels Alder reaction, Michel addition, Schiff base reactions, enzyme mediation, and

photopolymerization [226]. Yu et al. fabricated a self-healing IH using oxidized quaternized guar gum and carboxymethyl chitosan via Schiff base crosslinks for wound dressing [227]. An anti-inflammatory IH was synthesized using tyramine-modified gellan gum and silk fibroin through enzymatic crosslinking (horseradish peroxidase) for the release of betamethasone in the treatment of rheumatoid arthritis

[228]. A bifunctional peptide, juxta membrane, was synthesized and grafted to

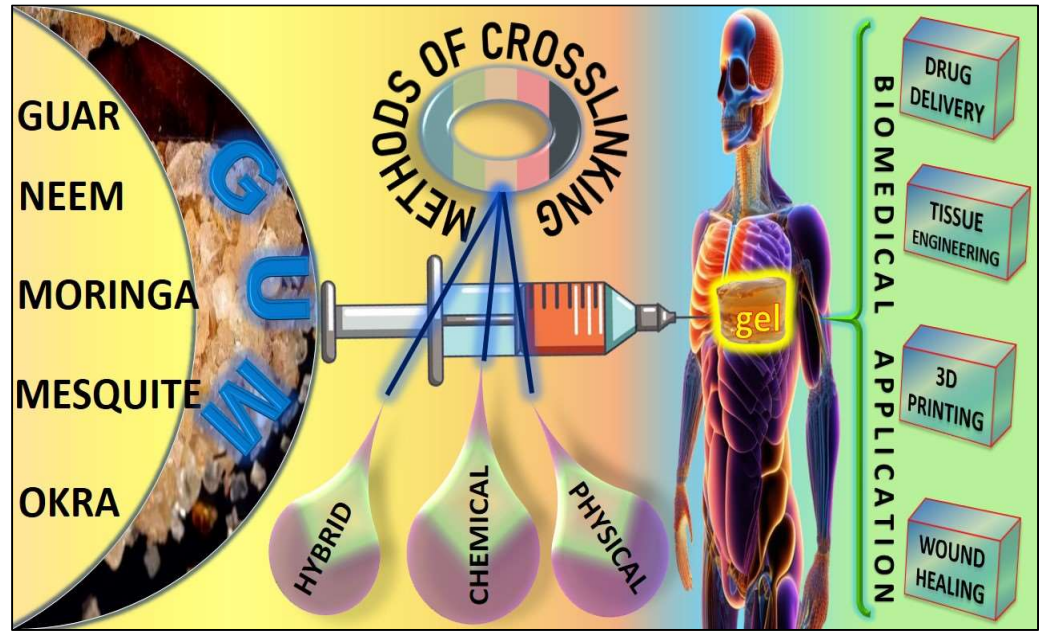


**Fig. 2.2** Pictorial representation of natural gum-based injectable hydrogel for biomedical applications.

hyaluronic acid through a photocrosslinker to generate a homogeneous bifunctional IH system, inhibiting tumor recurrence and enhancing wound healing [229]. A biodegradable high-strength IH was synthesized using poly(L-glutamic acid) and gellan gum via a step photo crosslinking mechanism for load-bearing tissue engineering applications [230]. A graphene oxide incorporated glycol chitosan and oxidized hyaluronic acid IH was developed using Schiff base crosslinks for tissue scaffold to treat bone defects [231]. Yikun Ren and colleagues developed an IH

crosslinked via amide linkage between the carboxylic group of hyaluronic acid and the amino group of tyramine to form the amide linkage, using the EDC/NHS-mediated coupling reaction and an amino group of quaternized chitosan and the carboxylic group of gallic acid to form the amide linkage, also using the EDC/NHS-mediated coupling reaction utilized for wound healing application [232]. An injectable chitosan-quince seed gum hydrogel encapsulated with curcumin-loaded-halloysite nanotubes was designed through Schiff base crosslinks for tissue engineering applications [233]. An IH was fabricated using N-carboxyethyl chitosan and oxidized hyaluronic acid using Schiff base crosslinks that improve bone regeneration and alveolar ridge promotion [234]. Pandit et al. synthesized an IH using N, O-carboxymethyl chitosan, and multialdehyde guar gum through Schiff base crosslinks for drug delivery applications [235]. A biocompatible and self-healing IH was fabricated using modified-β-chitin and alginate dialdehyde via Schiff base crosslinks for wound healing applications [236]. A self-healing IH was prepared by crosslinking two natural polysaccharides, carboxymethyl chitosan, and oxidized konjac glucomannan, based on the Schiff base bond loaded with exosomes and berberine for infected wound healing [237]. A selfhealing collagen-based was developed based on dynamic imine linkages between collagen and dialdehyde guar gum and diol-borate ester bonds between guar gum and borax for wound dressing application [238]. A pH and glucose dual-responsive IH was prepared through the cross-linking of Schiff's base and phenylboronate ester using phenylboronic-modified chitosan, poly(vinyl alcohol) and benzaldehyde-capped poly-(ethylene glycol) for diabetic wound healing [239]. A self-healing, injectable, and pHresponsive hydrogel was synthesized by N-carboxyethyl chitosan, hyaluronic acidaldehyde, and adipic acid dihydrazide through the formation of the reversible dynamic

bonds, acyl hydrazone, and imine bonds used as a bioactive dressing for enhancing diabetic wound healing [240]. Parinaz Nezhad-Mokhtari and coworkers fabricated a covalent crosslinked IH scaffold using oxidized guar gum incorporated with curcuminloaded zein nanoparticles to improve biological performance for wound healing applications [241]. Ruquan Zhang and colleagues developed a xanthan gum and silk fibroin-based IH using sodium trimetaphosphate as a crosslinker for drug release applications [242]. An injectable, shear-thinning, and self-healing hydrogel based on DNA, oxidized alginate, and silicate nanoparticles was fabricated through Schiff base crosslinks for the sustained delivery of simvastatin [243]. An aldehyde-functionalized hyaluronic acid and cysteine-capped ethylenediamine IH was formed through reversible hemithioacetal crosslinking based on thiazolidine chemistry to be applied as a general coupling for biomedical applications [244]. A hyaluronic acid and chitosan composite functionalized IH was synthesized using enzyme-catalyzed and Schiff base reaction to promote wound healing applications [245]. Amino groups in ε-polylysine undergo dynamic Schiff base reaction crosslinking with oxidized hyaluronic acid, and F-127 exhibits unique temperature sensitivity to form an injectable thermosensitive hydrogel, which was used to cover the wound at body temperature [246]. A bioinspired self-healing injectable nanocomposite hydrogel was developed based on oxidized dextran and gelatin by Schiff base cross-linking between dopamine-modified gelatin and oxidized dextran for bone regeneration [247]. The IH was designed with the natural macromolecular of the gallic acid-grafted quaternized chitosan and oxidized hyaluronic acid via Schiff base and Michael addition reaction for wound healing applications [248]. An injectable and self-healing hydrogel comprising of collagen, chitosan, and oxidation-modified konjac glucomannan, which acts

macromolecular cross-linker to construct dynamic Schiff-base bonds, was smartly designed for regenerative repairment of infected wounds [249]. An IH was developed by grafting dopamine onto hyaluronic acid and mixing it with carboxymethyl chitosan solution through a reversible Schiff base reaction for tissue adhesive material [250]. A Schiff base crosslinked IH was designed composed of carboxymethyl chitosan and oxidized konjac glucomannan through the Schiff base bond for tissue engineering and wound healing [251]. The dynamic Schiff-base reaction developed a biomultifunctional melatonin-loaded carboxymethyl chitosan and poly aldehyde dextranbased IHs to potentially manage periodontal diseases [252]. A polysaccharide-based IH was constructed consisting of a dynamic crosslinking network formed by the Schiff base and a covalent cross-linking network achieved by photo-initiated polymerization, offering a feasible way to tune the mechanical property of hydrogel after injection for skin repair applications [253]. An IH was constructed via a Schiff-base reaction of oxidized hyaluronic acid and carboxymethyl chitosan for bone repair applications [254]. An injectable multifunctional Schiff base cross-linked with gallic acid-modified chitosan and oxidized dextran hydrogels was rationally designed to accelerate wound healing [255]. An IH was developed using benzaldehyde-terminated polyethylene glycol crosslinked with hydroxypropyltrimethyl ammonium chloride chitosan via the Schiff base mechanism to promote diabetic wound healing [256]. An adhesive IH was developed using hydrazide-modified hyaluronic acid and-phthalaldehyde-terminated four-armed poly(ethylene glycol) via hydrazine linkage for sutureless wound closure [257]. An injectable, self-healing, transparent, and antibacterial hydrogel was fabricated based on quaternized chitosan and oxidized dextran crosslinked via the Schiff base mechanism used for wound dressings [258]. Sun et al. developed an IH

using oxidized konjac glucomannan, γ-poly(glutamic acid) modified with dopamine and L-cysteine and ε-polylysine by thiol-aldehyde addition and Schiff-base reactions to promote wound healing in burn wound infection [259]. An IH that comprises carboxymethyl chitosan and aldehyde functionalized alginate was developed, crosslinked through dynamic Schiff-base linkages for drug delivery to treat obesity [260]. An injectable nanocomposite was rationally designed as a sustained release platform for enhanced cartilage regeneration through the integration of a chitosanbased hydrogel, articular cartilage stem cells, and mesoporous SiO<sub>2</sub> nanoparticles loaded with anhydroicaritin via dynamic imine linkage for cartilage regeneration applications [261]. Schiff-base bonding was used to synthesize an IH based on polyaldehyde gum arabic and carboxymethyl chitosan for localized breast cancer treatment [262]. A biocompatible IH was designed based on amino-functionalized polyaspartamide crosslinked with naturally occurring dextran aldehyde via Schiff base mechanism for tissue adhesion applications [169]. An injectable adhesive dopamine functionalized oxidized hyaluronic acid and carboxymethyl chitosan collagen-based hydrogel was constructed via Schiff dynamic and ionic interaction for wound dressing [263]. A self-crosslinked IH was fabricated using oxidized alginate and carboxymethyl chitosan via Schiff base for dental enamel regeneration [264]. A facile one-pot approach was adopted to prepare a polysaccharide-based IH based on oxidized starch and chitosan via Schiff base crosslinks for drug release applications [265]. A selfhealing injectable nanocomposite hydrogels based on benzaldehyde-modified polyethylene glycol and chitosan, reinforced with graphene oxide via Schiff base crosslinking mechanism for the delivery of pomegranate extract for hard tissue engineering [266]. A carboxymethyl cellulose and chitosan hydrogel doped with

graphene oxide IH was developed through acylhydrazone bonds utilized for drug delivery [267]. A natural polysaccharide-based IH was designed using gellan gum and polyethylene glycol dimethacrylate using UV radiation for wound healing applications [268]. A gellan gum methacrylate-based polymer was used to fabricate injectable and photocrosslinkable hydrogels crosslinked through UV radiation utilized as innovative wound dressing material [269]. A photocrosslinkable, IH was designed and composed of locust bean gum and methacrylate, which was utilized for minimal invasive cartilage repair [270]. A biodegradable, high-strength, and IH was developed by one-step photocrosslinking of two bio macromolecules, polyethylene glycol acrylate poly(lglutamic acid) and methacrylate gellan gum used in load-bearing tissue regeneration [271]. A self-healing IH was synthesized composed of multialdehyde gum arabic and succinic anhydride chitosan via Schiff base crosslinks for anticancer drug delivery [272]. A degradable polysaccharide-based IH was formulated composed of carboxymethyl chitosan and oxidized alginate, doubly integrated with hydroxyapatite nanoparticles and calcium carbonate microspheres under physiological conditions through Schiff base mechanism for drug delivery and bone tissue engineering applications [273]. An injectable, self-healing, and biocompatible hydrogel was formulated based on N, O-carboxymethyl chitosan, and multialdehyde guar gum via Schiff base crosslinks for sustained anticancer drug delivery [274]. A self-healing and injectable polysaccharide-based hydrogel was prepared based on carboxymethyl chitosan and calcium pre-cross-linked oxidized gellan gum cross-linked by the Schiffbase reaction for bone tissue engineering [275]. An injectable, self-healable, and adhesive hydrogel was prepared using oxidized succinoglycan and chitosan using Schiff base crosslinks for pH-responsive drug delivery applications [276]. Curcuminloaded mesoporous polydopamine nanoparticles and metformin were introduced into the polymer matrix formed by the dynamic imine bonds and electrostatic interactions between carboxymethyl chitosan and oxidized hyaluronic acid to fabricate IHs for drug delivery applications [277]. A polysaccharide-based IH was prepared via Schiff base crosslinking of aldehyde-modified xanthan and carboxymethyl-modified chitosan for local drug delivery [278]. A covalently cross-linked composite chitosan-alginate hydrogel was prepared, possessing pH sensitivity to degradation for drug delivery [279]. A biocompatible and self-healing IH was designed based on modified-β-chitin and alginate for wound healing applications [280].

**Table 2.4** Natural gum-based injectable hydrogel using chemical crosslinks for biomedical applications

Srl. No.	Natural gum	Method	Application	Reference
1	Guar gum	Schiff base	Wound dressing	[227]
2	Gellan gum	Enzymatic crosslinking	Si RNA release	[228]
3	Hyaluronic Acid	Photocrosslinker	Wound healing	[229]
4	Gellan gum	Photocrosslinker	Tissue engineering	[230]
5	Hyaluronic acid	Schiff base crosslinking	Bone tissue engineering	[231]
6	Hyaluronic acid	Amide linkage	Wound healing	[232]
7	Quince seed gum	Schiff base crosslinking	Tissue engineering	[233]
8	Hyaluronic acid	Schiff base crosslinking	Bone regeneration	[234]
9	Guar gum	Schiff base crosslinking	Doxorubicin release	[235]

10	Sodium alginate	Schiff base crosslinking	Wound healing	[236]
11	Konjac glucomannan	Schiff base crosslinking	Wound healing	[237]
12	Guar gum	Schiff base and diolester bond	Wound dressing	[238]
13	Chitosan	Schiff base and phenyl boronate ester	Diabetic wound healing	[239]
14	Hyaluronic acid	Acylhydrazone and imine bond	Wound healing	[240]
15	Hyaluronic acid	Photocrosslinker	Tissue engineering	[281]
16	Guar gum	Hemiacetal bond	Curcumin release	[241]
17	Xanthan gum	Covalent crosslinks/sodium trimetaphosphate crosslinker	Bovine serum albumin release	[242]
18	Alginate	Schiff base crosslinking	Simvastatin release	[243]
19	Hyaluronic acid	Thiazolidine chemistry	Wound healing	[244]
20	Hyaluronic acid	Enzyme catalyzed and Schiff base	Wound healing	[245]
21	Hyaluronic acid	Schiff base crosslinking	Wound healing	[246]
22	Dextran	Schiff base crosslinking	Bone regeneration	[247]
23	Hyaluronic acid	Schiff base and Michael addition	Wound healing	[248]
24	Konjac glucomannan	Schiff base crosslinking	Wound healing	[249]
25	Hyaluronic acid	Schiff base crosslinking	Tissue adhesive material	[250]
26	Konjac glucomannan	Schiff base crosslinking	Tissue engineering	[251]

27	Dextran	Schiff base crosslinking	Treatment of periodontal diseases	[252]
28	Chitosan	Schiff base crosslinking	Skin repair	[253]
29	Hyaluronic acid	Schiff base crosslinking	Bore repair	[254]
30	Chitosan and dextran	Schiff base crosslinking	Wound healing	[255]
31	Chitosan	Schiff base crosslinking	Wound healing	[256]
32	Hyaluronic acid	Hydrazone linkage	Wound healing	[257]
33	Dextran	Schiff base crosslinking	Wound dressing	[258]
34	Konjac glucomannan	Schiff base and thiol aldehyde addition	Burn wound healing	[259]
35	Sodium alginate	Schiff base crosslinking	Treatment of obesity	[260]
36	Chitosan	Schiff base crosslinking	Cartilage regeneration	[261]
37	Gum arabic	Schiff base crosslinking	Cancer treatment	[262]
38	Dextran	Schiff base crosslinking	Tissue adhesion	[169]
39	hyaluronic acid	Schiff base crosslinking	Wound dressing	[263]
40	Sodium alginate	Schiff base crosslinking	Dental enamel regeneration	[264]
41	Chitosan	Schiff base crosslinking	Ampicillin sodium salt drug delivery	[265]
42	Chitosan	Schiff base crosslinking	Tissue engineering	[266]
43	Chitosan	Acylhydrazone	5-fluorouracil release	[267]
44	Guar gum	UV radiation	Wound healing	[268]
45	Gellan gum	UV radiation	Wound dressing	[269]
46	Locust bean gum	UV radiation	Cartilage repair	[270]

47	Gellan gum	Photocrosslinking	Tissue engineering	[271]
48	Guar gum	Schiff base crosslinking	Nanocurcumin release	[272]
49	Alginate gum	Schiff base crosslinking	Tetracycline hydrochloride release	[273]
50	Guar gum	Schiff base crosslinking	Doxorubicin release	[274]
51	Gellan gum	Schiff base crosslinking	Bone tissue engineering	[275]
52	Chitosan	Schiff base crosslinking	5-fluorouracil release	[276]
53	Hyaluronic acid	Schiff base crosslinking	Wound healing	[277]
54	Xanthan gum	Schiff base crosslinking	Tissue scaffolds	[278]
55	Alginate gum and chitosan	Schiff base crosslinking	5-fluorouracil release	[279]
56	Alginate gum	Schiff base crosslinking	Wound healing	[280]

Syed Ahmed Shah and researchers synthesized a curcumin-loaded IH using hyaluronic acid and pollulan through physical interaction and self-assembly mechanism for diabetic wound repair application [282]. Yueyuan Zheng and colleagues synthesized an IH using gellan gum and gelatin via physical crosslinks for wound dressing application [283]. Heparin and glycerol functionalized chitosan-based IH was fabricated using pH and temperature as a stimulus for wound healing application [284]. A curcumin-laden chondroitin sulfate grafted alginate-based thermoreversible IH was fabricated using the solvent casting method for potential use in drug delivery applications [285]. Monireh Kouhia and coworkers synthesized IH using gellan gum/lignocellulose nanofibrils enriched with melatonin-loaded forsterite nanoparticles

through ionic interaction used for cartilage tissue engineering [286]. A pH and thermosensitive IH was developed based on chitosan and hydroxyapatite composite materials loaded with heparin through sol-gel transition for drug delivery in bone regeneration [287]. A natural melanin and alginate-based IH was fabricated through a divalent cation crosslinking mechanism for cardiac repair [288]. Xu et al. developed an IH using gellan gum, chlorhexidine, and nano-hydroxyapatite through a coordination bond for enabling osteogenesis and inhibiting Enterococcus faecalis [289]. A gellan gum and collagen interpenetrating network IH was synthesized using magnesium chloride as a crosslinker for burn wound therapy [290]. An injectable, biocompatible, self-healable, and conductive material was developed using poly(3,4ethylenedioxythiophene), poly(styrenesulfonate), and guar gum through hydrogen bonding utilized as dressing for wound healing application [291]. Xie et al. developed an IH based on alginate loaded with minocycline through ionic interaction for bacteriainfected wound healing applications [292]. A uniform-unsaturated crosslinking strategy was designed to construct IH using sodium alginate and metal ions through coordination bonds for biomedical applications [293]. An IH was fabricated based on chitosan and cyclodextrin for local delivery of cinnamaldehyde in diabetic foot ulcers [294]. A guar gum-based supramolecular IH was developed by forming borate/didiol bonds for biomedical applications [295]. An injectable gellan gum /silk sericin hydrogel was fabricated via CaCl2 crosslinker as a cell carrier for cell delivery in retina tissue engineering [296]. A novel hydrogen-bonded polysaccharide IH consisting only of cationic guar gum and CuCl<sub>2</sub> was developed by mixing guar gum and Cu<sup>2+</sup> solution for tissue regeneration [297]. An injectable biocompatible natural guar gum-based hydrogel was developed via a facile and green method using CaCl<sub>2</sub> crosslinker to treat bone defects [298]. A chondroitin sulfate grafted alginate-based thermoreversible IH was designed using sol-gel transition via CaCl<sub>2</sub> crosslinker for drug delivery and accelerated diabetic wound healing [299]. A hear-sensitive IH was formulated composed of tragacanthic acid cross-linked with acetate salts for ocular drug delivery [300]. A polysaccharide, self-assembling-based IH system consisting of oxidized cellulose nanofibers and cationic guar gum crosslinked by electrostatic interactions and abundant hydrogen bonding localized therapeutic proteins delivery [301].

**Table 2.5** Natural gum-based injectable hydrogel using physical crosslinks for biomedical applications.

Srl. No.	Natural gum	Method	Application	Reference
1	Hyaluronic acid	physical interaction and self-assembly	Curcumin release	[282]
2	Gellan gum	Electrostatic interaction	Tannic acid release	[283]
3	Chitosan	pH and temperature	Wound healing	[284]
4	Sodium alginate	Physical interaction and self-assembly	Curcumin release	[285]
5	Gellan gum	Ionic interaction	Tissue engineering	[286]
6	Chitosan	Electrostatic interaction	Bone regeneration	[287]
7	Alginate	Divalent cation exchange	Cardiac repair	[288]
8	Gellan gum	Coordination bond	Tissue engineering	[289]
9	Gellan gum	Ionic interaction	Burn wound therapy	[290]
10	guar gum	Hydrogen bonding	Wound dressing	[291]
11	Alginate	Ionic interaction	Wound healing	[292]
12	Sodium Alginate	Coordination bond	Wound healing	[293]

13	Dextrin and chitosan	Host-guest interaction	Cinnamaldehyde release	[294]
14	Guar gum	Borate/didiol	Wound healing	[295]
15	Gellan gum	CaCl <sub>2</sub> crosslinker	Tissue engineering	[296]
16	Guar gum	Hydrogen bonding	Tissue regeneration	[297]`
17	Guar gum	CaCl <sub>2</sub> crosslinker	Bone defect treatment	[298]
18	Alginate gum	CaCl <sub>2</sub> crosslinker	Curcumin release	[299]
19	Tragacanth gum	Electrostatic interaction/Acetate salts crosslinker	Sunitinib release	[300]
20	Guar gum	Hydrogen bonding	Bovine serum albumin release	[301]

A bioinspired self-healing IH was synthesized through dynamic Schiff base crosslinks and coordinate bonds between sodium alginate, gelatin, and protocatechualdehyde, with ferric ion for wound healing application as tissue sealant [302]. A polysaccharide-based IH was fabricated based on glycol chitosan and oxidized hyaluronic acid using a double-dynamic network of dynamic Schiff base bond formation and dynamic coordination bond for promoting periodontium regeneration in periodontitis [303]. A self-healing, magnetic, and injectable biopolymer hydrogel was generated by a dual cross-linking mechanism for drug delivery and bone repair applications [304]. A temperature and pH dual-responsive injectable and self-healing hydrogel was fabricated through a dual crosslinking mechanism prepared by chitosan oligosaccharide and aldehyde hyaluronic acid to promote diabetic foot ulcer healing [305]. An injectable adhesive antibacterial hydrogel was developed using oxidized alginate and catechol-modified gelatin, crosslinks through double dynamic bonds

(Schiff base and catechol-Fe coordinate bond); polydopamine decorated silver nanoparticles were also introduced into the hydrogel network wound dressing for infected skin wounds [306]. A naturally derived IH was developed composed of bioactive ketogenic-linked chitosan and aldehyde-modified oxidized alginate via the highly efficient Schiff base reaction and multifarious physical interactions utilized for cartilage and other soft tissue implants [307]. An IH is fabricated using ubiquitous nature-derived biological macromolecules, quaternized chitosan, tannic acid, and oxidant hyaluronic acid, driven by multiple dynamic interactions under physiological conditions for wound dressing applications [308]. A polysaccharide-based double network IH was fabricated by mixing solutions of aldehyde-alginate and acrylic acidchitosan in the presence of adipic acid dihydrazide and FeCl<sub>2</sub> that resulted in dual crosslinking mediated by Schiff base and ionic interactions for drug delivery applications [309]. Shi et al. synthesized an injectable macro-porous hydrogel based on the "smashed gels recombination" strategy using chitosan/polyethylene glycolsilicotungstic acid double-network via dual dynamic interactions for cartilage tissue engineering [310]. A microstructure united heterogeneous IH was designed using sodium alginate through a dual crosslinking mechanism for wound healing applications [311]. A group of researchers fabricated an injectable nanocomposite hydrogel base on oxidized sodium alginate and gelatin in the presence of borax loaded with chitosan nanoparticles through a dual crosslinking mechanism for sustained protein delivery [312]. A self-healing-based IH was developed based on aldehydemodified hyaluronic acid and glycol chitosan using a double crosslinking network for promoting periodontium regeneration in periodontitis [313].

**Table 2.6** Natural gum-based injectable hydrogel using hybrid crosslinks for biomedical application.

Srl. No.	Natural gum	Method	Application	Reference
1	Sodium alginate	Schiff base and coordination bond	Tissue sealant	[302]
2	Hyaluronic acid	Schiff base and coordination bond	Tissue engineering	[303]
3	Gellan gum	Schiff base and emulsion cross-linking	tetracycline hydrochloride drug release and bone repair	[304]
4	Hyaluronic acid and chitosan	Schiff base and hydrogen bond	Diabetic foot ulcer healing	[305]
5	Sodium alginate	Schiff base and coordination bond	Infected skin wound repair.	[306]
6	Sodium alginate and chitosan	Schiff base and hydrogen bond	Tissue engineering	[307]
7	Hyaluronic acid	Imine bond, hydrogen bonds, and electrostatic interaction	Wound dressing	[308]
8	Sodium alginate and chitosan	Schiff base and ionic interaction	Doxorubicin and Ciprofloxacin release	[309]
9	Chitosan	Schiff base and electrostatic interaction	Cartilage tissue engineering	[310]
10	Sodium alginate	Hydrogen bonding and ionic interaction	Wound healing	[311]
11	Sodium alginate	Imine bond, hydrogen bond, electrostatic interaction, and borate ester bond	Protein delivery	[312]
12	Hyaluronic acid	Schiff base and coordination bond	Wound healing	[313]

2.3 Biomedical applications of natural gum-based hydrogels and injectable hydrogels crosslinks through Schiff-based bonds (Figure 2.3 and Figure 2.4).

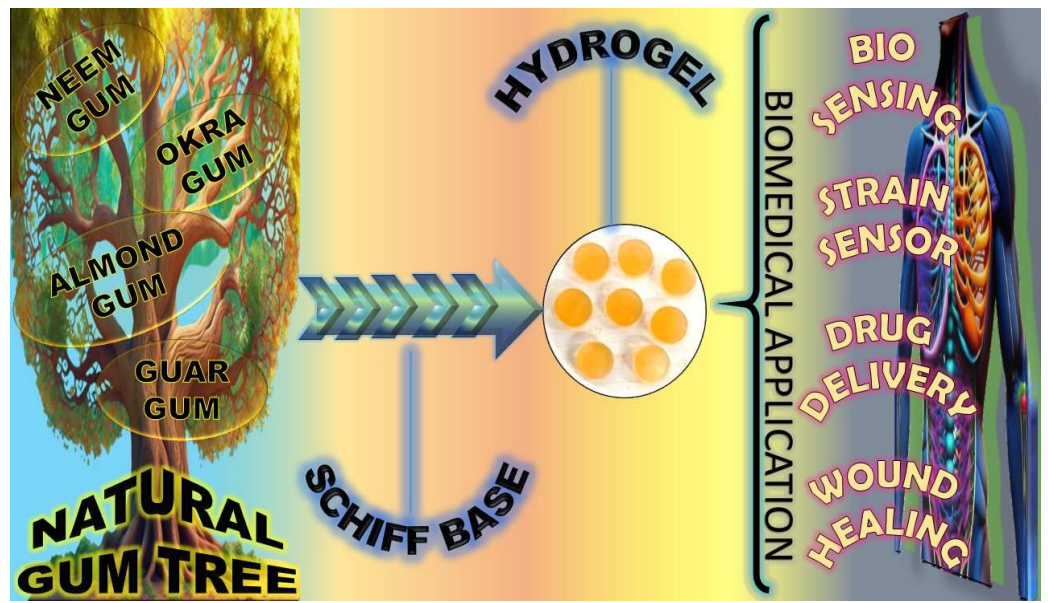


**Fig. 2.3** Pictorial representation of natural gum-based hydrogel using SB crosslinks for biomedical applications.

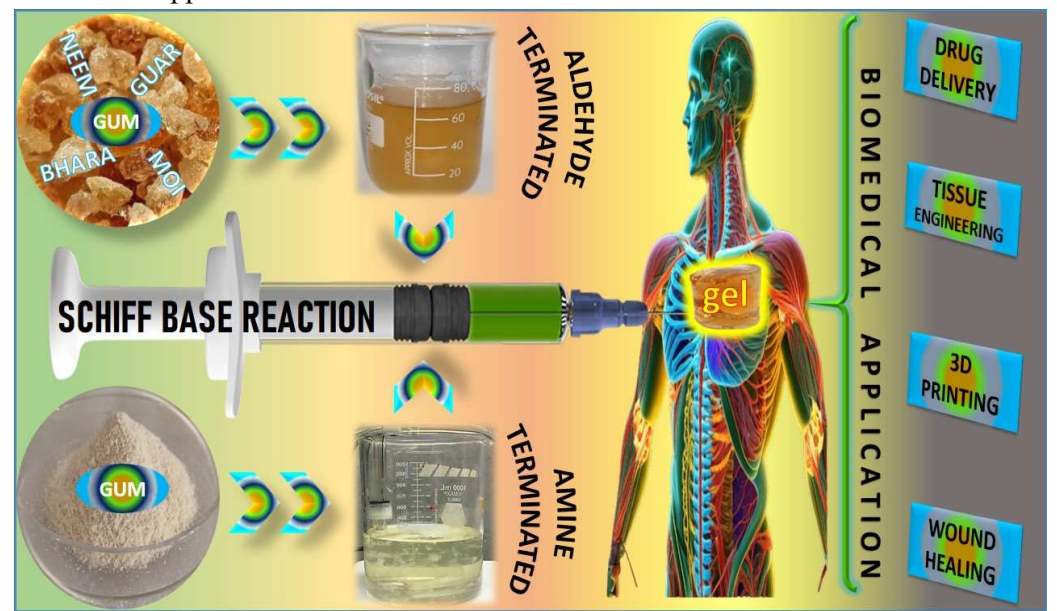


**Fig. 2.4** Pictorial representation of natural gum-based injectable hydrogel using SB crosslinks for biomedical applications.

The Schiff base crosslinking is found between amine, aldehyde, oxime, imine, and hydrazone functional groups. The Schiff base response is interceded by the nucleophilic attack of the nitrogen atom of the amino group on the electrophilic carbon atom of the ketone or aldehyde group, which happens in an aqueous arrangement under physiological circumstances. Also, it creates nontoxic items, guaranteeing good biocompatibility for the Schiff base response-based hydrogels [314]. Both groups' amounts determine the properties of IHs, such as gelling time and strength. Several advantages of using this technique include biocompatibility, reversibility, pH sensitivity, and simplicity utilized in biomedical applications. An IH was fabricated using N-carboxyethyl chitosan and oxidized hyaluronic acid using Schiff base crosslinks that improve bone regeneration and alveolar ridge promotion [234]. An oxidized dextran and phenylboronic acid-functionalized poly (ethylene imine) were used to develop an injectable local drug delivery system that could simultaneously improve drug loading efficiency of doxycycline and metformin through a dual crosslinking mechanism [315]. Deng et al. fabricated a Schiff base crosslinked IH using oxidized hyaluronic acid and carboxymethyl chitosan for abdominal tissue regeneration [316]. An IH was fabricated based on carboxymethyl chitosan and aldehyde functionalized sodium alginate via Schiff base reaction for wound healing [317]. A polysaccharide-based IH was fabricated based on glycol chitosan and oxidized hyaluronic acid using a double-dynamic network of dynamic Schiff base bond formation and dynamic coordination bond for promoting periodontium regeneration in periodontitis [303]. Pandit et al. synthesized an IH using N, O-carboxymethyl chitosan, and multialdehyde guar gum through Schiff base crosslinks for drug delivery applications [235]. A biocompatible and self-healing IH

was fabricated using modified-β-chitin and alginate dialdehyde via Schiff base crosslinks for wound healing applications [236]. A self-healing IH was prepared by crosslinking two natural polysaccharides, carboxymethyl chitosan and oxidized konjac glucomannan, based on the Schiff base bond loaded with exosomes and berberine for infected wound healing [237]. A self-healing collagen-based IH has been developed based on dynamic imine linkages between collagen and dialdehyde guar gum, as well as diol-borate ester bonds between guar gum and borax for wound dressing application [238]. A self-healing, injectable, and pH-responsive hydrogel was synthesized by Ncarboxyethyl chitosan, hyaluronic acid-aldehyde, and adipic acid dihydrazide through the formation of the reversible dynamic bonds, acyl hydrazone, and imine bonds used as a bioactive dressing for enhancing diabetic wound healing [240]. An injectable, shear-thinning, and self-healing hydrogel based on DNA, oxidized alginate, and silicate nanoparticles was fabricated through Schiff base crosslinks for the sustained delivery of simvastatin [243]. Amino groups in ε-polylysine undergo dynamic Schiff base reaction crosslinking with oxidized hyaluronic acid, and F127 exhibits unique temperature sensitivity to form an injectable thermosensitive hydrogel, which was used to cover the wound at body temperature [246]. A self-healing, magnetic, and injectable biopolymer hydrogel was generated by a dual cross-linking mechanism for drug delivery and bone repair applications [304]. A dual-responsive (temperature and pH) injectable and self-healing hydrogel was fabricated through a dual crosslinking mechanism prepared by chitosan oligosaccharide and aldehyde hyaluronic acid for promoting diabetic foot ulcer healing [305]. An injectable adhesive antibacterial hydrogel was developed using oxidized alginate and catechol-modified gelatin, crosslinks through double dynamic bonds, which were Schiff base and catechol-Fe

coordinate bond; polydopamine decorated silver nanoparticles were also introduced into the hydrogel network wound dressing for infected skin wounds [306]. An antibacterial, pro-healing IH was developed using oxidized pullulan polysaccharide and carboxymethyl chitosan via dynamic Schiff base crosslinks for early protection of open abdominal wounds [318]. A multifunctional IH scaffold was constructed by incorporating bioactive glass nanoparticles with a Schiff base crosslinking composed of carboxymethyl chitosan and oxidized cellulose for tissue engineering and drug delivery applications [319]. A bioinspired self-healing injectable nanocomposite hydrogel was developed based on oxidized dextran and gelatin by Schiff base crosslinking between dopamine-modified gelatin and oxidized dextran for bone regeneration [247]. The IH was designed with the natural macromolecular of the gallic acid-grafted quaternized chitosan and oxidized hyaluronic acid via Schiff base and Michael addition reaction for wound healing applications [248]. An injectable and selfhealing hydrogel comprising of collagen, chitosan, and oxidation-modified konjac glucomannan, which acts as a macromolecular cross-linker to construct dynamic Schiff-base bonds, was smartly designed for regenerative repairment of infected wounds [249]. An injectable, self-healing hydrogel was fabricated using N-succinyl chitosan and oxidized pectin via Schiff base reaction for biomedical applications [320]. An IH was developed by grafting dopamine onto hyaluronic acid and mixing it with carboxymethyl chitosan solution through a reversible Schiff base reaction for tissue adhesive material [250]. A naturally derived IH was developed composed of bioactive ketogenic-linked chitosan and aldehyde-modified oxidized alginate via the highly efficient Schiff base reaction and multifarious physical interactions utilized for cartilage and other soft tissue implants [307]. An IH is fabricated using ubiquitous

nature-derived biological macromolecules, quaternized chitosan, tannic acid, and oxidant hyaluronic acid, driven by multiple dynamic interactions under physiological conditions for wound dressing applications [308]. A Schiff base crosslinked IH was designed composed of carboxymethyl chitosan and oxidized konjac glucomannan through the Schiff base bond for tissue engineering and wound healing [251]. A biomultifunctional melatonin-loaded carboxymethyl chitosan and poly aldehyde dextranbased IHs were developed through the dynamic Schiff-base reaction to manage periodontal diseases potentially [252]. A polysaccharide-based double network IH was fabricated by mixing solutions of aldehyde-alginate and acrylic acid-chitosan in the presence of adipic acid dihydrazide and FeCl<sub>2</sub> that resulted in dual crosslinking mediated by Schiff base and ionic interactions for drug delivery applications [309]. A polysaccharide-based IH was constructed consisting of a dynamic crosslinking network formed by the Schiff base and a covalent cross-linking network achieved by photoinitiated polymerization, offering a feasible way to tune the mechanical property of hydrogel after injection for skin repair applications [253]. An IH was constructed via a Schiff-base reaction of oxidized hyaluronic acid and carboxymethyl chitosan for bone repair applications [254]. Shi et al. synthesized an injectable macro-porous hydrogel based on the "smashed gels recombination" strategy chitosan/polyethylene glycol-silicotungstic acid double-network via dual dynamic interactions for cartilage tissue engineering [310]. An injectable multifunctional Schiff base cross-linked with gallic acid-modified chitosan and oxidized dextran hydrogels was rationally designed to accelerate wound healing [255]. An IH was developed using benzaldehyde-terminated polyethylene glycol crosslinked with hydroxypropyltrimethyl ammonium chloride chitosan via the Schiff base mechanism

to promote diabetic wound healing [256]. An adhesive IH was developed using hydrazide-modified hyaluronic acid and-phthalaldehyde-terminated four-armed poly(ethylene glycol) via hydrazine linkage for sutureless wound closure [257]. An injectable, self-healing, transparent, and antibacterial hydrogel was fabricated based on quaternized chitosan and oxidized dextran crosslinked via the Schiff base mechanism used for wound dressings [258]. Sun et al. developed an IH using oxidized konjac glucomannan, γ-poly(glutamic acid) modified with dopamine and L-cysteine and ε-polylysine by thiol-aldehyde addition and Schiff-base reactions to promote wound healing in burn wound infection [259]. An IH that comprises carboxymethyl chitosan and aldehyde functionalized alginate was developed, and it was crosslinked through dynamic Schiff-base linkages for drug delivery to treat obesity [260]. An injectable nanocomposite was rationally designed as a sustained release platform for enhanced cartilage regeneration through the integration of a chitosan-based hydrogel, articular cartilage stem cells, and mesoporous SiO<sub>2</sub> nanoparticles loaded with anhydroicaritin via dynamic imine linkage for cartilage regeneration applications [261]. Schiff-base bonding synthesized an IH based on polyaldehyde gum arabic and carboxymethyl chitosan for localized breast cancer treatment [164]. A biocompatible IH was designed based on amino-functionalized polyaspartamide crosslinked with naturally occurring dextran aldehyde via Schiff base chemistry for tissue adhesion applications [321]. An injectable adhesive dopamine functionalized oxidized hyaluronic acid and carboxymethyl chitosan collagen-based hydrogel was constructed via Schiff dynamic and ionic interaction for wound dressing [263]. A self-crosslinked IH was fabricated using oxidized alginate and carboxymethyl chitosan via Schiff base for dental enamel regeneration [166]. A facile one-pot approach was adopted to prepare a polysaccharide-based IH based on oxidized starch and chitosan via Schiff base crosslinks for drug release applications [265]. A self-healing injectable nanocomposite hydrogels based on benzaldehyde-modified polyethylene glycol and chitosan, reinforced with graphene oxide via Schiff base crosslinking mechanism for the delivery of pomegranate extract for hard tissue engineering [266]. A group of researchers fabricated an injectable nanocomposite hydrogel base on oxidized sodium alginate and gelatin in the presence of borax loaded with chitosan nanoparticles through a dual crosslinking mechanism for sustained protein delivery [312]. A selfhealing and IH was synthesized composed of multialdehyde gum arabic and succinic anhydride chitosan via Schiff base crosslinks for anticancer drug delivery [272]. A degradable polysaccharide-based IH was formulated composed of carboxymethyl chitosan and oxidized alginate, doubly integrated with hydroxyapatite nanoparticles and calcium carbonate microspheres under physiological conditions through Schiff base mechanism for drug delivery and bone tissue engineering applications [273]. An injectable, self-healing, and biocompatible hydrogel was formulated based on N, Ocarboxymethyl chitosan, and multialdehyde guar gum via Schiff base crosslinks for sustained anticancer drug delivery [274]. A self-healing and injectable polysaccharidebased hydrogel was prepared based on carboxymethyl chitosan and calcium pre-crosslinked oxidized gellan gum cross-linked by the Schiff-base reaction for bone tissue engineering [275]. A self-healing-based IH was developed based on aldehydemodified hyaluronic acid and glycol chitosan using a double crosslinking network for promoting periodontium regeneration in periodontitis [313]. Curcumin-loaded mesoporous polydopamine nanoparticles and metformin were introduced into the polymer matrix formed by the dynamic imine bonds and electrostatic interactions

between carboxymethyl chitosan and oxidized hyaluronic acid to fabricate IHs for drug delivery applications [277]. A polysaccharide-based IH was prepared via Schiff base crosslinking of aldehyde-modified xanthan and carboxymethyl-modified chitosan for local drug delivery [278]. A covalently cross-linked composite chitosan-alginate hydrogel was prepared with pH sensitivity to drug delivery degradation [279]. A biocompatible and self-healing IH was designed based on modified-β-chitin and alginate for wound healing applications [280]. Self-healing hydrogels were prepared from partially oxidized hyaluronate and glycol chitosan in the presence of adipic acid dihydrazide via a combination of two dynamic bonds in the gels, including imine bonds obtained via a Schiff base reaction as well as acyl hydrazone for tissue engineering applications [322]. A dual dynamically crosslinked IH designed to serve as a physical postoperative anti-adhesion barrier by dynamic chemical oxime bonding from alkoxyamine-terminated Pluronic F127 and oxidized hyaluronic acid [323]. A hydrazine-modified elastin-like protein and aldehyde-modified hyaluronic acid were used to fabricate IHs through dynamic covalent hydrazone bonds for stem cell delivery [324]. An acylhydrazone and oxime cross-linked hyaluronic acid-based IH was developed for bioconjugation [325]. An adaptable elastin-like protein-hyaluronic acid IH platform was developed using dynamic covalent chemistry for tissue engineering [326]. A shear-thinning and self-healing IH crosslinked through dynamic covalent chemistry to develop 3D bioprinting scaffolds [327]. A biomimetic IH system was developed based on hyaluronic acid-adipic dihydrazide and the oligopeptide grafted oxidized pectin for tissue engineering applications [328]. An IH was formed by reacting hydrazide-modified hyaluronic acid and benzaldehyde-terminated F127 triblock copolymers for burn wound healing [329]. An IH was formulated through

dynamic covalent hydrazone cross-linking in the presence of a biocompatible benzimidazole-based catalyst for long-term stability for cell culture [330]. A selfcrosslinking hyaluronic acid-carboxymethylcellulose IH was developed for multilayered 3D-printed construct shape integrity and mechanical stability for soft tissue engineering using hydrazone crosslinking mechanism [331]. A hydrazone crosslinking chemistry and thiol-Michael addition reaction were utilized to form hyaluronic acid-based IHs for protein delivery [332]. A hydrazone-crosslinked gallol functionalized hyaluronic acid-based IH was synthesized for tissue adhesive applications [333]. Ganeswar Dalei et al. synthesized a hydrogel using Schiff base crosslinks composed of curcumin-loaded dialdehyde guar gum and chitosan for dual drug release in colorectal cancer therapy [334]. Xiaomin Zhang et al. have developed a doubly crosslinked hydrogel, which was constructed by Schiff-base crosslinking of oxidized gellan gum (pre-crosslinked by calcium ion) and carboxymethyl chitosan for tetracycline hydrochloride and silver sulfadiazine release applications [335]. The periodate-modified gum arabic was used as a natural-based, non-toxic cross-linker to synthesize hybrid bovine serum albumin-gum arabic aldehyde nano gels by Schiff base reaction through the inverse mini emulsion method for 5-fluorouracil drug release [336]. A hydrogel was synthesized using fenugreek gum and chitosan via Schiff base production for drug delivery application in the future [337]. A physical and selfcrosslinking mechanism was used to synthesize a hydrogel of chitosan, gelatin, and oxidized guar gum proposed for various applications [338]. A work described by researchers includes the synthesis of hydrogel using the conjugation of 9aminoacridine to gum arabic via Schiff's base for tumor treatment applications [339]. A self-healing hyaluronic acid-based hydrogel was fabricated through a facile dynamic

covalent Schiff base reaction for drug delivery, bioprinting, smart robots, and tissue regeneration [340]. Gelatin, oxidized gellan gum, and amino hydroxyapatite-based hybrid hydrogel were synthesized through Schiff base linkages for cartilage tissue engineering applications [341]. A hydrogel was designed by using gum arabic aldehyde with gelatin in the presence of acrylamide to prepare IPN hydrogel through Schiff base crosslinks [342]. A hydrogel based on aldehyde-modified xanthan gum and gelatin has been developed using Schiff's base reaction and utilized for tissue engineering applications [343]. A hydrogel scaffold of carboxyethyl chitosan and different oxidized cashew gums was developed and utilized for tissue engineering applications [344]. A facile one-pot approach was adopted to prepare a polysaccharidebased hydrogel of oxidized starch-chitosan crosslink through the Schiff base mechanism for ampicillin release applications [345]. A hydrogel composite with antibacterial and self-healing ability was prepared using cysteine-modified carboxymethyl chitosan, sodium oxidized alginate, and but-3-yn-2-one based on Schiff base and thiol-alkynone double cross-links mechanism for skin tissue engineering applications [346]. A highly stretchable, sensitive, and multifunctional polysaccharidebased dual-network hydrogel sensor was constructed using dialdehyde carboxymethyl cellulose, chitosan, poly(acrylic acid), and aluminum ions crosslink through Schiff base bonds and metal coordination mechanism for intelligent sensors, particularly for applications in wet and underwater environments [220]. A semi-interpenetrating hydrogel was designed from carboxymethyl guar gum and gelatin using the Schiff base crosslinks mechanism to release ciprofloxacin [123]. A group of researchers synthesized a hydrogel composed of aldehyde methylene sodium alginate, amino gelatin, and dithiothreitol-modified graphene oxide using Schiff base and Michael

addition reaction for bone regeneration application [347]. A hydrogel film was synthesized from dextran dialdehyde cross-linked with gelatin via Schiff base crosslinking mechanism for the sustained delivery of biologically active epidermal growth factor [348]. A self-healing hydrogel was fabricated using oxidized microcrystalline cellulose and carboxymethyl chitosan as wound dressing material [349]. The zein nanoparticles/aldehyde-modified guar gum/silk fibroin-based hydrogel networks were successfully developed to increase the curcumin bioavailability during wound treatment [350]. The hydrogel was synthesized via a Schiff base reaction between carboxymethyl chitosan and oxidized sodium alginate, followed by the polymerization of the acrylamide monomer utilized for wound healing applications [351]. A composite hydrogel was prepared using dialdehyde konjac glucomannan as a macromolecular cross-linking agent for chitosan through Schiff base crosslinks for wound healing applications [352]. A hydrogel based on a water-soluble derivative of chitosan, hydroxypropyl chitosan, and sodium alginate dialdehyde was derived using Schiff base crosslinks for corneal endothelium reconstruction [353]. A dextran-based nano gel with covalently conjugated doxorubicin was developed via Schiff base formation using the inverse microemulsion technique for wound healing applications [354]. A biodegradable and resilient hydrogel was prepared using a self-cross-linking method via Schiff base crosslinks between N-2-hydroxypropyl trimethyl ammonium chloride chitosan and oxidized sodium alginate for rhodamine release [355]. A biocompatible composite hydrogel was designed using casein and oxidized hyaluronic acid for controlled drug release [356]. A carboxymethyl chitosan/sodium alginate/oxidized dextran-based multifunctional hydrogel was developed through Schiff base reaction and amide reaction and firmly adhered to the skin for wound healing applications [357]. An oxidized cashew gum is mixed with gelatin to yield a covalently crosslinked hydrogel for tissue engineering applications [358]. A covalently crosslinked gelatin-βcyclodextrin hydrogel has been prepared via the Schiff-base reaction to release rutin [359]. A fungal mushroom-derived carboxymethyl chitosanpolydopamine-based hydrogels were derived through dynamic Schiff base crosslinking and hydrogen bonds with multifunctionality properties (tissue adhesive, hemostasis, self-healing, and antibacterial properties utilized as a wound dressing material for infected wounds [221]. Chitosan and cumin aldehyde were used for the gel formation by covalent bonding between the free amino group and the carbonyl group of chitosan & cumin aldehyde, respectively, for the release of levofloxacin [360]. A double-crosslinked multifunctional hydrogel based on quaternized chitosan, methacrylate anhydride-modified collagen, and oxidized dextran was developed for wound dressing applications [361]. A multifunctional ionic conductive doublenetwork hydrogel was prepared via FRP using a simple one-pot method based on AlCl<sub>3</sub>, acrylic acid, oxide sodium alginate, and aminated gelatin through metal coordination, and Schiff base for flexible strain sensor in biomedical fields [362]. The multifunctional double-crosslinking hydrogel was developed through the formation of catechol-catechol adducts and a Schiff-based reaction between amino groups in chitosan quaternary ammonium salt and aldehyde groups in oxidized dextrandopamine [363]. A pH-responsive carboxyethyl chitosan and oxidized pectin-based hydrogels were derived with self-healing, biodegradable, and antibacterial properties through Schiff base crosslinks for wound healing applications [364]. The carboxymethyl chitosan /oxidized dextran /γ-polyglutamic acid-based hydrogel was prepared via intramolecular lactam bonds, intermolecular amide bonds, and Schiff base

bonds for hemostasis of incompressible bleeding on wet wound surfaces [365]. A group of researchers developed a bi-layered composite hydrogel dressing consisting of breathable hydrophobic polyurethane/polydimethylsiloxane and membrane and double-crosslinked chitosan-based hydrogel with dynamic Schiff base bonds and non-dynamic photo-crosslinking bonds utilized as a skin wound repair [366]. Another group of colleagues designed and developed a series of multifunctional dynamic Schiff base network hydrogels composed of cystamine-modified hyaluronic acid, benzaldehyde-functionalized poly(ethylene glycol)-co-poly(glycerol sebacate), and polydopamine/polypyrrole nanocomposite with mild on-demand removability to enhance drug-resistant bacteria-infected wound healing [367]. A natural polymerbased conductive hydrogel with excellent mechanical properties, low water loss, and freeze-tolerance was formed by the Schiff base reaction between the hydrazide-grafted hyaluronic acid and the oxidized chitosan for flexible and wearable strain sensor in biomedical applications [368]. Halloysite nanotube-doped chitosan /oxidized dextran adhesive hydrogels were developed through a Schiff base reaction for rapid hemostasis and infected-wound repair in emergency injury events [369]. A hydrogel was fabricated by gallic acid grafted chitosan and oxidized Bletilla striata polysaccharide as the scaffold formed by two types of dynamic crosslinking, i.e., Schiff base and pyrogallol-Fe<sup>3+</sup> utilized for wound treatment purposes [222]. A hydrogel was designed using N-oleoyl chitosan and oxidized sodium alginate crosslinks through the Schiff base mechanism for metronidazole release applications [370]. A hydrogel for wearable electronics was fabricated using oxidized guar gum and acrylamide through Schiff base crosslinks [371]. Modified gum arabic cross-linked with gelatin scaffold used for hydrogel synthesis in biomedical applications [85]. A pH-sensitive and self-healable hydrogel was fabricated using gum arabic aldehyde and polyvinyl alcohol through Schiff base crosslinks for drug delivery applications [108]. A hydrogel was fabricated based on biopolymers chitosan and guar gum using glutaraldehyde crosslinker for sustained release of a commonly used orally prescribed analgesic, paracetamol [133]. Self-crosslinked chitosan/xanthan interpenetrated hypromellose hydrogels were developed through Schiff base crosslinking for the controlled delivery of ampicillin, minocycline, and rifampicin [139]. A binary blended hydrogel film was prepared composed of vanillin crosslinked chitosan /locust bean gum and then synthesized its complexes with Fe<sup>3+</sup>, Zn<sup>2+</sup> & Cu<sup>2+</sup> metal ions by solution casting method via Schiff base and metal ion bonding for biomedical applications [218].

**Table 2.7** Natural gum-based hydrogel using Schiff base crosslinks for biomedical applications.

Srl. No.	Natural gum	Method	Application	Reference
1	Guar gum	Schiff base	Curcumin and Aspirin release	[334]
2	Gellan gum	Schiff base	Tetracycline hydrochloride and silver sulfadiazine release applications	[335]
3	Gum arabic	Schiff base	5-fluorouracil drug release	[336]
4	Fenugreek gum	Schiff base	Propose for drug delivery application	[337]
5	Guar gum	Schiff base	Proposed for biological applications	[338]
6	Gum Arabic	Schiff base	Tumor treatment	[339]
7	Hyaluronic acid	Schiff base	Propose for drug delivery,	[340]

			bioprinting, intelligent robots, and tissue regeneration.	
8	Gellan gum	Schiff base	Cartilage tissue engineering applications	[341]
9	Gum arabic	Schiff base	Tissue engineering scaffolds and drug carriers are also applied to wearable devices.	[342]
10	Xanthan gum	Schiff base	Tissue engineering applications	[343]
11	Cashew gum	Schiff base	Tissue engineering applications	[344]
12	Chitosan	Schiff base	Ampicillin release	[345]
13	Sodium alginate	Schiff base	Skin tissue engineering	[346]
14	Chitosan	Schiff base and coordination bond	Sensor for human movements	[220]
15	Guar gum	Schiff base	Ciprofloxacin release	[123]
16	Sodium alginate	Schiff base and Michael Addition reaction	Bone regeneration	[347]
17	Dextran	Schiff base	Delivery of epidermal growth factor	[348]
18	Carboxymethyl chitosan	Schiff base	Wound dressing	[349]
19	Guar gum	Schiff base	Curcumin release	[350]
20	Sodium alginate	Schiff base	Wound healing	[351]
21	Konjac glucomannan	Schiff base	Wound healing	[352]

22	Sodium alginate	Schiff base	Corneal endothelium reconstruction	[353]
23	Dextran	Schiff base	Doxorubicin release	[354]
24	Sodium alginate	Schiff base and H-bonding	Rhodamine release	[355]
25	Hyaluronic acid	Schiff base	Salicylic acid release	[356]
26	Sodium alginate	Schiff base	Wound healing	[357]
27	Cashew gum	Schiff base	Tissue engineering	[358]
28	Dextrin	Schiff base	Rutin release	[359]
29	Chitosan	Schiff base and H-bond	Wound dressing	[221]
30	Chitosan	Schiff base	Levofloxacin release	[360]
31	Dextran	Schiff base	Wound dressing	[361]
32	Sodium alginate	Schiff base and metal coordination bond	Stain sensor	[362]
33	Chitosan	Schiff base	Tissue engineering	[363]
34	Chitosan	Schiff base	Wound healing	[364]
35	Dextran, chitosan	Schiff base	Wound healing	[365]
36	Chitosan	Schiff base	Skin wound repair	[366]
37	Hyaluronic acid	Schiff base	Wound healing	[367]
38	Hyaluronic acid	Schiff base	Stain sensor	[368]
39	Dextran, Chitosan	Schiff base	Wound repair	[369]
40	Chitosan	Schiff base and ionic interaction	Wound healing	[222]
41	Sodium alginate	Schiff base	Metronidazole release	[370]
42	Guar gum	Schiff base	Strain sensor	[371]
43	Gum arabic	Schiff base	Wound healing	[85]

44	Gum arabic	Schiff base	Rivastigmine	[108]
			release	
45	Guar gum	uar gum Schiff Paracetamol release		[133]
		base/Glutaraldehyde		
		crosslinker		
46	Xanthan gum	Schiff base	Propose for	[139]
			biomedical	
			engineering	
47	Chitosan and	Schiff base and	Wound healing	[218]
	locust bean gum	Coordination		
		crosslinks		

**Table 2.8** Natural gum-based injectable hydrogel using Schiff base crosslinks for biomedical applications

Srl. No.	Natural gum	Method	Application	Reference
1	Hyaluronic acid	Imine bond	Bone regeneration	[234]
2	Dextran	Imine bond	Doxycycline and metformin release	[315]
3	Hyaluronic acid	Imine bond	Tissue regeneration	[316]
4	Sodium alginate	Imine bond	Wound healing	[317]
5	Hyaluronic acid	Imine bond	Tissue engineering	[303]
6	Guar gum	Imine bond	Doxorubicin release	[235]
7	Sodium alginate	Imine bond	Wound healing	[236]
8	Konjac glucomannan	Imine bond	Wound healing	[237]
9	Guar gum	Imine bond	Wound dressing	[238]
10	Hyaluronic acid	Imine bond	Wound healing	[240]
11	Alginate	Imine bond	Simvastatin release	[243]
12	Hyaluronic acid	Imine bond	Wound healing	[246]
13	Gellan gum	Imine bond	Tetracycline hydrochloride drug release and bone repair	[304]

14	Hyaluronic acid and chitosan	Imine bond	Diabetic foot ulcer healing	[305]
15	Sodium Alginate	Imine bond	Skin wound	[306]
16	Carboxymethyl chitosan	Imine bond	Abdominal wound repair	[318]
17	Carboxymethyl chitosan	Imine bond	Doxorubicin release	[319]
18	Dextran	Imine bond	Bone regeneration	[247]
19	Hyaluronic acid	Imine bond	Wound healing	[248]
20	Konjac glucomannan	Imine bond	Wound healing	[249]
21	N-succinyl chitosan	Imine bond	Wound healing	[320]
22	Hyaluronic acid	Imine bond	Tissue adhesive material	[250]
23	Sodium alginate and chitosan	Imine bond	Tissue engineering	[307]
24	Hyaluronic acid	Imine bond	Wound dressing	[308]
25	Konjac glucomannan	Imine bond	Tissue engineering	[251]
26	Dextran	Imine bond	Treatment of periodontal disease	[252]
27	Sodium alginate	Imine bond	Doxorubicin and Ciprofloxacin release	[309]
28	Chitosan	Imine bond	Skin repair	[253]
29	Hyaluronic acid	Imine bond	Bore repair	[254]
30	Chitosan	Imine bond	Tissue engineering	[310]
31	Chitosan and dextran	Imine bond	Wound healing	[255]
32	Chitosan	Imine bond	Wound healing	[256]
33	Hyaluronic acid	Hydrazine linkage	Wound healing	[257]

34	Dextran	Imine bond	Wound dressing	[258]
35	Konjac glucomannan	Imine bond	Burn wound healing	[259]
36	Sodium Alginate	Imine bond	Obesity treatment	[260]
37	Chitosan	Imine bond	Cartilage regeneration	[261]
38	Gum arabic	Imine bond	Cancer treatment	[164]
39	Dextran	Imine bond	Tissue adhesion	[321]
40	Hyaluronic acid	Imine bond	Wound dressing	[263]
41	Sodium Alginate	Imine bond	Dental enamel regeneration	[166]
42	Chitosan	Imine bond	Ampicillin sodium salt drug delivery	[265]
43	Chitosan	Imine bond	Tissue engineering	[266]
44	Sodium alginate	Imine bond	Protein delivery	[312]
45	Guar gum	Imine bond	Nanocurcumin release	[272]
46	Alginate gum	Imine bond	Tetracycline hydrochloride release	[273]
47	Guar gum	Imine bond	Doxorubicin release	[274]
48	Gellan gum	Imine bond	Bone tissue engineering	[275]
49	Hyaluronic acid	Imine bond	Wound healing	[313]
50	Hyaluronic acid	Imine bond	Wound healing	[277]
51	Xanthan gum	Imine bond	Tissue scaffolds	[278]
52	Alginate gum and chitosan	Imine bond	5-fluorouracil drug release	[279]
53	Alginate gum and	Imine bond	Wound healing	[280]
54	Hyaluronic acid	Imine bond and hydrazine bond	Tissue engineering	[322]

55	Hyaluronic acid	Oxime bond	Postoperative anti- adhesion barrier	[323]
56	Hyaluronic acid	Hydrazone bond	Stem cell delivery	[324]
57	Hyaluronic acid	Acylhydrazone and oxime	Bioconjugation	[325]
58	Hyaluronic acid	Hydrazone bond	Cartilage regeneration	[326]
59	Hyaluronic acid	Hydrazone bond	Scaffolds	[327]
60	Hyaluronic acid	Hydrazone bond	Tissue engineering	[328]
61	Hyaluronic acid	Hydrazone bond	Burn wound healing	[329]
62	Hyaluronic acid	Hydrazone bond	Stability of cell culture	[330]
63	Hyaluronic acid	Hydrazone bond	Tissue engineering	[331]
64	Hyaluronic acid	Hydrazone bond	Protein delivery	[332]
65	Hyaluronic acid	Hydrazone bond	Tissue adhesive	[333]

# 2.4 Chitosan

Chitosan is a biodegradable, biocompatible, and non-toxic polymer derived from chitin, which is found in the cell walls of crustaceans, fungi, insects, some algae, microorganisms, and invertebrate animals. It is a copolymer composed of glucosamine and N-acetyl glucosamine, and its properties depend on the degree of acetylation and degree of deacetylation, as well as the molecular weight [372]. The derivatization of chitosan involves modifying its amino functional groups through processes like alkylation, acylation, and quaternization to create chitosan derivatives with enhanced properties for various applications. These modifications are crucial in escalating the application range of chitosan derivatives, improving their solubility, pH sensitivity, and targeting capabilities. Chemical modifications of chitosan can develop new materials with unique functionalities, making them valuable in fields such as drug

delivery, biomedicine, wound healing, and tissue engineering [373]. The properties of chitosan derivatives include variations in molecular weight, viscosity, solubility, crystallinity, and biological activities. Chitosan derivatives can have reduced molecular weight, viscosity, and crystallinity compared to native chitosan, leading to higher solubility. These derivatives exhibit improved functional and biological properties, such as antibacterial, antifungal, and antioxidant potentials, often related to their molecular weight [374]. Additionally, the charge density of chitosan derivatives depends on the degree of acetylation and pH, influencing their solubility and application range. Chemical modifications of chitosan can enhance its mechanical properties, solubility, and biocompatibility, making it a versatile material. The different methods of modifying chitosan include [375].

#### 2.4.1 Alkali treatment

This method involves treating chitosan with heated alkali solutions to remove impurities of proteins and pigments, partially destroy glycoside bonds, and reduce molecular weight. This method is commonly used to improve the quality of chitosan for industrial applications such as enzyme immobilization and biodegradable packing materials.

## 2.4.2 Acylation

This method involves introducing aromatic or aliphatic acyl groups to the amine chitosan group, which destroys chitosan's hydrogen bonding and improves its solubility. Short-chain acylated chitosan shows higher solubility than long-chain acylated chitosan.

## 2.4.3 Carboxylation

This method involves introducing carboxyl groups into the chitosan molecule, which can occur with the hydroxyl or amino group on the chitosan molecule alone or with the two active groups simultaneously. The commonly used reagents for carboxylation modification of chitosan include glyoxylic acid and chloroacetic acid. Introducing carboxyl groups substantially improves chitosan's water solubility, biocompatibility, and antibacterial properties.

## 2.4.4 Quaternization

This method involves introducing quaternary ammonium groups into the chitosan molecule, which improves its solubility in water and enhances its antibacterial properties.

#### 2.4.5 Esterification

This method involves introducing ester groups into the chitosan molecule, which improves its solubility in organic solvents and enhances its stability.

#### 2.4.6 Etherification

This method involves introducing ether groups into the chitosan molecule, which improves its solubility in water and enhances its stability for various industrial and biomedical applications.

Chitosan has been used in various fields due to its unique properties, such as its biodegradability, biocompatibility, non-toxicity, and functional groups, including food, medical, pharmaceutical, health care, agriculture, and environmental pollution protection, due to its reactive amino and hydroxyl groups, which confer it with

functional properties such as antimicrobial, antioxidant, gel-forming, biocompatibility, metal chelating, and easy processability [376]. Chitosan has been used as a drug carrier due to its biocompatible properties, and its degree of deacetylation and molecular weight can be modified to obtain different physicomechanical properties. It exhibits antifungal activity against various fungi, which depends on its concentration, molecular weight, degree of substitution, the type of functional groups added to the chitosan, and the kind of fungus [377]. Chitosan nanoparticles have been studied for drug delivery applications due to their biocompatibility, non-toxicity, and ability to form stable colloidal suspensions. Chitosan has been used in tissue engineering due to its biocompatibility, biodegradability, and ability to promote cell adhesion and growth [378]. It has been used as hydrogels, scaffolds, and nanofibers for tissue engineering applications [379]. Chitosan-based hydrogels have been used for cartilage tissue engineering due to their ability to mimic the mechanical properties of cartilage and promote chondrogenesis [380]. Chitosan-based scaffolds have been used for bone tissue engineering because they promote osteogenesis and provide a suitable environment for bone cell growth [381]. Chitosan-based nanofibers have been used for skin tissue engineering because they mimic the extracellular matrix and promote skin cell growth [382]. Chitosan has been used in gene delivery due to its ability to form complexes with DNA and protect it from degradation [383]. Chitosan-based microparticles have been used for gene delivery because they protect DNA from degradation, promote cell uptake, and sustain DNA release [384]. Chitosan-based hydrogels have been used for wound healing because they mimic the extracellular matrix, promote cell proliferation and migration, and provide a moist environment for wound healing [380]. Chitosan-based films have been used for wound healing because they provide a barrier to bacterial infection, promote cell proliferation and migration, and provide a moist environment for wound healing [385]. Chitosan-based nanofibers have been used for wound healing because they mimic the extracellular matrix, promote cell proliferation and migration, and provide a high surface area for drug delivery. Chitosan has been used in the food industry because it forms gels, films, and fibers and improves food products' texture, stability, and shelf life [386]. Chitosanbased hydrogel films have been used for food packaging because they provide a barrier for oxygen, water vapor, and aroma and improve food products' stability and shelf life [387]. It has been used in the form of hydrogels, nanoparticles, and membranes for environmental pollution protection applications [388]. Wang et al. synthesized a double-crosslinking-double-network design IH using catechol-modified chitosan and methacryloyl chitosan via the simultaneous crosslinking of carbon-carbon double bonds and catechol Fe<sup>3+</sup>chelation for tissue adhesion [389]. A catechol-modified quaternized chitosan was fabricated and incorporated into poly(d,l-lactide)poly(ethylene glycol)-poly(d,l-lactide) hydrogel to develop an IH through a covalent bond for wound dressing application [390]. A conductive IH was synthesized through enzymatic crosslinking based on silk fibroin/carboxymethyl cellulose/agarose containing polydopamine functionalized graphene oxide for burn healing applications [391]. An IH was fabricated using N-carboxyethyl chitosan and oxidized hyaluronic acid using Schiff base crosslinks that improve bone regeneration and alveolar ridge promotion [234]. Deng et al. fabricated a Schiff base crosslinked IH using oxidized hyaluronic acid and carboxymethyl chitosan for abdominal tissue regeneration [316]. Longlong Cui and coworkers fabricated an IH using carboxymethyl chitosan and hyaluronic acid functionalized with dopamine via horseradish peroxidase and

hydrogen peroxide crosslinks for skin injury repairing [392]. An IH was fabricated based on carboxymethyl chitosan and aldehyde functionalized sodium alginate via Schiff base reaction for wound healing application [317]. Pandit et al. synthesized an IH using N, O-carboxymethyl chitosan, and multialdehyde guar gum through Schiff base crosslinks for drug delivery applications [235]. A self-healing IH was prepared by crosslinking two natural polysaccharides, carboxymethyl chitosan and oxidized konjac glucomannan, based on the Schiff base bond loaded with exosomes and berberine for infected wound healing [237]. A self-healing, injectable, and pHresponsive hydrogel was synthesized by N-carboxyethyl chitosan, hyaluronic acidaldehyde, and adipic acid dihydrazide through the formation of the reversible dynamic bonds, acyl hydrazone, and imine bonds used as a bioactive dressing for enhancing diabetic wound healing [240]. A self-healing, magnetic, and injectable biopolymer hydrogel was generated by a dual cross-linking mechanism for drug delivery and bone repair applications [304]. An injectable carboxymethyl chitosan IH scaffold was formed via a coordination bond for antibacterial and osteogenesis in osteomyelitis [393]. An antibacterial and pro-healing IH was developed using oxidized pullulan polysaccharide and carboxymethyl chitosan hydrogel via dynamic Schiff base crosslinks for early protection of open abdominal wounds [318]. A multifunctional IH scaffold was constructed by incorporating bioactive glass nanoparticles with a Schiff base crosslinking composed of carboxymethyl chitosan and oxidized cellulose for tissue engineering and drug delivery applications [319]. The oxidized tannic acidmodified gold nano-crosslinker was synthesized and used to effectively crosslink with chitosan to prepare the bioactive self-healing IH through a coordinate bond for treating Parkinson's disease [394]. The IH was designed with the natural macromolecular of the gallic acid-grafted quaternized chitosan and oxidized hyaluronic acid via Schiff base and Michael addition reaction for wound healing applications [248]. An injectable, self-healing hydrogel was fabricated using N-succinyl chitosan and oxidized pectin via Schiff base reaction for biomedical applications [320]. An IH was developed by grafting dopamine onto hyaluronic acid and mixing it with carboxymethyl chitosan solution through a reversible Schiff base reaction for tissue adhesive material [250]. An IH is fabricated using ubiquitous nature-derived biological macromolecules, quaternized chitosan, tannic acid, and oxidant hyaluronic acid, driven by multiple dynamic interactions under physiological conditions for wound dressing applications [308]. An IH was fabricated through the dynamic Schiff-base bonds between hydroxypropyl chitosan and aldehyde-modified pluronic F127 as the delivery substrate for precise and efficient treatment of tumors [395]. A Schiff base crosslinked IH was designed composed of carboxymethyl chitosan and oxidized konjac glucomannan through the Schiff base bond for tissue engineering and wound healing [251]. A bio-multifunctional melatonin-loaded carboxymethyl chitosan and poly aldehyde dextran-based IHs were developed through the dynamic Schiff-base reaction to manage periodontal diseases potentially [252]. Hu et al. designed an IH composed of carboxymethyl chitosan and genipin encapsulated with tea tree oil through a Schiff base crosslinking mechanism utilized for the treatment of complex anal fistula wounds [396]. A supramolecular hydrogel was fabricated with orotic acid-modified chitosan and 2,6-diaminopurine via a dual crosslinking mechanism for gastrointestinal drug release [397]. An IH was constructed via a Schiff-base reaction of oxidized hyaluronic acid and carboxymethyl chitosan for bone repair applications [254]. An injectable, self-healing, transparent, and antibacterial hydrogel was fabricated based on

quaternized chitosan and oxidized dextran crosslinked via the Schiff base mechanism used for wound dressings [258]. The hydrogel is prepared using N, O-carboxymethyl chitosan, and 4-armed benzaldehyde-terminated polyethylene glycol via reversible Schiff base crosslinks for systemic sclerosis treatment [398]. A natural self-healing IH was prepared from carboxymethyl chitosan and dialdehyde cellulose mixed with doxorubicin using dynamic Schiff-base and hydrogen linkages for drug delivery applications [399]. Yurui Wang and coworkers fabricated an adhesive-based IH composed of catechol-modified chitosan, N-isopropyl acrylamide, and NaHCO3 by a dual crosslinking mechanism for wound healing applications [400]. An IH that comprises carboxymethyl chitosan and aldehyde functionalized alginate was developed, and it was crosslinked through dynamic Schiff-base linkages for drug delivery to treat obesity [260]. A pH-responsive, injectable, and self-healing hydrogel was prepared by reacting oxidized hydroxypropyl cellulose with carboxymethyl chitosan via dynamic Schiff base linkages for targeted drug release [401]. An injectable, self-healing hydrogel was developed using quaternized chitosan and oxidized pectin via Schiff base crosslinks for potential use as a wound dressing material [402]. A multifunctional IH was fabricated using carboxymethyl chitosan, oxidized fucoidan, and polyphenol-metal nanoparticles of tannic acid-capped gold nanoparticles through Schiff base reaction for postoperative synergistic photothermal melanoma therapy and skin regeneration [403]. Schiff-base bonding synthesized An IH based on polyaldehyde gum arabic and carboxymethyl chitosan for localized breast cancer treatment [164]. A Schiff base crosslinked IH was synthesized by benzaldehyde-substituted agarose oligosaccharide and carboxymethyl chitosan through the Schiff base mechanism for wound dressing applications [404]. A selfhealing and conductive IH was developed based on oxidized pectin, N-succinyl chitosan, and graphene oxide via Schiff base crosslinks for tissue engineering applications [405]. A Schiff base crosslinked IH was synthesized using aldehyde-4arm polyethylene glycol and carboxymethyl chitosan via Schiff base crosslinks for wound healing applications [406]. Chitosan and polyethylene glycol-based IH were designed by integrating photo-crosslink with Schiff base reaction for intervertebral disc repair [407]. An injectable adhesive dopamine functionalized oxidized hyaluronic acid and carboxymethyl chitosan collagen-based hydrogel was constructed via Schiff dynamic and ionic interaction for wound dressing [263]. A self-crosslinked IH was fabricated using oxidized alginate and carboxymethyl chitosan via Schiff base for dental enamel regeneration [166]. The thermo responsive, injectable, and self-healing hydrogel was prepared through the Schiff base between aldehyde-functionalized poly(2-(2-methoxy ethoxy) ethyl methacrylate)-co-oligo(ethylene glycol) methacrylate-co-2-hydroxyethyl methacrylate) and hydroxypropyl chitosan for cancer therapy [408]. A carboxymethyl cellulose and aminated poloxamer 407-based thermosensitive IH was designed via a Schiff base mechanism to treat neovascular ocular diseases [409]. Li et al. constructed a hydrogel network by ionic bonding interactions between quaternized chitosan and epigallocatechin gallate-Zn complexes for wound dressing applications [410]. A self-healing and IH was synthesized using multialdehyde gum arabic and succinic anhydride chitosan via Schiff base crosslinks for anticancer drug delivery [272]. A degradable polysaccharide-based IH was formulated composed of carboxymethyl chitosan and oxidized alginate, integrated with hydroxyapatite nanoparticles and calcium carbonate microspheres under physiological conditions through Schiff base mechanism for drug delivery and

bone tissue engineering applications [273]. An injectable, self-healing, and biocompatible hydrogel was formulated based on N, O-carboxymethyl chitosan, and multialdehyde guar gum via Schiff base crosslinks for sustained anticancer drug delivery [274]. A self-healing and injectable polysaccharide-based hydrogel was prepared based on carboxymethyl chitosan and calcium pre-cross-linked oxidized gellan gum cross-linked by the Schiff-base reaction for bone tissue engineering [275]. In situ, IHs were prepared based on carboxymethyl chitosan and alginate by polyelectrolyte complexation for wound healing applications [411]. A self-healingbased IH was developed based on aldehyde-modified hyaluronic acid and glycol chitosan using a double crosslinking network for promoting periodontium regeneration in periodontitis [313]. Curcumin-loaded mesoporous polydopamine nanoparticles and metformin were introduced into the polymer matrix formed by the dynamic imine bonds and electrostatic interactions between carboxymethyl chitosan and oxidized hyaluronic acid to fabricate IHs for drug delivery applications [277]. A polysaccharidebased IH was prepared via Schiff base crosslinking of aldehyde-modified xanthan and carboxymethyl-modified chitosan for local drug delivery [278]. A covalently crosslinked composite chitosan-alginate hydrogel was prepared with pH sensitivity to drug delivery degradation [279]. A biocompatible and self-healing IH was designed based on modified-β-chitin and alginate for wound healing applications [280]. Self-healing hydrogels were prepared from partially oxidized hyaluronate and glycol chitosan in the presence of adipic acid dihydrazide via a combination of two dynamic bonds in the gels, including imine bonds obtained via a Schiff base reaction as well as acyl hydrazone for tissue engineering applications [322].

Table 2.9 Biomedical application of derivatized chitosan as an injectable hydrogel.

Srl.	Type of derivatized	Application	References
No.	chitosan		
1	Methacryloyl chitosan	Tissue adhesion	[389]
2	Quaternized chitosan	Wound dressing	[390]
3	Carboxymethyl chitosan	Burn healing	[391]
4	N-carboxyethyl chitosan	Bone regeneration	[234]
5	Carboxymethyl chitosan	Tissue regeneration	[316]
6	Carboxymethyl chitosan	Skin injury repair	[392]
7	Carboxymethyl chitosan	Wound healing	[317]
8	N, O-carboxymethyl chitosan	Doxorubicin release	[235]
9	Carboxymethyl chitosan	Wound healing	[237]
10	N-Carboxyethyl chitosan	Wound healing	[240]
11	Carboxymethyl chitosan	Tetracycline hydrochloride release and bone repair	[304]
12	Carboxymethyl chitosan	Wound healing	[393]

13	Carboxymethyl	Wound healing	[318]
	chitosan		
14	Carboxymethyl	Wound healing	[319]
	chitosan		
15	O-carboxymethyl	Wound dressing	[394]
	chitosan		
16	Quaternized chitosan	Tissue engineering	[248]
17	N-succinyl chitosan	Wound healing	[320]
18	Carboxymethyl	Tissue adhesive material	[250]
	chitosan		
19	N-Carboxyethyl	Wound dressing	[308]
	chitosan		
20	Hydroxypropyl	Tumor treatment	[395]
	chitosan		
21	Carboxymethyl	Wound healing	[251]
	chitosan		
22	Carboxymethyl	Treatment of periodontal disease.	[252]
	chitosan		
23	Carboxymethyl	Anal fistula wound treatment	[396]
	chitosan		
24	Carboxymethyl	Gastrointestinal drug release	[397]
	chitosan		
25	Carboxymethyl	Bone repair	[254]
	chitosan		
26	Quaternized chitosan	Wound dressing	[258]

27	N, O-carboxymethyl	Sclerosis treatment	[398]
	chitosan		
28	Carboxymethyl	Doxorubicin release	[399]
	chitosan		
29	Quaternized chitosan	Wound healing	[400]
30	Carboxymethyl	Obesity treatment	[260]
	chitosan		
31	Carboxymethyl	Phenylalanine release	[401]
	chitosan		
32	Quaternized chitosan	Wound dressing	[402]
33	Carboxymethyl	Skin regeneration	[403]
	chitosan		
34	Carboxymethyl	Cancer treatment	[164]
	chitosan		
35	Carboxymethyl	Wound dressing	[404]
	chitosan		
36	N-succinyl chitosan	Tissue engineering	[405]
37	Carboxymethyl	Wound healing	[406]
	chitosan		
38	Methacrylate chitosan	Intervertebral disc repair	[407]
39	Carboxymethyl	Wound dressing	[263]
	chitosan		
40	Carboxymethyl	Dental enamel regeneration	[166]
	chitosan		
<u> </u>			

41	Hydroxypropyl	Cancer therapy	[408]
	chitosan		
42	Carboxymethyl	Treatment of neovascular ocular	[409]
	chitosan	diseases	
43	Quaternized chitosan	Wound dressing	[410]
44	Succinic anhydride chitosan	Nanocurcumin release	[272]
45	Carboxymethyl	Tetracycline release	[273]
	chitosan		
46	Carboxymethyl	Doxorubicin release	[274]
	chitosan		
47	Carboxymethyl	Bone tissue engineering	[275]
	chitosan		
48	Carboxymethyl	Wound healing	[411]
	chitosan		
49	Glycol chitosan	Wound healing	[313]
50	Carboxymethyl	Wound healing	[277]
	chitosan		
51	Carboxymethyl	Tissue scaffolds	[278]
	chitosan		
52	Carboxymethyl	5-fluorouracil drug release	[279]
	chitosan		
53	Carboxymethyl	Wound healing	[280]
	chitosan		
54	Glycol chitosan	Tissue engineering	[322]
L	<u>l</u>		

# 2.5 Moringa oleifera gum

MOG is a natural polymer obtained from the stem of the Moringa oleifera tree. The gum exudate released from the stem is initially white, which, on long exposures, turns reddish-brown or brownish-black in color. Other names include horseradish tree, drumstick tree, African Moringa, radish tree, arango, badumbo, ben, bentree, ben oil tree, caragua, murunga, murinna, moringo, la mu shu, maranga-calalu, and teberindo, in Sanskrit: Subhanjana, in hindi: Saguna and Sainjna, in Gujarati: Suragavo, in Tamil: Mulaga and Munaga, in Malayalam: Murinna and Sigru, in Punjabi: Sainjna and Soanjna, in Unani: Sahajan, in other countries such as Africa the *Moringa oleifera* is commonly called by the name as the "Miracle Tree" or "Never Die Tree" and this has been honored as "Botanical of The Year-2017" through the National Institute of Health which cures 300 diseases [412]. The tree natively exists across various Asian and African countries, including India, Sri Lanka, Pakistan, Bangladesh, Afghanistan, Madagascar, and the Arabian Peninsula. The MOG has been identified and characterized using parameters such as particle characters, angle of repose, bulk density, tape density, Hausner ratio, and loss on drying. The properties of MOG include its composition primarily of polysaccharides, flavonoids, proteins, and various carbohydrates like d-xylose, l-arabinose, d-glucuronic acid, d-galactose, d-mannose, and 1-rhamnose. Furthermore, MOG has been characterized for its biodegradability, biocompatibility, and role as a stabilizing and reducing agent with diverse applications in various fields. MOG has been explored for its gel-forming nature to develop hydrogel wound dressings, indicating its potential in wound care and drug delivery applications [413]. The gum has been studied for its therapeutic properties, including antipyretic, antioxidant, antiasthmatic, astringent, and rubefacient properties. It has

been used traditionally to treat various ailments such as syphilis, gastrointestinal problems, and rheumatism [414]. MOG has been recognized for its techno-functional properties and applications in the food industry. It is considered a valuable source of commercial functional food and non-food products, highlighting its potential to enhance food products with added benefits [415]. Ahmad et al. synthesize a superabsorbent hydrogel based on MOG and polyvinyl alcohol cross-linked with borax for smart polymer-wide promising applications [416]. A MOG polysaccharides-based hydrogel was prepared with poly(acrylic acid) by radiation-induced crosslinking for slow drug delivery applications [417]. A low cost and biocompatible hydrogels were synthesized using chitosan and MOG biopolymers through Maillard reaction with glutaraldehyde as a crosslinker for removal of anionic Azo-dye (congo red) [418]. A MOG polysaccharides-based hydrogel was prepared with poly(acrylic acid) by radiation-induced crosslinking for slow drug delivery applications [417].A MOG and sterculia gum polysaccharides-based hydrogel was designed through grafting and crosslinking polymerization via NNMBA crosslinker for wound dressing applications [419]. A hydrogel was formed by radiation-induced crosslinked copolymerization of acrylamide onto moringa gum for drug delivery applications [420]. MOG and sterculia gum polysaccharides have been explored to design the network structure in hydrogels, which can act as a wound dressing for better wound healing using NNMBA crosslinker [413]. A radiation-induced graft copolymerization technique made N-vinyl imidazole hydrogels onto MOG polysaccharides for biomedical applications [421]. The dietary fiber moringa gum was modified through graft copolymerization with polyvinylpyrolle in the presence of NNMBA as a crosslinker to form a three-dimensional network structure in copolymeric hydrogels for drug delivery applications [422]. Singh et al.

developed a hydrogel based on dietary fiber moringa gum and poly(2-acrylamido-2-methylpropane sulphonic acid) crosslinked with NNMBA and loaded with ciprofloxacin for wound dressings applications [423]. A moringa gum polysaccharides-based hydrogel was designed to enhance wound healing using a radiation-induced crosslinking technique as a slow drug carrier [424]. Singh *et al.* developed ciprofloxacin-impregnated dietary fiber psyllium-moringa gum-alginate network hydrogels via a green approach crosslinked with a CaCl<sub>2</sub> crosslinker for use

**Table 2.10** Various applications of MOG-based hydrogel

Srl.	Natural	Method	Application	References
No.	gum			
1	MOG	Radiation-induced crosslinking	Ciprofloxacin release	[417]
2	MOG	FRP/NNMBA	Wound dressing	[419]
3	MOG	Gamma radiation	Levofloxacin release	[420]
4	MOG	FRP/NNMBA	Wound dressing	[413]
5	MOG	Gamma radiation	Levofloxacin release	[421]
6	MOG	FRP/NNMBA	Meropenem release	[422]
7	MOG	FRP/NNMBA	Ciprofloxacin release	[423]
8	MOG	Gamma radiation	Wound dressing	[424]
9	MOG	Ionic interaction/CaCl <sub>2</sub> crosslinker	Ciprofloxacin release	[425]
10	MOG	FRP/NNMBA	Doxorubicin release	[426]
11	MOG	Microwave irradiation	Metronidazole release	[427]

12	MOG	Borax	Superabsorbent	[416]
		crosslinker	polymer	
13	MOG	Glutaraldehyde	Removal of anionic	[418]
			azo dye (congo red)	

in a gastro-retentive drug delivery system [425]. MOG–based pH-responsive nanogel was functionalized as a doxorubicin carrier via free radical polymerization through the γ-irradiation method using acrylamide and NNMBA crosslinker [426]. A pH-sensitive and biocompatible microwave-irradiated MOG-carrageenan interpenetrating isotropic polymeric network hydrogel was formulated for controlled drug delivery [427].

## 2.6 Mesquite gum

Mesquite gum (*Prosopis juliflora*) is a natural gum obtained from the sap of various mesquite species native to the southwestern United States and northern Mexico. MG is a viscous, sticky substance that hardens into a brittle, glassy solid when dried. Depending on the source and processing method, it has a pale yellow to reddish-brown color. The gum is soluble in water, forming highly viscous solutions. The main constituents of MG are galactose and arabinose. It also contains small amounts of proteins, lipids, and minerals. MG has been found to have a 4-O methyl glucuronogalactan core, which is a high proportion of  $1\rightarrow 3'$  linked  $\beta$ -D-galactopyranose residues. The structure of the polysaccharides is highly branched, providing the gum with its unique properties [36]. MG has various applications across various industries due to its unique physical, chemical, and functional properties [428]. MG is used in the food industry as a thickening and stabilizing agent in sauces, dressings, gravies, and condiments; emulsifier and fat replacer in dairy products, ice

cream, and other food emulsions; binding and gelling agent in baked goods, confectionery, and processed meats, clarifying and filtering agent in fruit juices and wines [429]. In pharmaceutical and cosmetic industries, MG is used as a binder and disintegrant in tablet and capsule formulations; suspending and emulsifying agent in lotions, creams, and ointments; viscosity modifier and stabilizer in personal care products like shampoos and toothpaste; bio adhesive and film-forming agent for drug delivery systems [430]. It has been utilized in other industrial applications such as adhesive and binding agent in paper, textiles, and wood products, flocculant and coagulant in water treatment and wastewater purification, ink and coating additive for improved viscosity, stability, and film-forming properties, encapsulation and controlled release agent for flavors, fragrances, and other active ingredients [431]. Additionally, the gum has been used in agricultural areas as a soil conditioner and flocculant for water purification in agrarian settings, seed coating and germination enhancer, biopesticide, and antifungal agent for crop protection [432]. The versatility of MG is attributed to its excellent emulsifying, stabilizing, and thickening properties, as well as its biodegradability and relative abundance. Its natural origin, sustainability, and safety profile make it a preferred alternative to synthetic gums and polymers in various industries.

#### 2.7 Neem Gum

NG is a natural extract from the neem tree (*Azadirachta indica*) by induced or natural injury. The gum is extracted from the trunk and branches of the neem tree. It is a sticky, resinous substance that hardens upon drying. It is a clear, bright, and amber-colored material non-bitter in taste and soluble in cold water [433]. NG has been traditionally used in Ayurveda for oral health care and is commonly known as the toothbrush tree

in India, where neem twigs are frequently used to clean the teeth. NG primarily comprises polysaccharides, which comprise around 60-80% of its structure. The main polysaccharides in NG are arabinogalactans, galactans, and glucans with traces of proteins, lipids, and minerals. The polysaccharides in NG have a highly branched structure. The backbone consists of  $(1\rightarrow 3)$ -linked  $\beta$ -D-galactopyranose units. Side chains are composed of  $(1\rightarrow 6)$ -linked  $\alpha$ -L-arabinofuranose and  $(1\rightarrow 6)$ -linked  $\beta$ -Dgalactopyranose units. The polysaccharides contain hydroxyl, carboxyl, and other functional groups. These groups contribute to the gum's ability to form hydrogen bonds and interact with other molecules [434]. The functional groups also confer antioxidant and antimicrobial properties. NG is hydrophilic and water-soluble, forming viscous solutions. It has excellent emulsifying, suspending, stabilizing, and thickening properties. It is resistant to heat, acids, and enzymes. NG has various applications in the food, cosmetic, and pharmaceutical industries [435]. NG has various applications across various industries due to its unique physical, chemical, and biological properties [436]. It is used in the food industry as a thickening and stabilizing agent in sauces, dressings, and jams; emulsifier in mayonnaise, ice cream, and other oil-in-water emulsions; gelling and binding agent in confectionery, bakery, and dairy products; clarifying agent in fruit juices and wines [437]. NG is utilized in the pharmaceutical industry as a binder and disintegrant in tablet and capsule formulations, a suspending and emulsifying agent in syrups, lotions, and ointments, a film-forming agent for controlled drug delivery systems, a mucoadhesive agent for improved bioavailability of drugs [434]. It has been broadly used in the cosmetic industry as an emulsifier and stabilizer in creams, lotions, and gels; thickening agent in shampoos, toothpaste, and skin care products; emollient and moisturizing agent in skin and hair care formulations;

antimicrobial preservative in cosmetic products [438]. NG is also used in agricultural applications such as seed coating and germination enhancers, soil conditioners and flocculants for water purification, biopesticides, and fungicides for crop protection [439]. Additionally, NG has some industrial applications also, such as adhesive and binding agents in paper, textiles, and packaging materials, flocculants and coagulants in water treatment processes, ink and coating additives for improved viscosity and stability, encapsulation and delivery agents for fragrances and flavors. The versatility of NG is attributed to its excellent emulsifying, stabilizing, thickening, and binding properties and its antimicrobial and antioxidant activities. Its natural origin, biodegradability, and safety profile make it a preferred alternative to synthetic gums and polymers in various industries. Rishabha Malviya synthesized a hydrogel composed of acrylamide graft copolymers of Azadirachta indica gum and characterized the prepared hydrogel as a flocculating agent and ineffective removal of cationic dye methylene blue from aqueous solution using microwave irradiation [440]. A biodegradable, hemocompatible, and antimicrobial NG grafted with polyacrylamide hydrogel was prepared using a microwave for biomedical applications [441]. A NG based pH-responsive hydrogel matrix was prepared under microwave irradiation using an NNMBA crosslinker for the sustained release of anticancer drug [442]. The NGbased hydrogel wound dressings were designed by the graft-copolymerization reaction in the presence of cross-linker NNMBA with encapsulation of the antibiotic drug cefuroxime to improve wound healing [443]. NG and their semisynthetic derivatives acrylamide graft copolymer of NG and carboxymethylated NG synthesized a hydrogel by free radical-induced microwave-assisted polymerization for drug release applications [444]. Durgacharan et al. synthesize acrylamide grafted NG polymer

hydrogel using free-radical based microwave-assisted polymerization reaction for drug release retardation ability [445]. Singh et al. synthesize a hydrogel using Azadirachta indica gum grafted with copolymerization of 2-hydroxyethyl methacrylate in the presence of an NNMBA crosslinker for use in drug delivery carrier of methylprednisolone [446]. A similar research was carried out using graft copolymerization of the polyacrylamide onto Azadirachta indica gum polysaccharide NNMBA in the presence of crosslinker to form the interpenetrating network structure in hydrogels for use in biomedical applications [447]. A hydrogel was designed by graft-copolymerization reaction of carbopol, NG, and acrylamide using an NNMBA crosslinker for drug release applications [448]. An acrylamide-grafted NG hydrogel was synthesized using a free-radical-based microwave-assisted polymerization reaction to deliver ciprofloxacin [449]. Baljit Singh and coworkers formulated a hydrogel composed of graft-copolymerization of polyvinylpyrrolidone onto Azadirachta indica gum polysaccharide in the presence of NNMBA crosslinker for use in drug delivery applications [450]. Azadirachta indica gum-based hydrogel was synthesized using acrylic acid as a monomer and NNMBA as a crosslinker for drug delivery [451]. A NG polysaccharides-based hydrogel was developed functionalizing with carbazole and poly(acrylamide) using an NNMBA crosslinker for wound healing purposes [452]. A non-toxic and tissue-compatible NG-based polyvinyl acetate grafted NG amphiphilic graft copolymer hydrogel was designed using the microwave-assisted free radical technique for drug delivery applications [453]. Kirti Rajput designed a dual crosslinked low methoxy pectin-neem gum-mediated interpenetrating polymer network floating mucoadhesive microbeads by using the ionic gelation for lansoprazole gastro-retentive delivery [454]. A bacterial cellulose-carbopol hydrogel

loaded with *Azadirachta indica* gum was prepared using NNMBA crosslinker for burn wound healing [455].

Table 2.10 Various applications of neem gum-based hydrogel

Srl.	Natural	Method	Method Application	
No.	gum			
1	NG	Microwave	Propose for biomedical	[441]
		irradiation		
2	NG	FRP/NNMBA	Methotrexate release	[442]
3	NG	FRP/NNMBA	Cefuroxime release	[443]
4	NG	Microwave	Etoricoxib release	[444]
		irradiation		
5	NG	Microwave	Propranolol HCl release	[445]
		irradiation		
6	NG	FRP/NNMBA	Methylprednisolone release	[446]
7	NG	FRP/NNMBA	Methylprednisolone release	[447]
8	NG	FRP/NNMBA	Levofloxacin release	[448]
9	NG	Microwave	Ciprofloxacin	[449]
		irradiation	Hydrochloride release	
10	NG	FRP/NNMBA	Methylprednisolone release	[450]
11	NG	FRP/NNMBA	Methylprednisolone release	[451]
12	NG	FRP/NNMBA	Moxifloxacin release	[452]
13	NG	Microwave	Curcumin release	[453]
		irradiation		

14	NG	Ionic gelation	lansoprazole release	[454]
15	NG	FRP/NNMBA	Wound healing	[455]
16	NG	microwave irradiation	Removal of methylene blue	[440]

#### 2.8 Okra Gum

Okra gum (Abelmoschus esculentus) is a natural polysaccharide primarily composed of glucose, galactose, rhamnose, galacturonic acid, and glucuronic acid. OG is typically extracted from okra pods using water or aqueous solutions, followed by precipitation, purification, and drying processes [456]. OG is generally considered as safe (GRAS) for food use and a natural alternative to synthetic thickeners and stabilizers [457]. It has good thermal and acid stability and is compatible with various other ingredients [458]. OG is commonly used as a thickener, stabilizer, and emulsifier in various food products, such as frozen desserts, sauces, dressings, and beverages [459]. It benefits products that require stability at high temperatures or low pH levels. OG is valued for its functional properties and status as a natural, plant-based hydrocolloid. It is popular in various industries seeking natural and sustainable alternatives to synthetic additives [460]. OG has applications in pharmaceuticals, cosmetics, and other sectors [461]. It is a binder, disintegrant, and controlled-release agent in pharmaceutical products. It is also used in personal care products like shampoos and lotions for its thickening and stabilizing properties [462]. Singh et al. synthesize an eco-friendly okra-psyllium-based hydrogel through the free radical crosslinking method by using citric acid-ammonium persulphate as a crosslinkerinitiator system for efficient removal of uranium and crystal violet dye from aqueous

media [463]. A green hydrogel was synthesized and composed of okra polysaccharide reinforced with poly-vinyl alcohol and guar gum cross-linked by citric acid, which was used to release nano-curcumin [464]. A xanthan gum, a κ-carrageenan-based hydrogel with okra powder, was examined to develop hydrogel pads for drug delivery [465]. A pH-sensitive OG /gelatin-based polymeric blend hydrogel was created through an aqueous polymerization method using an NNMBA crosslinker loaded with cytarabine to treat various cancerous diseases [50]. A stretchable and self-healing based hydrogel was prepared using okra polysaccharide, polyvinyl alcohol, and borax as crosslinker enriched with a conductive layer of silver nanowires for fast-response and ultrasensitive strain sensors [466]. A biodegradable and hemocompatible alginate/okra hydrogel film was prepared using a solvent-casting method using a CaCl<sub>2</sub> crosslinker, and it has promising stability for use in biological applications [467]. The OG was chemically modified with acrylic acid by free radical polymerization using an ethylene glycol dimethacrylate crosslinker to formulate hydrogel for controlled release of Calendula officinalis [468]. A hydrogel was designed to contain okra pods/chia seeds mucilage using an NNMBA crosslinker for drug delivery applications [469]. The polymeric microspheres were synthesized and composed of OG and alginate using a CaCl<sub>2</sub> crosslinker for the controlled release of oxcarbazepine [49].

**Table 2.11** Various applications of okra gum-based hydrogel

Srl. No.	Natural gum	Method/crosslinker	Application	References
1	OG	Citric acid crosslinker	Nanocurcumin release	[464]

2	OG	FRP/NNMBA	Drug delivery	[465]
3	OG	FRP/NNMBA	Cytarabine release	[50]
4	OG	Borax crosslinker	Strain sensor	[466]
5	OG	CaCl <sub>2</sub> crosslinker	Wound healing	[467]
6	OG	ethylene glycol dimethacrylate crosslinker	Bovine serum albumin release	[468]
7	OG	FRP/NNMBA	Nettle extract release	[469]
8	OG	CaCl <sub>2</sub> crosslinker	Oxcarbazepine release	[49]
9	OG	Citric acid crosslinker	Removal of uranium and crystal violet dye	[463]

#### **CHAPTER 3**

#### **MATERIALS AND METHODS**

#### 3.1 Materials

MOG and NG were purchased from Nutramine Life Science, New Delhi, India, and MG and OG were purchased from Indianjadibooti Pvt. Ltd., Tamilnadu, India. Chitosan was procured from Otto Chemical Pvt. Ltd. (Degree of deacetylation >85%, pH - 7 to 9, viscosity (1% w/v) - <200cps). Sodium periodate (NaIO<sub>4</sub>) and hydroxylamine hydrochloride (HONH<sub>2</sub>HCl) were obtained from CDH chemicals. Ethylene glycol, isopropyl alcohol, and monochloroacetic acid were acquired from Thomas Baker Chemicals Pvt. Ltd. Sodium hydroxide (NaOH) pellets from Fisher Scientific Chemical. Ethanol used of minimum 99.9% purity. M/S Unicure India Limited provided the Ciprofloxacin HCl drug as a gift. Mili Q (MQ) water was used for all the reactions. All the chemicals and solvents were used as received.

# 3.2 Methods

## 3.2.1 Oxidation of gum

# 3.2.1.1 Oxidation of MOG

Oxidation of MOG was carried out to generate aldehyde groups using NaIO<sub>4</sub> as per the protocol described by Zang *et al.* with slight modification [470]. Briefly, a known

amount of MOG (1% w/v) was dissolved in MQ water on a digital magnetic stirrer for 24 hours at 400 RPM at 27°C. After complete dissolution, a varying amount of NaIO<sub>4</sub> (1%, 3%, 5%, 7% w/v) was added into the aqueous solution in a stepwise manner, and the reaction was continued for 24 hours at 27°C in dark conditions to prevent auto acceleration. The unreacted NaIO<sub>4</sub> was removed with an excess of ethylene glycol. The solution was poured into a glass petridish and placed inside the hot air oven at 50°C until a constant weight was achieved. The MOG sample oxidized with 1%, 3%, 5%, and 7% w/v of NaIO<sub>4</sub> was abbreviated as MOG-CHO-1, MOG-CHO-3, MOG-CHO-5, and MOG-CHO-7 respectively. A pH metric titration was used to calculate the aldehyde percentage of oxidized MOG (Equation 1). Briefly, a known amount of oxidized gum (0.1 g) was dissolved in 20 ml of 0.25 mol L<sup>-1</sup> of hydroxyl amine hydrochloride and titrated against 0.1 M NaOH. Aldehyde groups in the oxidized MOG reacted with the hydroxyl amine hydrochloride and released HCl, which reacted with NaOH (Schemes 3.1 and 3.2).

$$MOG - (CHO)_n + H_2N - OH \cdot HCl \rightarrow MOG - (CH = N - OH) + H_2O + HCl$$
 (Scheme 3.1)

$$HCl + NaOH \rightarrow NaCl + H_2O$$
 (Scheme 3.2)

CHO% = 
$$\frac{194.18 \times C \times \Delta v \times 10^{-3}}{2 \times w} \times 100$$
 (1)

C – Concentration of NaOH

Δv – Difference in the volume of NaOH

w - Weight of oxidized MOG

## 3.2.1.2 Oxidation of MG

MG was oxidized to produce aldehyde groups using sodium periodate. In summary, MQ water was combined with a known amount of MG (1 % w/v) and stirred at 400 RPM for 24 hours at 27 °C. After complete dissolution, NaIO<sub>4</sub> was gradually added to the aqueous solution at different concentrations (0.5 %, 1 %, 2 %, and 3 % w/v). The reaction lasted 24 hours at 27 °C in the dark to avoid auto-acceleration. The reaction was stopped using the ethylene glycol. The solution was dialyzed against MQ water for around four days to remove the unreacted product. The mixture was then put into a plastic petri dish and kept in a hot air oven at 50 °C. The MG samples oxidized with 0.5 %, 1 %, 2 % and 3 % NaIO<sub>4</sub> are abbreviated as MG-CHO-0.5, MG-CHO-1, MG-CHO-2, and MG-CHO-3 respectively.

The aldehyde percentage of oxidized MG gum was ascertained by pH metric titration (Equation 2). Briefly, 20 mL of hydroxyl amine hydrochloride solution containing 0.1 g of known oxidized gum at 0.25 mM was used to titrate the mixture against 0.1 mL of NaOH. The hydroxyl amine's hydrochloride and the aldehyde groups in the oxidized MG combine to form HCl, which then combines with sodium hydroxide (Schemes 3.3 and 3.4).

$$\label{eq:mg-choice} \text{MG} - (\text{CHO})_n + \text{H}_2 \text{N} - \text{OH} \cdot \text{HCl} \rightarrow \text{MG} - (\text{CH} = \text{N} - \text{OH}) + \text{H}_2 \text{O} + \text{HCl} \quad \text{(Scheme 3.3)}$$

$$HCl + NaOH \rightarrow NaCl + H_2O$$
 (Scheme 3.4)

$$CH0\% = \frac{{}^{194.18 \times C \times \Delta v \times 10^{-3}}}{{}^{2 \times w}} \times 100 \tag{2}$$

C – Concentration of NaOH

Δv – Difference in the volume of NaOH

w - Weight of oxidized MG

## 3.2.1.3 Oxidation of NG

Oxidation of NG was carried out to generate aldehyde groups using sodium periodate. MQ water was mixed with a known quantity of NG (1 % w/v) for 24 hours at 400 RPM at 27 °C. After complete dissolution, NaIO<sub>4</sub> was incrementally added to the aqueous solution in varied concentrations (0.1 %, 0.3 %, 0.5 %, and 1 % w/v), and the reaction was continued for 24 hours at 27 °C in the dark to prevent auto-acceleration. The ethylene glycol was used to terminate the reaction. The solution was dialyzed against MQ water for around 4 days to eliminate the unreacted product. Then, the solution was added to a plastic petri dish and heated in a hot air oven at 50 °C. The NG samples oxidized with 0.1 %, 0.3 %, 0.5 % and 1 % NaIO<sub>4</sub> are abbreviated as NG-CHO-0.1, NG-CHO-0.3, NG-CHO-0.5, and NG-CHO-1 respectively.

A pH metric titration was used to determine the aldehyde percentage of oxidized NG gum (Equation 3). A known quantity of oxidized gum (0.1 g) was dissolved in 20 mL of hydroxyl amine hydrochloride solution at a concentration of 0.25 M and titrated against 0.1 M NaOH. Aldehyde groups in the oxidized NG react with the hydroxyl amine hydrochloride to generate HCl, reacting with the sodium hydroxide (Schemes 3.5 and 3.6).

$$NG - (CHO)_n + H_2N - OH \cdot HCl \rightarrow NG - (CH = N - OH) + H_2O + HCl$$
 (Scheme 3.5)  
 $HCl + NaOH \rightarrow NaCl + H_2O$  (Scheme 3.6)

$$CH0\% = \frac{{}^{194.18 \times C \times \Delta v \times 10^{-3}}}{{}^{2 \times w}} \times 100 \tag{3}$$

C – Concentration of NaOH

Δv – Difference in the volume of NaOH

w – Weight of oxidized NG

## 3.2.1.4 Oxidation of OG

Oxidation of OG was carried out to generate aldehyde groups using sodium periodate. Briefly, a known quantity of OG was dissolved in MQ water for 24 hours at 400 RPM at 50 °C. Centrifugation was carried out at 3000 RPM for 15 minutes to eliminate the undissolved content of OG, followed by the separation of supernatant, which contains only the soluble part of OG. The soluble part was dried in a hot air oven (yield=85±5%) and dissolved in MQ water (1 % w/v). Then, sodium periodate (1.5 g) was incrementally added to the dissolved OG solution, and the reaction was continually stirred for 24 hours at 50 °C in the dark to prevent auto-acceleration. The ethylene glycol was used to terminate the reaction. The solution was dialyzed against MQ water for four days to eliminate the unreacted product. Then, the oxidized OG (OG-CHO) solution was poured into a polycarbonate petri dish and put in a hot air oven at 50 °C. The pH metric titration was used to determine the aldehyde percentage of OG-CHO, which was found to be 56±1.7% (Equation 4) (Schemes 3.7 and 3.8).

$$NG - (CHO)_n + H_2N - OH \cdot HCl \rightarrow NG - (CH = N - OH) + H_2O + HCl (Scheme 3.7)$$
  
 $HCl + NaOH \rightarrow NaCl + H_2O$  (Scheme 3.8)

CH0% = 
$$\frac{194.18 \times C \times \Delta v \times 10^{-3}}{2 \times w} \times 100$$
 (4)

C – Concentration of NaOH

Δv – Difference in the volume of NaOH

w - Weight of oxidized OG

#### 3.2.2 Derivatization of Chitosan

CMCh was synthesized following a procedure outlined in the literature, with slight modifications [471]. Briefly, 5 g of Chitosan was dispersed in 80 mL of isopropyl alcohol and stirred at 25°C. Subsequently, 25 mL of a 10 mol L-1 aqueous sodium hydroxide solution was divided into five equal parts and added to the suspension over 25 minutes. The entire alkaline suspension was continuously stirred at 800 rpm for 30 minutes. Then, monochloroacetic acid (10 g) was added dropwise at 5-minute intervals to each of the five parts. The reaction mixture was maintained at 60 °C and stirred for 3 hours. Finally, CMCh was obtained as a solid by filtering the reaction mixture and rinsing it multiple times with an 80% v/v ethanol solution. The resulting dried CMCh powder was obtained via oven drying.

The Degree of substitution (DS %) of CMCh was determined using back titration [472]. Briefly, 0.5 g of CMCh was dissolved in 100 mL of 0.04 M NaOH and, after complete dissolution, titrated against 0.05 M HCl using phenolphthalein as an indicator. The analyses were carried out in triplicate, and the DS % was determined using Equation 5.

$$DS \% = \frac{0.162 A}{1 - 0.058 A} \times 100 \tag{5}$$

$$A = \frac{(\text{Conc of NaOH} \times \text{Vol of NaOH}) - [\text{Conc of HCl} \times (\text{Vb} - \text{Vs})]}{m}$$

Vb – Volume of HCl consumed without CMCh

Vs – Volume of HCl consumed with CMCh

m – Weight of dry CMCh

# 3.2.3 Synthesis of IHs

#### 3.2.3.1 MOG-based IH

The known amount of oxidized MOG was dissolved in MQ water for about 24 hours at 700 RPM at 27°C (precursor 1). Similarly, CMCh (5% w/v) was dissolved in PBS at pH 7.4 at 700 RPM at 27°C (precursor 2). Then, two syringes of 18 gauge (G) were filled with equal amounts of the precursors and extruded simultaneously into a glass vial (10ml) at physiological temperature (37°C). Immediate gel formation was observed.

#### **3.2.3.2 MG-based IH**

The known amount of oxidized MG gum was dissolved in MQ water at 700 RPM and 27 °C (precursor 1). CMCh (5 % w/v) was dissolved using a similar process in PBS at pH 7.4, 700 RPM, and 27 °C (precursor 2). Next, at physiological temperature (37 °C), equal volumes of both precursors were concurrently extruded into two distinct syringes of 21 G, each carrying 5 mL of precursors. Gel formation began immediately.

#### **3.2.3.3 NG-based IH**

The known quantity of oxidized NG was dissolved in MQ water (precursor 1) at 700 RPM for 24 hours at 27 °C. A similar procedure was used to dissolve CMCh (5 % w/v) in PBS at pH 7.4 at 700 RPM at 27 °C (precursor 2). After that, equal amounts of both precursors were simultaneously extruded into a vial through two separate syringes of 18 gauzes, each holding 5 mL<sup>-1</sup> of precursors at a physiological temperature (37 °C). Gel formation started right away.

## **3.2.3.4 OG-based IH**

The known quantity of OG-CHO was dissolved in MQ water (precursor 1) for 4 hours at 700 RPM and 27 °C. A similar procedure was used to dissolve CMCh (5 % w/v) in PBS at pH 7.4 for 700 RPM at 27 °C (precursor 2). After that, both precursors were simultaneously extruded into a vial through two separate syringes of 26 G at 37°C. After some time, gelation occurred.

#### 3.3 Characterization

The Fourier transform spectroscopy test was performed in ATR mode on a Perkin Elmer 2000 instrument for qualitative analysis. The samples were analyzed in the frequency range of 500–4000 cm<sup>-1</sup> and a resolution of 4 cm<sup>-1</sup>. <sup>1</sup>H NMR was recorded on Bruker advance III, 500 MHz, using D<sub>2</sub>O and CDCl<sub>3</sub> as the solvent. Chemical shift (δ) values were reported in ppm using tetramethyl silane as an internal reference. The morphological features were studied in a scanning electron microscope (ZEISS, EVO 18). The double adhesive carbon tape was used to mount gold-coated samples. The photomicrographs were recorded at different magnifications. The UV–visible absorption spectra were recorded using a UV-1800 spectrophotometer (Shimadzu, Japan).

# 3.3.1 Tube Inversion Test

A tube inversion test was performed in which different concentrations of precursor 1 and precursor 2 were simultaneously extruded into a glass vial of 10 ml capacity at 37°C. The physical status of the IH was examined by tilting the vial at 45° and then inverted completely at physiological temperature. The flow of gel was observed visually. IH was not able to flow gravimetrically itself, which confirmed the gelation.

The test was performed three times to know the precise gelation time of the synthesized IH.

## 3.3.2 Gel content

A known amount of IH (W<sub>a</sub>) was dipped in 100 ml of MQ water for 48 hours at 37°C. The water-insoluble IH was removed and dried to a constant weight (W<sub>b</sub>) in a hot air oven at 50°C. The percentage of gel content (GC %) was calculated using Equation 6. The trials were done in triplicate, and the analysis was carried out using the mean value of the three observations.

$$GC \% = \frac{W_b}{W_a} \times 100 \tag{6}$$

## 3.3.3 Porosity

The liquid displacement method was used to calculate the porosity of the IH [473]. A vial containing ethanol was filled with a known quantity of oven-dried IHs (Xb) and left for 24 hours. Parafilm was used to completely enclose the vial to prevent the ethanol from evaporating and spilling. After a day, the samples were taken from the vial and weighed (Xa). Equation (7) was utilized to ascertain the IH's porosity.

$$P\% = \frac{Xa \times V}{Xb} \times 100 \tag{7}$$

## 3.3.4 Load-bearing capacity and structural integrity

Synthesized IH was cut into three cylindrical discs of equal height and diameter. An empty glass beaker of 250 ml capacity (101 g) was allowed to stand vertically on the IH to analyze the IH's load-bearing capacity for 12 hours. Furthermore, IH was also examined for structural integrity by holding it through a stainless steel spatula over a height of 30 cm for 30 minutes above the ground gravimetrically.

## 3.3.5 Syringeability and injectability evaluation

The ability to inject the precursors using a needle is referred to as syringeability. Two syringes of 18 G with 10 ml capacity were used to conduct this test. The initial weight of the syringes was measured (W<sub>1</sub>). The precursors (10ml) were loaded in the syringes and extruded simultaneously. Both syringes' weights were measured upon extrusion (W<sub>2</sub>). The syringeability (SP %) was calculated using the equation 8. The trials were done in triplicate, and the analysis was carried out using the mean value of the three observed values.

$$SP \% = \frac{W_1}{W_2} \times 100 \tag{8}$$

Both precursors were extruded into a single syringe to calculate the injectability evaluation. After gelation, the synthesized IH was allowed to come out by manually applying pressure on the plunger and forming an image (DTU, J.K., and ③) in glass petridish.

#### 3.3.6 Self-healing evaluation

Self-healing was analyzed qualitatively according to the protocol used by Sadeghi-Abandansari and colleagues [474]. In order to evaluate the self-healing ability of the prepared IHs, two identical IH samples were synthesized separately in test tubes. To enable a clear visual distinction during the healing process, one of the IH samples was deliberately loaded with a colored dye, while the second IH sample was left unloaded, serving as a control. After gelation, the two cylindrical hydrogel specimens were carefully removed from their respective molds and brought into contact by manually joining their cross-sectional surfaces. This configuration allowed the interface between

the two specimens to act as the healing zone, where the intrinsic dynamic interactions within the polymeric network could facilitate reformation of bonds. The assembled samples were left undisturbed under ambient conditions for a predetermined interval of time, ensuring that sufficient molecular diffusion and reversible bonding could occur across the interface to achieve effective healing. Following this incubation period, the healed IH was gently transferred into a syringe to assess its cohesiveness and mechanical robustness. The IH was then extruded through the syringe into a polypropylene mold, demonstrating not only its injectability but also the degree of integrity regained after the healing process. The ability of the IH to be extruded as a continuous structure without visible disruption provided qualitative evidence of its self-healing efficiency.

# 3.3.7 Rheological properties of synthesized injectable hydrogel

At a temperature of 37 °C, an MCR-101 rheometer (Anton Paar, Japan) with a parallel plate was used to analyze various rheological parameters. The distance between the platform and the spindle was maintained at 0.5 mm during all experiments. A time sweep study was conducted in isothermal mode (37°C) to analyze the gelation behavior. The IHs underwent a one-hour incubation period (37°C) before testing. A flow sweep experiment in the range of 0.01–100 s<sup>-1</sup> was carried out to test the shearthinning capabilities and changes in viscosity. An amplitude sweep test was performed to ascertain the hydrogel's linear viscoelastic range (LVE). A varied strain amplitude (high 100% and low 1%) was then applied to the IHs to ascertain the mechanical properties under strain. Frequency sweep tests were conducted at 1% amplitude, covering a frequency range of 0.01 to 100 rad s<sup>-1</sup>. The self-healing behavior was quantitatively analyzed using a rheometer. An alternative strain sweep test with a fixed

angular frequency of 1 rad s<sup>-1</sup> was carried out. An amplitude oscillatory strain test was performed with high and low strain values.

# 3.3.8 Swelling ratio

The swelling ratio was evaluated in PBS under different pH conditions at physiological temperature. At pH 5.5 (acidic), it simulates the skin/wound environment that supports healing; at pH 7.4 (neutral), it reflects normal blood and tissue conditions; and at pH 8.5 (alkaline), it represents infected or chronic wounds, thereby modeling healthy, healing, and diseased states.

## 3.3.8.1 Swelling study from dry form (Method 1)

Briefly, oven-dried IHs were weighed and put in 50 mL of PBS at all pH. After a predetermined interval, gels were removed from their respective beakers, and the surface water was wiped out using filter paper and weighed.

## 3.3.8.2 Swelling study from gel form (Method 2)

The freshly synthesized IHs in gel form is immediately added to 50 mL of PBS at all pH. The swelling ratio (SR %) was determined by the amount of water absorbed by the IHs using Equation 9.

$$SR \% = \left[\frac{Ws - Wd}{Wd}\right] \times 100 \tag{9}$$

Where,

Wd - Dried weight of the IH

Ws – Swollen weight of the IH

The network parameters of IH were calculated in terms of the number of average molecular mass present between crosslinks ( $\overline{M}_c$ ), crosslink density ( $\rho$ ), and mesh size

( $\xi$ ). Florry – Rehner equation was used to calculate the number of average molecular mass between crosslinks.

$$\overline{M_c} = -\rho_{v^V m.1} \phi^{1/3} [\ln(1-\phi) + \phi + \chi \phi^2]^{-1}$$

Where,

 $\rho_p$  – density of polymer

 $v_{m,1}$  – molar volume of solvent

 $\phi$  – polymer volume fraction in the swollen state

 $\chi$  – Florry - Huggins interaction parameter

To calculate the Florry - Huggins interaction parameter, the following equation was used

$$\chi = \left[\phi(1-\phi)^{-1} + N\ln(1-\phi) + N\phi\right] \left[2\phi - \phi^2 N - \phi^2 T^{-1} \left(\frac{d\phi}{dT}\right)^{-1}\right]^{-1}$$

Where,

$$\phi = \left[ \left( \frac{\rho_p}{\rho_S} \right) \left( \frac{m_S - m_0}{m_0} \right) + 1 \right]^{-1}$$

$$N = \left(\frac{\phi^{2/3}}{3} - \frac{2}{3}\right) \left(\phi^{1/3} - \frac{2}{3}\phi\right)^{-1}$$

Where,

 $\rho_p$  – density of polymer

 $\rho_s$  – density of solvent

 $m_s$  – mass of polymer in the swollen state

 $m_o$  – a mass of polymer in a dry state

 $\left(\frac{d\phi}{dT}\right)$  – it was obtained by plotting the graph between volume fraction data and temperature. For this purpose, the swelling ratio was evaluated at 27°C, 37°C, and 47°C in MQ for 24 hours.

Crosslink density was calculated by using the following equation

$$\rho = \frac{1}{\bar{\nu}(\bar{M}_c)} = \frac{\rho_p}{\bar{M}_c}$$

Here,  $\bar{\nu} = \frac{1}{\rho_p}$  is the specific volume of the polymer.

The following equation was calculated using the mesh or mean pore size (nm).

$$\xi = 0.071 \phi^{-1/3} (\overline{M}_c)^{1/2}$$

## 3.3.9 Drug loading and release kinetics

Ciprofloxacin HCl (pKa values 6.1 and 8.7) is used as a model drug due to its high water solubility and change in ionization charge with wound pH. This allows faster release in acidic or alkaline infected wounds, while maintaining more sustained release at physiological pH, thereby supporting effective antibacterial action and wound healing. The calibration curve for the drug was prepared using a UV-visible spectrophotometer. To create precursor 3, an oxidized solution of each natural gum was mixed with a 3 mL aqueous solution of ciprofloxacin HCl (6 mg mL<sup>-1</sup>). The drugloaded IH was prepared by combining equal parts of precursor 2 and precursor 3. Drug release from IH was measured in two different ways.

# 3.3.9.1 Drug release from dry form of IHs (Method 1)

Synthesized IH was initially incubated for 4 hours at 37°C to enable complete crosslinking and then kept in a hot air oven at 50°C to dry completely. Button form drug-loaded IH was put in 100 mL PBS at all pH at 37°C.

## 3.3.9.2 Drug release from gel form of IHs (Method 2)

The freshly prepared drug-loaded IH was put in 100 mL PBS at all pH at 37°C.

For both drug release studies, the aliquots were taken at predetermined intervals from each medium and simultaneously refilled with fresh medium so that the overall volume of the release medium remained the same. Here, it was assumed that the drug molecules in the IH were distributed uniformly. The trials were done in triplicate, and the analysis was carried out using the mean value of the three observations. The amount of drug released was measured using UV-visible spectroscopy.

The Korsmeyer-Peppas (K-P) model was used to study the drug release pattern (Equation 10).

$$\frac{M_t}{M_m} = kt^n \tag{10}$$

Where  $M_t$  and  $M_{\infty}$  represent the cumulative drug concentrations released at time "t" and time infinity, respectively. "n" is the release exponent, which is used to describe the release mechanism, and "k" is the release rate constant, which depends on the matrix's geometry and structure.

#### 3.3.10 Cytotoxicity evaluation

The cytotoxicity of the IHs was assessed by the MTT test using the L-929 fibroblast cell line (obtained from NCCS Pune, India). The cells (between 5000 and 8000 cells per well) were grown in DMEM media with 10% FBS and 1% antibiotic solution for a whole day at 37°C and 5% CO<sub>2</sub> in 96-well plates. IH (Cipro loaded and unloaded) formulations varying in concentration from 1 to 1000 μg mL<sup>-1</sup> were applied to the cells the next day. MTT Solution was added to the cell culture and incubated for an

additional two hours at a final concentration of 250 µg mL<sup>-1</sup> following a 24-hour incubation period. After the experiment was over, the culture supernatant was discarded, and the cell layer matrix was dissolved in 100 µL of Dimethyl Sulfoxide (DMSO) and measured at 540 and 660 nm using an Elisa plate reader (iMark, Biorad, USA). Utilizing Graph Pad Prism-6 software, IC-50 was computed. Images were taken with an AmScope digital camera (10 MP Aptima CMOS) under an inverted microscope (Olympus ek2). The wells without IH were considered as the control.

## 3.3.11 Hemolysis assay

Human blood was centrifuged at 1000 g for 15 minutes at 4 °C to separate plasma and buffy coat, which were then removed. The erythrocytes were washed three times with PBS and prepared as a 1 % suspension in PBS. Subsequently, 500  $\mu$ L of the 1% erythrocyte suspension was dispensed into a 96-well plate and incubated for 30 minutes at 37 °C in the presence or absence of 100  $\mu$ L test samples across a concentration range of 1-1000  $\mu$ g mL<sup>-1</sup>. After incubation, 400  $\mu$ L of PBS was added to the samples. For the positive control representing 100 % hemolysis, 400  $\mu$ L of RBC lysis buffer was added to the control sample. Following centrifugation, 100  $\mu$ L of the supernatant solution was transferred to a fresh 96-well plate, and the absorbance was measured at 540 nm using a microplate reader (iMark, BioRad).

#### 3.3.12 Antibacterial assay

The antibacterial activity was evaluated using the zone inhibition method, also known as the Kirby-Bauer method. Both *S. aureus* and *E. coli* were selected as representative models for gram-positive and gram-negative bacteria, respectively. The Mueller–Hinton agar plates were inoculated by spreading with 100 µL of each bacterium culture

(approx cell density  $1.5 \times 10^8$  CFU/ mL) and followed by placing the discs containing  $10~\mu\text{L}$  of different concentrations (0 to 100~mg/mL). One disc (5 mm) on each plate was loaded with solvent alone, serving as the vehicle control, while a Ciprofloxacin disc ( $10~\mu\text{g}$ ) was used as the positive control. The plates were then incubated at  $37~^\circ\text{C}$  for 24 hours. The clear zones around the discs were measured and recorded to assess the antibacterial activity. Three replicates were conducted for each compound against each bacterium.

# 3.3.13 Hydrolytic degradation

After attaining the equilibrium swelling, a known quantity of IH (dry and gel form) was submerged in PBS at pH 7.4 and 37°C (w<sub>a</sub>); at a predetermined interval, the samples were removed from the solution, wiped out the surface, and reweighed (w<sub>b</sub>). Percentage degradation (HD %) was calculated using weight loss using Equation 11. The trials were done in triplicate, and the analysis was carried out using the mean value of the three observations.

$$HD \% = \frac{w_a - w_b}{w_a} \times 100 \tag{11}$$

# Statistical analysis

All experimental measurements are reported as the mean ± standard deviation (SD) to provide an estimate of the variability and reliability of the data. Each experiment was independently repeated a minimum of three times to ensure reproducibility and consistency of the results. To determine whether observed differences between experimental groups were statistically significant, a one-way analysis of variance (ANOVA) was performed. Differences were considered statistically significant at a

confidence level of p < 0.05. All statistical calculations, data organization, and analyses were conducted using Microsoft Excel 2010 software, which facilitated data processing and graphical representation of the results.

#### **CHAPTER 4**

# SYNTHESIS AND CHARACTERIZATION OF INJECTABLE HYDROGEL BASED ON MULTIALDEHYDE Moringa oleifera GUM CROSSLINKED WITH CARBOXYMETHYL CHITOSAN VIA SCHIFF BASE MECHANISM

## 4.1 Introduction

This chapter describes the synthesis of an IH based on oxidized *Moringa oleifera* gum, and carboxymethyl chitosan crosslinked through the Schiff base mechanism at 37°C (Fig. 4.1). The IH's physical, structural, and morphological properties are evaluated. The swelling behavior is assessed in PBS at pH 5.4 and 7.4 at 37°C. The ciprofloxacin HCl drug is loaded *in situ* in dry and gel form of IH, and drug release kinetics are assessed in PBS at pH 5.5 and 7.4 at 37°C. Furthermore, the biocompatibility evaluation is assessed through cytotoxicity assay and hemolysis assay. Furthermore, the biodegradability of the IHs is also evaluated in PBS at pH 7.4 at 37°C.

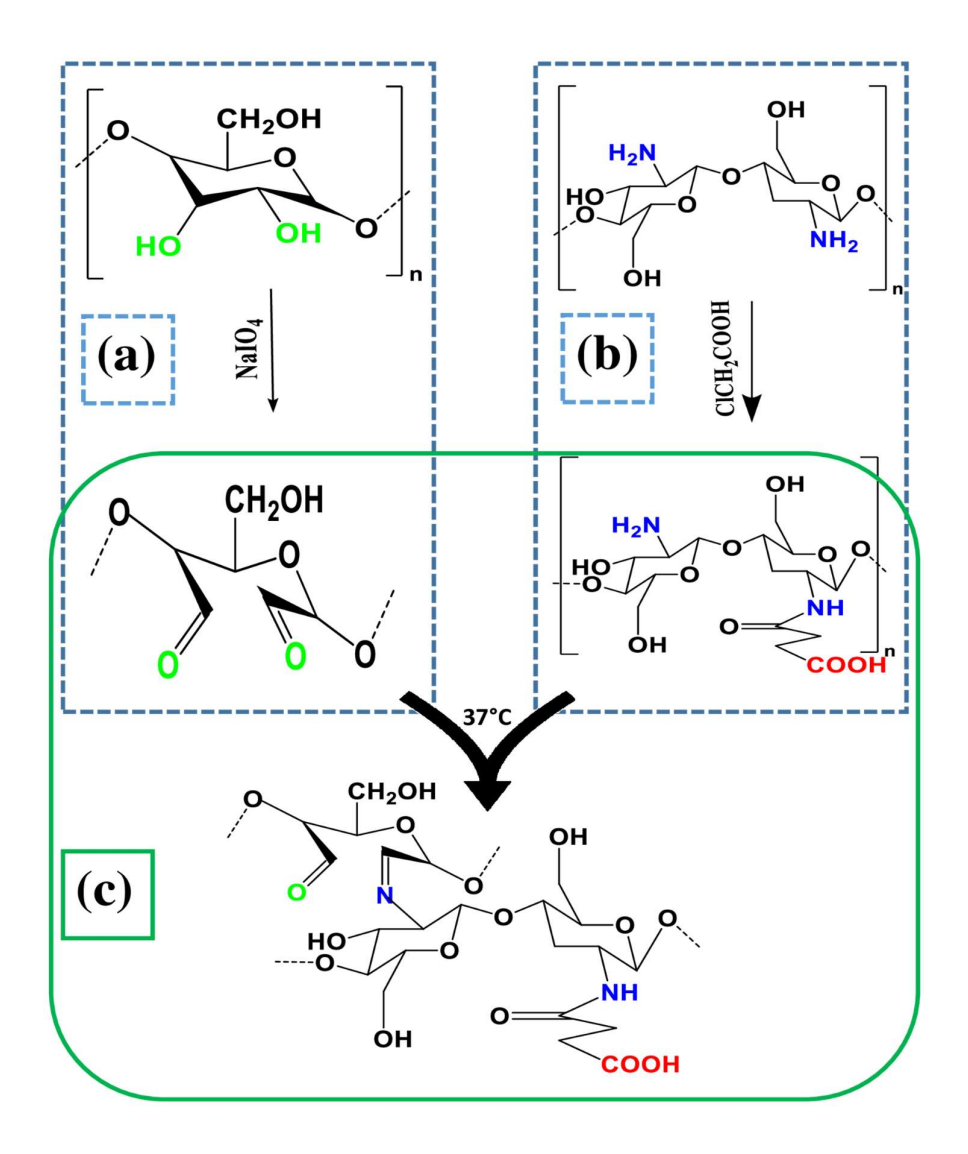


**Fig. 4.1** (a) Oxidation of *Moringa oleifera* gum (MOG-CHO-3), (b) Derivatization of chitosan (CMCh), (c) Synthesis of injectable hydrogel (IH-3-7)

# 4.2 Effect of Concentration of NaIO<sub>4</sub> on Gelation time

Table 4.1. shows the effect of the derivatization of MOG on gelation time. With the increase in the concentration of the NaIO<sub>4</sub>(1% w/v to 3% w/v), gelation time decreases and becomes almost constant with further increase (3% w/v to 7% w/v). This behavior was primarily because increasing the concentration of the oxidizing agent increases

the conversion of hydroxyl groups to aldehyde groups. The amount of aldehyde % was calculated and was found to be increased from 46.5±2.3 % to 87.8±2.6 %. This behavior was explained by calculating the ratio of aldehyde % to the amine group present on CMCh (Table 1). Results indicated that a 1% (w/v) addition of NaIO<sub>4</sub> gives a value of 0.75, while an almost constant value was obtained with the addition of 3, 5, and 7 % (w/v) of NaIO<sub>4</sub>, i.e., 1.31, 1.30 and 1.30 respectively. For various types of polysaccharide hydrogels, it is necessary to adjust the ratio of the aldehyde group to the amino group to achieve an effective Schiff base reaction. An improper ratio of the aldehydic to the amino group would result in a longer gelation time. Nair et al. synthesized an IH using derivatized hyaluronic acid and chitosan, and hyaluronic acid was derivatized using NaIO<sub>4</sub>. The required amount of NaIO<sub>4</sub> was added, successful oxidation degrees of 10, 15, and 25% were achieved, and the observed gelation time was 8 seconds [16]. Similar work has been reported by Su et al, in which they reported the same procedure of derivation of hyaluronic acid; briefly, hyaluronic acid was oxidized by the addition of a different amount of NaIO4 to achieve the various oxidation degrees, and results show that with an increase in concentration of NaIO<sub>4</sub> increase the oxidation degree from 27% to 60%, which decreases the gelation time from 175 seconds to 145 seconds [475]. From this study, the concentration of sodium periodate was optimized at 3% w/v for further studies.

**4.3 Effect of Concentration of Oxidized** *Moringa Oleifera* Gum on Gelation time Table 4.2. shows the effect of the concentration of oxidized MOG on gelation time. Here, the concentration of the oxidizing agent was kept constant at 3% w/v. The table clearly shows that with an increase in concentration of oxidized MOG (1% w/v to 7% w/v), a decrease in gelation time is observed (40 minutes to 4 minutes). Further, the

increment of oxidized MOG (9% w/v) increases the gelation time (30 minutes) because the number of aldehyde groups in oxidized MOG is more than the amine group in CMCh.

Therefore, a surplus amount of aldehyde groups may hinder the formation of gels. This is primarily because a total number of aldehyde functional groups is more likely to react with the amine groups of derivatized chitosan. Furthermore, this behavior is explained with the simple unitary method in which, as a ratio (Table 2) continuously increases from 1.31 to 11.8, gelation time decreases (40±5 minutes to 4±1 minutes). Pandit *et al.* reported a work in which they fabricated IH using oxidized gum Arabic by adding 0.5 g of NaIO4 and achieved an oxidation degree of around 44%; they varied the amount of derivatized gum Arabic (20% to 40%) by which gelation time was decreased (42 seconds to 29 seconds) [476]. From the above study, the concentration of oxidized *Moringa oleifera* gum (MOG-CHO-3) is optimized as 7% w/v. Sample IH-3-7 is found to be optimized IH to be used for further characterization.

Table 4.1 Effect of concentration of NaIO<sub>4</sub> on gelation time of injectable hydrogels

Sample code	MOG % (w/v)	NaIO <sub>4</sub> % (w/v)	Aldehyde % (A)	Amine concentration in CMCh (%) (B)	Ratio $= \frac{A}{B}$	Gelation time (minutes)
IH-1-1	1	1	46.5±2.3	67±2.11	0.75	30±3.5
IH-3-1	1	3	87.8±2.6	67±2.11	1.31	9±2.5
IH-5-1	1	5	87±2.5	67±2.11	1.30	10±2
IH-7-1	1	7	87.6±2.6	67±2.11	1.30	9±1.5

**Table 4.2** Effect of concentration of oxidized *Moringa oleifera* gum (MOG-CHO-3) on gelation time

Sample	Conc. of	The aldehyde	Amine	Ratio	Gelation
code	MOG- CHO-3	concentration present in	group present in	$=\frac{\mathbf{A}\times\mathbf{B}}{\mathbf{C}}$	time (minutes)
	(% w/v)	<b>МО</b> G-СНО-3	CMCh (%)		
	<b>(B)</b>	(%) (A)	(C)		
IH-3-1	1	87.8±2.5	67±2.11	1.31	40±5
IH-3-3	3	87.8±2.5	67±2.11	3.9	10±2.5
IH-3-5	5	87.8±2.5	67±2.11	6.5	8±1.5
IH-3-7	7	87.8±2.5	67±2.11	9.2	4±1
IH-3-9	9	87.8±2.5	67±2.11	11.8	30±5

# 4.4 Physical properties of injectable hydrogel

The physical properties of color, gel content, porosity, syringeability, self-healing ability, and network parameters are given in Table 4.3. The gel content and porosity of IH-3-7 are found to be  $60\pm2\%$  and  $35\pm2.5\%$ , respectively.

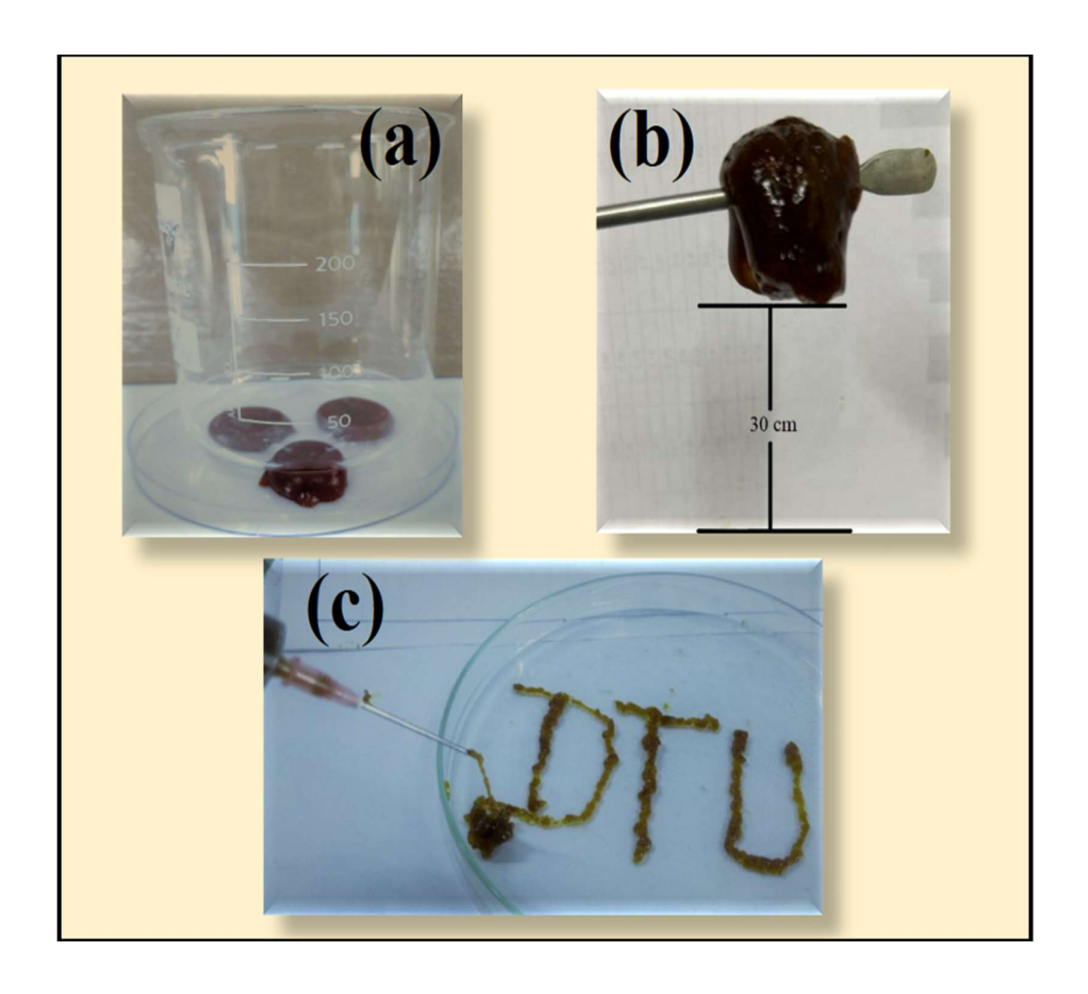


**Fig. 4.2** Physical properties of injectable hydrogel (a) Load bearing capacity (b) structural integrity (c) injectability

The higher gel content suggests the IH-3-7 has a good crosslink network via an imine bond. The porosity of IH-3-7 was described in terms of mesh size and the average molecular weights between crosslinks. Additionally, porosity determination helps understand the voids in the IH. Lima *et al.* published a research article based on Schiff base crosslinking using oxidized galactomannan and N-succinyl chitosan, in which they evaluated porosity determination of 69% [477]. Yan *et al.* fabricated an IH using Schiff base chemistry between poly(L-glutamic acid) and chitosan, in which the observed gel content was 79% [478].

According to a study on load-bearing capacity, IH-3-7 has sufficient strength to support a load of roughly 101 g for 12 hours (Fig. 4.2.a) without any structural damage to its shape. Furthermore, it maintains its shape while holding into a "U" shape using a stainless-steel spatula over a height of 30 cm for 30 minutes above the ground (**Fig.** 4.2.b). The tests confirmed that the IH-3-7 has load-bearing strength and structural integrity.

The syringeability percentage was calculated, and the result obtained was nearly 99±0.5%. This data confirmed that IH-3-7 possesses good syringeability properties when extruded through an 18 G needle. Wang et al. reported a research article in which they transformed copper sulfide into an IH which was further utilized for photothermal therapy. They used a syringe of various sizes (26 G, 25 G, 23 G, 18 G) and revealed that 26 G gave the best result among all [479]. Additionally, their injectability was investigated to make the synthesized hydrogels appropriate for clinical procedures. No worldwide guidelines or regulations govern how to conduct the test; however, various research articles have reported several injectability tests [480, 481]. The gauge of the needle used in calculating the values must be the same as used in the industrial setting to administer hydrogel precursors subcutaneously, ranging from 18-21 G to 26-27 G. This study successfully carried out the injectability evaluation test using an 18 G. Fig. 4.2.c shows an image (DTU) formed by extruded IH-3-7 using a 10mL capacity needle (18 G) in glass petridish. Easy flow through the needle confirmed the ease of accessibility. Qu et al. synthesized an IH using N-carboxyethyl chitosan and di benzaldehyde-terminated poly(ethylene glycol) by Schiff base reactions, in which they evaluated injectability in vivo using a 22 G needle and found ease out of IH after gel formation [482].

**Table 4.3** Physical properties of IH-3-7

Property	value
Color	Dark maroon
Gel content	60±3.5%
Porosity	35±2.5%
Syringeability	99±0.5%
Average molecular weight between crosslinks	2.1613×10 <sup>3</sup> g/mol
Crosslink density	2×10 <sup>-4</sup> mol/cm <sup>3</sup>
Mesh size	4.570 nm

Self-healing behavior was observed after 3 hours when two cylindrical shaped IH-3-7 (one is loaded with yellow dye another is remain unloaded) are placed together (Fig. 4.3.a). The IH-3-7 was dark maroon in color. Therefore, the addition of yellow dye was not visible, and manually joining the two cylinders was not visible. Further, these cut cylinders were placed in the 10 mL capacity syringe to form a disc-shaped sample. When the mold was inverted, the disc shape sample was found intact after 3 hours (Fig. 4.3.b). The two samples were seen integrating after 3 hours, demonstrating that the reversible Schiff-base bond connection was rebuilt to repair the cut surfaces, which confirmed the self-healing behavior of IH-3-7. Qu *et al.* synthesized an IH using Schiff base crosslinks between quaternized chitosan and benzaldehyde-terminated Pluronic; their self-healing evaluation showed that synthesized IH took 2 hours to self-heal [483].

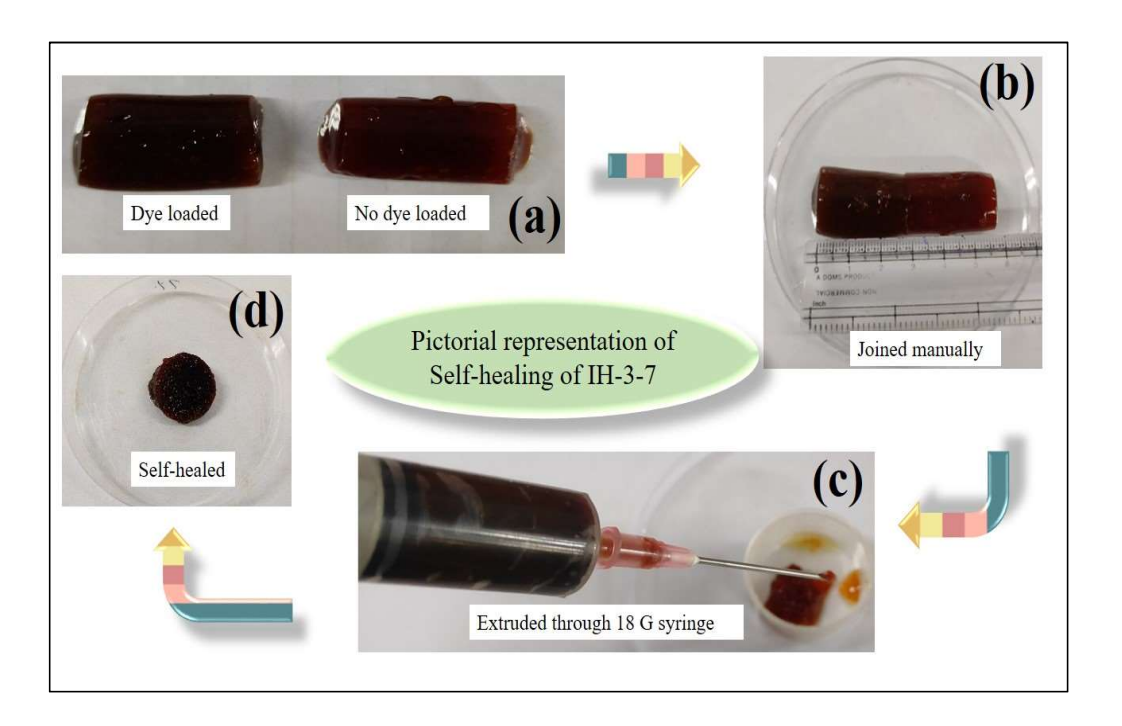


**Fig. 4.3** (a) IH-3-7 cut into two halves, (b) Gels were joined together manually, (c) Filled and extruded through an 18 G needle, and (d) button-shaped self-healed IH-3-7

# **4.5 Structural Properties**

Structural properties of the IH-3-7 are characterized using FT-IR and <sup>1</sup>H NMR. Fig. 4.4a to 4.4c show the FT-IR spectra of the MOG, MOG-CHO-3, Chitosan, CMCh, and IH-3-7. A broad peak is observed at 3397 cm<sup>-1</sup> which is due to the presence of the hydroxyl group (O-H stretching), peak at 2920 cm<sup>-1</sup>, which corresponds to C-H stretching of the alkane group, and 1603 cm<sup>-1</sup> which is due to the presence of glucuronic acid (-COOH stretching), in addition to this, peak at 1040 cm<sup>-1</sup> attributed to the polysaccharide structure, are observed in the FT-IR spectra of pure MOG (Fig. 4.4a) [484]. After MOG reacts with sodium periodate, significant peaks are observed at 1730 and 873 cm<sup>-1</sup> (Fig. 4.4a), mainly attributed to the production of symmetrical

vibration of aldehydes and hemiacetal bonds, respectively. Another comparative research study shows similar outcomes for the oxidized product [485]. The FT-IR spectra of pure chitosan (Fig. 4.4b) show the amino group's bending vibrational peak at 1570 cm<sup>-1</sup>, the Chitosan saccharide's C-O-C asymmetric structure at 1250 cm<sup>-1</sup>, and the C-O stretching vibration at 1024cm<sup>-1</sup>. The FT-IR spectrum of CMCh (Fig. 4.4b) reveals the existence of two additional peaks at 1644 and 1420 cm<sup>-1</sup>, which are attributable to symmetric and asymmetric stretching vibrational modes of the -COO group, respectively, and indicate the successful derivatization of chitosan and confirmed the presence of carboxymethyl groups on CMCh [486]. IH-3-7 hydrogel's FT-IR spectrum (Fig. 4.4c) shows a peak at 1642 cm<sup>-1</sup>, which demonstrates imine structure formation due to the dynamic Schiff base crosslinking reaction between the amine group of CMCh and the aldehyde groups of MOG-CHO. Further, the development of the Schiff base connection is shown by the loss of the aldehyde peak in the IH-3-7 spectrum [487].

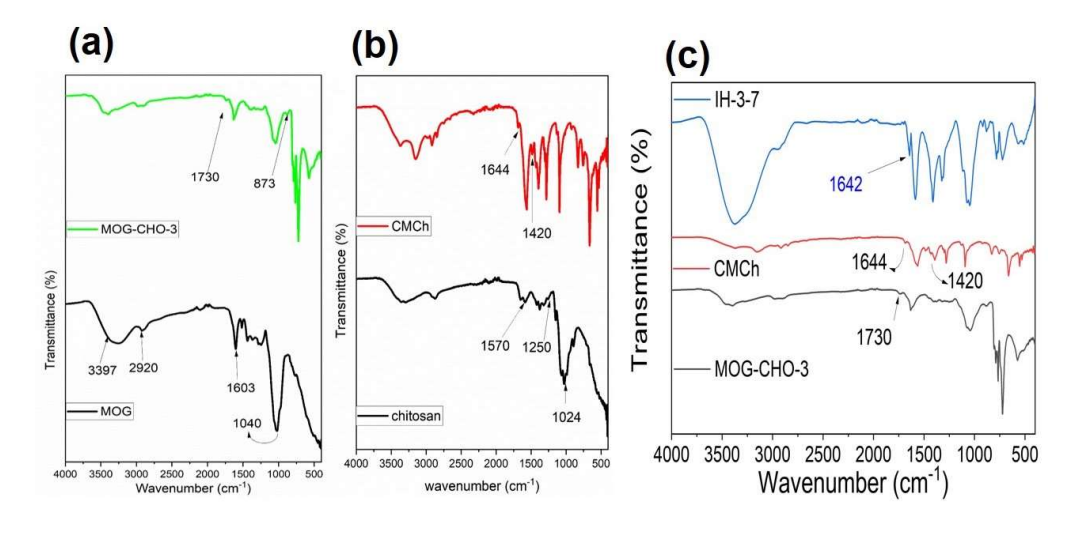


**Fig. 4.4** FT-IR spectra of (a) MOG, MOG-CHO-3 (b) chitosan, CMCh and (c) MOG-CHO-3, CMCh, IH-3-7.

<sup>1</sup>H-NMR was conducted for MOG and oxidized MOG samples. Fig. 4.5a shows that the peak caused by the tetramethyl silane reference appeared at 0 ppm. CDCl<sub>3</sub> was used to dissolve MOG. The peak at 7.25 shows the aromatic hydrogen. The peak at 4.42 ppm confirms the hydroxyl group. The aldehyde group's –hydrogen is shown at 2.15 ppm. The significant concentration of the hydrogen justified the polysaccharide (rhamnose) to be present in the MOG's soluble portion. The peak at 1.24 ppm suggests the presence of methyl hydrogen in rhamnose. These chemical shifts are similar to those previously reported by Koley *et* al. for pure MOG [488]. A new distinctive peak of the aldehydic proton is observed at 9.31 ppm, which confirms the oxidation of MOG (Fig. 4.5.b)

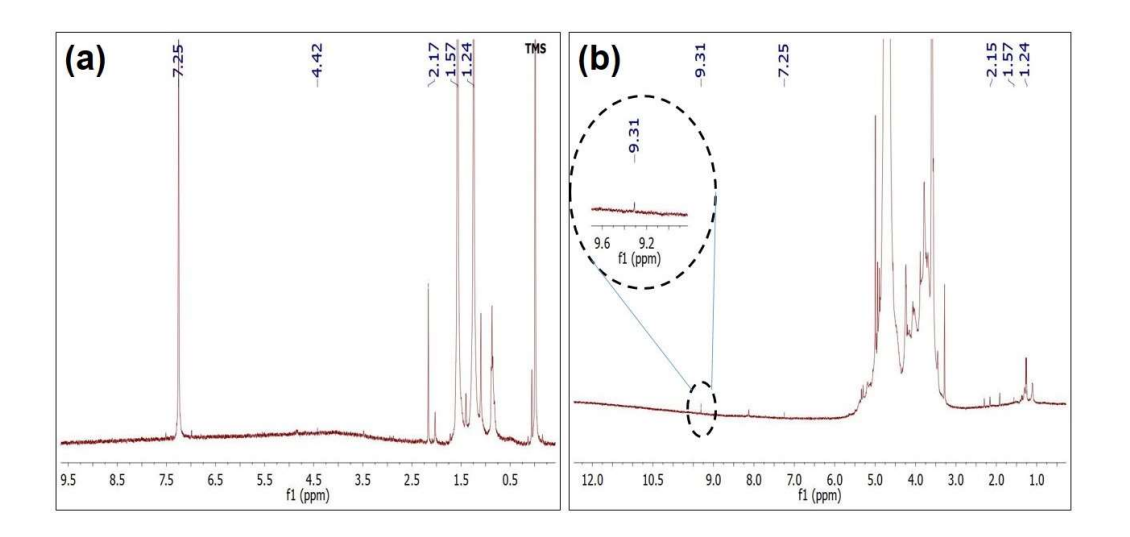


Fig. 4.5 <sup>1</sup>H-NMR spectra of (a) MOG (b) MOG-CHO-3

## 4.6 Rheological Properties

To check the shear thinning behavior, a continuous flow sweep test (1-1000 1 s<sup>-1</sup>, 1% constant strain) was performed at 37°C, in which the IH-3-7 hydrogel being sandwiched between the parallel plates of the instrument was permitted to squeeze at progressively higher shear rates. It is observed that as the shear rate increases, the medium's viscosity reduces (23324 to 9.52 m Pa.s), which shows the shear thinning behavior of hydrogel. The shear thinning behavior of hydrogel may be due to the breakage of Schiff base linkage at a high shear rate (Fig. 4.6.a). The shear thinning behavior of IH-3-7 further supports the data on syringeability and injectability. Wei *et al.* fabricated an IH using N-carboxyethyl chitosan and oxidized konjac glucomannan by Schiff base crosslinks; a flow sweep test was conducted, and results depicted a decrease in viscosity with an increased shear rate [489].

When measuring the amplitude sweep test of IH-3-7, it was subjected to several strain levels between 0.1 and 100% at 37°C (Fig. 4.6.b) to check the linear viscoelastic region (LVE). The LVE region is between 0.1 and 5 % of strain. A strain value of 1% was selected for all kinetic studies involving gelation. The maximum value of storage modulus (G') and loss modulus (G") is obtained at 138 Pa and 5 Pa, respectively. At different strain levels, hydrogels showed larger G' than G" values, and the crossover point at 40% of shear strain shows hydrogel changing its physical form from solid to liquid. Balitaan *et* al fabricated an IH using a Schiff base reaction between acrylamide-modified  $\beta$  -chitin and alginate dialdehyde. In the amplitude sweep test, strain value varied from (10° to 10<sup>4</sup>) %, and all the IHs showed higher storage modulus values than loss modulus [490].

In the frequency sweep test, the IH-3-7 shows a higher storage modulus than the loss modulus, which confirms its stiff and elastic behavior (Fig. 4.6.c). The high crosslink density results in a higher value of G' (115.83 pa) in IH-3-7 (Fig. 5c), limiting chain mobility and deformability. Li *et* al synthesized an IH using Schiff base chemistry and performed rheological studies. A frequency sweep test was performed (0.1 to 10 rad/s), and a higher value of G' (120 Pa) than G' (9.8 Pa) was found [491].

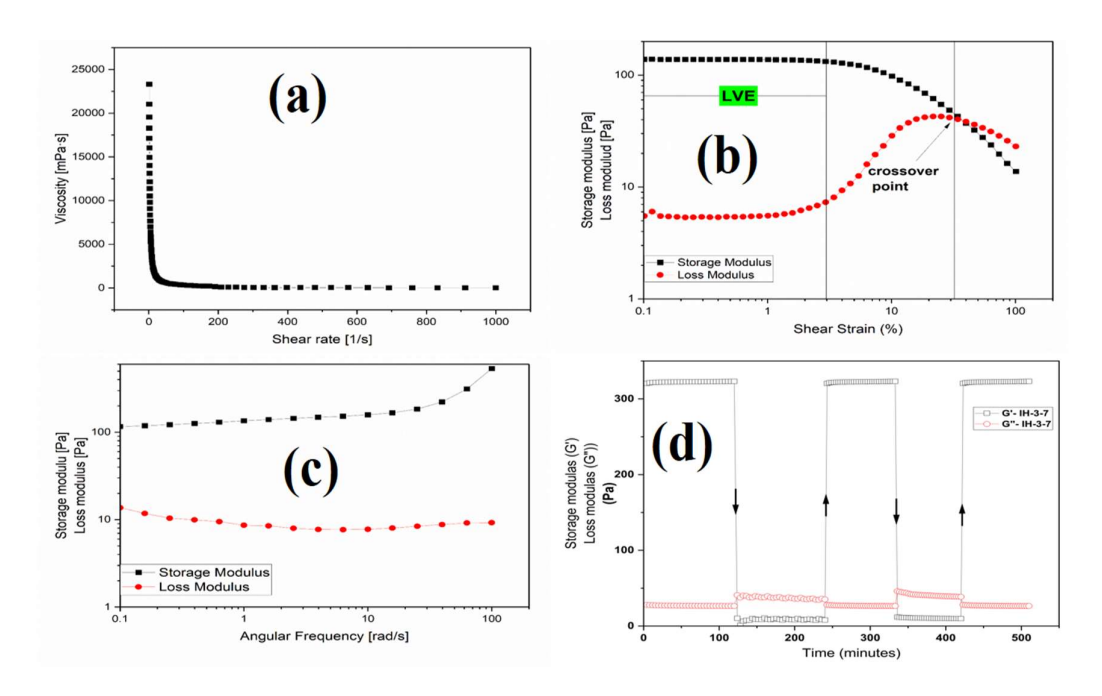


**Fig. 4. 6** Rheological study of IH-3-7 at 37°C (a) Flow sweep test (b) Amplitude sweep test (c) frequency sweep test (d) step-strain analysis

Oscillatory step-strain analyses were carried out to examine the self-healing characteristic of the IH-3-7. The G' value had a high magnitude value at low strain values (1%); as the strain shifted to high values (200%), the G' value was found to be closest to G" (Fig. 4.6.d). This resulted from the structure deforming at high strain values. The behaviors were stable over multiple cycles, indicating the self-healing capability and stability of the dynamic Schiff base and dynamic coordination network.

# 4.7 Morphological Evaluation

Scanning electron microscopy (SEM) images of IH-3-7 are presented in Fig. 4.7.a-b. SEM image (Fig. 4.7.a) shows scaly and heterogeneous spaces with porous hydrogel network structure. Surface morphology shows interconnected dense pores. A cuboidal granulated structure is also observed, possibly due to the unreacted part of MOG. The average diameter of pores was calculated using Image J software and found to be 4±1 μm. To confirm the unreacted part of MOG, an SEM analysis was carried out on dried IH after the gel content test. The SEM image is shown in Fig. 4.7.b. A clear image with interconnected pores structure is observed with an average pore size of 25.5±2 μm. Immersion in MQ water removes the unreacted content (gel content test). A porous structure is beneficial for drug delivery applications, as the drug can easily diffuse out from the hydrogel [492]. Grewal *et* al derivatized MOG and studied its properties, in which SEM images of pure MOG showed granular and scaly structures [493]. Guan *et* al fabricated an IH using Schiff base chemistry between oxidized dextran and gelatin, in which an SEM study reveals the surface pore size was 40 μm [494].

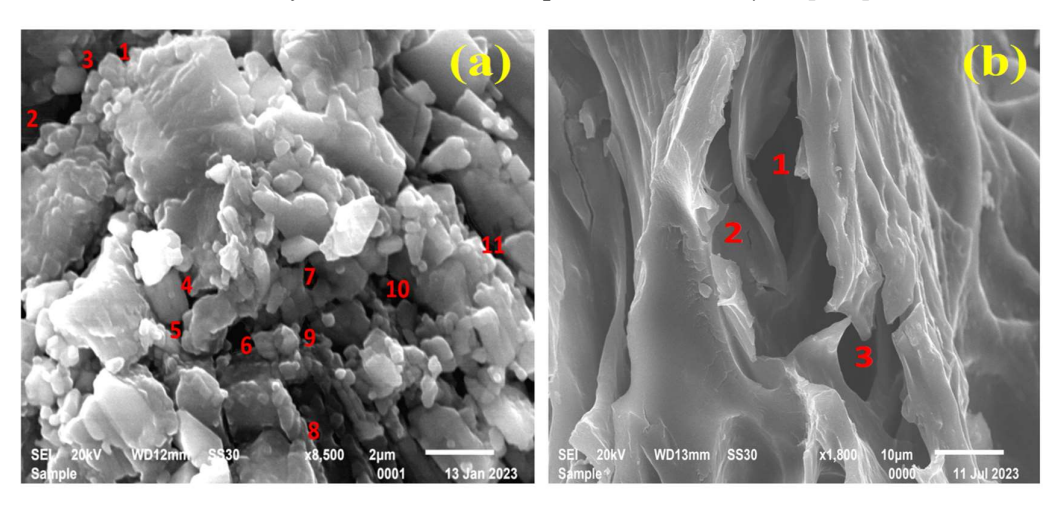


Fig. 4.7 SEM micrograph of IH-3-7 (a) before gel content (b) after gel content

# 4.8 Swelling Study

The swelling behavior of synthesized IHs is investigated in PBS at pH 5.5 and 7.4 at 37°C.

# 4.8.1 Swelling Study from Dry Form of IH-3-7 (Method 1)

Fig. 4.8.a shows the swelling behavior of IH-3-7 in dry form. Graph of swelling studies shows a maximum swelling ratio percentage of 415% at pH 5.5 and 209% at pH 7.4 in 110 minutes.

# 4.8.2 Swelling Study from Gel Form of IH-3-7 (Method 2)

The swelling behavior of IH-3-7 in its gel form is depicted in Fig. 4.8.b. Maximum swelling percentages are observed for pH 5.5 (830%) rather than pH 7.4 (430%) in 110 minutes.

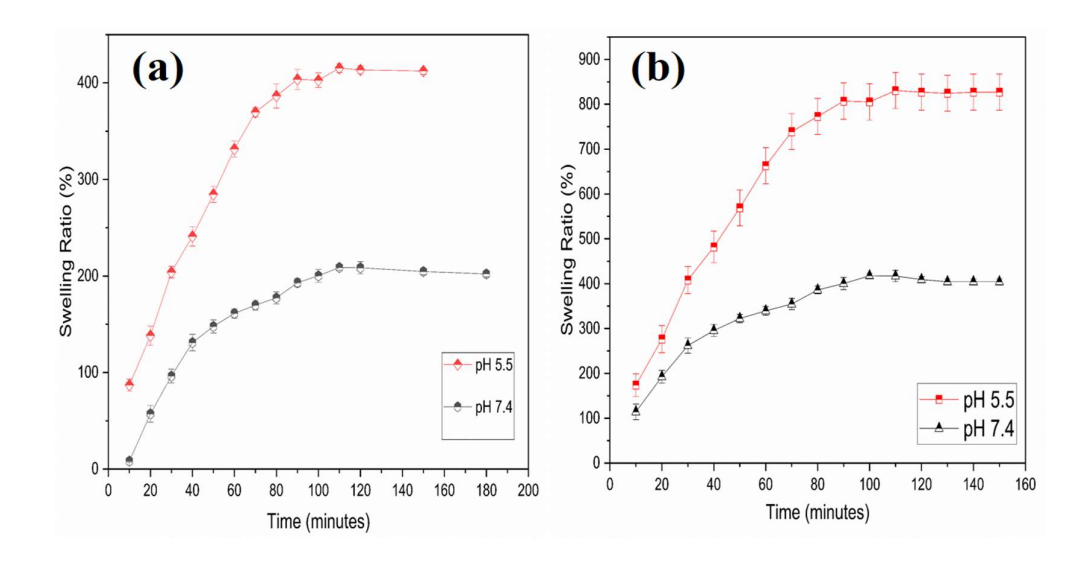


**Fig. 4.8** The swelling ratio of IH-3-7 in PBS (pH 5.5 and pH 7.4) at 37°C (a) dry form (b) gel form

Although the trend of swelling behavior for the dry form is similar to the freshly prepared gel form of IH-3-7, the swelling percentage is higher in the gel state of IH-3-7, which is also the requirement of IH. Furthermore, the swelling behavior of IH-3-7 relies on the pH of the solution (5.5 and 7.4). The swelling plots show that the swelling decreases as the pH increases, demonstrating pH-responsive swelling behavior. Protonation of the amino groups in chitosan occurs around pH 5.5, creating an electrostatic repulsion force between intra- and inter-polymeric chains. The outcome is a loosening of the polymeric network, which improves water pH of 7.4, which reduces the swelling percentage. In the literature swelling studies are reported for dry hydrogel. In a research article published by Pandit et al, in which they synthesized an IH using Schiff base crosslinks, swelling studies reveal that synthesized IH having the highest degree of crosslinking displays 151% swelling at pH 5.5. The inclusive trend shows higher swelling at a lower pH of 5.5 than at a high pH (7.4) at a given time interval [476]. Singh et al synthesized a hydrogel using Moringa oleifera gum and Sterculia gum in which the least swelling was observed (2.94 g/g) in pH 2.2 buffer in 24 hours [495].

# 4.9 Drug Release Study

The drug release behavior of IH-3-7 was assessed using ciprofloxacin HCl as a model drug. Ciprofloxacin HCl is an antibiotic for treating skin, urinary system, and respiratory tract bacterial infections. Two different strategies were applied, as described in the experimental section.

# 4.9.1 Drug Release from Dry Form of IH-3-7 (Method 1)

Initially, more drug release was observed in pH 7.4 than in pH 5.5 until 60 to 70 minutes; then, the release pattern was inverted. In other words, more release is observed in pH 5.5 (~ 847 μg 100mL<sup>-1</sup> g<sup>-1</sup> of IH-3-7) than in pH 7.4 (~ 719.12 μg 100mL<sup>-1</sup> g<sup>-1</sup> of IH-3-7) at a given time interval (~130 minutes). Additionally, it might be possible that, due to the higher level of swelling at pH 5.5, the same IH-3-7 showed higher drug release than at pH 7.4. The strength of the Schiff base connection weakens, and the electrostatic repulsive interactions among the protonated amino groups rise when the pH is lowered from 7.4 to 5.5, resulting in greater gaps for drug release (Fig. 4.9.a). A relatable research article published by Wu *et al.* in which an IH was fabricated using Schiff base chemistry and 5-fluorouracil drug release studies reported that higher release was observed at pH 6.0 (80%) than at PBS 7.0 (58.9%) [496]. Singh *et* al fabricated a hydrogel using *Moringa oleifera* gum and *Sterculia* gum in which the least release of levofloxacin drug was observed (60.387 mg L<sup>-1</sup>) in pH 2.2 buffer and follows non-Fickian diffusion [495].

#### 4.9.2 Drug Release from Gel Form of IH-3-7 (Method 2)

The synthesized gel form of IH-3-7 underwent the release of ciprofloxacin HCl at pH 5.5 and pH 7.4 at 37°C (Fig. 4.9.b). A higher amount of drug is released at pH 5.5 than 7.4. The maximum drug release in pH 5.5 is 993.65 µg 100mL<sup>-1</sup> g<sup>-1</sup> of IH-3-7. This is major because the effectiveness of the Schiff base linkage weakens, and the electrostatic repulsive interactions between the protonated amino groups are higher at low pH, resulting in greater gaps for the release of drugs. The drug release behavior is well correlated with swelling behavior.

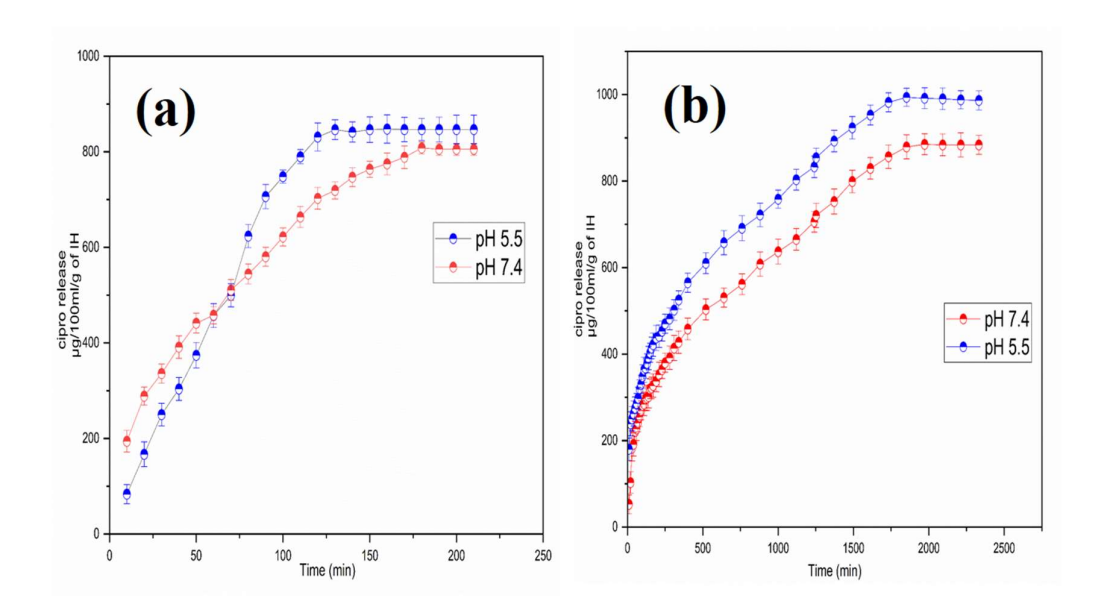


**Fig. 4.9** Drug release behavior of IH-3-7 in PBS (pH 5.5 and pH 7.4) at 37°C (a) Dry form (b) Gel form

While comparing the two methods, a uniform rate of drug release is observed, and it becomes constant after a certain time. Most of the drug release occurred in 150 minutes from the dry form of IH-3-7 (method-1). In the case of gel form, the drug release is found to be slow, and the overall drug release happened in 2000 minutes (method-2). In the actual situation, when IH is used for the wound site, method 2 is more realistic than method 1. The slow release of the drug will help reduce microbial growth at the wound site during the healing process.

**Table 4.4** K-P kinetic model parameters for IH-3-7

	P	Parameters associated with the K-P model					
Sample code		pH 7.4			рН 5.5		
	k	n	R <sup>2</sup>	k	n	R <sup>2</sup>	
IH-3-7 (dry form)	8.19	0.48	0.99	1.39	0.89	0.99	
IH-3-7 (gel form)	4.53	0.41	0.99	7.87	0.33	0.99	

K-P model provides the most accurate description of the antibiotic drug release mechanism for IH-3-7 as the regression coefficient (R<sup>2</sup>) is found to be 0.99. In the case of IH-3-7 dry form, the release exponent value "n" is found to be 0.86 at pH 5.5. It means that the drug follows the non-Fickian mechanism and the diffusion rate is higher than the relaxation rate of the hydrogel matrix. While at higher pH, the "n" value is less than 0.5. In the case of the IH-3-7 gel form, the "n" value is found to be less than 0.5 for both pH. This means that the drug follows the Fickian diffusion mechanism, and the drug diffusion rate is less than the hydrogel matrix's relaxation rate (Table 4.4.). Li *et* al reported that the 5-Fluorouracil drug release from IH generated by oxidized pectin and chitosan follows mostly Fickian diffusion at pH 6.8 and non-Fickian diffusion at pH 7.4 [497].

# 4.10 Cytotoxicity Evaluation

IHs must be biocompatible with host cells to serve as biomaterials for drug delivery applications. Therefore, MTT assay was used to study the cytotoxicity of IH-3-7 using

L-929 fibroblast cell lines in both the unloaded and drug-loaded stages. Up to 50 μg mL<sup>-1</sup> concentration, the unloaded IH-3-7 IH's MTT test shows no toxicity with 50% cell survival (Fig. 4.10.a). The cell viability decreased when the unloaded IH-3-7 concentration was above 50 μg mL<sup>-1</sup>. The existence of unreacted carbonyl groups in the MOG-CHO-3, which may interact with the cell proteins, may cause a modest reduction in cell viability. Additionally, the drug-loaded IH-3-7 showed insignificant toxicity up to 500 μg mL<sup>-1</sup> dose range, with 60% of the cells still viable after 24 hours of treatment. However, drug-loaded IH-3-7 showed cell viability of roughly 46% at a higher dosage (1000 μg mL<sup>-1</sup>), regarded as marginal toxicity and a sign of good biocompatibility against L-929 fibroblast cell lines.

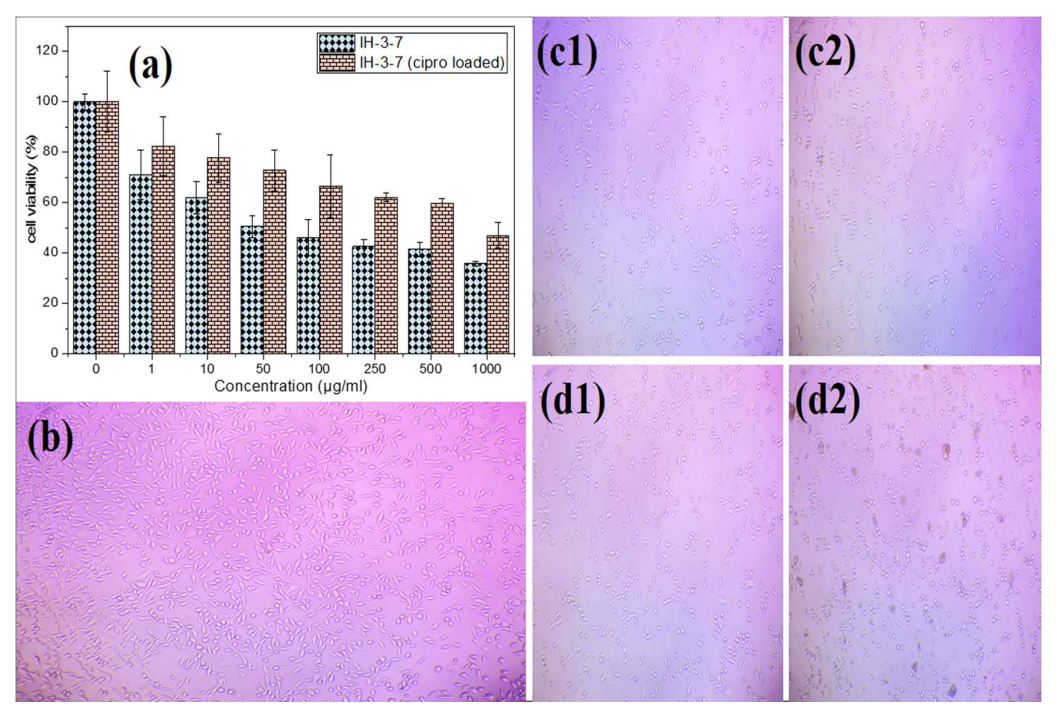


**Fig. 4.10** (a) Cell viability of IH-3-7 and cipro-loaded IH-3-7. Inverted phase microscopic images of (b) control. IH-3-7 treated L-929 cell line at (c1) 1μg mL<sup>-1</sup> (c2) 50 μg mL<sup>-1</sup>. Cipro loaded IH-3-7 treated L-929 cell line at (d1)1 μg mL<sup>-1</sup> (d2) 500 μg mL<sup>-1</sup> against fibroblast cell line L-929.

Drug molecules (Ciprofloxacin) may interact with host cell proteins to cause this reduction in cellular viability at higher concentrations. Furthermore, it was noted that the L-929 cells' morphology did not significantly change due to the treatment with drug-loaded and unloaded IH. The inverted phase microscopic images of the formulated IH are displayed in Fig. 4.10 (b to d2). The outcomes demonstrate that L-929 fibroblast cell lines interacted well with IH-3-7 in both loaded and unloaded forms. Consequently, the cytotoxicity evaluation showed no toxicity.

# 4.11 Hemolysis assay

Hemolysis, the rupture or lysis of red blood cells (erythrocytes), is a critical factor in assessing the biocompatibility of IH-3-7. Evaluating hemolysis for IH-3-7 is essential to determine its compatibility with blood, which is key for its potential use as a biomaterial in biomedical applications. The hemolysis rates of IH-3-7 across all tested concentrations (1 to 1000 µg mL<sup>-1</sup>) remain below 4%, meeting the standard criteria for acceptable hemolysis rates in biomaterials (Fig. 4.11.). This indicates that IH-3-7 exhibits negligible hemolytic activity, maintaining hemolysis rates well within the acceptable threshold. Therefore, IH-3-7 demonstrates good biocompatibility with blood components, making it a promising candidate for biomedical applications involving blood contact.

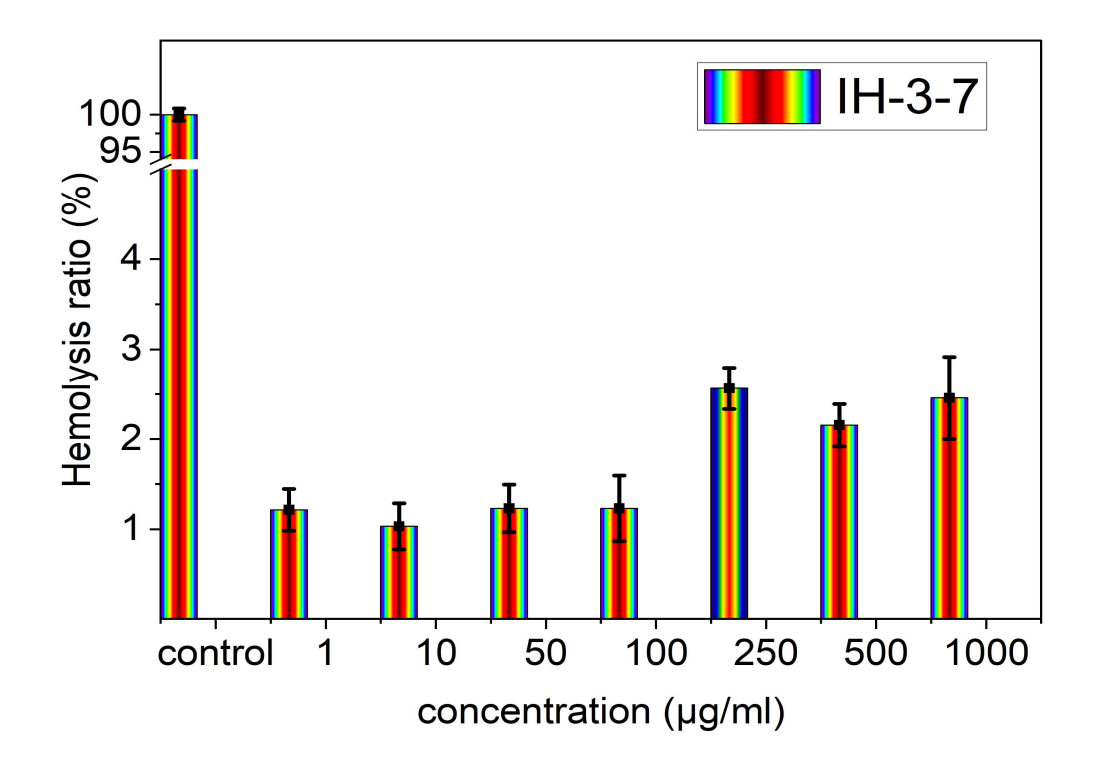
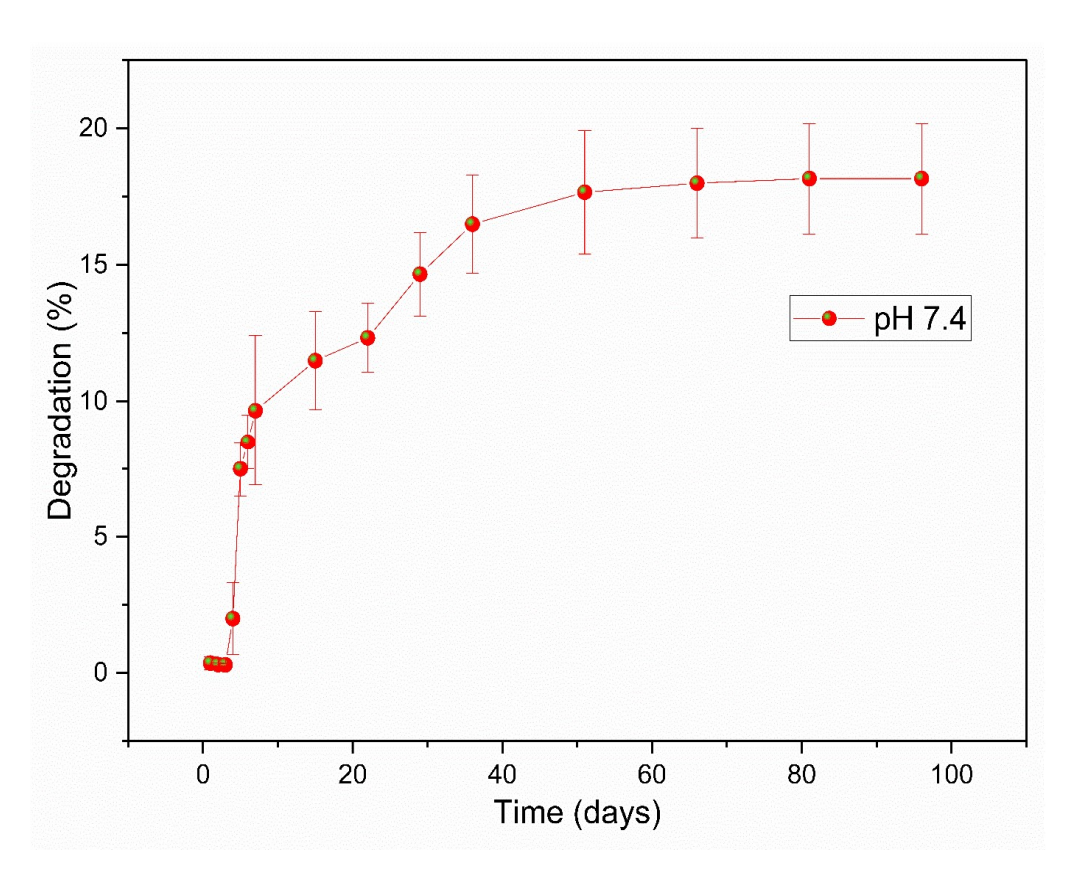


Fig. 4. 11 Hemolysis ratio of IH-3-7

# 4.12 Hydrolytic degradation studies

The biodegradability of IH-3-7 was studied in PBS at pH 7.4 at 37°C (Fig. 4.12.). The study was carried out for 96 days. Nearly 18% degradation was observed in around 88 days, which is considered gradual degradation; after that, it becomes constant. The degradation rate of hydrogel is dependent on the crosslink density. The IH-3-7 has a crosslink density of 2×10<sup>-4</sup> mol/cm<sup>3</sup>. Due to high crosslink density, the rate of degradation is slow. Liu *et* al fabricated an IH using Schiff base chemistry between sericin and oxidized dextran and found a slow degradation rate (~50% after 60 days) [498].



**Fig. 4. 12** Hydrolytic degradation behavior of IH-3-7 in PBS at pH 7.4 at 37°C for 96 days.

# 4.13 Conclusion

Dynamic Schiff base linkage designed self-healing polysaccharide IH based on oxidized *Moringa oleifera* gum with multi-aldehyde groups and carboxymethyl chitosan. The optimized concentration of sodium periodate is 3 % w/v, which converts the vicinal hydroxyl group to the aldehyde group of *Moringa oleifera* gum. The optimized ratio of the aldehyde percentage of oxidized moringa gum to the amine percentage of carboxymethyl chitosan is 9.2 to form an IH in ~4 minutes. The IH-3-7 is ideal for syringeability and injectability evaluation because of its exceptional

viscoelastic and shear-thinning properties. The hydrogel is self-healed in 3 hours. The swellability and drug-release behavior of IH are pH-dependent and well-correlated. The IH-3-7 showed drug release behavior using model drug ciprofloxacin HCl, with a greater release at pH 5.5 than at physiological pH 7.4. The slow drug release is found in the gel form of IH-3-7, which is useful for wound healing applications. The drug release mostly follows the Fickian diffusion mechanism. Synthesized IH-3-7 is observed to be gradually degrading in pH 7.4 at 37°C and is used to release antibiotic drugs at the wounded sites slowly. Furthermore, the cytotoxicity evaluation showed no toxicity against the L-929 fibroblast cell line.

#### **CHAPTER 5**

# SYNTHESIS AND CHARACTERIZATION OF INJECTABLE HYDROGEL BASED ON MULTIALDEHYDE MESQUITE GUM CROSSLINKED WITH CARBOXYMETHYL CHITOSAN VIA SCHIFF BASE MECHANISM

#### 5.1 Introduction

This chapter reports the synthesis of multi-aldehyde groups on mesquite gum by employing NaIO<sub>4</sub> as an oxidant (Fig. 5.1.a). To make chitosan more soluble in water in neutral environments, carboxymethyl groups were added to the molecule to form CMCh (Fig. 5.1.b). The aldehyde groups of oxidized mesquite gum covalently crosslinked with the NH<sub>2</sub> of CMCh through Schiff base crosslinking at 37 °C without requiring any hazardous or chemical crosslinking agents (Fig. 5.1.c). The study investigated the synthesized IHs' self-healing capability, rheological behavior, swelling ability, drug release assay in PBS at varying pH levels (5.4, 7.4, and 8.5), biocompatibility, antibacterial properties, and hydrolytic degradability.

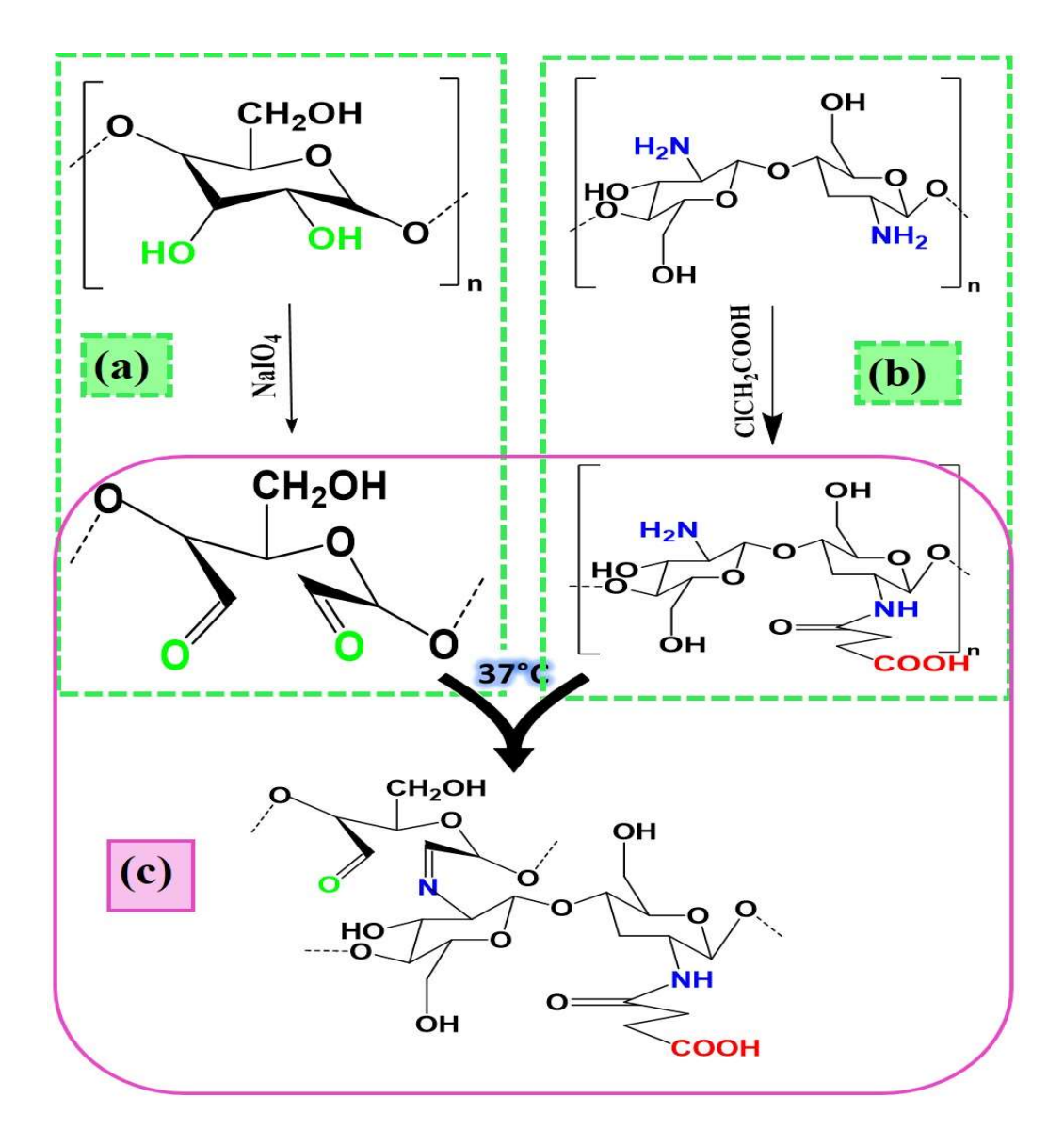


**Fig. 5. 1** (a) Oxidation of mesquite gum (MG-CHO) (b) Derivatization of chitosan (CMCh) (c) Fabrication of IH

# 5.2 Effect of concentration of NaIO<sub>4</sub> on gelation time

The impact of MG derivatization on aldehyde content then on gelation time is displayed in Table 5.1. Gelation time drops from  $30\pm3.5$  to  $7\pm2.1$  minutes. An increase in NaIO<sub>4</sub> concentration (0.5 % to 2 % w/v) nearly stays constant (8 $\pm2.5$  minutes), with an additional rise in NaIO<sub>4</sub> concentration (3 % w/v). This behavior was caused mainly

by an increase in the oxidizing agent's concentration, which increases the conversion of hydroxyl groups to aldehyde groups. After analysis, the percentage of aldehyde was discovered to have increased from 33.5±2.8 % to 50.2±2.5 %. This behavior was explained by determining the ratio of aldehyde % to the amine group on CMCh.

The results show that adding 2 % (w/v) of NaIO4 results in a value of 47.6±1.5 %, whereas adding 3 % (w/v) of NaIO4 results in an almost constant value of 50.2±2.5 %. To accomplish a successful Schiff base reaction, the ratio of the aldehyde group to the amino group must be adjusted for different polysaccharide hydrogels. An incorrect ratio would lead to longer gelation times. Hyaluronic acid that had been derivatized using NaIO4 and chitosan were combined to create an IH by Nair *et al*. After adding the necessary quantity of NaIO4, successful oxidation degrees of 10, 15, and 25 % were obtained with 8-second gelation time [16] Based on this investigation, the optimal NaIO4 concentration for subsequent research was determined to be 2 % w/v.

**Table 5.1** Effect of concentration of NaIO<sub>4</sub> on gelation time of injectable hydrogel

Sample code	MG % (w/v)	NaIO <sub>4</sub> % (w/v)	Aldehyde % (A)	Amine group % present in CMCh (B)	Ratio $= \frac{A}{B}$	Gelation time (minutes)
IH- MG <sub>0.5</sub> -1	1	0.5	33.5±2.8	67±2.11	0.5	30±3.5
IH-MG <sub>1</sub> -	1	1	40.8±1.7	67±2.11	0.6	15±2.6
IH-MG-	1	2	47.6±1.5	67±2.11	0.7	7±2.1
IH-MG <sub>3</sub> -	1	3	50.2±2.5	67±2.11	0.7	8±2.5

# 5.3 Effect of concentration of oxidized MG on gelation time

The impact of oxidized MG content on gelation time is displayed in Table 5.2. The NaIO<sub>4</sub> concentration was maintained at 2 % w/v (MG-CHO-2). The table unequivocally demonstrates that a reduction in gelation time (7±2.1 minutes to 2±1 minutes) was noted with a rise in MG-CHO-2 concentration (1 % w/v to 5 % w/v). This is mainly because derivatized chitosan's amine groups were more likely to react with an overall number of aldehyde functional groups. At the same time, adding 7 % w/v of MG-CHO-2 increases the gelation time (3±1.5 minutes) because there are now more aldehyde groups in the MG-CHO-2 than amine groups in the CMCh. As a result, too many aldehyde groups could prevent the formation of gels. Moreover, the basic unitary approach was used to explain this tendency. A comprehensive analysis of the computation was conducted, and the magnitude value of the ratio increased steadily (0.7 to 5) with the increased MG-CHO-2 (1 % w/v to 7 % w/v). According to a study by Pandit et al., they created IH using oxidized gum arabic and 0.5 g of NaIO<sub>4</sub>. They were able to reach an oxidation degree of about 44% by varying the amount of derivatized gum arabic (20 % to 40 %), which resulted in a reduction in gelation time (42 seconds to 29 seconds) [476].

**Table 5.2** Effect of concentration of oxidized MG (MOG-CHO-2) on gelation time.

Sample code	Concentration of MG-CHO-2 (% w/v) (B)	Aldehyde % of MG- CHO-2 (A)	Amine group in CMCh (%) (C)	$ \begin{array}{c} \textbf{Ratio} \\ = \frac{\mathbf{A} \times \mathbf{B}}{\mathbf{C}} \end{array} $	Gelation time (minutes)
IH-MG-	1	47.6	67±2.11	0.7	7±2.1
IH-MG-	3	47.6	67±2.11	2.13	5±1.5

IH-MG- 5	5	47.6	67±2.11	3.55	2±1
IH-MG-	7	47.6	67±2.11	5	3±1.5

# **5.4 Physical properties of IHs**

Table 5.3 lists the physical characteristics, including gel content, porosity, syringeability, and network parameters. It is observed that IH-MG-1, IH-MG-3, and IH-MG-5 have gel contents of 62±1 %, 73±1 %, 81±2 %, and porosities 75.42±1.5 %, 61.24±1.2 %, and 49.23±1.4 %, respectively. The increased gel content and lower porosity of IHs are attributed to well-formed imine bond crosslinks. Additionally, with increasing porosity, the average molecular weights between crosslinks increase, the mesh size increases, and the crosslink density decreases. This is because a more compact structure developed when the concentration of MG-CHO-2 was raised (1 % to 5 % w/v). Determining the porosity of the IH also aids in understanding the spaces where liquids get trapped or stuck. Aghajanzadeh *et al.* designed an injectable hydrogel using Schiff base crosslinks between oxidized xanthan gum and gelatin, and a porosity determination of 50 % was observed [499].

Self-healing behavior was checked by placing two half-sliced, cylindrical IHs of distinct colors together; the self-healing property was ascertained qualitatively. The self-healing IH in both hues was put into a 20 mL syringe and extruded using a 21 G needle. After 30 minutes, a picture of "DTU" was created. The image displays the blending of yellow color with the IH's existing color (dirty white). The continuous strands emerge from a needle to provide a "DTU" image, confirming the IHs' self-

healing properties by showing the reversibility of the Schiff-base bond, which is further utilized to fix the cut surfaces of wounds (Fig. 5.2).

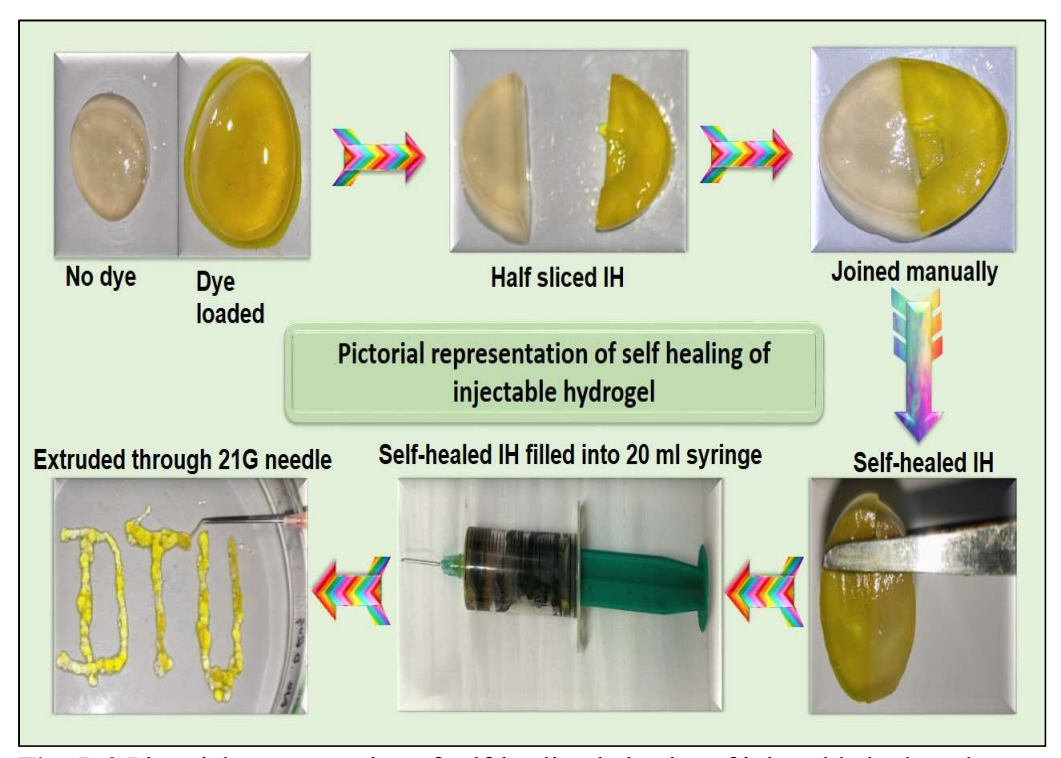


Fig. 5. 2 Pictorial representation of self-healing behavior of injectable hydrogel

For all concentrations of MG-CHO-2, the computed syringeability percentage was almost 99±0.5 %. The data verified that IHs produced and extruded with a 21 G needle exhibit favorable syringeability characteristics. Wang *et al.* described their process of turning copper sulfide into an IH that was then used for photothermal therapy. They tested syringes in different diameters (26 G, 25 G, 23 G, and 18 G), and the results showed that the 26 G syringe produced the best outcome overall [479].

Additionally, the injectability of the developed IHs was examined to determine their suitability for use in clinical operations. There are currently no international standards or criteria governing the conduct of the test, yet several injectability tests have been published in different research articles [480, 481]. The gauge of the needle used to

calculate the values must match the range of 18–21 G to 26–27 G used in the industrial context to deliver IH precursors subcutaneously. Using a 21 G needle, the injectability evaluation test in this study was completed satisfactorily. A picture of "DTU" created by extruding IH in a glass petridish with a 10 mL (21 G) needle capacity (Fig. 5.3.). The needle's smooth flow verified the ease of injectability of IH. Zhang *et al* designed an IH using protein-polysaccharide for chondrogenic differentiation of bone marrow mesenchymal stem cells. After gel formation, it was found to be easily injected through a 22 G syringe and formed the shape "SCU"[500].



Fig. 5. 3 Pictorial representation of injectability of IH through 21G needle.

Table 5.3 Physical properties of IHs

Property	Value				
	IH-MG-1	IH-MG-3	IH-MG-5		
Gel content	62±1 %	73±1 %	81±2 %		
Porosity	75.42±1.5 %	61.24±1.2 %	49.23±1.4 %		
Syringeability	99.21±0.5 %	98.76±04 %	98.11±0.6 %		
Average molecular weight	43.2×10 <sup>-2</sup> g	51.3×10 <sup>-2</sup> g	67.4×10 <sup>-2</sup> g		
between crosslinks	mol <sup>-1</sup>	mol <sup>-1</sup>	mol <sup>-1</sup>		
Crosslink density	1.1 mol cm <sup>-3</sup>	1.5 mol cm <sup>-3</sup>	1.9 mol cm <sup>-3</sup>		
Mesh size	7.2×10 <sup>-2</sup> nm	5.1×10 <sup>-2</sup> nm	4.3×10 <sup>-2</sup> nm		

# 5.5 Structural properties

FT-IR and proton NMR characterize the IH's structural characteristics. The FT-IR spectra of the MG, MG-CHO-2, chitosan, CMCh, and IH-MG-5 are displayed in Fig. 5.4.a to 5.4.c. The FT-IR spectra of pure MG exhibit absorptions attributed to O–H and C–H at 3290 and 2922 cm<sup>-1</sup>, respectively. A peak on 1600 cm<sup>-1</sup> is designated to amide I, indicative of the protein content within the MG. The vibration modes of C–O and C–O–H groups of carbohydrates (glucose, mannose, and galactose) are evidenced by peaks around 1150 cm<sup>-1</sup> and 900 cm<sup>-1</sup>. Furthermore, the occurrence of pyranose glycosidic acetal groups is suggested by the peaks at 834 and 776 cm<sup>-1</sup>[35]. A significant peak is observed at 1727 cm<sup>-1</sup>, which confirms the presence of the aldehyde group (Fig. 5.4.a), which qualitatively supports observation obtained from the oxidation of MG. The FT-IR spectra of pure chitosan show that the bending vibrational

peak of the amino group is located at 1570 cm<sup>-1</sup>. The C-O-C asymmetric structure of the chitosan saccharide is located at 1250 cm<sup>-1</sup>, and the C-O stretching vibration is located at 1024 cm<sup>-1</sup>. The presence of two additional peaks in the FT-IR spectrum of CMCh at 1644 and 1420 cm<sup>-1</sup> indicates symmetric and asymmetric stretching vibrational modes of the -COO group, respectively. These peaks show that chitosan derivatization was successful and that carboxymethyl groups are present on CMCh [471] (Fig. 5.4.b). A peak at 1642 cm<sup>-1</sup> in the FT-IR spectrum of the IH-MG-5 indicates the formation of an imine structure as a result of a dynamic Schiff base crosslinking reaction between the amine group of CMCh and the aldehyde groups of MG-CHO-2. Removing the aldehyde peak in the IH-MG-5 spectrum further illustrates the evolution of the Schiff base linkage [478] (Fig. 5.4.c).

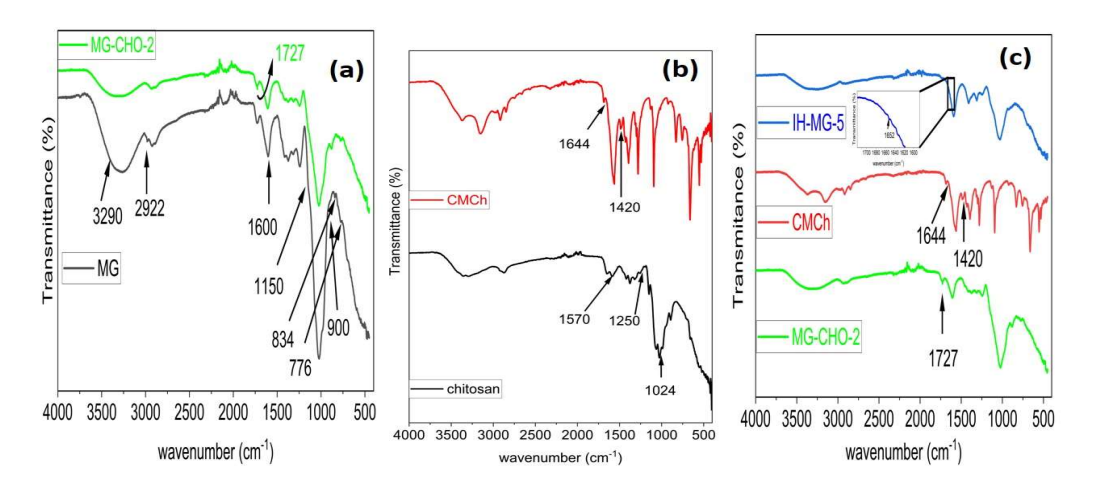


**Fig. 5. 4** FT-IR spectra of (a) MG, MG-CHO-2 (b) chitosan, CMCh and (c) MG-CHO-2, CMCh, IH-MG-5.

As FT-IR shows, structural properties are also supported by the proton NMR spectroscopy technique. D<sub>2</sub>O was used as a solvent to oxidize MG before <sup>1</sup>H-NMR analysis. The presence of methyl groups is the cause of the peak at 1.3 ppm. The spectra

showed congested signals in the 2.16, 3.65-4.30, and 4.9 ppm spectrum bands, which corresponds to the distinctive characteristics of the anomeric proton in polysaccharides due to the existence of sugar residues. The primary peak, identified by D<sub>2</sub>O, was observed at 4.7 ppm (Fig. 5.5.a). A new distinctive peak of the aldehydic proton is observed at 9.31 ppm, confirming MG's oxidation, which supports the data obtained from the FT-IR graph (Fig. 5.5.b) [303]. The <sup>1</sup>H-NMR spectra of the chitosan show a peak at 1.24 ppm due to the presence of protons in the acetyl group. The anomeric

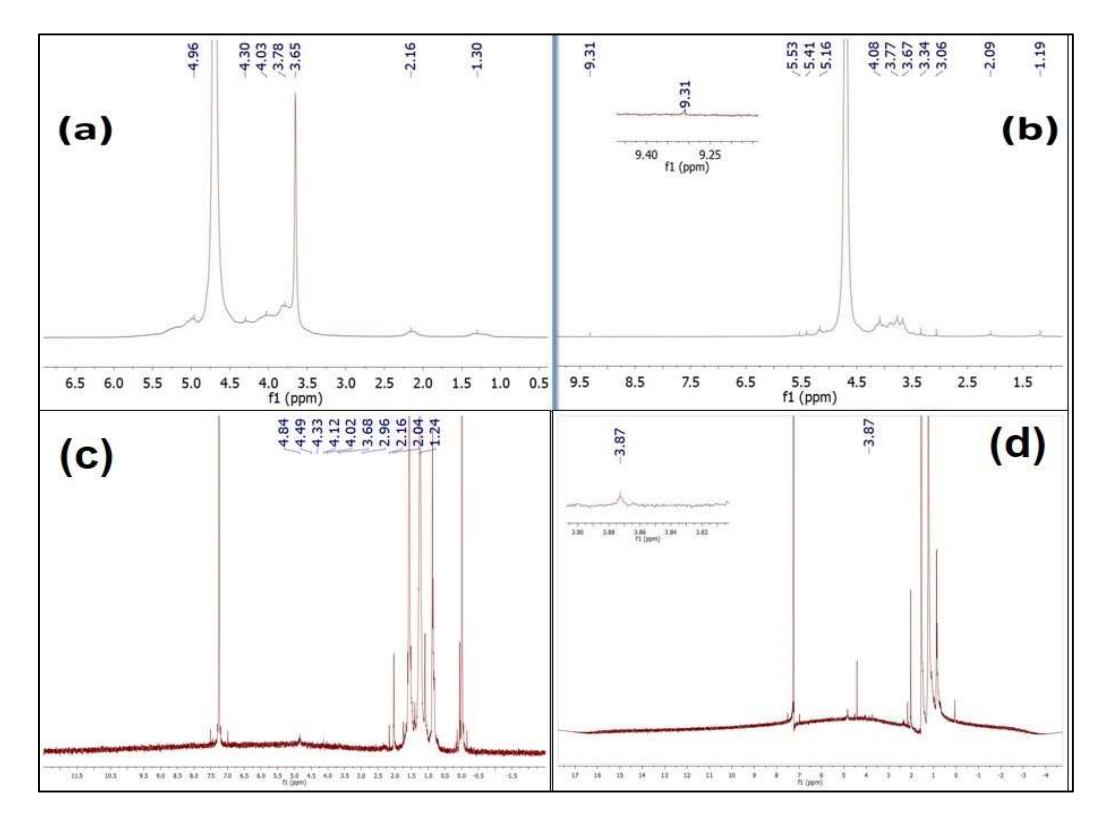


**Fig. 5. 5** <sup>1</sup>H-NMR spectra of (a) MG (b) MG-CHO-2 (c) chitosan (d) CMCh protons of glucosamine show a peak at 2.96 ppm, while the non-anomeric protons of the chitosan structural backbone are responsible for the peaks ranging from 3.68 to 4.84 ppm (Fig. 5.5.c). Additionally, a new peak was observed at 3.87 ppm due to the presence of the –CH<sub>3</sub>COO<sup>-</sup> group (Fig. 5.5.d) [501].

## 5.6 Rheological properties

A rheometer operating at a constant strain of 1 % and a set frequency of 1 rad s<sup>-1</sup> was used to conduct the time sweep study. Precursors 1 and 2 were simultaneously extruded in a 1:1 ratio at 37 °C on the rheometer platform, and they were then left to crosslink on the platform itself. In isothermal mode (37 °C), the variations in storage modulus (G') and loss modulus (G") over time were measured. After the initial few seconds, the G' value increased because the viscosity of the liquid increased, and the Schiff base reaction proceeded slowly. The G' value peaked at 2086.2 Pa for IH-MG-5 after 300 seconds, surpassing that of IH-MG-3 at 760.02 Pa and IH-MG-1 at 257.35 Pa. This is because the concentration of MG-CHO-2 increased (1 % w/v to 5 % w/v) along with the concentration of the Schiff base bond, which led to compact polymer networks and more excellent mechanical characteristics. This interaction between the NH<sub>2</sub> groups of CMCh and the aldehyde group of MG-CHO-2 caused the G' to increase quickly. Additionally, the G" values for IH-MG-1, IH-MG-3, and IH-MG-5 are 6.12, 23, and 272 Pa, respectively. Fig. 5.6.a indicates no discernible variations in the G" values of the IHs with varying weight ratios of MG-CHO-2. Liang et al. synthesized an IH using Schiff base chemistry between chitosan-grafted-dihydrocaffeic acid and oxidized pollulan; the time sweep study shows that G' surpassed the G" with time [485].

To assess the shear thinning behavior, IHs were placed between the parallel plates of the rheometer and allowed to squeeze at increasingly more excellent shear rates during a continuous flow sweep test (1-100 1 s<sup>-1</sup>, 1 % strain) conducted at 37 °C. When IH-MG-5 is compared to IH-MG-1 and IH-MG-3, it has the most excellent MG-CHO-2 value and, thus, the highest initial viscosity value. The viscosity was found to decrease with increasing shear rate (1151700 to 1592 m Pa.s for IH-MG-5, 842490 to 926.3 m

Pa.s for IH-MG-3, and 371700 to 578.45 m Pa.s for IH-MG-1), indicating that the IHs exhibits shear thinning behavior. This behavior could be caused by the Schiff base linkage breaking at a high shear rate (Fig. 5.6.b). The shear thinning behavior of IH further supports the data on syringeability, injectability, and self-healing properties.

The linear viscoelastic region (LVE) of the IHs was measured using the amplitude sweep test at multiple strain levels ranging from 0.1 to 100 % at 37 °C (Fig. 5.6.c). Using the amplitude sweep test, the LVE of IHs was found between 0.1 and 5 % of the strain values. A strain value of 1 % was chosen for all gelation-related kinetic investigations. At different strain values, it was found that the IHs had more excellent G' values than G" values. The crossovers for the IHs appeared at 14.8 %, indicating that the hydrogel was converting from a solid to a liquid. Thus, IHs possess a higher amount of MG-CHO-2, resulting in more excellent elasticity, which is necessary for these IHs to resist the administration-linked strains during their injectable formulation. The variable angular frequency shear in the range of 0.1–100 rad s<sup>-1</sup> was delivered to the IHs at a constant amplitude (1 %) to perform a frequency sweep test (Fig. 5.6.d). The figure shows that these IHs demonstrated mechanical robustness with more excellent G' values than G" values throughout all investigated frequency ranges. These IHs are both elastic and stiff, as observed by the more excellent value of G' than G". Because the IH-MG-5 has a higher crosslinking density, which limits the mobility of chains within the hydrogel matrix, it exhibited higher values of G' (1518 Pa) than the IH-MG-1 (247 Pa) and IH-MG-3 (934 Pa). The frequency sweep test's G' values showed a similar pattern to the amplitude sweep.

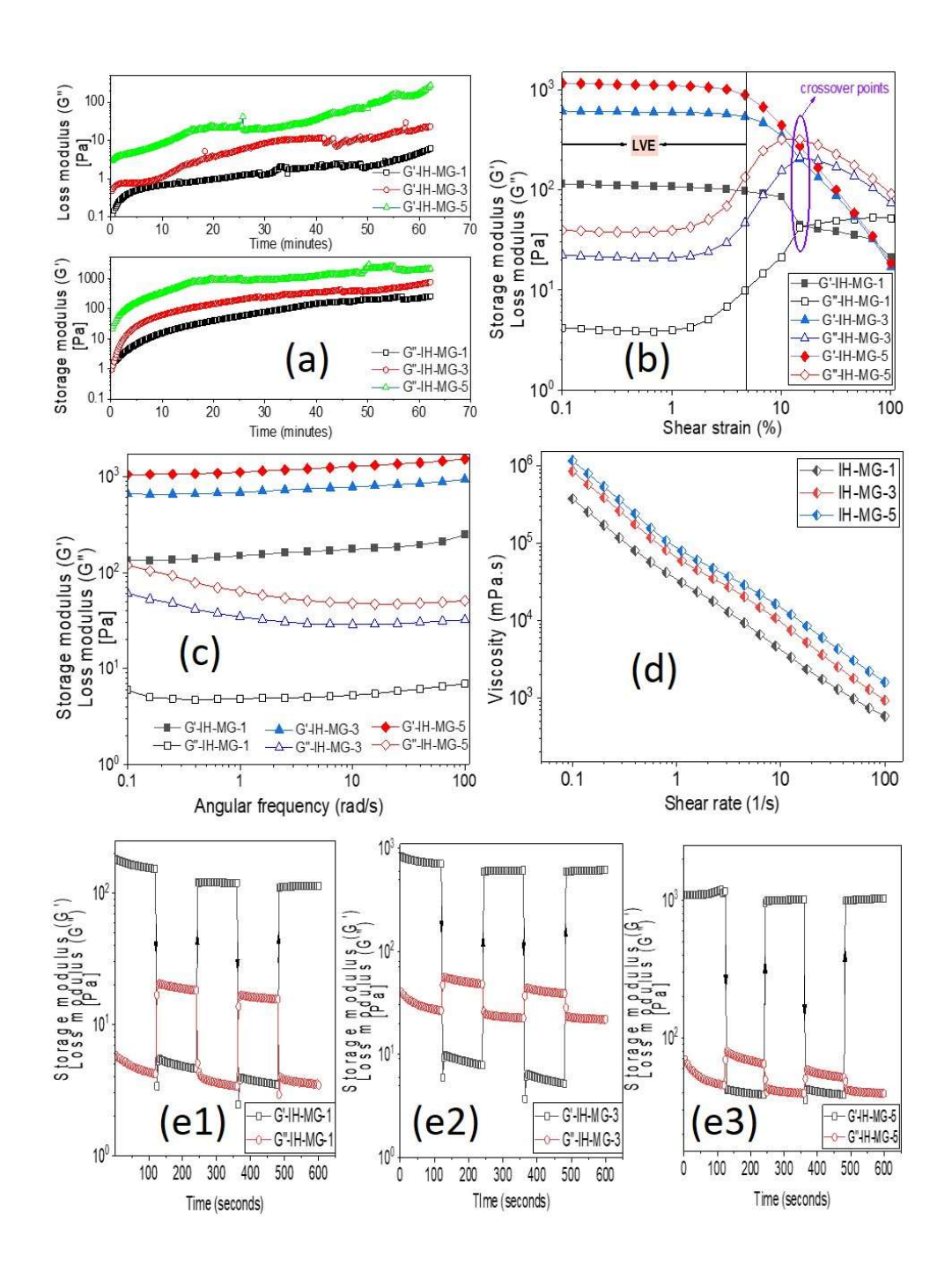


**Fig. 5.6** Rheological study at 37°C (a) Isothermal time sweep study (b) flow sweep behavior (c) Amplitude sweep study (d) Frequency sweep study IH-MG-1, IH-MG-3, and IH-MG-5. Step-strain measurement of (e1) IH-MG-1 (e2) IH-MG-3 (e3) IH-MG-

Balitaan *et al.* synthesized an IH using a Schiff base crosslink between acrylamide-modified  $\beta$  -chitin and alginate dialdehyde. The amplitude sweep test, frequency sweep test, and viscosity measurement were conducted, and results showed that IH possesses better mechanical properties with shear thinning characteristics [490].

A series of rheological recovery tests were carried out to quantify the self-healing properties of IHs. This behavior was evaluated by oscillatory step-strain measurement. The G' value had a high magnitude at low strain (1 %), and in all IHs, as the strain shifted to high values (200 %), the G' value was found to be closest to G". This resulted from the structure deforming at high strain values. The behaviors were stable over multiple cycles, indicating the self-healing capability and stability of the dynamic Schiff base and dynamic coordination network. After all cycles of alternate strain (low to high), the highest recovery was found in the case of IH-MG-5 (95 %, Fig. 5.6.e1), followed by IH-MG-3 (78.33 %, Fig. 5.6.e2) and IH-MG-1 (63 %, Fig. 5.6.e3) for a given interval of time as shown in Equation 5.1.

Recovery 
$$\% = 100 - \frac{\text{initial G'} - \text{final G'}}{\text{initial G'}} \times 100$$
 (5.1)

Qu et al. synthesized an IH using N-carboxyethyl chitosan and dibenzaldehydeterminated poly(ethylene glycol) via Schiff base chemistry in which self-healing analysis was examined qualitatively and quantitatively [482].

# 5.7 Morphological evaluation

The surface morphology of the IHs synthesized with varied amounts of MG-CHO-2 (1, 3, and 5 % w/v) was investigated using the SEM (Fig. 5.7.). The SEM images were captured at 1300 X and 1800 X for all IHs. The SEM pictures demonstrate the

relationship between the structure and the composition of the IHs. Image J software was used to calculate the average diameter of the pores. When compared with IH-MG-3 (21 μm, Fig. 5.7.b1, 5.7.b2) and IH-0.5-1 (34 μm, Fig. 5.7.a1, 5.7.a2), the IH-0.5-5 shows a tight network structure and a comparatively smaller pore size (14 μm, Fig. 5.7.c1, 5.7.c2). The SEM images additionally show that the IHs exhibit a continuous three-dimensional porous network at different MG-CHO-2 concentrations (1 %, 3 %, and 5 % w/v). The porosity quickly decreased when the MG-CHO-2 concentration in the IHs increased. The linked pores of the IHs network might provide enough vacancies for the loading of drugs and also help with their release. Wang *et al.* fabricated an IH using Schiff-based chemistry composed of phenylboronic acid grafted polylysine and oxidized dextran; SEM study revealed a porous structure having size ranges from 209 to 37 μm [502].

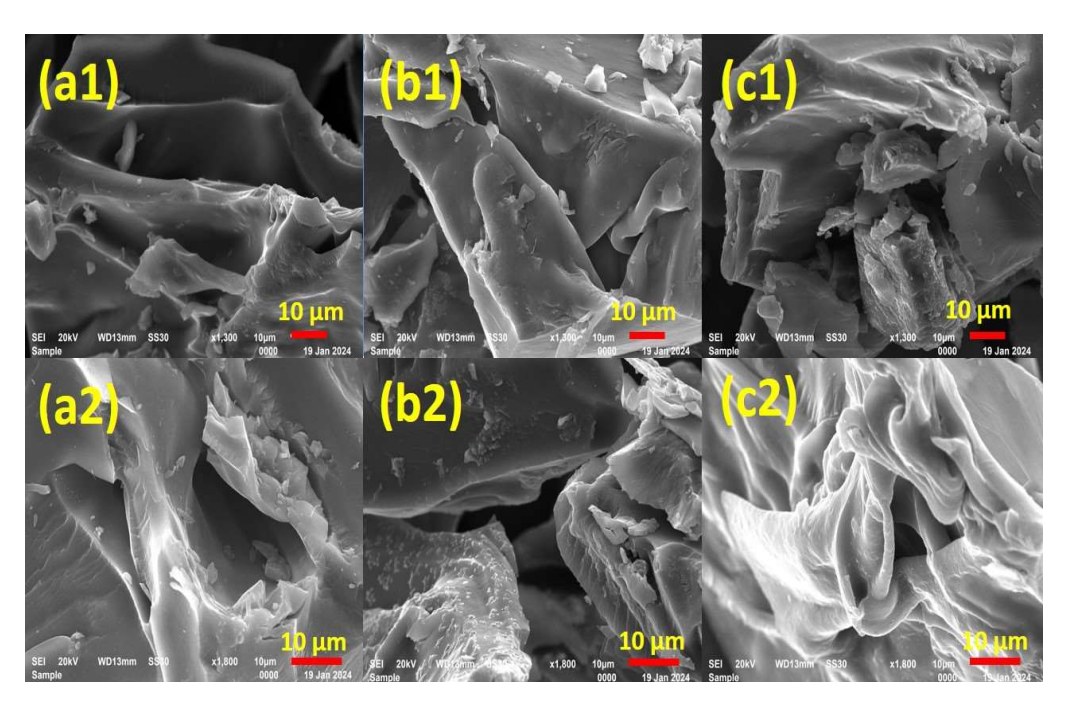


**Fig. 5.7** SEM images at 1300X (a1) IH-MG-1 (b1) IH-MG-3 (c1) IH-MG-5 and 1800X (a2) IH-MG-1 (b2) IH-MG-3 (c2) IH-MG-5

## 5.8 Swelling Study of IHs

The swelling behavior of synthesized IHs is investigated in PBS at three pH levels (pH 5.5, pH 7.4, and pH 8.5) at 37°C.

# 5.8.1 Swelling study from dry form of IHs (Method 1)

The swelling ratio decreases quickly with the increasing quantity of MG-CHO-2 at low pH levels (pH 5.5). The IH-MG-1 exhibits a swelling ratio of about 810 %. Fig. 5.8.a shows that the IH-MG-3 and IH-MG-5 had swelling ratios of around 714 % and 555 %, respectively. The swelling ratio values of IH-MG-1, IH-MG-3, and IH-MG-5 in physiological pH (7.4) are 514, 460, and 420 %, respectively (Fig. 5.8.b). The swelling ratios are also calculated in alkaline pH (8.5), where the swelling ratios for IH-MG-1, IH-MG-3, and IH-MG-5 were found to be 784, 692, and 528 %, respectively (Fig. 5.8.c).

#### 5.8.2 Swelling study from gel form of IHs (Method 2)

In an acidic environment (pH 5.5), the swelling ratio decreases rapidly as the concentration of MG-CHO-2 increases. The IH-MG-1 exhibits a swelling ratio of roughly 611 %. Conversely, the swelling ratios of the hydrogels IH-MG-3 and IH-MG-5 are around 535 and 483 %, respectively (Fig. 5.8.d). At physiological pH (7.4), Fig. 5.8.e displays the swelling ratios for IH-MG-1, IH-MG-3, and IH-MG-5, 484, 442, and 401 %, respectively. For swelling ratios in alkaline pH (8.5), the values for IH-MG-1, IH-MG-3, and IH-MG-5 are 557, 501, and 452 %, respectively (Fig. 5.8.f).

The reason is that when the concentration of MG-CHO-2 rises (from 1 % w/v to 5 % w/v), the IHs network structure becomes more compact. This leads to a more severe

constraint on the mobility of the polymer chains, which minimizes their exposure to water. Because CMCh's amino groups are hydrophilic, they hydrate with water quickly and rapidly. In contrast, the imine group, found in the IHs, is assumed to be hydrophobic. The increased concentration of MG-CHO-2 in synthesized IHs may result in a more significant concentration of hydrophobic moieties. This slows the IH swelling rate by reducing its ability to form hydrogen bonds with water. Consequently, in both dry and gel form across all pH ranges (5.5, 7.5, and 8.5), the IH (IH-MG-5), which has a higher concentration of MG-CHO-2, exhibits a lower swelling ratio than IH-MG-1 and IH-MG-3. Furthermore, as pH rises (from 5.5 to 7.4), the swelling ratios of IH-MG-1, IH-MG-3, and IH-MG-5 (in both dry and gel form) decrease and then increase again to pH 8.5, indicating their pH-sensitive swelling behavior. At pH 5.5, an acidic pH, the amino groups in CMCh undergo protonation, leading to electrostatic repulsion between intra- and interpolymeric chains. As a result, the IHs network's ruptured structure enhances water absorption. However, at pH 7.4 (higher pH), deprotonation within the amine group of CMCh causes a decrease in the swelling ratio in IHs. Higher swelling ratios can be caused by further increasing the pH to 8.5, which could lead to a loose network topology in IHs (dry and gel form). Therefore, the study mentioned above demonstrates that the concentration of MG-CHO-2 and the pH of the swelling media affect the swelling ratios of the dry and gel forms of IHs. Kumar et al. fabricated an IH using Moringa oleifera gum and carboxymethyl chitosan crosslinked through the Schiff base mechanism; the swelling study was conducted for dry and gel forms of IHs. At pH 5.5, more drug release was observed than at pH 7.4 [503].

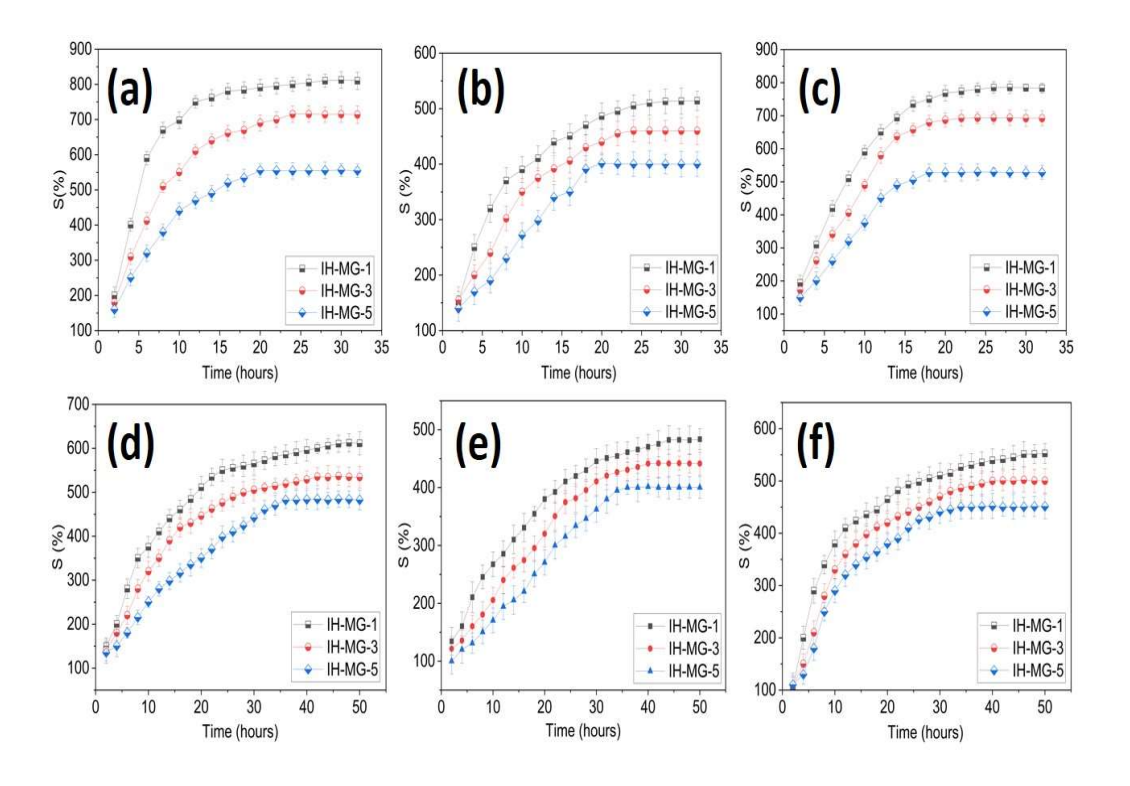


**Fig. 5. 8** Swelling behavior of IHs in PBS in dry form at (a) pH 5.5 (b) pH 7.4 (c) pH 8.5 and in gel form at (d) pH 5.5 (e) pH 7.4 (f) pH 8.5 at 37°C.

# 5.9 Drug release behavior

The IHs drug release behavior was assessed in PBS at pH 5.5, 7.4, and 8.5 at 37 °C using ciprofloxacin HCl as the model drug. Skin, urinary tract, and respiratory tract bacterial infections are treated with the antibiotic drug ciprofloxacin HCl. Two distinct methods were employed, as stated in the description of the experimental section (Fig. 5.7).

# 5.9.1 Drug release from dry form of IHs (Method 1)

At low pH (pH 5.5), the Cipro release increases rapidly as MG-CHO-2 concentrations rise. With the least amount of MG-CHO-2, the IH- MG-1 yields a cipro release of 13110 μg 100 mL<sup>-1</sup> g<sup>-1</sup> of IH. Conversely, Fig. 5.a shows that the IH-MG-3 and IH-

MG-5 release cipro at approximately 11130 and 9125 μg 100 mL<sup>-1</sup> g<sup>-1</sup> of IH, respectively. At physiological pH (7.4), the Cipro release for IH-MG-1, IH-MG-3, and IH-MG-5 is 9566, 8011, and 6896 μg 100 mL<sup>-1</sup> g<sup>-1</sup> of IH, respectively (Fig. 5.7b). IH-MG-1, IH-MG-3, and IH-MG-5 have cipro release values in alkaline pH of 12326, 10210, and 8895 μg 100 mL<sup>-1</sup> g<sup>-1</sup> of IH, respectively (Fig. 5.7c). A relatable research article published by Yin *et al.* in which they fabricated an IH using Schiff base chemistry between oxidized microcrystalline cellulose from pineapple peel were crosslinked with carboxymethyl chitosan and rutin release studies show a pH-dependent release behavior [504].

# 5.9.2 Drug release from gel form of IHs (Method 2)

The IH-MG-1, which contains the least concentration of MG-CHO-2, has a cipro release of around 16101 μg 100 mL<sup>-1</sup> g<sup>-1</sup> of IH. Moreover, Fig. 5.7d shows that the cipro release values for IH-MG-3 and IH-MG-5 are 13787 μg 100 mL<sup>-1</sup> g<sup>-1</sup> of IH and 11500 μg 100 mL<sup>-1</sup> g<sup>-1</sup> of IH. For IH-MG-1, IH-MG-3, and IH-MG-5, the cipro release values at physiological pH (7.4) are 12110, 11160, and 9150 μg 100 mL<sup>-1</sup> g<sup>-1</sup> of IH, correspondingly (Fig. 5.7e). The values for IH-MG-1, IH-MG-3, and IH-MG-5 for cipro release in alkaline pH (8.5) are 15590, 13111, and 10112 μg 100 mL<sup>-1</sup> g<sup>-1</sup> of IH, respectively (Fig. 5.7f). This can be explained by the fact that the hydrogel network structure gets more compressed when the concentration of MG-CHO-2 rises (from 1 % w/v to 5 % w/v), increasing crosslink density (0.7 to 1.2 g cm<sup>-3</sup>). This reduces exposure to the release of Cipro by drastically restricting the mobility of the polymer chains. The hydrophilic nature of the amino groups in CMCh makes it easy for them to hydrate with water immediately. The imine group, which is thought to have hydrophobic moieties, is present in the IHs. On the other hand, IHs may have more

hydrophobic moieties due to the higher concentration of MG-CHO-2 in them. As a result, the IH's capacity to create hydrogen bonds with water diminishes, slowing the release of cipro. Because of this, the IH-MG-5 has a larger concentration of MG-CHO-2 than IH-MG-1 and IH-MG-3, and it also shows a lower cipro release in both dry and gel form across all pH ranges (5.5, 7.5, and 8.5). Furthermore, as pH rises (5.5 to 7.4), the cipro release of IH-MG-1, IH-MG-3, and IH-MG-5 (dry and gel form) reduces, suggesting a pH-sensitive behavior.

The amino groups of CMCh undergo protonation at pH 5.5, an acidic pH, which causes electrostatic repulsion between intra and interpolymeric chains. Cipro release is, therefore, improved by the ruptured structure of the IH network. Nevertheless, deprotonation within the amine group of CMCh reduces the release of Cipro in IH at pH 7.4 (higher pH). An even higher pH of 8.5 may cause a looser network structure in IHs (dry and gel form), leading to a greater cipro release—the drug released more slowly from gel form than from the dry form of IHs in all pH ranges. Additionally, method 2 is more practical than method 1 in the real world, where the IHs will be used for the wound site. During the healing phase, the drug's gradual release will aid in the decrease of microbial development at the wound site. Therefore, the previously stated tests show that the pH of the solution and the quantity of MG-CHO-2 present are essential factors in the cipro release of IHs in both their dry and gel forms. Kumar *et al.* synthesized an IH using a Schiff base crosslink between *Moringa oleifera* gum and carboxymethyl chitosan; the drug release study was conducted in a dry and gel form of IH. More drug release was observed at pH 5.5 than 7.4 [503].

The K-P model gives the most realistic explanation of the process of antibiotic drug release using IHs (Table 5.4.). Diffusion that is erosion- and diffusion-controlled is

referred to as non-Fickian or anomalous diffusion when the release exponent value "n" is between 0.5 and 1. Fickian diffusion is obtained when  $n \le 0.5$ , and supercase transport II is indicated by  $n \ge 1$  [476]. The  $R^2$  value for each IH's release behavior is determined to be greater than 0.99. All synthesized IHs had an "n" value greater than 0.5 and less than 1. Hence, the "n" value verified that all IHs displayed non-Fickian or anomalous diffusion over the whole pH range in both dry and gel form. Furthermore, the diffusion rate exceeds the hydrogel matrix's relaxation rate in every instance.

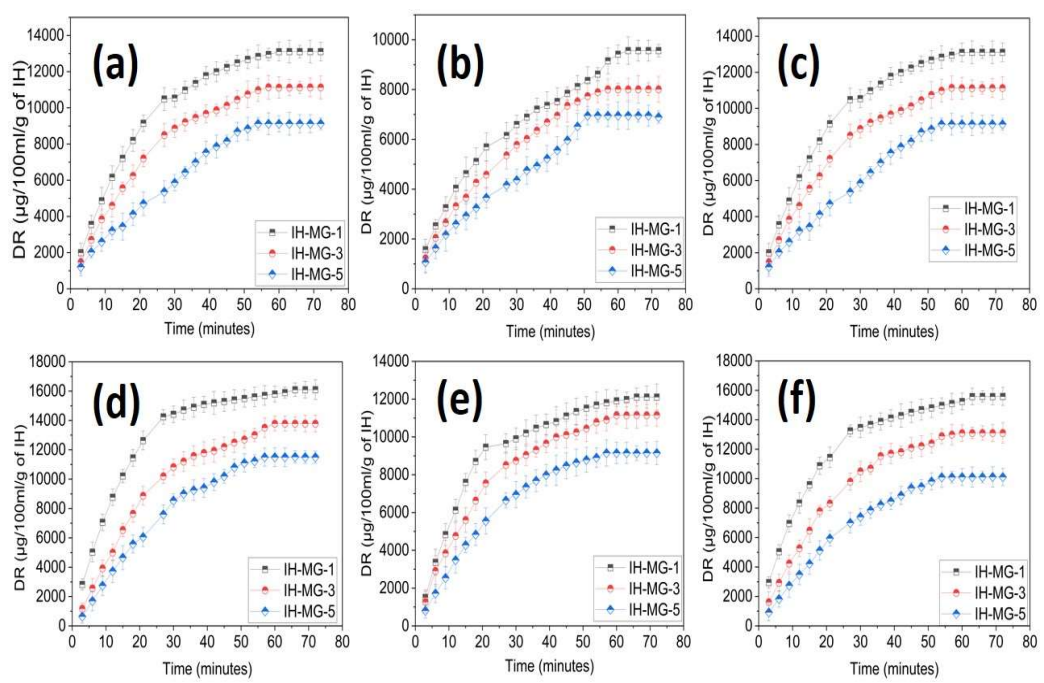


**Fig. 5. 9** Drug release behavior of IHs in PBS in dry form (a) at pH 5.5 (b) pH 7.4 (c) pH 8.5 and in gel form (d) at pH 5.5 (e) at pH 7.4 (f) at pH 8.5 at 37°C.

**Table 5.4** K-P kinetic model parameters for IH-MG-1, IH-MG-3, and IH-MG-5 in dry and gel form in PBS at pH 5.5, 7.4, and 8.5

pH of PBS	Physical state of IH	Sample code	Parameters associated with the K-P model		
			k	n	R <sup>2</sup>
		IH-MG-1	7.69	0.72	0.99
	Dry	IH-MG-3	6.30	0.76	0.99
pH 5.5		IH-MG-5	6.51	0.67	0.99
pii 3.3		IH-MG-1	9.76	0.68	0.99
	Gel	IH-MG-3	3.98	0.87	0.99
		IH-MG-5	3.00	0.86	0.99
рН 7.4		IH-MG-1	9.27	0.60	0.99
	Dry	IH-MG-3	8.08	0.65	0.99
		IH-MG-5	7.99	0.61	0.99
		IH-MG-1	6.05	0.85	0.99
	Gel	IH-MG-3	6.43	0.78	0.99
		IH-MG-5	4.22	0.87	0.99
		IH-MG-1	5.57	0.85	0.99
	Dry	IH-MG-3	4.11	0.88	0.99
nH 9.5		IH-MG-5	5.58	0.79	0.99
рН 8.5		IH-MG-1	10.88	0.63	0.99
	Gel	IH-MG-3	6.45	0.79	0.99
		IH-MG-5	3.84	0.88	0.99

# 5.10 In vitro cytotoxicity assay

IHs must be biocompatible with the host cells to serve as biomaterials for drug delivery applications. Therefore, an L-929 fibroblast cell line was used to test the cytotoxicity of synthesized IH. The IH-MG-1, IH-MG-3, and IH-MG-5 show negligible toxicity in the MTT experiment, with cell viability of 53%, 58%, and 62% up to 500  $\mu$ g/mL, respectively (Fig. 5.10 a). This could be because the MG-CHO-2 contains unreacted

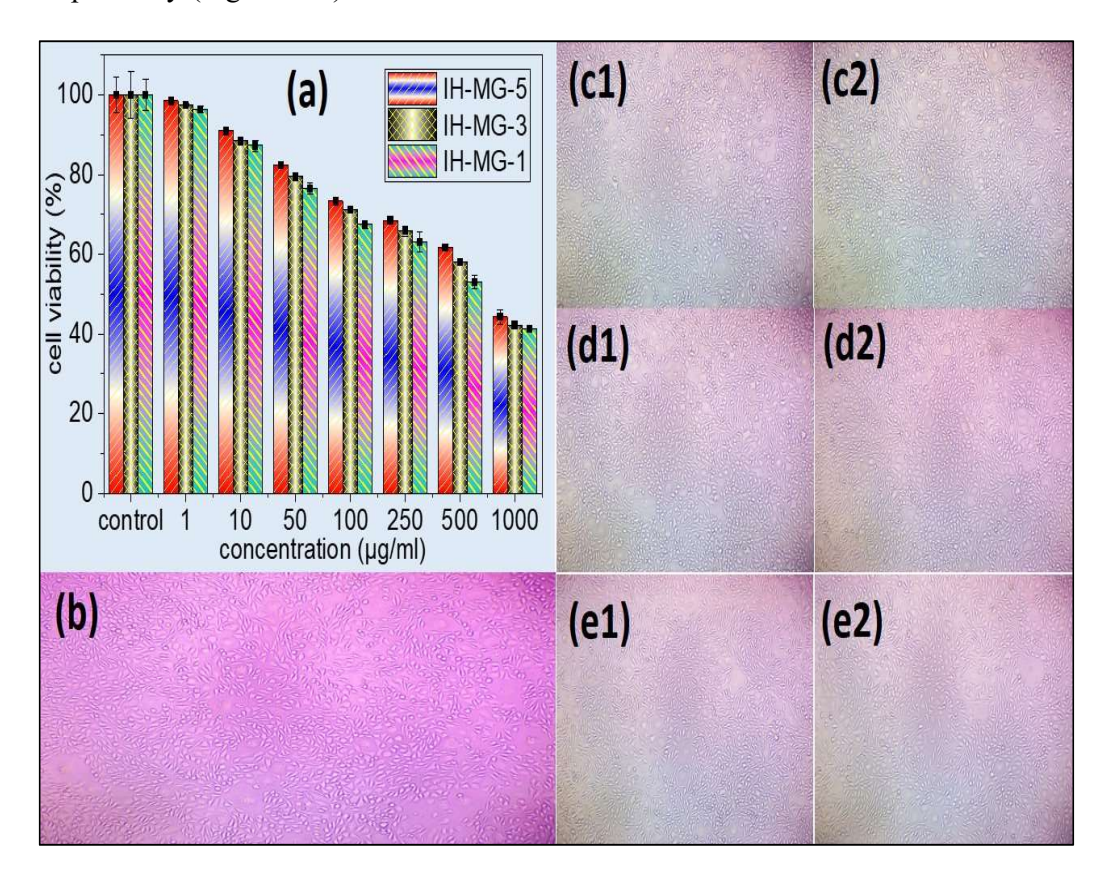


**Fig. 5. 10** (a) Cytotoxicity of injectable hydrogels. Inverted phase microscopic images of (b) control. IH-0.5-1 treated L-929 cell line at (c1) 1μg mL<sup>-1</sup> (c2) 500 μg mL<sup>-1</sup>. IH-0.5-3 treated L-929 cell line at (d1)1μg mL<sup>-1</sup> (d2) 500 μg mL<sup>-1</sup>. IH-0.5-5 treated L-929 cell line at (e1) 1μg mL<sup>-1</sup> (e2) 500 μg mL<sup>-1</sup>

carbonyl groups that may interact with the proteins in the cells. The concentration of MG-CHO-2 was found to cause a modest decrease in cell viability. The synthesized IHs' inverted phase microscopic images are displayed in Fig. 5.10b to e2. The outcomes demonstrate that the cytotoxicity of all IHs is compatible with L-929 fibroblast cell lines. A similar study was conducted by Kumar *et al.* in which they synthesized an injectable using Schiff base crosslinks between oxidized NG and carboxymethyl chitosan, *in vitro* cytotoxicity results show that synthesized IH was found to be biocompatible against L-929 fibroblast cell lines [505].

# 5.11 Hemolysis assay

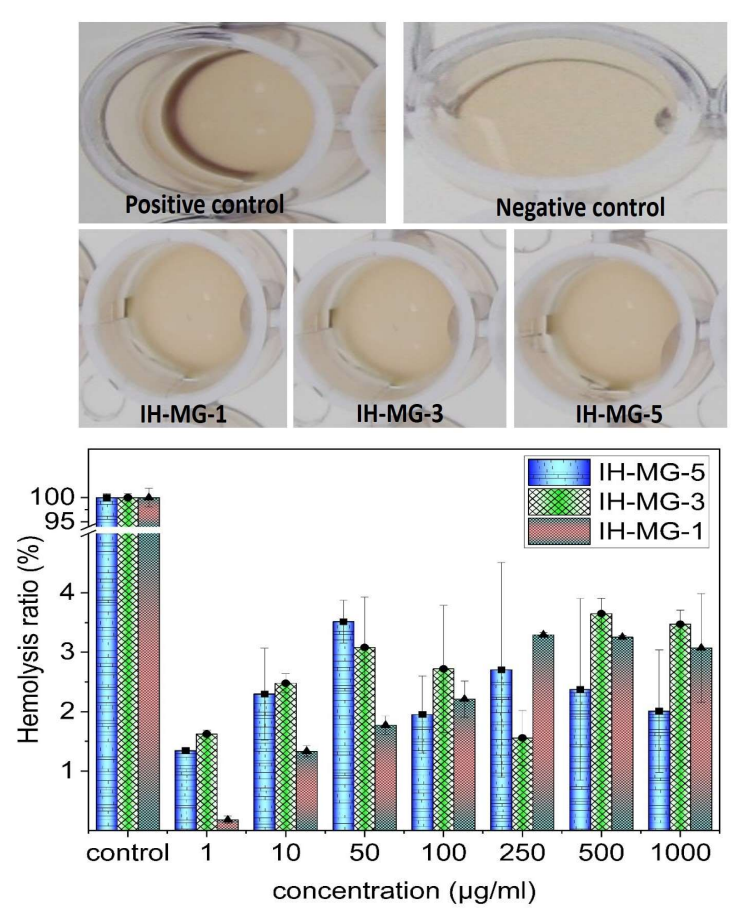


Fig. 5. 11 Statistical representation of hemolysis ratio of IHs

Figure 5.11 shows that the IHs have a similar color to PBS, while the RBC lysis group is bright red. The hemolysis rates of IHs with different concentrations are all < 4 %, which meets the standard of hemolysis rates of biomaterials. Therefore, IH-MG-1, IH-MG-3, and IH-MG-5 demonstrated a negligible hemolysis capability for all concentrations (1 to 1000  $\mu$ g mL<sup>-1</sup>).

# 5.12 Antibacterial assay

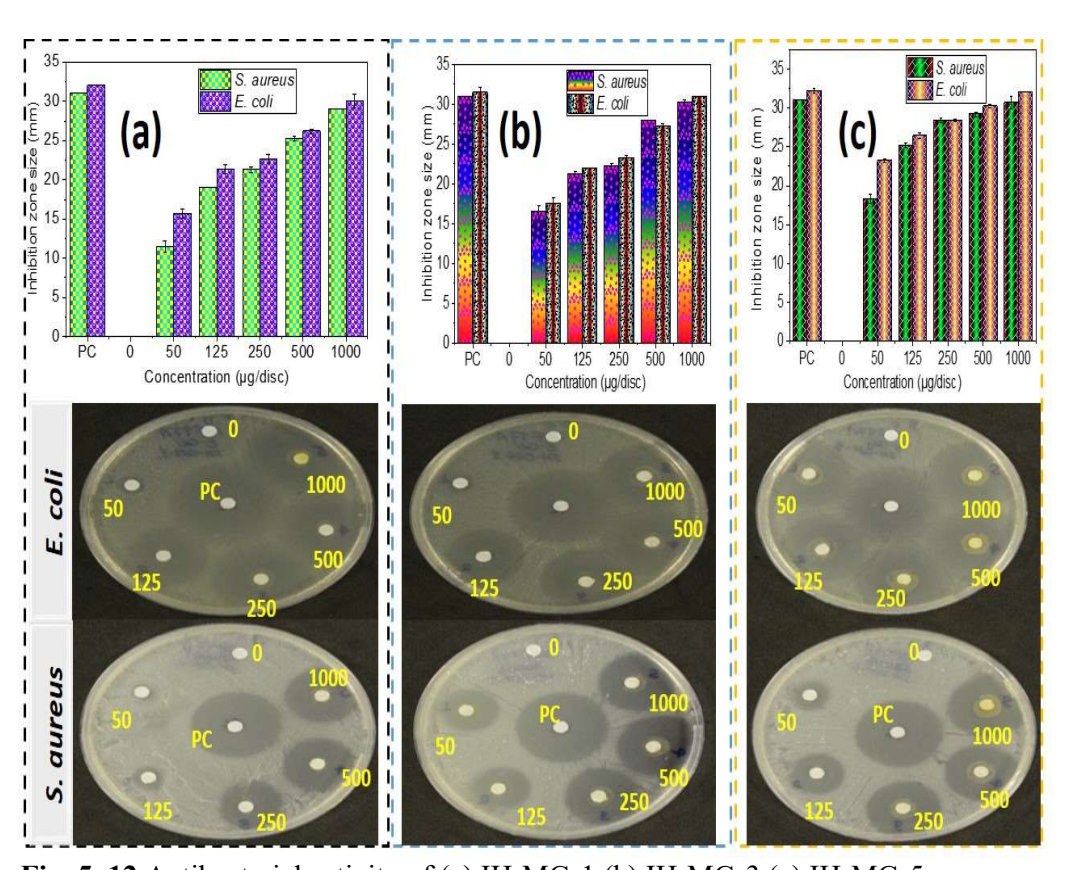


Fig. 5. 12 Antibacterial activity of (a) IH-MG-1 (b) IH-MG-3 (c) IH-MG-5

The IH's bactericidal properties were assessed using *S. aureus* and *E. coli* for 24 hours at 37°C. All IHs exhibited inhibitory effects against each bacterium across all concentrations (50 to 1000 µg disc<sup>-1</sup>) up to 24 hours at 37°C (Fig. 5.12.). This phenomenon was ascribed to chitosan, which could induce the leakage of

proteinaceous and other intracellular components from bacteria. Chitosan, containing amino groups and exhibiting a positive electrical charge, traps bacteria with negative charges via electrostatic forces, thus effectively inhibiting bacterial growth. A group of researchers published a research article based on Schiff base chemistry between oxidized konjac glucomannan and chitosan; all synthesized IHs showed an antibacterial nature [506].

## 5.13 Hydrolytic degradation

days (Fig. 5.13.a).

days. The weight loss resulting from the hydrolysis of Schiff base bonds in these IHs is evidence of their breakdown, as demonstrated by studies on hydrolytic degradation. Hydrolytic degradation from dried IHs (Method-1): In roughly 30 days, IHs with the highest percentage of MG-CHO-2 (IH-MG-5) degraded the least (53.12 %). On the other hand, the IH with the lowest amount of MG-CHO-2 (IH-MG-1) was discovered

to be the most degraded (70.21 %). Furthermore, IH-MG-3 degraded 60.48 % in 30

Synthesized IHs' biodegradability was investigated in PBS (pH 7.4) at 37 °C for 30

Hydrolytic degradation from gel form of IHs (Method 2): In 30 days, IHs—which contains the highest percentage of MG-CHO-2 (IH-MG-5)—observed a 66 % degradation. In contrast, with the lowest MG-CHO-2 (IH-MG-1) percentage, IH observed a 92.45 % deterioration in 30 days. Furthermore, the concentration of MG-CHO-2 (IH-MG-3) is in the middle of these two degrades by 80 % in PBS (pH 7.4) within 30 days (Fig. 5.13.b).

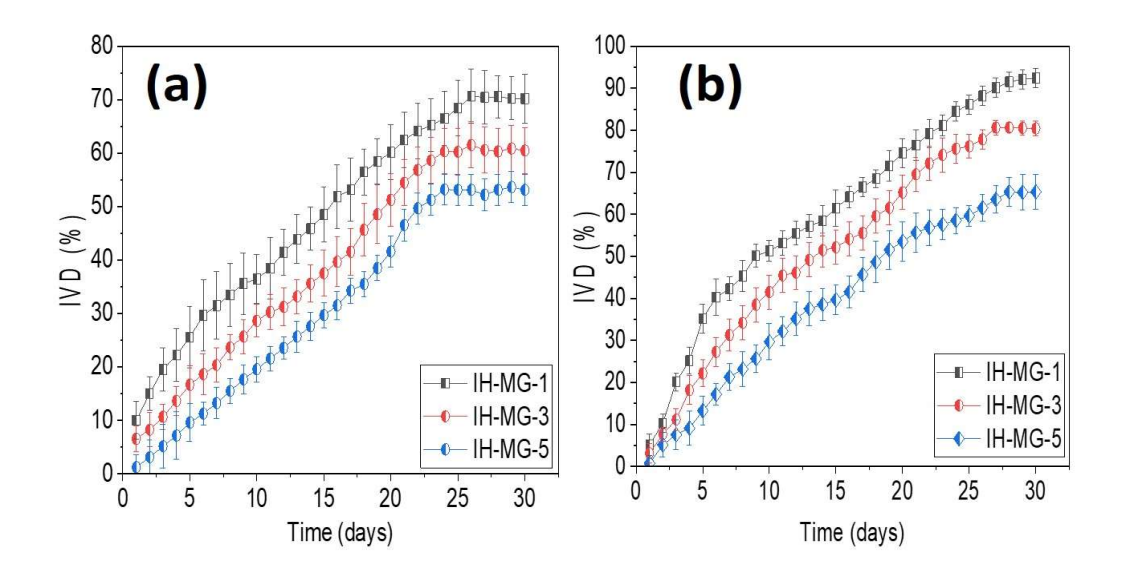


**Fig. 5. 13** Hydrolytic degradation behavior of IHs in PBS (pH 7.4) at 37°C (a) dry form (b) gel form.

The relationship between the crosslinking density and the degradation rate can explain this result. The crosslinking density and concentration of MG-CHO-2 significantly influence the hydrolytic breakdown of these IHs. As the amount of MG-CHO-2 increased, the crosslinking density increased, and the rate of IH breakdown decreased. Liu *et al.* fabricated an IH using Schiff base chemistry between sericin and oxidized dextran and found a slow degradation rate (~50 % after 60 days) [498].

## **5.14 Conclusions**

For the first time, self-healing polysaccharide-based IHs comprising oxidized MG with multi-aldehyde groups and carboxymethyl chitosan are fabricated via dynamic Schiff base linkage. The optimized sodium periodate concentration was 2 % w/v, which caused MG's vicinal hydroxyl group to change into an aldehyde group. Since the synthesized IHs have excellent viscoelastic and shear-thinning properties, they are

perfect for syringeability and injectability evaluation. IHs have a pH-dependent swellability and drug-release behavior strongly associated with crosslink density. Using ciprofloxacin HCl as a model drug, the IHs demonstrated that the drug release at pH 5.5 was higher in PBS than at pH 7.4, followed by further increases in pH 8.5. The gel form of IHs is a slow-release drug that can be used for wound healing. The non-Fickian diffusion mechanism governs the release of the drug. Hemolysis assay and *in vitro* cytotoxicity evaluation confirm the biocompatibility of synthesized IHs with antibacterial properties against Gram-positive and Gram-negative bacteria. Furthermore, synthesized IHs have been shown to gradually degrade in PBS (pH 7.4) at 37 °C. This suggests that they may be helpful for the progressive release of antibiotics at the sites of wounds.

#### **CHAPTER 6**

# SYNTHESIS AND CHARACTERIZATION OF INJECTABLE HYDROGEL BASED ON MULTIALDEHYDE NEEM GUM CROSSLINKED WITH CARBOXYMETHYL CHITOSAN VIA SCHIFF BASE MECHANISM

## **6.1 Introduction**

This chapter describes the fabrication of multi-aldehyde groups on neem gum utilizing NaIO<sub>4</sub> as an oxidant, which converts the hydroxyl groups of neem into aldehyde groups (Fig. 6.1.a). CMCh is synthesized by adding carboxymethyl groups to the chitosan molecule (Fig. 6.1.b). Without any hazardous or chemical crosslinking agents, the aldehyde groups of oxidized neem gum covalently crosslinked with the primary amine group of CMCh through Schiff base crosslinking at 37 °C (Fig. 6.1.c). The synthesized IHs' self-healing capability, rheological behavior, swelling ability, and drug release assay in PBS at different pH levels (5.4, 7.4, and 8.5). Furthermore, *in vitro* cytotoxicity, antibacterial assay, and hydrolytic degradation are also assessed.

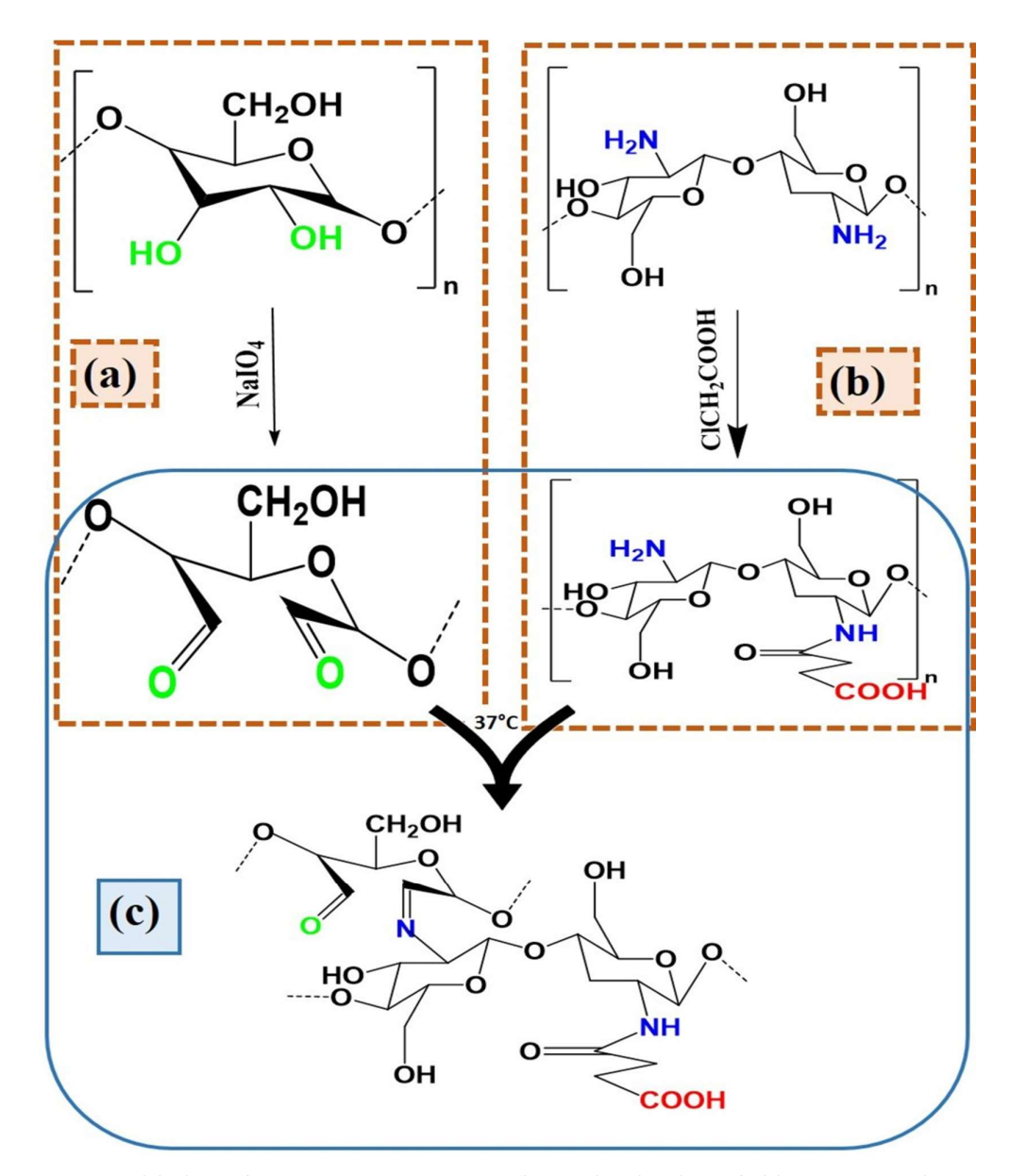


Fig. 6. 1 (a) Oxidation of neem gum (NG-CHO) (b) Derivatization of chitosan (CMCh)(c) Fabrication of IH

# 6.2 Effect of concentration of NaIO<sub>4</sub> on gelation time

Table 6.1. shows the effect of the concentration of NaIO<sub>4</sub> on aldehyde content followed by gelation time. With the increase in the concentration of oxidizing agent (0.1 % w/v to 0.5 % w/v), gelation time decreases ( $40\pm3$  to  $18\pm1.3$  minutes) and becomes almost

constant (20±1.5 minutes) with further increase in the concentration of NaIO<sub>4</sub> (1 % w/v). This behavior was primarily because increasing the concentration of the oxidizing agent increases the conversion of hydroxyl groups to aldehyde groups. The amount of aldehyde percentage was calculated and was found to be increased from 31.5±0.52 % to 56.8±1.41 % (Table 5.1). Further increase in the concentration of oxidizing agent (1 % w/v), the conversion of the aldehyde group remains constant. This behavior was explained by calculating the ratio of aldehyde percentage to the amine group present on CMCh (Table 5.1). A group of researchers synthesized an IH using derivatized hyaluronic acid and chitosan, and hyaluronic acid was derivatized using NaIO<sub>4</sub>. The required amount of NaIO<sub>4</sub> was added, successful oxidation degrees of 10, 15, and 25 % were achieved, and the observed gelation time was eight seconds [16]. Another group of researchers reported similar work, which used the same procedure for deriving hyaluronic acid by adding a different amount of NaIO<sub>4</sub>. Results show that an increase in the concentration of NaIO<sub>4</sub> increases the oxidation degree from 27 % to 60 %, which decreases the gelation time from 175 sec to 145 seconds [475]. From this study, the concentration of sodium periodate was optimized at 0.5 % w/v for further studies.

Table 6.1 Effect of concentration of NaIO<sub>4</sub> on gelation time of IHs

Sample code	NG % (w/v)	NaIO4 % (w/v)	Aldehyde % in NG-CHO (A)	Amine group in CMCh (%) (B)	Ratio $= \frac{A}{B}$	Gelation time (minutes)
IH-0.1-1	1	0.1	31.5±0.52	67±2.11	0.47	40±3
IH-0.3-1	1	0.3	40.7±0.43	67±2.11	0.61	32±2
IH-0.5-1	1	0.5	56.8±1.41	67±2.11	0.85	18±1.3

IH-1-1 1 1	56.1±0.83	67±2.11	0.84	20±1.5
------------	-----------	---------	------	--------

## 6.3 Effect of concentration of oxidized NG on gelation time

Table 6.2. shows the effect of the concentration of oxidized NG on gelation time. Here, the NaIO<sub>4</sub> concentration was kept constant at 0.5 % w/v. It is observed that with an increase in the concentration of NG-CHO-0.5 (1 % w/v to 5 % w/v), a decrease in gelation time was observed (18±1.3 minutes to 3±0.5 minutes). Furthermore, this behavior was explained using the simple unitary method. Table 2 shows the detailed analysis of the calculation, as the magnitude value of the ratio continuously increased from 1 % w/v to 5 % w/v of NG-CHO-0.5, and the observed gelation time was also decreased (18±1.3 minutes to 3±0.5 minutes). This is primarily because higher numbers of aldehyde functional groups are assessable to react with the amine groups of derivatized chitosan. For various types of polysaccharide hydrogels, it is necessary to adjust the ratio of the aldehyde group to the amino group to achieve an effective Schiff base reaction. Longer gelation times would result from an improper ratio. A research article has reported that they fabricated IH using oxidized gum Arabic by adding 0.5 g of NaIO<sub>4</sub> and achieved an oxidation degree of around 44 %; they varied the amount of derivatized gum Arabic (20 % to 40 %), by which gelation time was decreased (42 seconds to 29 seconds) [476].

Table 6.2 Effect of concentration of oxidized NG (NG-CHO-0.5) on gelation time

	Conc. of	Aldehyde %	Amine		Gelation
Sample	NG-CHO-	of NG-CHO-	group in	Ratio	
code	0.5 (% w/v)	0.5	CMCh (%)	$=\frac{\mathbf{A}\times\mathbf{B}}{\mathbf{C}}$	time
	(B)	(A)	(C)	C	(minutes)

IH-0.5-1	1	56.8±1.41	67±2.11	0.85	18±1.3
IH-0.5-3	3	56.8±1.41	67±2.11	2.54	11±1
IH-0.5-5	5	56.8±1.41	67±2.11	4.24	3±0.5

## 6.4 Physical properties of IHs

The physical properties of gel content, porosity, syringeability, and network parameters are given in Table 6.3. The gel content and porosity of IH-0.5-1, IH-0.5-3, and IH-0.5-5 are found to be 58±1 %, 67±1 %, 76±2 %, 71±2 %, 59±1 %, and 47±2 %, respectively. Good crosslinks via imine bonds are responsible for IHs' higher gel content and lower porosity. Also, the higher the porosity, the higher the mesh size, the higher the average molecular weights between crosslinks, and the lower the crosslink density. This is because a more compact structure was formed as the concentration of NG-CHO-0.5 was increased (1 w/v % to 5 % w/v). Yan and coworkers have fabricated an IH using Schiff base chemistry between poly(L-glutamic acid) and chitosan, in which the observed gel content was 79 % [478]. Another group of researchers published a research article based on Schiff base crosslinking using oxidized galactomannan and N-succinyl chitosan, in which they evaluated a porosity determination of 69 % [477].

The self-healing property was determined qualitatively when two half-sliced cylindrical-shaped IHs with different colors were placed together as per the procedure described in the experimental section. After completing 1 hour, self-healed IH bearing both colors were filled in a 20 mL syringe and extruded through an 18 G needle. A "DTU" image has been created. The picture shows the mixing of green color with the existing color of IH (light yellow). The continuous strands come through a needle, forming a "DTU" image. This demonstrates that the reversible Schiff-base bond

connection was rebuilt to repair the cut surfaces, confirming IHs' self-healing behavior (Fig. 6.2). Jin Qu and coworkers synthesized an IH using Schiff base crosslinks between quaternized chitosan and benzaldehyde-terminated Pluronic; their self-healing evaluation showed that synthesized IH took 2 hours to self-heal [483].

The syringeability percentage was calculated, and the result obtained was nearly 99 % for all concentrations of NG-CHO-0.5. This data confirmed that synthesized IHs possess good syringeability properties when extruded through an 18 G needle. Wang and colleagues reported a research article in which they transformed copper sulfide into an injectable hydrogel which was further utilized for photothermal therapy. They used syringes of various sizes (26 G, 25 G, 23 G, 18 G), revealing that 26 G gave the best result among all [479].



Fig. 6. 2 Pictorial representation of macroscopically self-healing of injectable hydrogel

Additionally, their injectability was investigated to make the synthesized hydrogels appropriate for clinical procedures. No worldwide guidelines or regulations govern how to conduct the test; however, various research articles have reported several

injectability tests [480, 481]. The gauge of the needle used in calculating the values must be the same as used in the industrial application to administer hydrogel precursors subcutaneously, ranging from 18-21 G to 26-27 G. This study successfully carried out the injectability evaluation test using an 18 G. Fig. 6.3. shows an image (DTU) formed by extruded IH using a 10 mL capacity needle (18 G) in glass petridish. Easy flow through the needle confirmed the ease of accessibility. An IH was formulated using N-carboxyethyl chitosan and dibenzaldehyde-terminated poly(ethylene glycol) by Schiff base reactions; in *vivo* injectability evaluation was performed using a 22 G needle and found ease out of IH after gel formation [482].



Fig. 6. 3 Injectability evaluation of synthesized injectable hydrogel

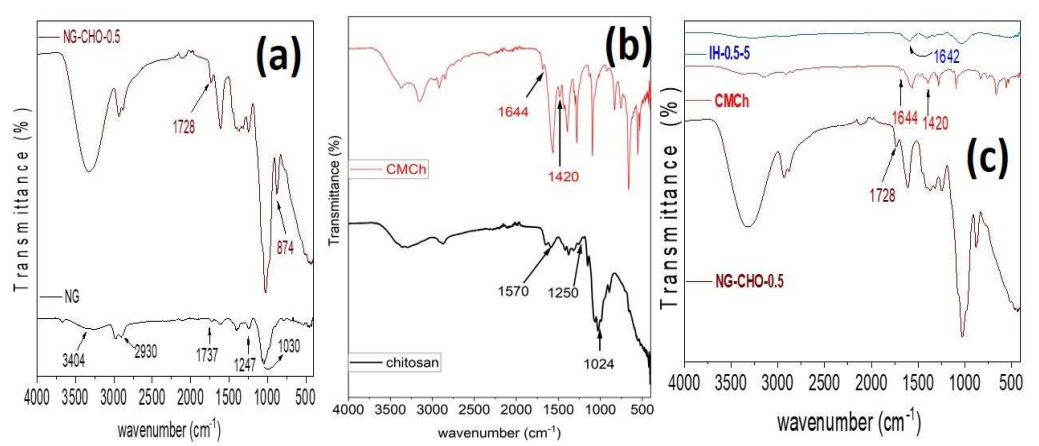
Table 6.3 Physical properties of IHs

Property	value				
Troperty	IH-0.5-1	IH-0.5-3	IH-0.5-5		
Gel content	58±1 %	67±1 %	76±2 %		
Porosity	71±2 %	59±1 %	47±2 %		
Syringeability	99±0.51 %	98.89±0.53 %	98.72±0.72 %		
Average molecular weight between crosslinks	5.8 ×10 <sup>2</sup> g mol <sup>-1</sup>	4.5×10 <sup>2</sup> g mol <sup>-1</sup>	3.8×10 <sup>2</sup> g mol <sup>-1</sup>		
Crosslink density	0.7 mol cm <sup>3</sup>	1.01 mol cm <sup>3</sup>	1.2 mol cm <sup>3</sup>		
Mesh size	5.1×10 <sup>-2</sup> nm	4×10 <sup>-2</sup> nm	3.3×10 <sup>-2</sup> nm		

## **6.5 Structural properties**

Structural properties of the IH showing the least gelation time (IH-0.5-5) are characterized using FT-IR spectroscopy and <sup>1</sup>H-NMR. Fig. 6.4a to 6.4c show the FT-IR spectra of the NG, NG-CHO-0.5, Chitosan, CMCh, and IH-0.5-5. FT-IR measurements of pure NG revealed absorption bands at 3404 cm<sup>-1</sup> caused by -OH stretching vibrations in the NG polysaccharide, 2930 cm<sup>-1</sup> due to -C-H stretching mode of -CH<sub>3</sub> groups in the NG, peaks at 1737 cm<sup>-1</sup> caused by C=O stretching vibrations of carboxylic acid present in the NG. Along with the peak at 1247 cm<sup>-1</sup> is due to the C-O-C asymmetric stretching vibrations, a strong absorption band at 1030 cm<sup>-1</sup> appeared, which belongs to C-O-C stretching vibration, can be seen in the FT-IR spectra of pure NG (Fig. 6.4a) [507]. After NG reacts with sodium periodate, significant peaks are seen at 1727 and 874 cm<sup>-1</sup> (Fig. 6.4a), mainly attributed to the production of symmetrical vibration of aldehydes and hemiacetal bonds, respectively. Another

comparative research study shows similar outcomes for the oxidized product [485]. The FT-IR spectra of pure Chitosan (Fig. 6.4b) show the amino group's bending vibrational peak at 1570 cm<sup>-1</sup>, the chitosan saccharide's C-O-C asymmetric structure at 1250 cm<sup>-1</sup>, and the C-O stretching vibration at 1024 cm<sup>-1</sup>. The FT-IR spectrum of CMCh (Fig. 6.4b) reveals the existence of two additional peaks at 1644 and 1420 cm<sup>-1</sup>, which are attributable to symmetric and asymmetric stretching vibrational modes of the –COO<sup>-</sup> group, respectively, and indicate the successful derivatization of chitosan and confirmed the presence of carboxymethyl groups on CMCh [486]. IH-0.5-5 IH's FT-IR spectrum (Fig. 6.4.c) shows a peak at 1642 cm<sup>-1</sup>, which demonstrates imine structure formation due to dynamic Schiff base crosslinking reaction between the amine group of CMCh and the aldehyde groups of NG-CHO. Further, the development



of the Schiff base connection is shown by the loss of the aldehyde peak in the IH-0.5-5 spectrum [487].

Fig. 6. 4 FT-IR spectra of (a) NG, NG-CHO-0.5 (b) chitosan, CMCh and (c) NG-CHO-0.5, CMCh, IH-0.5-5

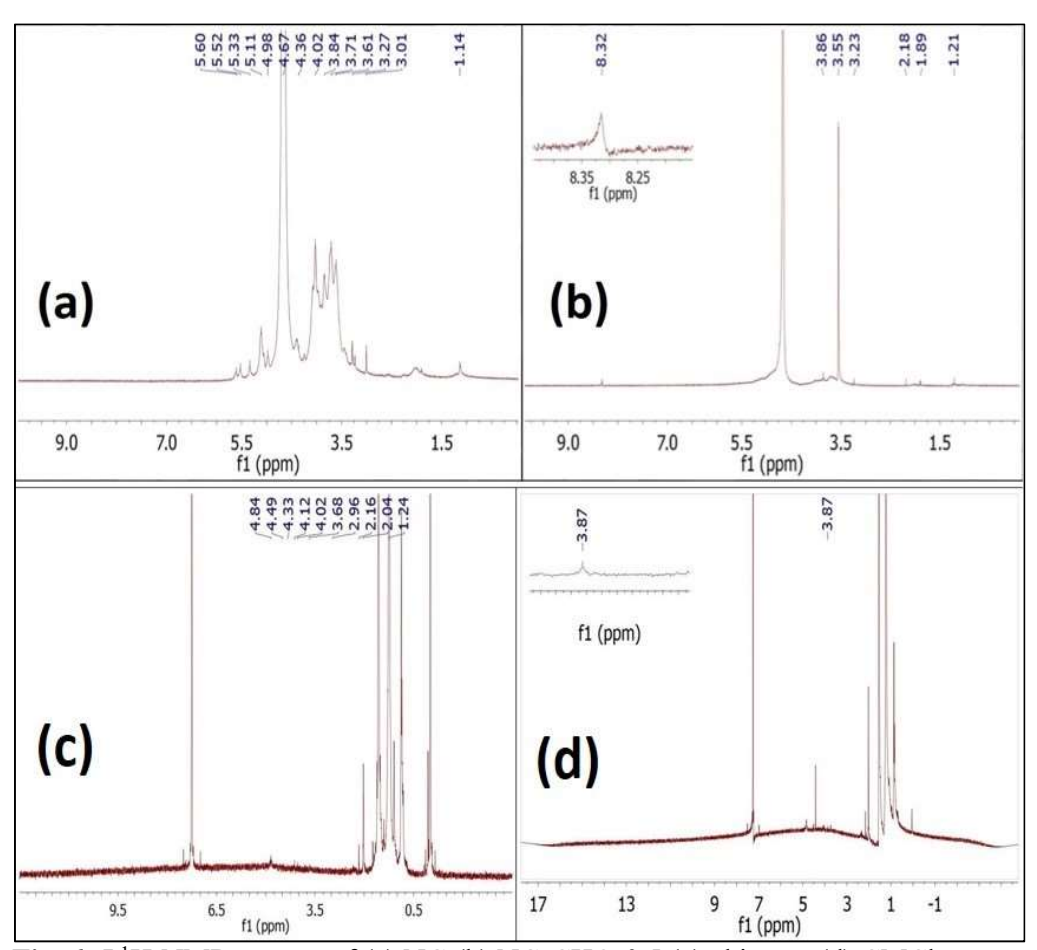


Fig. 6. 5 <sup>1</sup>H-NMR spectra of (a) NG (b) NG-CHO-0.5 (c) chitosan (d) CMCh

Proton NMR also supports structural characterization. <sup>1</sup>H-NMR was conducted for NG and oxidized NG using D<sub>2</sub>O as solvent (Fig. 6.5). Due to the presence of sugar residues, the spectra displayed signals in the 3-6 ppm spectrum band, corresponding to the characteristic properties of polysaccharides sugar proton [508]. The peak at 3.13 ppm is due to the acetyl group (COCH<sub>3</sub>) in NG. The peak at 1.3 ppm is due to the presence of methyl groups. The increase in signal strength between 3.3 and 3.8 ppm indicated evidence of an O-CH<sub>3</sub> group [509]. The peak at 4.36 to 5.36 was due to the –OH group. The central peak observed was between 4.67 ppm, which D<sub>2</sub>O designated. The non-anomeric protons (H<sub>2</sub> - H<sub>6</sub>) contributed signals in the range of 3.3-4.5 ppm (Fig. 6.5a).

A new distinctive peak of the aldehydic proton is observed at 8.32 ppm, confirming NG's oxidation (Fig. 6.5b).

# 6.6 Rheological properties

The time sweep study was evaluated using a rheometer at a fixed frequency (1 rad s<sup>-1</sup>) and constant strain (1 %). Precursors 1 and 2 were simultaneously extruded at the rheometer platform in a 1:1 ratio and allowed to crosslink at 37 °C. The changes in storage modulus (G') and loss modulus (G") over time were determined in isothermal mode (37 °C). The G' value rose after the first few seconds because the Schiff base reaction continued slowly as the mixture's viscosity rose. After 3000 seconds, the G' value reached the highest for IH-0.5-5 (584.75±27 Pa) than IH-0.5-3 (514.71±19 Pa), followed by IH-0.5-1 (122.99±15 Pa). This is because when NG-CHO-0.5 concentration increased (1 % w/v to 5 % w/v), resulting in tighter polymer networks and more excellent mechanical characteristics. A quick interaction between the aldehyde group of NG-CHO-0.5 and NH<sub>2</sub> groups of CMCh caused the G' to proliferate. Although the G" values in the IHs with different weight ratios of NG-CHO-0.5 (1 %, 3 %, and 5 % w/v) showed no apparent differences (Fig. 6.6.a).

When measuring the amplitude sweep test, the IHs were subjected to several strain levels between 0.01 and 100 % at 37 °C (Fig. 6.6.b) to check the linear viscoelastic region (LVE). The LVE of the IH with a medium amount of NG-CHO-0.5 (IH-0.5-1) was measured with the help of the amplitude sweep test and was found to have strain values between 0.01 and 4 %. A strain value of 1 % was selected for all kinetic studies involving gelation. It was observed that the IHs exhibited higher values of G' than G" values at variable strain values, and the crossovers for the IH-0.5-5, IH-0.5-3, and IH-0.5-1 appeared at 30 %, 27 %, and 22 % respectively, which shows IHs changing its

physical form from solid to liquid. Thus, IH possesses a higher amount of NG-CHO-0.5, resulting in more excellent elasticity, which is necessary for these IHs to resist the administration-linked strains during their injectable formulation, thus supporting syringeability. Balitaan *et al.* fabricated an IH using a Schiff base reaction between acrylamide-modified  $\beta$  -chitin and alginate dialdehyde. In the amplitude sweep test, strain value varied from (10° to 10<sup>4</sup>) %, and all the IHs showed higher storage modulus values than loss modulus [490].

For a frequency sweep test, the variable angular frequency shear in the 0.1–100 rad s<sup>-1</sup> range was applied to the IHs at a constant amplitude (1 %) (Fig. 6.6.c). Across all the tested frequency ranges, these IHs exhibited mechanical robustness with higher G' values than G" values. The higher value of G' than G" indicates these IHs' elastic and rigid nature. The IH-0.5-5 hydrogel showed higher values of G' (509.03±29 Pa) than the IH-0.5-1 (188.76±16 Pa) and IH-0.5-3 (378.85±20 Pa) due to the higher crosslinking density, which restricts the mobility of chains within the hydrogel matrix. The G' values obtained from the frequency sweep test followed the same pattern as the amplitude sweep. A group of researchers synthesized an IH using Schiff base chemistry and performed rheological studies. A frequency sweep test was performed (0.1 to 10 rad s<sup>-1</sup>), and a higher value of G' (120 Pa) was found than G" (9.8 Pa) (G'> G") [510].

To check the shear thinning behavior, a continuous flow sweep test (1-100 s<sup>-1</sup>, 1 % constant strain) was performed at 37 °C, in which IHs were sandwiched between the parallel plates of the instrument and were permitted to squeeze at progressively higher shear rates. IH-0.5-5 has the highest concentration of NG-CHO-0.5, so the highest viscosity value at the beginning is compared to IH-0.5-1 and IH-0.5-3. It is observed

that as the shear rate increases, the viscosity reduced (800680±576 to 497.27±31 m Pa. s for IH-0.5-5, 657740±482 to 329.96±25 m Pa. s for IH-0.5-3, and 226430±354 to 131.83±14 m Pa. s for IH-0.5-1), which shows shear thinning behavior of IH. This behavior may be due to the breakage of Schiff base linkage at a high shear rate (Fig. 6.6.d). The shear thinning behavior of IH further supports the data on syringeability and injectability. Wei and colleagues fabricated an IH using N-carboxyethyl chitosan and oxidized konjac glucomannan via Schiff base crosslinks. A flow sweep test was conducted, and the results depicted a decrease in viscosity with an increased shear rate [489].

Further, the self-healing properties of synthesized IHs were quantitatively determined using a series of rheological recovery experiments. Oscillatory step-strain measurements were used to assess the injectable hydrogels' self-healing capacity. At a low strain value (1 %), the storage modulus has a high magnitude value; as the strain shifted to a high value (200 %), the value was observed near the loss modulus in all IHs. This was because the structure got distorted at a high strain value. The behaviors remained consistent across three cycles, demonstrating the dynamic Schiff base and dynamic coordination network's stability and self-healing ability. The percentage recovery after the third cycle was calculated using Equation 5. The high crosslink density of IH-0.5-5 is responsible for the self-healing property. After all cycles of alternate strain (low to high), the highest recovery was found in the case of IH-0.5-5 (68±5 %, Fig. 6.6.e3), followed by IH-0.5-3 (65±4 %, Fig. 6.6.e2) and IH-0.5-1 (54±2 %, Fig. 6.6.e1) for a given interval of time (Equation 6.1).

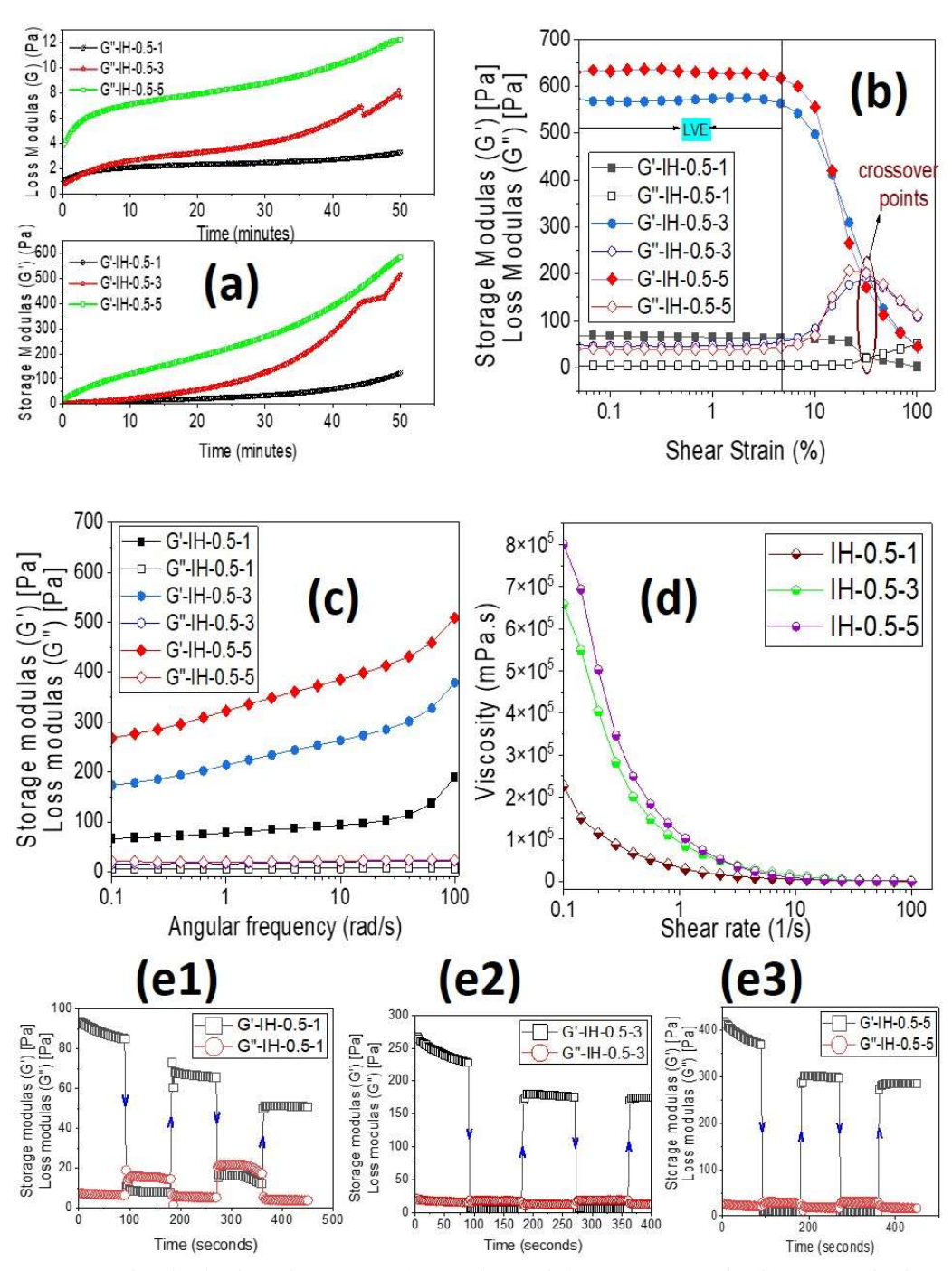


**Fig. 6. 6** Rheological study at 37°C (a) Isothermal time sweep study (b) G'G" v/s shear strain showing LVE region and crossover point (c) G'G" v/s angular frequency showing stiff and elastic nature (d) Viscosity v/s shear rate showing shear-thinning

behavior. Oscillatory step-strain measurements of (e1) IH-0.5-1 (e2) IH-0.5-3 (e3) IH-0.5-5

Recovery 
$$\% = 100 - \frac{\text{initial G'} - \text{final G'}}{\text{initial G'}} \times 100$$
 (6.1)

Huilong Guo and colleagues synthesized an IH using Schiff base chemistry in which alternate strain sweep shows the self-healing behavior using high (500 %) and low strain (1 %) [303].

# 6.7 Morphological Evaluation

The surface morphology of the IHs with three different concentrations of NG-CHO-0.5 (1, 3, and 5 % w/v) was examined through FESEM (Fig. 6.7.). The FESEM images show a correlation between the IHs composition and the structure. The average pore diameter was calculated using histograms of Image J software. FESEM pictures reveal that the IHs display a continuous three-dimensional porous network at varying NG-CHO-0.5 concentrations (1 to 5 % w/v). The IH-0.5-5 exhibits a tight network structure and relatively smaller pore size (80±10 μm, Fig. 6.7. c1, c2) when compared to IH-0.5-3 (105±4.45 μm, Fig. 6.7. b1, b2) and IH-0.5-1 (120±10.22 μm, Fig. 6.7. a1, a2). This is because when the NG-CHO-0.5 concentration in the IHs rose, the porosity rapidly reduced (71±2% to 47±2%, Table 3). The IHs network of interconnected pores may offer enough voids for the loading of drugs and also help with their release. Guan and coworkers fabricated an IH using Schiff base chemistry between oxidized dextran and gelatin, in which an SEM study revealed the surface pore size was 40 μm [494].

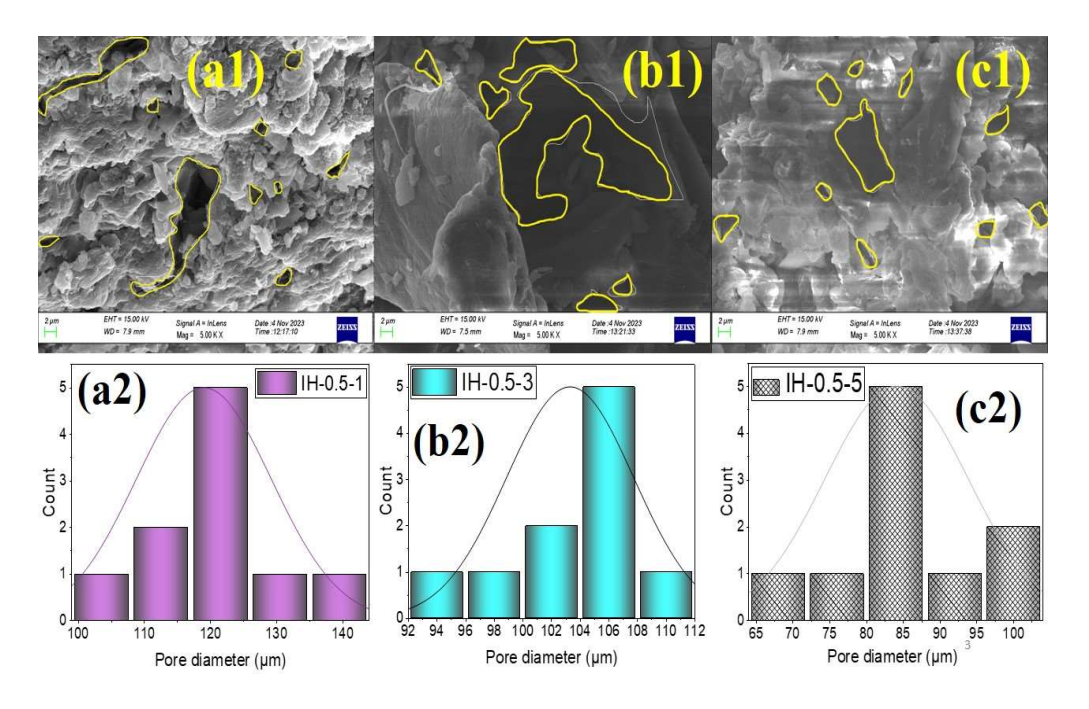


**Fig. 6. 7** FESEM images at different magnifications of (a1) IH-0.5-1, (b1) IH-0.5-3, (c1) IH-0.5-5 with respective histograms (a2, b2, and c2).

# 6.8 Swelling study of IHs

The swelling behavior of synthesized IHs is investigated in PBS at three pH levels (pH 5.5, pH 7.4, and pH 8.5) for both dry and gel forms at 37°C.

# 6.8.1 Swelling study from dry form of IHs (Method 1)

In the case of the dry form of IHs, with decreasing concentrations of NG-CHO-0.5 and at a low pH (pH 5.5), the swelling ratio rapidly increases. IH-0.5-1, which has a lower NG-CHO-0.5 concentration, shows a swelling ratio of roughly 611±20 %. While the swelling ratios of the hydrogels IH-0.5-3 and IH-0.5-5 were around 313±19.42 % and 162±23 %, respectively (Fig. 6.8.a). In physiological pH (7.4), the swelling ratio values of IH-0.5-1, IH-0.5-3, and IH-0.5-5, are 327±12 %, 198±12 %, and 158±10 %, respectively (Fig. 6.8.b). Swelling ratios are also determined in alkaline pH (8.5), and

the values for IH-0.5-1, IH-0.5-3, and IH-0.5-5 are  $394\pm14$  %,  $335\pm12$  %, and  $190\pm10$  % respectively (Fig. 6.8.c).

## 6.8.2 Swelling study from gel form of IHs (Method 2)

In the case of the freshly synthesized gel form of IHs, the swelling ratio increases quickly in an acidic environment (pH 5.5) with decreasing concentration of NG-CHO-0.5. The IH-0.5-1, which contains less NG-CHO-0.5, has a swelling ratio of about 476±20 %. The IH-0.5-3 and IH-0.5-5, on the other hand, have swelling ratios of about 250±21.23 % and 190±27 %, respectively (Fig. 6.8.d). Fig. 6.8.e shows the swelling ratios for IH-0.5-1, IH-0.5-3, and IH-0.5-5 are 253±14 %, 192±12 %, and 161±10 %, respectively, at physiological pH (7.4). The values for IH-0.5-1, IH-0.5-3, and IH-0.5-5 are  $306\pm14\%$ ,  $233\pm10\%$ , and  $206\pm12\%$  for swelling ratios in alkaline pH (8.5) (Fig. 6.8.f). The IHs network structure becomes more compact as NG-CHO-0.5 concentration increases (1 % w/v to 5 % w/v). As a result, the mobility of the polymer chains is more severely constrained, resulting in less exposure to water. The amino groups in CMCh are hydrophilic, making it simple to hydrate with water quickly. On the other hand, the imine group in the IHs is considered hydrophobic. So, IHs may have more hydrophobic moieties due to the higher concentration of NG-CHO-0.5. As a result, the IH's capacity to make hydrogen bonds with water decreases, lowering its swelling rate. As a result, the hydrogel IH-0.5-5, which has a higher concentration of NG-CHO-0.5, displays less swelling ratio comparatively to IH-0.5-1 and IH-0.5-3 in both dry and gel form in all pH ranges (5.5, 7.5 and 8.5). Additionally, swelling ratios of IH-0.5-1, IH-0.5-3, and IH-0.5-5 (dry and gel form) decrease with increasing pH (5.5 to 7.4) and further increase when pH rises to 8.5. For acidic pH (5.5), the amino groups of CMCh undergo protonation, which causes electrostatic repulsion between

inter- and intrapolymeric chains. Thus, the ruptured structure of the IHs network improves the water uptake. However, deprotonation within the amine group of CMCh reduces the swelling ratio in IHs at pH 7.4 (higher pH). Further, the carboxyl groups of CMCh become more ionized at pH 8.5, which increases the electrostatic repulsion and creates a loose network structure in IHs (dry and gel form), resulting in higher swelling ratios. Thus, the above studies show that the swelling ratios of dry and gel forms of IHs depend on the pH of the solution and the concentration of NG-CHO-0.5 [274][511]. Additionally, it was observed that the swelling ratio is higher in the dried form than in the gel form of IHs across all pH ranges. This is because there is already some extent of water molecules available. So, the gel form absorbs fewer water molecules than a dried form of IHs. Furthermore, the swelling percentage required for drug delivery varies depending on the application. A higher swelling percentage is often desired to prolong drug release and improve efficacy and adherence. The higher level of swelling allows the IH's matrix to expand and release the drug over a longer period, maintaining therapeutic levels in the body [512] [513]. Kumar et al. synthesized an IH based on Moringa oleifera gum and carboxymethyl chitosan crosslinked through the Schiff base mechanism. A swelling study was conducted for dry and gel forms of IHs. The dry form shows the highest swelling in pH 5.5 (415 %) than pH 7.4 (209 %). In the case of gel form, the highest swelling was observed at pH 5.5 (830 %) and then at pH 7.4 (430 %) [503].

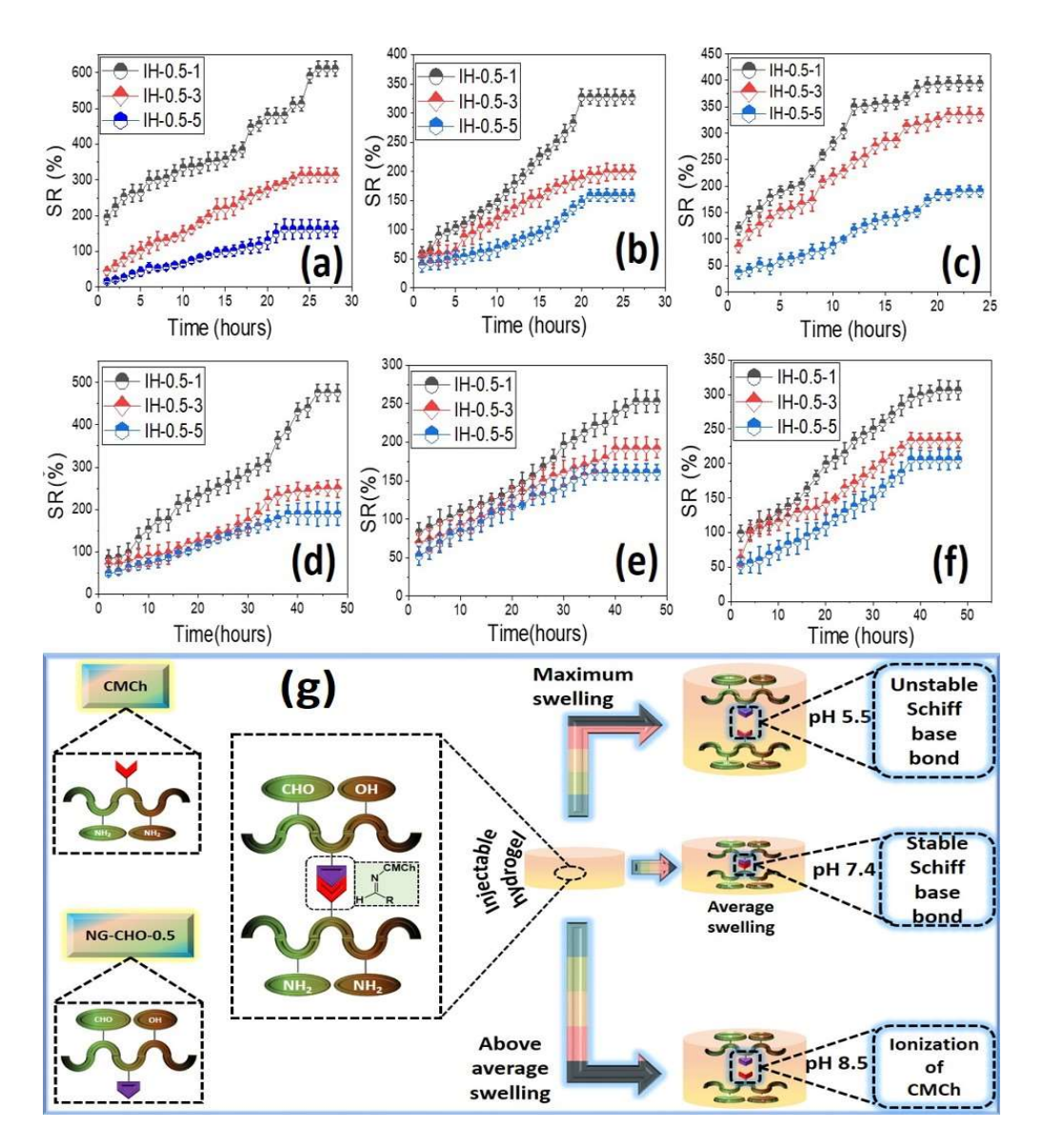


**Fig. 6. 8** Swelling behavior of IHs in PBS in dry form at 37°C (a) pH 5.5 (b) pH 7.4 (c) pH 8.5 and in gel form at (d) pH 5.5 (e) pH 7.4 (f) pH 8.5 (g) mechanism of swelling.

# 6.9 Drug release behavior

Using ciprofloxacin HCl as the model drug, the IH's drug release behavior was evaluated in PBS at pH 5.5, 7.4, and 8.5 at 37 °C. The antibiotic drug ciprofloxacin HCl is used to treat bacterial infections of the skin, urinary tract, and respiratory tract.

According to the experimental section's description, two separate approaches were used.

## 6.9.1 Drug release study from dry form of IHs (Method 1)

The Cipro release increases quickly at low pH (pH 5.5) with decreasing concentrations of NG-CHO-0.5. The IH-0.5-1 contains the least concentration of NG-CHO-0.5, giving a cipro release of about 9621±220 μg 100mL <sup>-1</sup> g<sup>-1</sup> of IH. On the other hand, the IH-0.5-3 and IH-0.5-5 give cipro release of about 6489±353.21 and 5012±523 μg 100mL <sup>-1</sup> g<sup>-1</sup> of IH, respectively (Fig. 6.9.a). The Cipro release for IH-0.5-1, IH-0.5-3, and IH-0.5-5 is 5125±144, 4662±191, and 3536±170 μg 100mL <sup>-1</sup> g<sup>-1</sup> of IH, respectively, at physiological pH (7.4) (Fig. 6.9.b). In alkaline media (pH 8.5), cipro release values for IH-0.5-1, IH-0.5-3, and IH-0.5-5 are 7165±221, 6358±219, and 5514±148 μg 100mL <sup>-1</sup> g<sup>-1</sup> of IH, respectively (Fig. 6.9.c). A relatable research article published by Wu and colleagues in which they fabricated an IH using Schiff base chemistry and 5-fluorouracil drug release studies reported that higher drug release was observed at pH 6.0 (58.9 %) than at PBS 7.0 (80 %) [496].

# 6.9.2 Drug release study from gel form of IHs (Method 2)

The second approach conducted the Cipro release through the gel form of IHs. The IH-0.5-1 includes the least concentration of NG-CHO-0.5, giving a Cipro release of 12723±793 μg 100mL <sup>-1</sup> g<sup>-1</sup> of IH. Furthermore, the Cipro release values for IH-0.5-3 and IH-0.5-5 are 11467±770 μg 100mL <sup>-1</sup> g<sup>-1</sup> of IH and 6446±70 μg 100mL <sup>-1</sup> g<sup>-1</sup> of IH, respectively (Fig. 6.9.d). At physiological pH (7.4), the Cipro release values for IH-0.5-1, IH-0.5-3, and IH-0.5-5 are 8626±238, 4197±346, and 3056±190 μg 100mL <sup>-1</sup> g<sup>-1</sup> of IH, respectively (Fig. 6.9.e). For cipro release in alkaline pH (8.5), the values

for IH-0.5-1, IH-0.5-3, and IH-0.5-5 are  $10127\pm499$ ,  $8346\pm388$ , and  $5000\pm289~\mu g$   $100 mL^{-1}~g^{-1}$  of IH, respectively (Fig. 6.9.f).

This can be explained by the fact that as the concentration of NG-CHO-0.5 rises (from 1 % w/v to 5 % w/v), the IHs network structure becomes more compact, which results in an increased crosslink density (0.7 to 1.2 g cm<sup>-3</sup>). As a result, the mobility of the polymer chains is more severely limited, leading to reduced exposure to the release of Cipro. Since amino groups in CMCh are hydrophilic, it is simple to hydrate with water immediately. On the other hand, the IHs contain the imine group, which is regarded to have a hydrophobic tendency. Because there is a more significant concentration of NG-CHO-0.5 in IHs, they may contain more hydrophobic moieties. The IH's ability to form hydrogen bonds with water declines, decreasing the pace of Cipro release. As a result, the IH-0.5-1 has a higher Cipro release than IH-0.5-3 and IH-0.5-5 in both dry and gel forms across all pH ranges (5.5, 7.5, and 8.5). Additionally, the Cipro release of IH-0.5-1, IH-0.5-3, and IH-0.5-5 (dry and gel form) decreases as pH increases (5.5 to 7.4), indicating a pH-sensitive behavior. This was because the Schiff base bond was unstable at low pH (5.5) and easy to break, which caused the structure of the IHs to be destroyed, and the physically trapped drug Cipro was released along the concentration gradient. When the pH value was increased (pH = 7.4), the Schiff base bond was relatively stable, and the release rate of Cipro was relatively slow due to the effect of physical interaction. Furthermore, at pH 8.5, CMCh carboxyl groups become more ionized, increasing electrostatic repulsion and forming a free network structure in IHs (dry and gel), increasing Cipro release. In the actual situation, when the IHs are used at the wound site, the second approach is more realistic than the first approach. The drug's slow release will help reduce microbial growth at the wound site during healing.

Thus, the experiments demonstrate that the Cipro release of IHs in their dry and gel forms relies on the solution's pH and the amount of NG-CHO-0.5. The release of Cipro was found to be slower in gel form than in the dry form of IHs across all pH ranges. In dry form, PBS enters the IHs to release the drug, while in gel form, the drug follows a diffusion mechanism to release. This can be further explained using the Korsemeyer–Peppas (K-P) model.

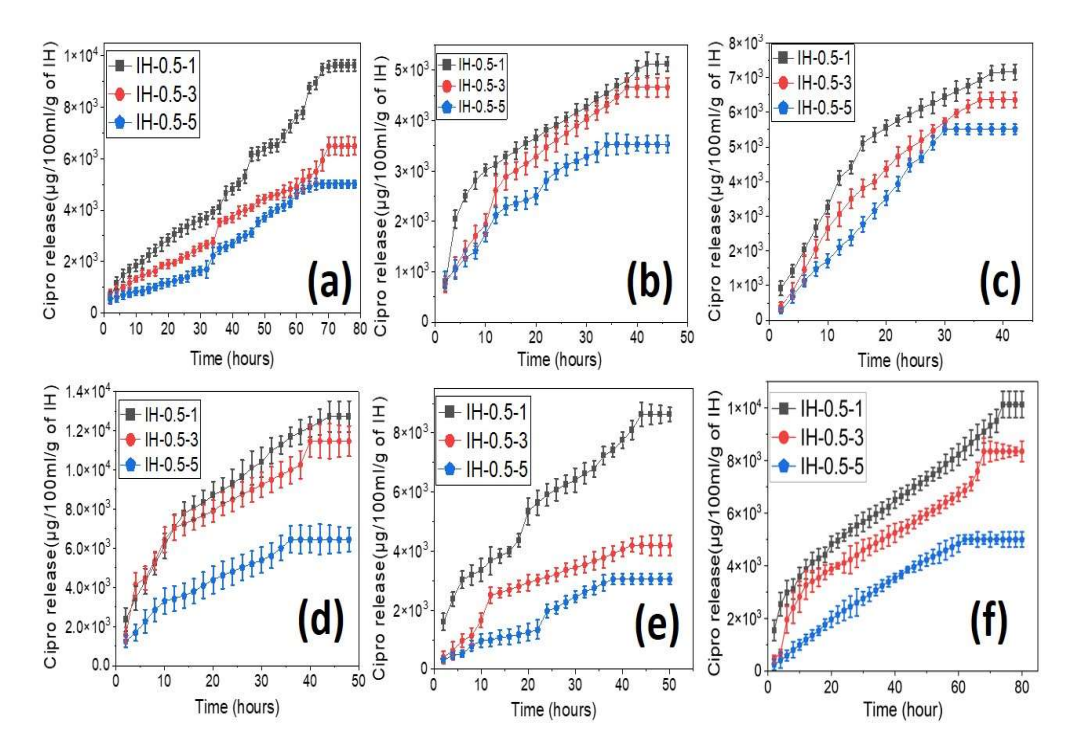


**Fig. 6. 9** Drug release behavior of IHs in PBS in dry form at 37°C (a) pH 5.5 (b) pH 7.4 (c) pH 8.5 and in gel form at (d) pH 5.5 (e) pH 7.4 (f) pH 8.5

K-P model provides the most accurate description of the antibiotic drug release mechanism through synthesized IHs (Table 6.4). When release exponent value "n" is equal to or less than 1, it denotes non-Fickian or anomalous diffusion, a combination of diffusion- and erosion-controlled rate release. When n=0.5, it denotes Fickian diffusion. Case II is indicated when n=1, and super case transport 2 is shown when n

> 1. For the release behavior of all the IHs, the value for R<sup>2</sup> is found to be more than 0.99. The "n" value was more than 0.5 and less than 1, observed in all synthesized IHs. So, the "n" value confirmed that all IHs showed non-Fickian or anomalous diffusion across all pH ranges in dry and gel form. Additionally, the diffusion rate is higher than the relaxation rate of the hydrogel matrix in all cases. Li and researchers reported that the 5-Fluorouracil drug release from IH generated by oxidized pectin and chitosan follows mostly Fickian diffusion at pH 6.8 and non-Fickian diffusion at pH 7.4 [497]. **Table 6.4** K-P kinetic model parameters for IH-0.5-1, IH-0.5-3, and IH-0.5-5 in dry and gel form in PBS at pH 5.5, 7.4, and 8.5

pH of PBS	Physical state of IH	Sample code	Parameters associated with the K-P model			
			k	n	R <sup>2</sup>	
	Dry	IH-0.5-1	3.31	0.74	0.99	
		IH-0.5-3	2.62	0.80	0.99	
рН 5.5		IH-0.5-5	3.20	0.74	0.99	
p11 3.3		IH-0.5-1	8.19	0.76	0.99	
	Gel	IH-0.5-3	11.54	0.68	0.99	
		IH-0.5-5	13.51	0.54	0.99	
	Dry	IH-0.5-1	14.48	0.61	0.99	
		IH-0.5-3	7.45	0.80	0.99	
11.5.4		IH-0.5-5	12.83	0.60	0.99	
pH 7.4	Gel	IH-0.5-1	14.32	0.61	0.99	
		IH-0.5-3	7.45	0.80	0.99	
		IH-0.5-5	12.83	0.60	0.99	
		IH-0.5-1	5.83	0.90	0.99	
	Dry	IH-0.5-3	4.71	0.92	0.99	
рН 8.5		IH-0.5-5	3.74	0.94	0.99	
		IH-0.5-1	5.46	0.93	0.99	
	Gel	IH-0.5-3	9.62	0.51	0.99	
		IH-0.5-5	2.42	0.92	0.99	

# 6.10 In vitro cytotoxicity evaluation

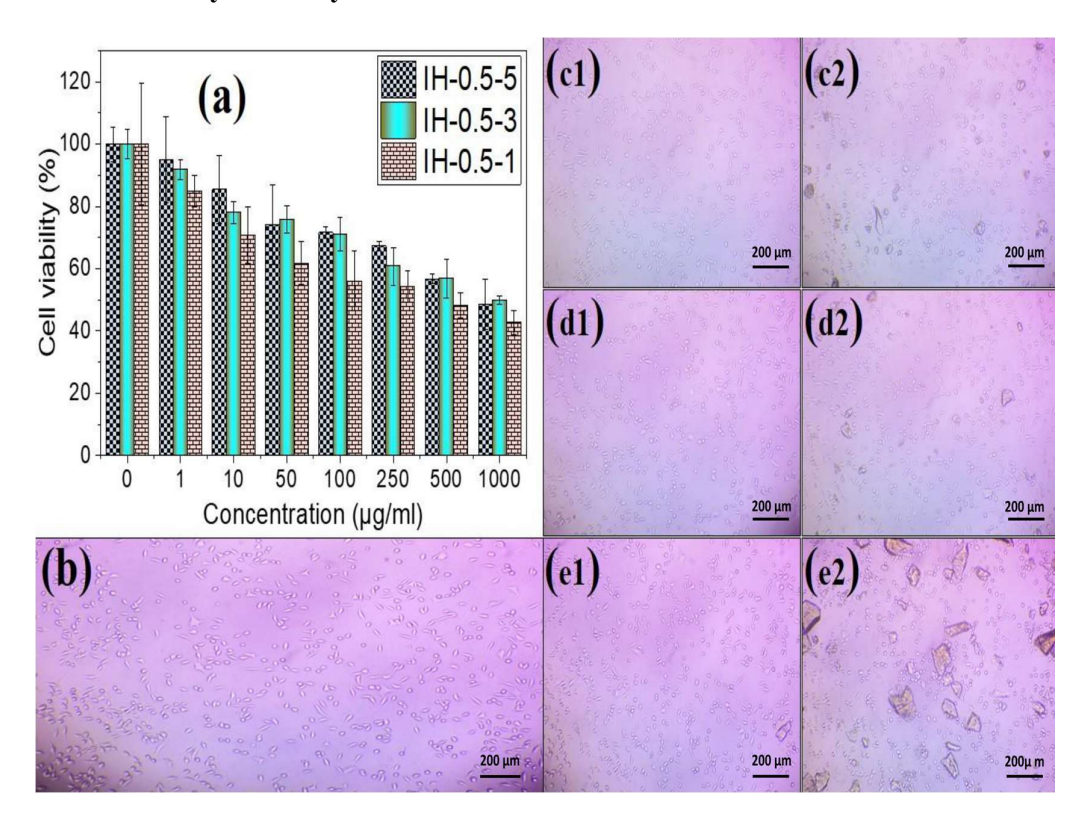


**Fig. 6. 10** (a) Cytotoxicity of injectable hydrogels. Inverted phase microscopic images of (b) control. IH-0.5-1 treated L-929 cell line at (c1) 1μg mL<sup>-1</sup> (c2) 500 μg mL<sup>-1</sup>. IH-0.5-3 treated L-929 cell line at (d1)1μg mL<sup>-1</sup> (d2) 500 μg mL<sup>-1</sup> IH-0.5-5 treated L-929 cell line at (e1) 1μg mL<sup>-1</sup> (e2) 500 μg mL<sup>-1</sup>

The main requirement for IHs to function as biomaterials for drug delivery applications is their biocompatibility with the host cells. Thus, the cytotoxicity of formulated IHs was investigated toward the L-929 fibroblast cell line. The MTT assay of the IH-0.5-1, IH-0.5-3, and IH-0.5-5 exhibits insignificant toxicity with cell viability of 54±1.53 %, 60±4.05 %, and 67±6.24 % up to 500μg mL<sup>-1</sup>, respectively (Fig. 6.10.a). This may be due to the presence of unreacted carbonyl groups present in the NG-CHO-0.5, which can interact with the cell proteins. A slight decrease in cell viability was

observed as the concentration of NG-CHO-0.5 decreased [514]. Fig. 6.10 (b to e2) shows synthesized inverted phase microscopic pictures of IHs. The results show that all IHs were compatible with fibroblast cells. Therefore, the IHs have exhibited good biocompatibility toward L 929 fibroblast cell lines.

## 6.11 Hemolysis assay

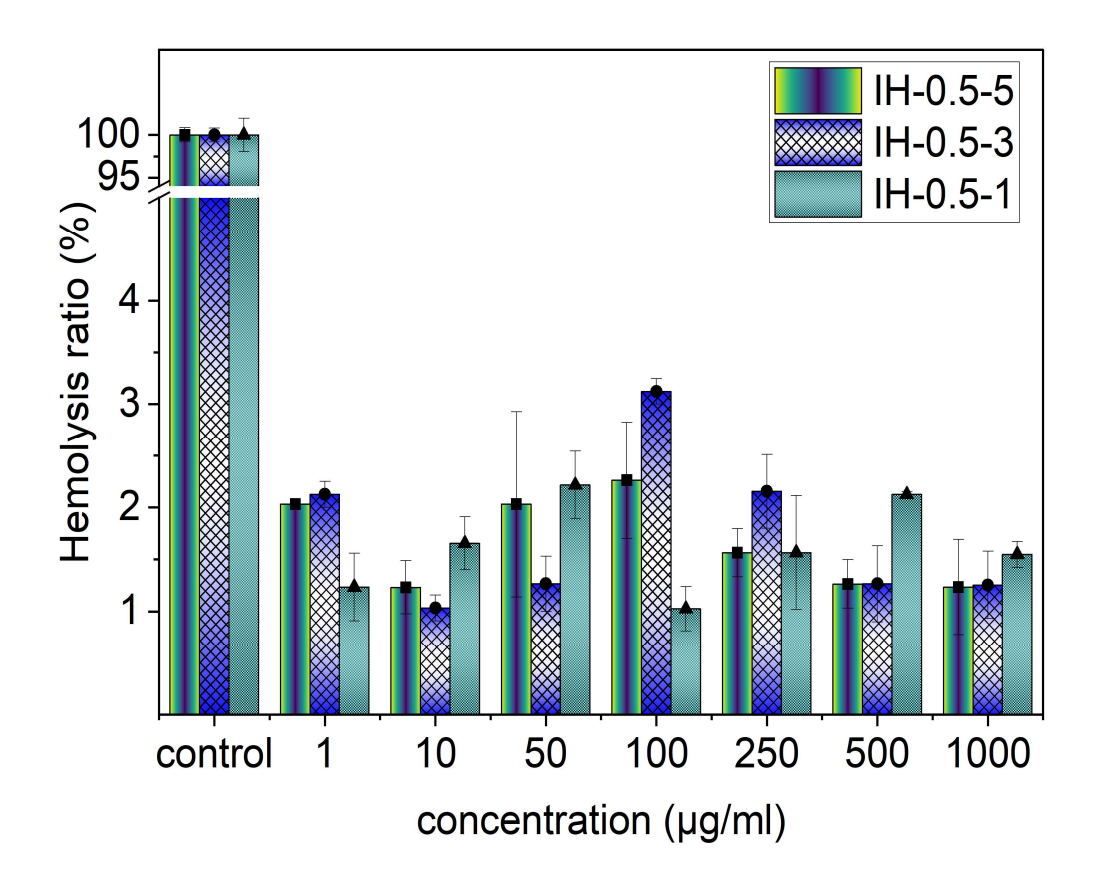


Fig. 6. 11 Hemolysis assay for IHs

Fig. 6.11 shows that the IHs have a color similar to PBS, while the RBC lysis group is bright red. The hemolysis rates of the IHs at various concentrations are all below 4%, meeting the standard for biomaterial hemolysis rates. As a result, IH-0.5-1, IH-0.5-3, and IH-0.5-5 exhibit negligible hemolytic activity across all tested concentrations (1)

to  $1000~\mu g~mL^{-1}$ ). A hemolysis ratio below 4% indicates that the IHs are non-toxic and suitable for promoting safe and effective wound healing.

# 6.12 Antibacterial assay

IHs must be antibacterial to prevent bacteria from entering the wound, eliminate microbes, and reduce inflammation. The antibacterial properties of Schiff base IHs are pH-responsive, with the highest activity observed at acidic pH levels. This is due to the reversible nature of the Schiff base linkages, which are more stable under acidic conditions [515]. The antibacterial assessment of IHs was examined using S. aureus and E. coli for 24 hours at 37°C. Fig. 6.12. displays the antibacterial test results of positive control along with IH-0.5-1, IH-0.5-3, and IH-0.5-5 (50 to  $1000 \,\mu g \, disc^{-1}$ ). All IHs exhibited inhibitory effects against each bacterium across all concentrations up to 24 hours at 37°C. These inhibitory effects have come from two major approaches. Firstly, Chitosan has inherent antibacterial properties due to its polycationic nature and ability to disrupt bacterial cell walls. Since the amino group in CMCh exhibits a positive electrical charge, it traps bacteria with negative charges via electrostatic forces, thus effectively inhibiting bacterial growth. Additionally, it could induce the leakage of proteinaceous and other intracellular components from bacteria. Secondly, dynamic imine bonds have been proven to have certain antibacterial functions. Therefore, the combination of active Schiff base and protonated amino group in CMCh endows IHs with excellent antibacterial properties by defending the cell wall from the dispersion of active ingredients toward the cytoplasm. Thus, the imine bond in IHs further enhances the antibacterial effects. Li et al. synthesized an IH based on hyaluronic acid and chitosan via enzyme-catalyzed and Schiff-based crosslinks, showing excellent antibacterial results against S. aureus and E. coli [516].

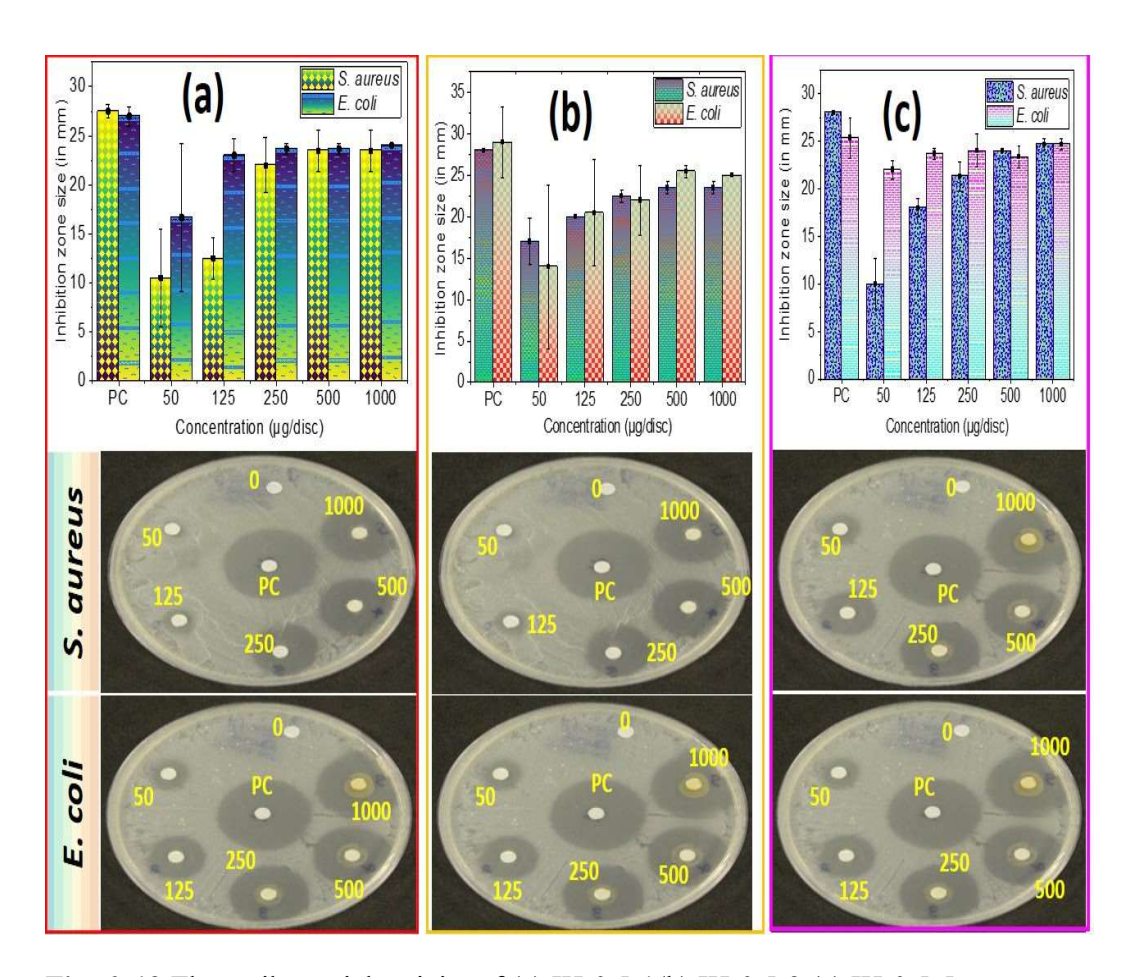
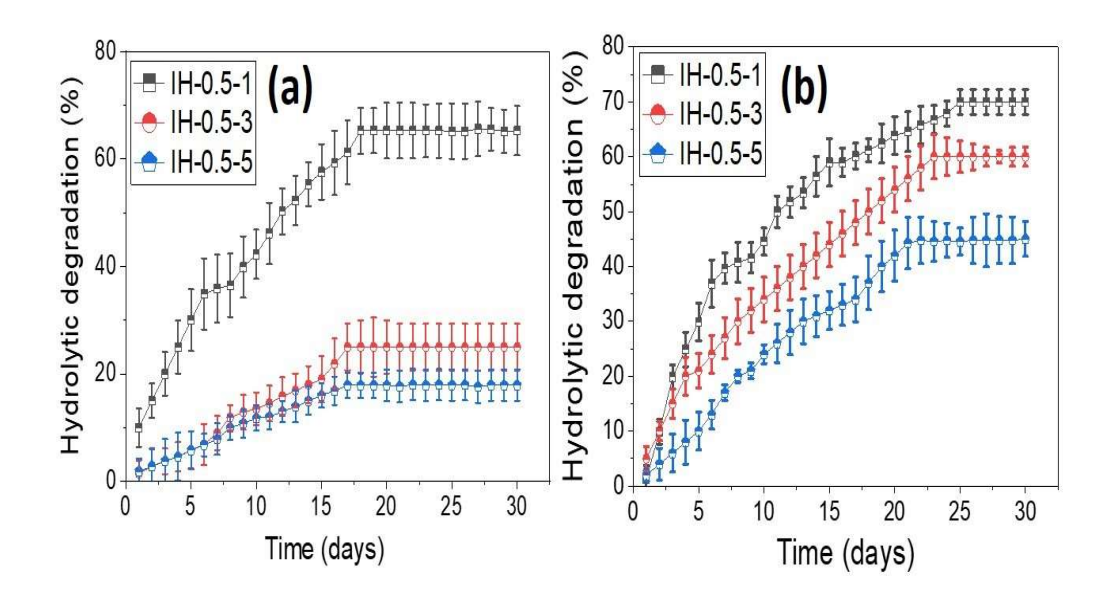


Fig. 6. 12 The antibacterial activity of (a) IH-0.5-1(b) IH-0.5-3 (c) IH-0.5-5

# 6.13 Hydrolytic degradation

The imine bond undergoes hydrolytic cleavage in PBS (pH 7.4) at 37°C. This hydrolytic degradation results in the breakdown of the polymer network and the formation of smaller molecular weight fragments. As the hydrolytic degradation progresses, the smaller molecular weight fragments produced become soluble in the PBS (pH 7.4) at 37 °C and dissolve or disperse into the liquid medium. It is important to note that degradation and dissolution can occur simultaneously or sequentially [517]. The hydrolytic biodegradability of synthesized IHs was studied in PBS (pH 7.4) at 37 °C for 30 days. Two approaches were used to quantify the result (Fig. 6.13.). The

first approach conducted a hydrolytic degradation study using the dry form of IHs. The IH with the highest concentration of oxidized NG (IH-0.5-5) degraded the least (20±4 %). Meanwhile, the IH with the lowest concentration of oxidized NG (IH-0.5-1) was the most degraded (65±5%). Additionally, IH-0.5-3 showed 25±4% degradation (Fig. 6.13.a). In the second approach, freshly synthesized gel forms of IHs were used to conduct the study. Here, the same type of degradation behavior was observed. The IH, having the highest concentration of oxidized NG (IH-0.5-5), observed 45±7 % degradation. At the same time, IH, which has the lowest concentration of oxidized NG (IH-0.5-1), observed 70±3 % degradation. Additionally, the concentration of oxidized NG between these two (IH-0.5-3) shows 60±10 % degradation (Fig. 6.13.b). The correlation between the degradation rate and crosslinking density can explain this finding. The concentration of NG-CHO-0.5 and crosslinking density significantly impact the hydrolytic degradation of these IHs. As the concentration of NG-CHO-0.5 was increased, the crosslink density increased, making it more difficult for water molecules to penetrate and cleave the Schiff base bond of IHs. As a result, the rate of hydrolytic degradation was declined. Pandit et al. fabricated an IH using N, O-carboxymethyl chitosan, and multialdehyde guar gum crosslink through the Schiff base mechanism; the IH having higher concentrations of oxidized guar gum degraded the least (85 %) and the IH having most minuscule amount of oxidized guar gum degraded the most (~99 %) up to 24 days at 37°C in pH 7.4 [274].



**Fig. 6. 13** Hydrolytic degradation behavior of IHs in PBS (pH 7.4) at 37°C (a) dry form (b) gel form

## **6.14 Conclusion**

The biodegradable, biocompatible, and self-healing IHs have been fabricated using dynamic Schiff base linkages between multi-aldehyde groups of oxidized NG and CMCh. The optimized concentration of sodium periodate is 0.5 %w/v, which converts the hydroxyl group to the aldehyde group of NG. The ideal ratio of the concentration of NG-CHO-0.5 to CMCh decides the least gelation time (18±1.6 to 3±0.5 minutes), which seems enough for administration. The synthesized IHs are ideal for syringeability and injectability evaluation because of their exceptional viscoelastic, shear-thinning, and self-healing properties. Because of self-healing behavior, IHs rapidly recover their mechanical integrity to provide a protective, conformable matrix. The swellability and drug-release behavior of IHs are pH-dependent and well-correlated with crosslink density. The IHs showed drug release behavior using model drug ciprofloxacin HCl, with a more significant release in PBS at pH 5.5 than at pH

7.4 and pH 8.5. The prolonged drug release is found in the gel form of IHs, which supports wound healing. The drug release behavior follows the non-Fickian diffusion mechanism. *In vitro*, cytotoxicity evaluation towards L-929 fibroblast cell lines and antibacterial assay favor the biocompatibility of synthesized IHs. Furthermore, IHs are observed to have better hydrolytic degradation in PBS (pH 7.4) at 37 °C.

#### **CHAPTER 7**

# SYNTHESIS AND CHARACTERIZATION OF INJECTABLE HYDROGEL BASED ON MULTIALDEHYDE OKRA GUM CROSSLINKED WITH CARBOXYMETHYL CHITOSAN VIA SCHIFF BASE MECHANISM

#### 7.1 Introduction

This chapter describes the synthesis process of multi-aldehyde okra gum using NaIO<sub>4</sub> as an oxidizing agent, and CMCh to design the IH crosslinked through the Schiff base mechanism at 37°C. The aldehyde groups of oxidized okra gum covalently crosslinked with the NH<sub>2</sub> groups of CMCh, eliminating the need for hazardous or chemical crosslinking agents. The research delves into syringeability, injectability, self-healing properties, swelling behavior, and drug release profiles in PBS under various wound pH conditions (5.5, 7.4, and 8.5) at 37°C. The biocompatibility, antibacterial assays, and *in vitro* degradation of the synthesized IHs are also evaluated in PBS (pH 7.4) at 37°C.

## 7.2 Gelation time

The gelation time of an IH is an important parameter that determines its practical usability and clinical application. The time at which the liquid precursor solution

transforms into a stable, three-dimensional hydrogel network structure at 37°C is defined as gelation time. The ratio of OG-CHO to CMCh varied, and the effect on gelation time was observed. The tube inversion test shows that OG1C2, OG1C1, and OG2C1 gelation times are  $10\pm2$ ,  $5\pm1.2$ , and  $3\pm1.5$  minutes, respectively (Fig. 7.1.a). IHs can have a gelation time ranging from a few seconds to several hours, depending on the total polymer concentration or ratio of liquid precursor solutions [518]. The ratio of aldehyde groups of OG-CHO to amine groups of CMCh was calculated using the simple unitary method and reported in Table 7.1. It was observed that as the ratio of the aldehyde group of OG-CHO to the amine group of CMCh increased, the time of gel formation decreased, primarily because a total number of aldehyde functional groups is more likely to react with the amine groups of CMCh. The oscillatory time sweep study on the rheometer was carried out to calculate the gelation time. The gelation point is a crossover point where the storage modulus (G') overcomes the loss modulus (G"). The time required to reach the gel point is called the gelation time. Fig. 7.1.b to 7.1.d show the oscillatory time sweep behavior of IHs. The gelation time of OG1C2, OG1C1, and OG2C1 was 9±3, 5±1.5, and 2±1 minutes, respectively, which supports the tube inversion test. Since OG2C1 has the shortest gelation time, it was considered an optimized IH for further characterization. A similar article published by Zhang et al. in which an IH was synthesized using carboxymethyl chitosan and hyaluronic acid through Schiff base and acyl hydrazide bonding, where gel time formation using tube inversion test supported the time sweep study conducted by rheometer [519].

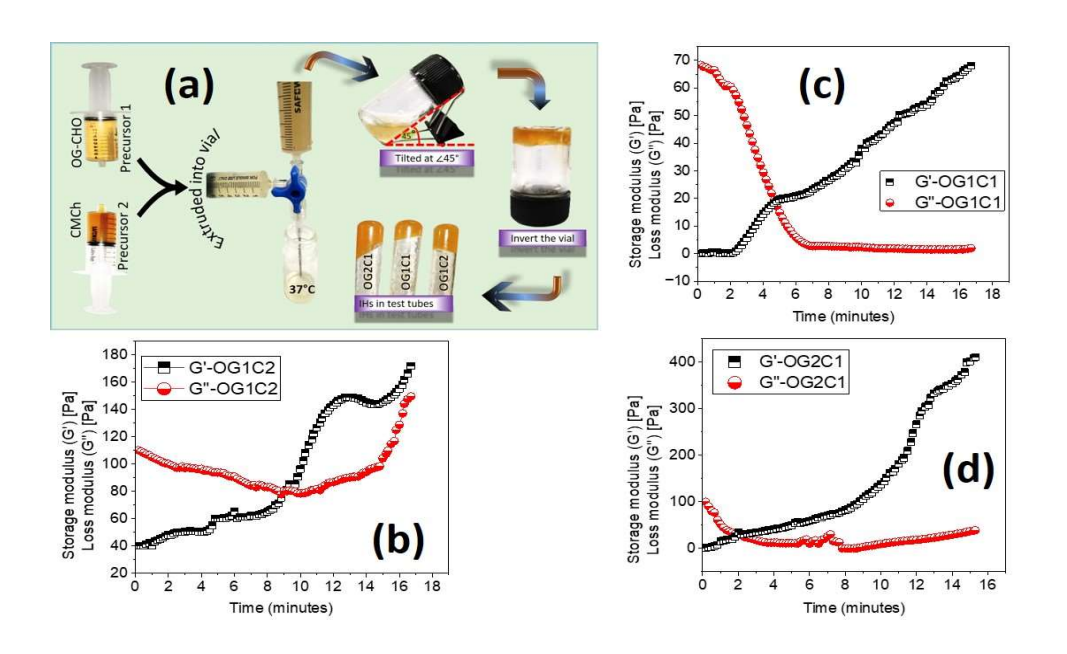


**Fig. 7. 1** (a) Tube inversion test. Time sweep study of (b) OG1C2 (c) OG1C1 (d) OG2C1 at 37°C.

Table 7.1 The concentration of precursors for the synthesis of IHs

Injectable	Conc. of	Volume	Conc. of	Volume	Ratio	Gelation
hydrogels	aldehyde	of OG-	amine	of	$-\frac{\mathbf{A} \times \mathbf{B}}{}$	time
	group in	СНО (	group in	CMCh (	$-\overline{\mathbf{C} \times \mathbf{D}}$	(minutes)
	OG-CHO	mL)	CMCh	mL) (D)		
	(% w/v)	(B)	(%)			
	(A)		(C)			
OG1C2	56±1.7	1	67±2.11	2	0.42	9±3
OG1C1	56±1.7	1	67±2.11	1	0.82	5±1.5
OG2C1	56±1.7	2	67±2.11	1	1.67	2±1

# 7.3 Physical properties of OG2C1

Table 7.2 presents the physical characteristics such as gel content, porosity, syringeability, and network parameters. The gel content and porosity for OG2C1 are

recorded as 84±2% and 66±3%, respectively. The higher gel content and lower porosity of IHs are attributed to effective crosslinking via imine bonds. This results in the construction of a more compact 3D structure formation. Yan and coworkers have fabricated an IH using Schiff base chemistry between poly(L-glutamic acid) and chitosan, in which the observed gel content was 79% [478]. Another group of researchers published a research article based on Schiff base crosslinking using oxidized galactomannan and N-succinyl chitosan, in which they evaluated a porosity determination of 69% [477].

The calculated syringeability percentage was nearly 99±0.5%, which confirmed the synthesized good syringeability ability when extruded through a 26 G needle. Wang *et al.* reported on an IH made from transformed copper sulfide, which was then used for photothermal therapy. They tested the hydrogel's injectability using syringes of various sizes (26 G, 25 G, 23 G, and 18 G) and found that the 26 G needle shows the best results [479]. To ensure the synthesized IHs are suitable for clinical use, the researchers investigated their injectability. There are no global guidelines or regulations governing injectability testing, but various research articles have reported different injectability test methods [520][519]. The needle gauge used for testing should match the size used clinically to administer the hydrogel precursors subcutaneously, typically ranging from 18-21 G to 26-27 G. In this study, the injectability evaluation was successfully carried out using a 26 G needle. Fig. 7.2. shows an image of the extruded injectable hydrogel-forming structure ("J.K." and "©") when expressed from a 10 mL capacity 26 G needle into a glass petri dish. The easy flow through the needle confirmed the hydrogel's ready accessibility for administration. Vahedi *et al.* synthesized an IH using gelatin and

polyethylene glycol dibenzaldehyde by Schiff base reactions, in which they evaluated the injectability test using a 20 G syringe and formed a letter "R" and "N"[519].

Self-healing IHs are one of the biomaterials that have emerged in recent years, with the capacity to heal any damage autonomously. The hydrogel is a commanding material for tissue restoration and is injected through a smaller syringe, making it one of the least intrusive biomaterials. They offer the advantages of personalized treatments and the precision delivery of bioactives or therapeutics. The self-healing ability of the hydrogel is enabled via the development of a crosslinked system with dynamic and reversible bonding to allow the capacity to heal in a timescale of seconds, which is a requirement for any application in tissue restoration [521]. To demonstrate the self-healing property, two differently colored hydrogels were fabricated and cut into semicircular shapes. The cut surfaces were then brought together to allow selfhealing. It was observed that the cut surface gradually healed during the healing process. After 1 hour, the two samples had integrated, indicating that the cut surfaces had healed together by reconstructing reversible Schiff-base bond linkages (Fig. 7.3). Additionally, due to the shear-thinning property of the hydrogel (viscosity decreases with increasing shear stress), the OG2C1 exhibited extrusion ability through a needle. After injection, it could regain its gel state in different shapes, supporting good injectable properties. These properties make the IH suitable for minimally invasive drug delivery, potentially reducing scarring and pain and promoting faster patient recovery. The results suggest that the dynamic reaction among functional groups is the main driving force behind the hydrogel's self-healing capability, rather than simple physical adhesion between the broken interfaces. The constant cleavage and regeneration of imine bonds on Schiff-base bonds allow the interaction between CMCh

molecules of the separated networks, creating space for network reconstruction. Consequently, new Schiff-base bonds form on the contact surfaces of the separated hydrogels, leading to the reconstitution of the network and captured water during the self-healing process.

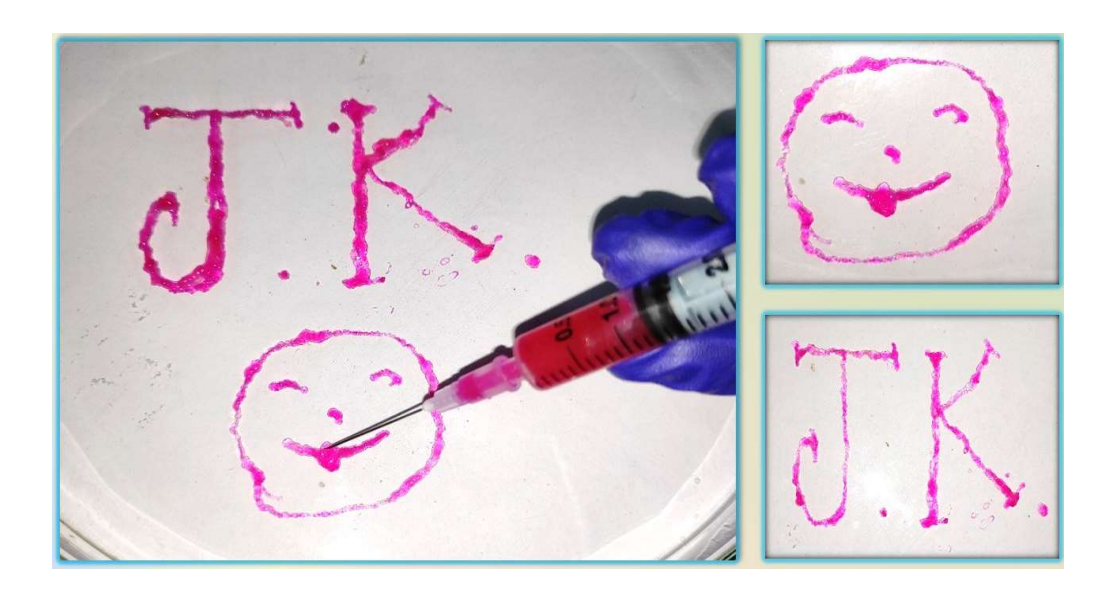


Fig. 7. 2 Injectability evaluation of OG2C1 using 26 G needle.

**Table 7.2** Physical properties of OG2C1

Property	value		
Troperty	OG2C1		
Gel content	84 %		
Porosity	66 %		
Syringeability	99 %		
Average molecular weight between crosslinks	2.8 ×10 <sup>2</sup> g mol <sup>-1</sup>		
Crosslink density	0.9 mol cm <sup>-3</sup>		
Mesh size	7.5×10 <sup>-3</sup> nm		

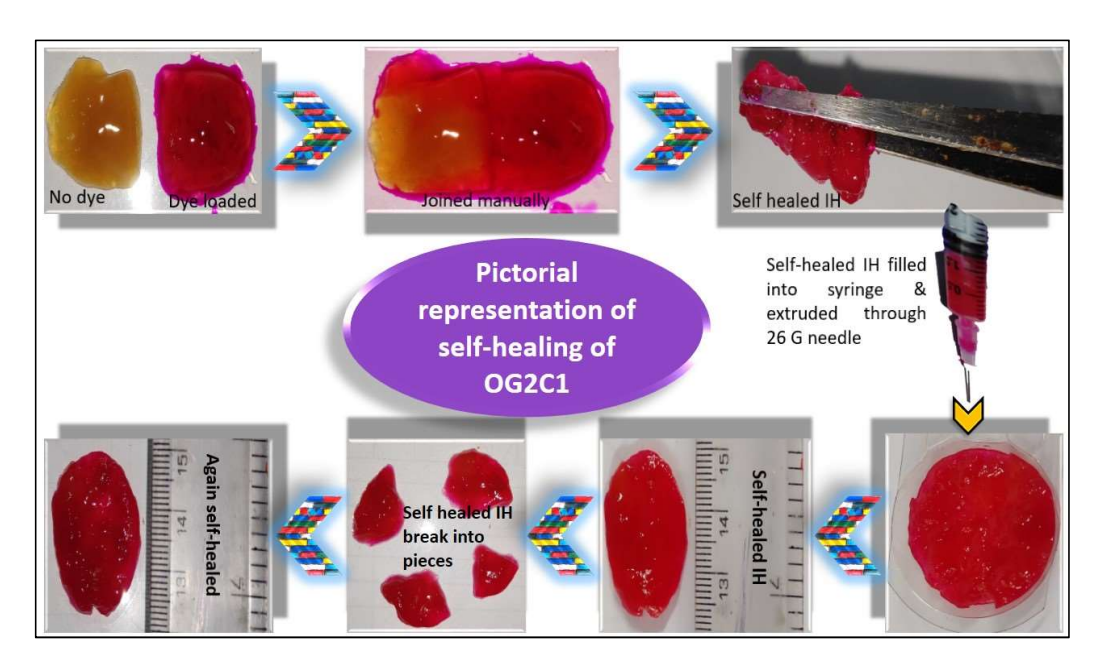
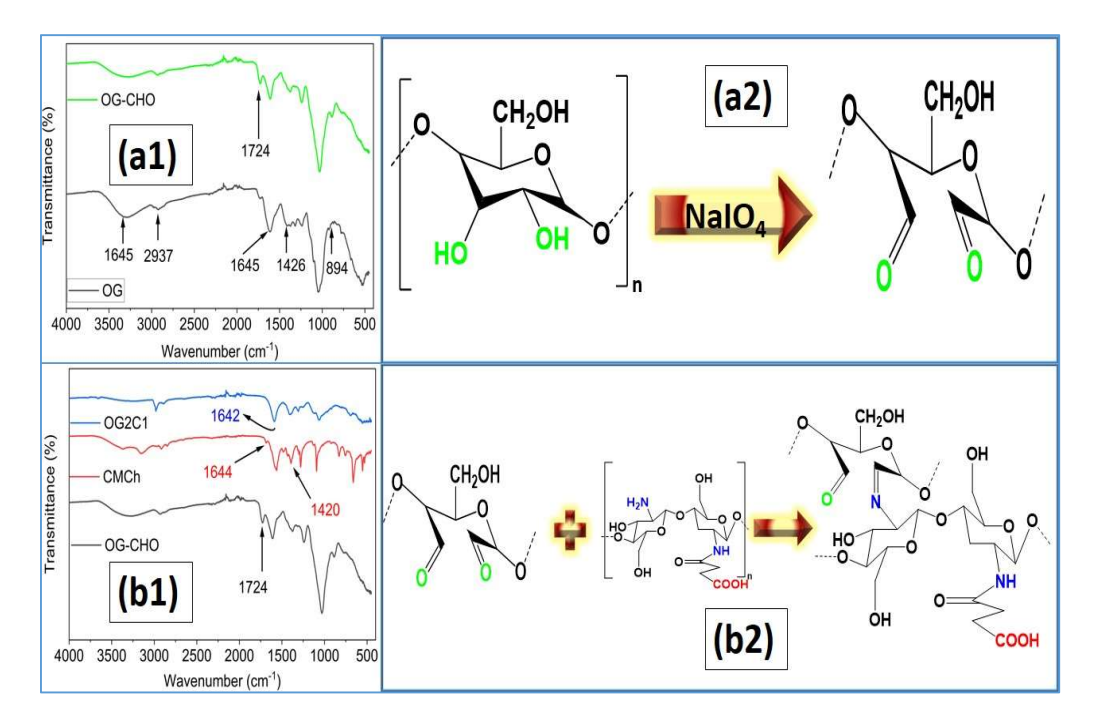


Fig. 7. 3 Pictorial representation of Self-healing of OG2C1

# 7.4 Structural properties

Structural properties of OG2C1 were characterized using FT-IR spectroscopy and <sup>1</sup>H-NMR. Okra gum FT-IR spectrum demonstrates a broad band at 3404 cm<sup>-1</sup>, which proves carboxylic acid existence, and this is due to O–H near the carboxylic acid band; another peak at 2937 cm<sup>-1</sup> is visible, which represents methylene (CH<sub>2</sub>) functional group. The peak at 1645 cm<sup>-1</sup> represents amide-I occurrence. Due to the hydroxyl group, the deformation band is visible at 1426 cm<sup>-1</sup>. The peak at 894 cm<sup>-1</sup> was because of polysaccharides (Fig. 7.4.a1). After OG reacts with sodium periodate, significant peaks were observed at 1724 cm<sup>-1</sup> (Fig. 7.4.b1), mainly attributed to the production of symmetrical vibration of aldehydes bonds. Another comparative research found Similar outcomes for the oxidized polysaccharide [485]. The FT-IR spectrum of CMCh (Fig. 7.4.b1) reveals the existence of two additional peaks at 1644 and 1420 cm<sup>-1</sup>, which are attributable to symmetric and asymmetric stretching vibrational modes

of the -COO group, respectively, and indicate the successful derivatization of chitosan and confirmed the presence of carboxymethyl groups on CMCh [486]. The OG2C1 FT-IR spectrum (Fig. 7.4.b1) shows a peak at 1642 cm<sup>-1</sup>, which demonstrates imine structure formation due to dynamic Schiff base crosslinking reaction between the amine group of CMCh and the aldehyde groups of OG-CHO [487].



**Fig. 7. 4** FT-IR spectra of (a1) OG, OG-CHO (b1) OG-CHO, CMCh, OG2C1. Reaction Schemes of (a2) oxidation of OG (b2) synthesis of OG2C1

Proton NMR also supports structural properties. The <sup>1</sup>H-NMR spectrum of chitosan, CMCh, OG, and OG-CHO are described using D<sub>2</sub>O as a solvent. <sup>1</sup>H-NMR spectra of the chitosan show a peak at 1.24 ppm due to protons in the acetyl group. The anomeric protons of glucosamine show a peak at 2.96 ppm, while the non-anomeric protons of the chitosan structural backbone are responsible for the peaks ranging from 3.68 to 4.84 ppm (Fig. 7.5.a). Additionally, a new peak was observed at 3.87 ppm due to the

presence of the –CH<sub>3</sub>COO- group (Fig. 7.5.b). Due to the presence of the methyl group of rhamnose, the spectra displayed congested signals in the 1.23 and 1.92 ppm spectrum bands. The peak available at 3.60-3.69 was due to the –OH and CH of mannose. Signals at chemical shift equal to 3.81-3.60 ppm, assigned to the CH<sub>2</sub> group of arabinose. Signals in the 3.63 and 3.79 ppm range are transferred to the proton linked to C<sub>6</sub> and C<sub>4</sub> of galactose [43] (Fig. 7.5.c). A new distinctive peak of the aldehydic proton is observed at 8.11 ppm, confirming OG oxidation (Fig. 7.5.d).

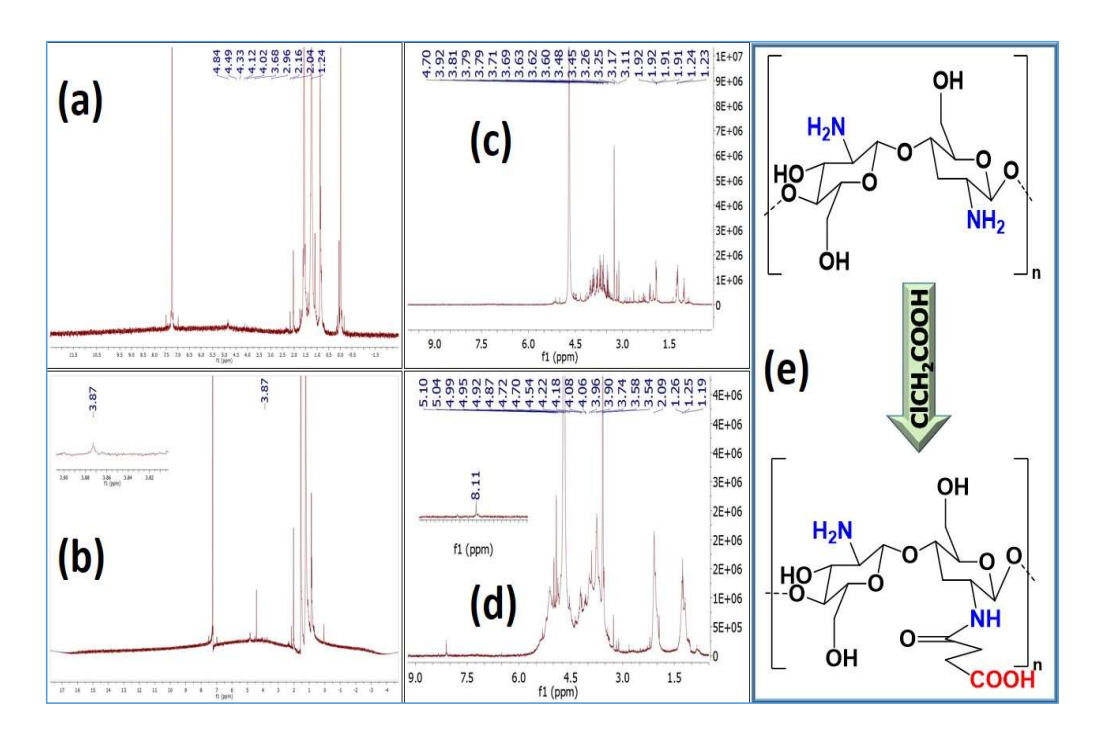


**Fig. 7. 5** <sup>1</sup>H- NMR spectra of (a) chitosan (b) CMCh (c) OG (d) OG-CHO (e) reaction scheme of derivatization of chitosan

## 7.5 Rheological study

To evaluate the shear thinning characteristics, a continuous flow sweep test was conducted at 37°C, ranging from 1 to 1000 s<sup>-1</sup> with a constant 1% strain, wherein

OG2C1 was placed between the parallel plates of the instrument. As the shear rate increased, a reduction in viscosity was observed (from 650840 to 41 m Pa.s), indicating the shear thinning behavior. This phenomenon may be attributed to the rupture of Schiff base linkages at higher shear rates (Fig. 7.6.a). The shear thinning property of the IH further corroborates the findings on its syringeability and injectability.

During the amplitude sweep test of the OG2C1, it underwent varying strain levels ranging from 0.1 to 100% at 37°C (Fig. 7.6.b) to delineate the LVE. The LVE ranges from 0.1 to 5% strain, with a chosen % strain value of 1% for all gelation kinetic studies. The maximum storage modulus (G') and loss modulus (G") were recorded at 138 Pa and 5 Pa, respectively. Across different strain levels, the hydrogels consistently exhibited higher G' values than G", with a crossover point at 32 % shear strain, indicating a transition in the hydrogel's physical state from solid to liquid.

A frequency sweep test was employed to explore the rheological characteristics of the OG2C1 hydrogel, as illustrated in Fig. 7.6.c. The G' was consistently more significant than the G", indicating that the IH possesses stiffness and elasticity. This elevated G' (360 Pa) observed in OG2C1 can be attributed to its high crosslink density, which restricts chain mobility and deformability.

A series of rheological recovery tests were conducted to assess the quantitative analysis of self-healing properties of OG2C1. The IH restorative capacity was examined through oscillatory step-strain measurements. At low strain levels (1%), the G' value exhibited a significantly high magnitude. However, as the strain increased to higher values (200%), the G' value approached G", indicating structural deformation under high strain conditions (Fig. 7.6.d). These behaviors remained stable across multiple

cycles, underscoring the self-healing capability and durability of the dynamic Schiff base and dynamic coordination network within the IH. After completing all cycles of alternating strain from low to high, the recovery percentage (Equation 7.1) was calculated and found to be 78 %.

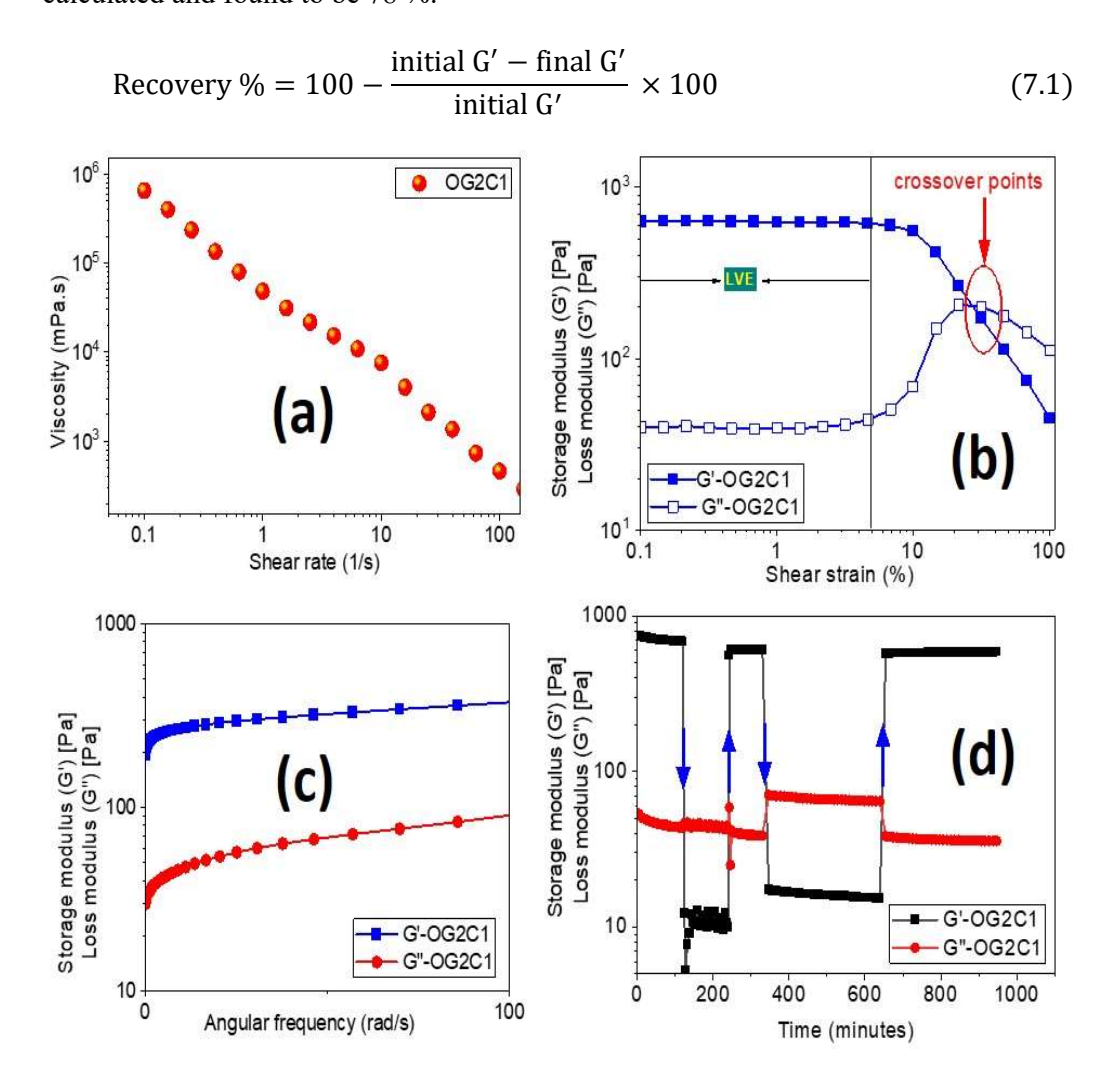


**Fig. 7. 6** Rheological study of OG2C1 at 37°C (a) Flow sweep study (b) Amplitude sweep study (c) Frequency sweep study (d) Step-strain analysis

Li et al. synthesized an IH using Schiff base crosslinks between dialdehyde-modified hyaluronic acid and cystamine dihydrochloride and measured the self-healing

properties qualitatively and quantitatively. Their results showed that the IH could self-heal within 2 hours [340].

# 7.6 Morphological evaluation

The surface morphology of OG2C1 reveals a scaly surface with a porous network structure in the form of several rings. These circular-shaped structures are dense pores interconnected to irregular surfaces. Using Image J software, the average pore diameter was 70 to 95  $\mu$ m (Fig. 7.7). The porous structure is advantageous for drug delivery applications as it allows for easy diffusion of drugs from the IH.

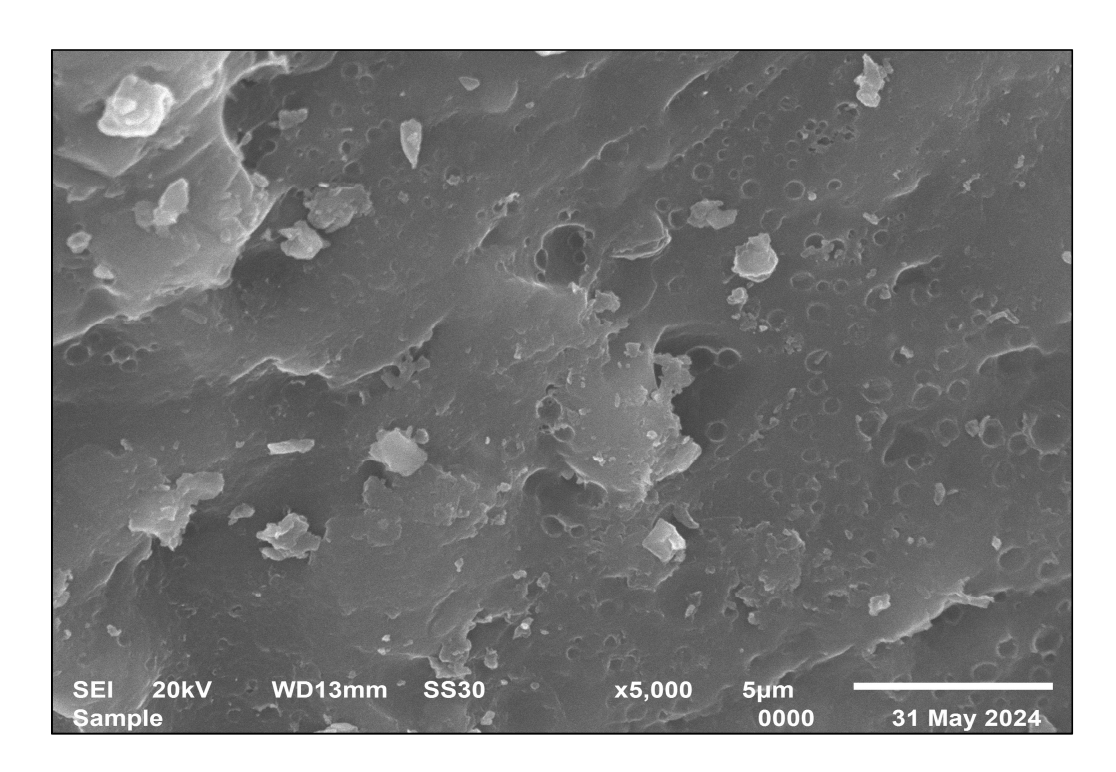


Fig. 7. 7 SEM image of OG2C1 at 5000X.

# 7.7 Swelling study

Two methods were used to investigate the swelling behavior of the OG2C1 in PBS at pH 5.5, 7.4, and 8.5 at 37°C.

# 7.7.1 Swelling study from dry form of OG2C1 (Method 1)

Fig. 7.8.a illustrates Method 1, which examined the swelling from the dry form of OG2C1. The observed swelling ratio percentages are 997% at pH 5.5, 713 % at pH 7.4, and 970 % at pH 8.5.

# 7.7.2 Swelling study from gel form of OG2C1 (Method 2)

In Method 2, the swelling behavior of the gel form of OG2C1 was studied (Fig. 7.8.b). The observed swelling ratio percentages are 750 % at pH 5.5, 635 % at pH 7.4, and 724 % at pH 8.5.

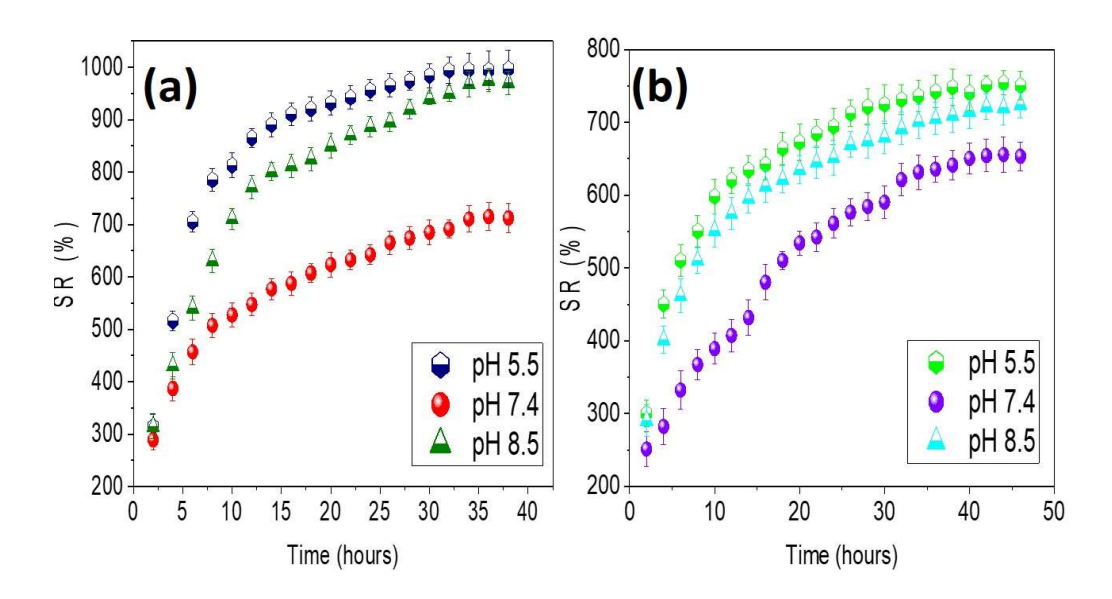


**Fig. 7. 8** Swelling study of OG2C1 in PBS (pH 5.5, 7.4, and 8.5) at 37°C (a) dry form (b) gel form.

The swelling trend remains consistent between the freshly prepared gel form and the dry state of the IH. The swelling ratios of the dry and gel forms of OG2C1 decrease as the pH increases from 5.5 to 7.4. However, the swelling ratios increase when the pH is further raised to 8.5. At acidic pH 5.5, the amino groups of the CMCh undergo

protonation. This leads to electrostatic repulsion between the interpolymeric and intrapolymeric chains, improving water uptake and resulting in a higher swelling ratio. In contrast, at the more neutral pH of 7.4, deprotonation occurs within the amine groups of CMCh. This reduces the swelling ratio of the IH. When the pH is increased to 8.5, the IH network structure becomes looser, which results in even higher swelling ratios for both the dry and gel forms. Overall, the swelling ratios of the dry and gel forms of IHs depend on the pH of the solution. It was also observed that the swelling ratio is higher in the dried form than in the gel form across all pH ranges. The dried form initially has less water content to absorb more water molecules than the gel form.

# 7.8 Drug release study

Using Cipro as the model drug, the drug release behavior of the IH was evaluated in PBS at pH 5.5, 7.4, and 8.5 at 37 °C. Cipro is an antibiotic drug used to treat bacterial infections of the skin, urinary tract, and respiratory tract. According to the experimental section, two separate approaches were used to study the drug release. The drug release trend was consistent between the freshly prepared gel form and the dry form of the IH.

## 7.8.1 Drug release study from dry form of OG2C1 (Method 1)

In the first approach, where the drug release was evaluated from the dried form of the OG2C1, the Cipro release decreased (7017  $\mu g$  100mL<sup>-1</sup> g<sup>-1</sup> of OG2C1 to 5516  $\mu g$  100mL<sup>-1</sup> g<sup>-1</sup> of OG2C1) as the pH increased from 5.5 to 7.4. However, the release increased further at the alkaline pH of 8.5, reaching around 6020  $\mu g$  100mL<sup>-1</sup> g<sup>-1</sup> of OG2C1 (Fig. 7.9.a).

# 7.8.2 Drug release study from gel form of OG2C1 (Method 2)

In the second approach, the drug release was studied from the freshly synthesized gel form of the IH. Here, the Cipro release also decreased (9146  $\mu$ g 100mL<sup>-1</sup> g<sup>-1</sup> of OG2C1 to 5912  $\mu$ g 100mL<sup>-1</sup> g<sup>-1</sup> of OG2C1) as the pH increased from 5.5 to 7.4, and then increased (8436  $\mu$ g 100mL<sup>-1</sup> g<sup>-1</sup> of OG2C1) again at the alkaline pH of 8.5 (Fig. 7.9.b). The Cipro release from both the dried and gel forms of the IH followed a similar trend, i.e., the Cipro release decreased as the pH was raised from 5.5 to 7.4 but then increased when the pH was further raised to 8.5.

This behavior can be explained as, at pH 5.5 (an acidic pH), the amino groups of CMCh undergo protonation, which results in electrostatic repulsion between inter- and intrapolymeric chains. Therefore, the IH network's ruptured structure enhances levo release. However, at pH 7.4 (higher pH), deprotonation inside the amine group of CMCh causes a decrease in the release of Cipro in IH. Further raising the pH to 8.5 could result in a loose network structure in IHs (dry and gel form); the more significant Cipro release is the outcome. In the actual situation, when the IH is used at the wound site, the second approach is more realistic than the first approach. The drug's slow release will help reduce microbial growth at the wound site during the healing process. Thus, the experiments demonstrate that the levo release of IHs in their dry and gel forms relies on the solution's pH. The release of Cipro was found to be slower in gel form than in the dry form of IHs across all pH ranges. In dried form, PBS enters the IHs to release the drug, while in gel form, the drug follows a diffusion mechanism to release. This can be further explained using the Korsemeyer–Peppas (K-P) model.

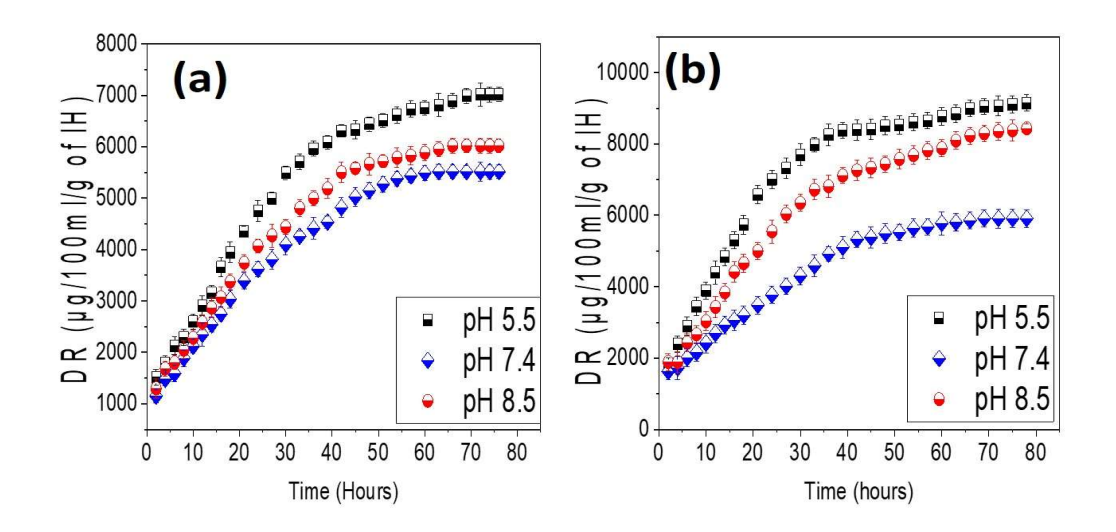


**Fig. 7. 9** Drug release study of OG2C1 in PBS (pH 5.5, 7.4, and 8.5) at 37°C (a) dry form (b) gel form.

The K-P model provides the most accurate description of the antibiotic drug release mechanism through the IH, as shown in Table 3. When the release exponent value "n" is equal to or less than 1, it denotes non-Fickian or anomalous diffusion. This indicates a combination of diffusion- and erosion-controlled drug release. When n=0.5, it denotes Fickian diffusion, where the drug release is solely controlled by diffusion. Case II transport is indicated when n=1, and Super Case II transport is indicated when n>1. For the release behavior of IH, the coefficient of determination ( $R^2$ ) value is more than 0.99. This shows an excellent fit of the experimental data to the K-P model. The "n" value was observed to be more than 0.45 and less than 1 for all the synthesized IHs. This confirms that all the IHs exhibited non-Fickian or anomalous diffusion as the drug release mechanism across all the tested pH ranges (5.5, 7.4, and 8.5) for both the dry and gel forms. Additionally, the analysis indicates that the diffusion rate is higher than the relaxation rate of the hydrogel matrix in all cases. In summary, the K-P model accurately describes the drug release mechanism from the IH, which follows

a non-Fickian or anomalous diffusion pattern, with the diffusion rate being higher than the polymer relaxation rate.

**Table 7. 3** K-P kinetic model parameters for OG2C1 in dry and gel form in PBS at pH 5.5, 7.4, and 8.5

Sample	Parameters associated with the K-P model										
code	I	Н 7.4		pH 5.5			рН 8.5				
	k	n	R <sup>2</sup>	k	n	R <sup>2</sup>	k	n	R <sup>2</sup>		
OG2C1	11.344	0.534	0.99	11.823	0.523	0.99	11.529	0.539	0.99		
(dry)											
OG2C1	15.141	0.453	0.99	11.566	0.578	0.99	13.368	0.509	0.99		
(gel)											

# 7.9 In vitro cytotoxicity assay

The main requirement for IH to function as biomaterials for drug delivery applications is their biocompatibility with the host cells. Therefore, the L-929 fibroblast cell lines were used to test the cytotoxicity of OG2C1 in both the unloaded and drug-loaded forms (Fig. 7.10). The morphology of the L-929 fibroblast cells did not undergo significant changes due to the treatment with both the drug-loaded and unloaded IH formulations. Since the cell viability was more than 90% for both cases (loaded and unloaded forms), the MTT test results for the OG2C1 show no toxicity. In conclusion, the *in vitro* cytotoxicity assay showed no toxicity of the OG2C1 against the L-929 fibroblast cell line, indicating good biocompatibility.

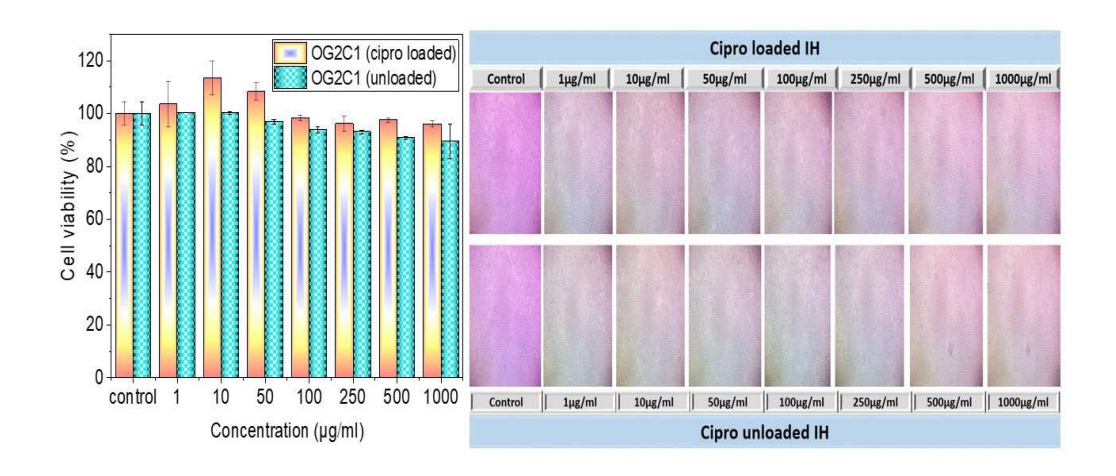


Fig. 7. 10 In vitro cytotoxicity assessment of OG2C1

## 7.10 Hemolytic activity

Hemolysis refers to the rupture or lysis of red blood cells (erythrocytes), an essential parameter in evaluating the biocompatibility of biomaterials. Evaluating the hemolysis of the IH would be an important step to fully assess its suitability as a biomaterial for biomedical applications, as it would indicate the material's compatibility with blood components. Fig. 7.11. shows that the color of the OG2C1 is similar to that of the PBS, while the positive control group representing RBC lysis appears bright red. The results indicate that the hemolysis rates of the OG2C1 at all concentrations (1 to 1000 μg mL<sup>-1</sup>) are less than 4%, which meets the standard criteria for acceptable hemolysis rates of biomaterials. Therefore, OG2C1 has demonstrated a negligible hemolytic capability across the concentration range of 1 to 1000 μg mL<sup>-1</sup>, suggesting good biocompatibility with blood components. The OG2C1 exhibited minimal hemolytic activity, as evidenced by the low hemolysis rates below the standard threshold, indicating its suitability for biomedical applications where contact with blood is expected.

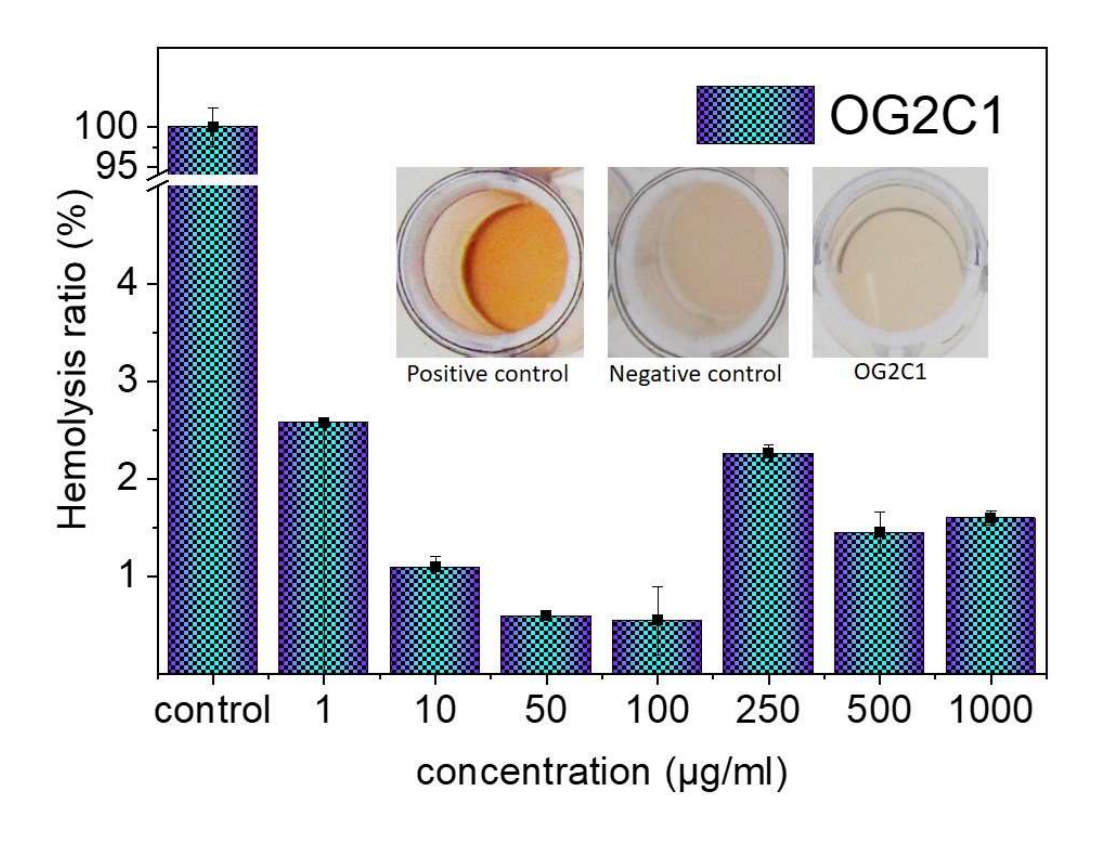
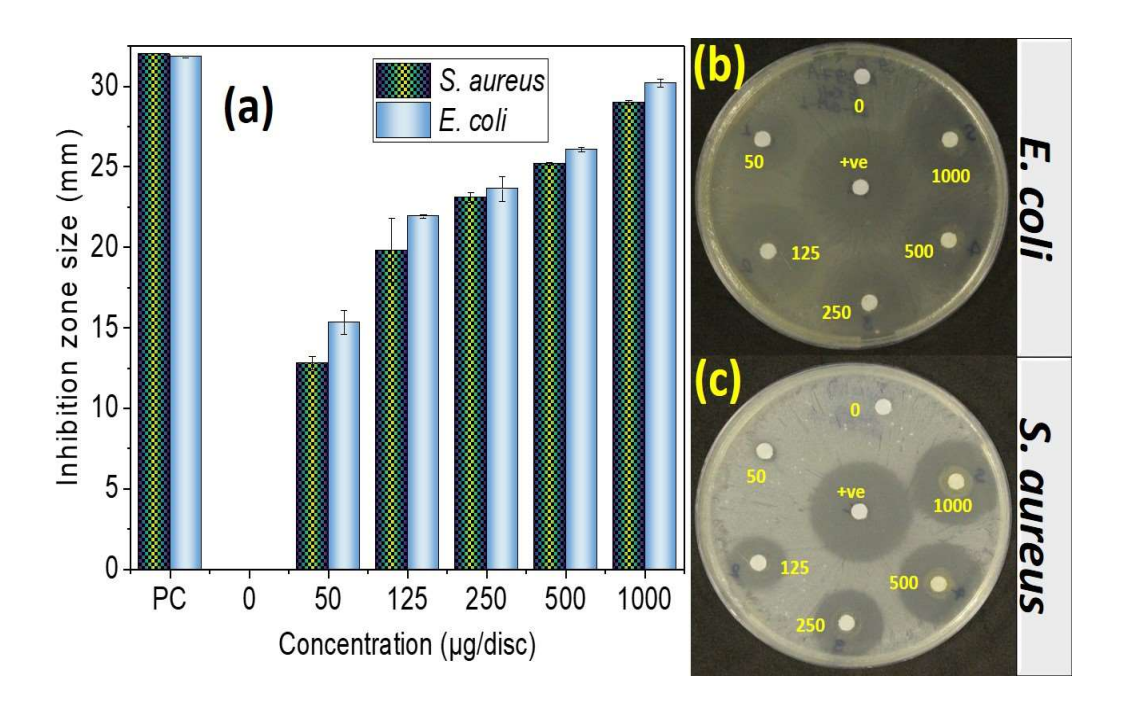


Fig. 7. 11 Hemolysis evaluation of OG2C1

# 7.11 Antibacterial assay

To prevent bacteria from entering the wound, stop microorganisms from growing, and reduce inflammation, the IH should possess antibacterial properties. The antibacterial activity of the OG2C1 was assessed against *S. aureus* and *E. coli* for 24 hours at 37°C (Fig. 7.12.b to c). This includes the data for the positive control and the OG2C1 at concentrations ranging from 50 to 1000 μg disc<sup>-1</sup> (Fig. 7.12.a). The findings show that the OG2C1 exhibited inhibitory effects against both bacterial species across all the tested concentrations up to 24 hours at 37°C. This antibacterial activity is attributed to the presence of chitosan in the OG2C1 formulation. With its positively charged amino groups, chitosan can effectively trap bacteria with negative charges through

electrostatic forces. This mechanism helps to inhibit the growth of bacteria. Additionally, chitosan can induce the leakage of proteinaceous and other intracellular components from the bacterial cells, further contributing to the observed antibacterial properties. The OG2C1 demonstrated potent antibacterial activity against both *S. aureus* and *E. coli*, an essential characteristic for its potential application as a wound dressing material to prevent microbial infection and promote healing.



**Fig. 7. 12** (a) Antibacterial assessment bar diagram of OG2C1. Antibacterial evaluation of OG2C1 against (b) *E. coli.* (b) *S. aureus*.

# 7.12 In vitro degradation

The biodegradability of OG2C1 was studied in PBS at pH 7.4 at 37 °C (Fig. 7.13). Studies on *in vitro* degradation have shown that OG2C1 degrades, as observed by the weight loss that results from the hydrolysis of Schiff base bonds. The study was carried out for 30 days. Two approaches were used to quantify the result. In the first approach,

a hydrolytic degradation study was conducted from the dried form of OG2C1 and found to be 85%. In the second approach, freshly synthesized OG2C1 was used to perform the study, and the degradation was to be 98%. Higher degradation was observed in the gel form of OG2C1 compared to the dry form, which is also required for the practical application of IH in wound healing.

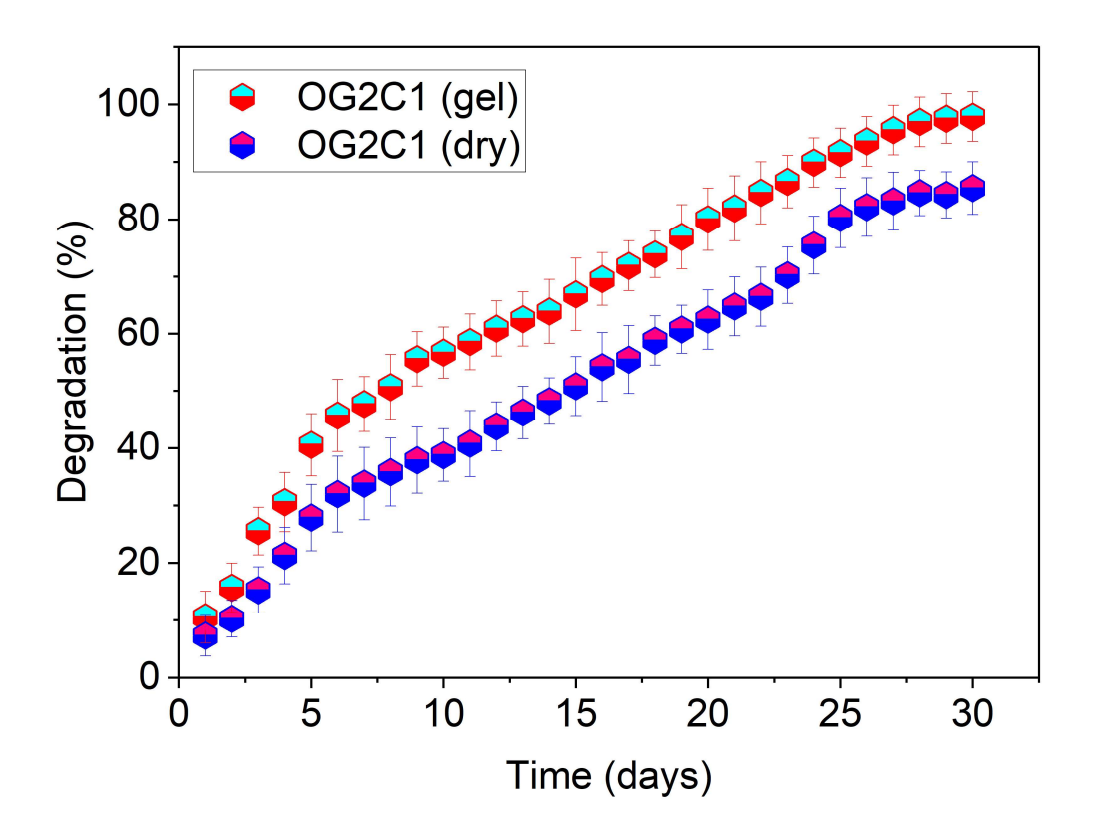


Fig. 7. 13 Hydrolytic degradation of OG2C1 at pH 7.4 in dry and gel form at 37°C.

# 7.13 Conclusion

In conclusion, dynamic Schiff linkage was employed to create self-healing natural gum-based IH using OG-CHO and CMCh. The optimal concentration of sodium periodate was 1.5 g, effectively converting vicinal hydroxyl groups to aldehyde groups in OG. The OG2C1 shows the least gelation time (2 minutes) among all synthesized

IHs. The OG2C1 demonstrated excellent syringeability and injectability due to its viscoelastic and shear-thinning properties, self-healing within 1 hour. The OG2C1 possesses a pH-dependent swellability and drug-release behavior strongly associated with crosslink density. Using ciprofloxacin HCl as a model drug, the OG2C1 demonstrated higher drug release in PBS at pH 5.5 compared to pH 7.4, with further increases observed at pH 8.5. The gel form of OG2C1 enables slow drug release, making it suitable for wound-healing applications. The drug release follows a non-Fickian diffusion mechanism. Hemolysis assays and *in vitro* cytotoxicity evaluations confirm the biocompatibility of the OG2C1, which also exhibits antibacterial properties against both Gram-positive and Gram-negative bacteria. Additionally, the OG2C1 has enhanced degradation in PBS (pH 7.4) at 37°C.

#### **CHAPTER 8**

## OVERALL CONCLUSION, FUTURE SCOPE AND SOCIAL IMPACT

#### **8.1 Overall Conclusion**

In this thesis work, a series of IHs using multialdehyde MOG, NG, MG, and OG crosslinked with CMCh via the Schiff base mechanism were synthesized at physiological temperature. These biopolymers were chosen due to their medicinal properties, biocompatibility, and biodegradability. The MOG, MG, NG, and OG were oxidized with NaIO<sub>4</sub> to form an aldehyde group, and chitosan was derivatized using monochloroacetic acid in the presence of sodium hydroxide to form CMCh. The aldehyde groups in the oxidized natural gums (MOG, MG, NG, and OG) reacted with the amino groups in CMCh, creating a stable imine bond. FT-IR and <sup>1</sup>H-NMR confirmed the oxidation of natural gum and the synthesis of injectable hydrogels. Morphological evaluation by FESEM and SEM confirmed the porous structure of injectable hydrogels. The Schiff base crosslinking method was chosen for its ability to create dynamic covalent bonds, allowing for self-healing and injectable properties. This crosslinking method facilitated the formation of a robust hydrogel network and enabled the hydrogel to be injectable, an essential feature for minimally invasive biomedical applications. All synthesized IHs have enough gelation time for administration and cross-linking during wound healing. The physical properties, such

as gel content, porosity, injectability, syringeability, and network parameters, were evaluated. The reversible Schiff base crosslinks allowed for shear-thinning and injectability, enabling minimally invasive application to the wound site. The swelling ability and cipro-release assay were assessed in PBS (pH 5.5, 7.4, and 8.5) at 37°C for dry and gel forms of IHs, revealing a pH-dependent swelling and drug-release behavior strongly associated with crosslink density. The rheological analysis demonstrated that injectable hydrogel's suitable viscoelastic properties and self-healing ability are essential for maintaining structural integrity under physiological conditions. In vitro, cytotoxicity using L-929 fibroblast cell lines and hemolysis assays confirmed the biocompatibility of the IHs, which also exhibit antibacterial properties against both Gram-positive and Gram-negative bacteria. Furthermore, hydrolytic degradation studies revealed that the IHs exhibited a controlled degradation profile. This is necessary for drug release applications, where a sustained release of therapeutic agents is desired, and tissue engineering, where gradual degradation supports new tissue formation. Table 8.1 summarizes the characterization data of the optimized IHs and compares them with findings from previously published studies, focusing on swelling behavior, drug release kinetics, and degradation profiles.

**Table 8.1.** Comparison of optimized IHs with literature data on swelling, drug release, and degradation.

	Parameters	IH-3-7	IH-0.5-5	IH-MG-5	OG2C1
al es	Aldehyde %	87.8	56.8	47.6	56
Physical properties	DS of CMCh (%)	67	67	67	67
P. pr	Pore size (µm)	25.5	80	14	80

		ntion tin	ne	9	3	2	2	
	Gel	content	(%)	60	76	81	84	
	Porc	sity (%	)	35	47	49.23	66	
ırameter	Average M <sub>w</sub> between crosslinks (g mol <sup>-1</sup> )			2.2×10³	3.8×10 <sup>2</sup>	67.4×10 <sup>-2</sup>	2.8×10 <sup>2</sup>	
Network Parameter		sslink de l cm <sup>-3</sup> )	ensity	2×10 <sup>-4</sup>	1.2	1.9	0.9	
Ž	Mes	h size (	nm)	4.570	3.3×10 <sup>-2</sup>	4.3×10 <sup>-2</sup>	7.5×10 <sup>-2</sup>	
			5.5	415	162	555	997	
(0)	Dry	dia	7.4	209	158	420	713	
Swelling ratio (%)		pH of swelling media	8.5	-	190	528	970	
lling r			5.5	830	190	483	750	
Swe	Gel		7.4	430	161	401	635	
			8.5	-	206	452	724	
fo			5.5	847	5012	9125	7017	
ml <sup>-1</sup> g <sup>-1</sup> of	Dry	media	7.4	719	3536	6896	5516	
		lease	8.5	-	5514	8895	6020	
use (µg IH)		lrug re	5.5	994	6446	11500	9146	
Drug release (µg 100 IH)	Gel	pH of drug release media	7.4	884	3056	9150	5912	
Dru		ď	8.5	-	5000	10112	8436	
			1					
		Parameters associated with the K-P model						

				n	k	n	k	n	k	n	k
e e		<b>.</b>	5.5	0.89	1.39	0.74	3.2	0.67	6.51	0.52	11.82
\eleas	Dry		7.4	0.48	8.19	0.60	12.8	0.6	8	0.53	11.34
rug F			8.5	-	-	0.94	3.74	0.79	5.58	0.54	11.53
Kinetics of Drug Release	Gel	Gel	5.5	0.33	7.87	0.54	13.5	0.86	3	0.58	11.57
inetics			7.4	0.41	4.53	0.60	12.8	0.87	4.22	0.45	15.14
			8.5	-	-	0.92	2.42	0.88	3.82	0.51	13.37
Hydrolytic degradation (%)	Ge	Gel (30 days)		~18 (88 days)		4	5	66	5	Ģ	98
Hy	Dry (30 days)		-		20		53.12		85.45		

# Comparison of the performance of optimized IHs with the literature

	Val	lues			
Parameter	From	From present	Outcome	References	
	Literature	study			
			Better		
Swelling (%)	Upto 500	Upto 1000	uptake/drug	[522]	
			diffusion.		
Drug Release	n ~ 0.75 (for		Higher drug		
Kinetics	`	$n = \sim 0.9$	load and	[523]	
Kinetics	some cases)		release.		
Degradation	~60-70 in ~42	45-98% in 30-60	Controlled	[524]	
(%)	days	days	degradation	[524]	

# 8.2 Future Scope

Optimizing the synthesized injectable hydrogel's drug loading and release profiles for specific therapeutic agents, particularly for wound healing, cancer therapy, or localized drug delivery, is still unexplored. Further, this research could also involve scaling up production and clinical trials and exploring other biomedical applications, such as tissue engineering or regenerative medicine, given the natural bioactivity and potential wound-healing properties. Additionally, many more natural gums are still unexplored and can be used to synthesize injectable hydrogel for biomedical applications using various crosslinking techniques except Schiff base mechanisms. Besides biomedical applications, synthesized IHs can be used for many more applications.

## 8.3 Social Impact

The social impact of this work could be significant, especially in healthcare. By developing a natural, biocompatible, and potentially cost-effective system for localized drug delivery, this work could lead to more accessible and effective treatments for diseases and conditions such as chronic wounds, infections, or localized cancers. This would be particularly beneficial in resource-limited settings where access to advanced medical treatments is constrained. Additionally, using plant-based materials promotes sustainability and reduces dependence on synthetic polymers, aligning with global efforts toward greener and more environmentally friendly medical technologies. This research could improve patient outcomes, reduce healthcare costs, and contribute to more equitable healthcare solutions globally. It could revolutionize the treatment of chronic wounds, infections, and localized cancers and improve therapeutic outcomes, reducing side effects. Such systems are particularly useful in resource-poor environments, where expensive medical technologies are not accessible. The use of

biodegradable, plant-based materials makes these hydrogels more sustainable and inexpensive than synthetic ones, thereby making healthcare cheaper and innovative treatments more accessible worldwide. The biodegradability of these materials also supports efforts to reduce medical waste and environmental damage, thus leading to eco-friendly healthcare products. Economically, the cultivation and processing of plant-based gums can support the livelihoods of rural households, creating jobs and empowering local communities. This research not only addresses health inequities by providing affordable, effective treatment options but also advances several United Nations Sustainable Development Goals, such as promoting good health, fostering economic growth, and encouraging responsible consumption and production. Overall, this work has the potential to transform healthcare by improving patient outcomes, reducing the environmental footprint of medical technologies, and fostering a more sustainable and equitable global health system.

## **REFERENCES**

- [1] Jacob, S.; Nair, A. B.; Shah, J.; Sreeharsha, N.; Gupta, S.; Shinu, P. (2021). Emerging role of hydrogels in drug delivery systems, tissue engineering and wound management, *Pharmaceutics*, Vol. 13, Issue 3, pp. 357. doi:10.3390/pharmaceutics13030357
- [2] Almawash, S.; Osman, S. K.; Mustafa, G.; El Hamd, M. A. (2022). Current and Future Prospective of Injectable Hydrogels—Design Challenges and Limitations, *Pharmaceuticals*, Vol. 15, Issue 3, pp. 371. doi:10.3390/ph15030371
- [3] Dattilo, M.; Patitucci, F.; Prete, S.; Parisi, O. I.; Puoci, F. (2023). Polysaccharide-Based Hydrogels and Their Application as Drug Delivery Systems in Cancer Treatment: A Review, *Journal of Functional Biomaterials*, Vol. 14, Issue 2, pp. 55. doi:10.3390/jfb14020055
- [4] Kapoor, D. U.; Garg, R.; Gaur, M.; Pareek, A.; Prajapati, B. G.; Castro, G. R.; Suttiruengwong, S.; Sriamornsak, P. (2024). Pectin hydrogels for controlled drug release: Recent developments and future prospects, *Saudi Pharmaceutical Journal*, Vol. 32, Issue 4, pp. 102002. doi:10.1016/j.jsps.2024.102002
- [5] Farasati Far, B.; Naimi-Jamal, M. R.; Safaei, M.; Zarei, K.; Moradi, M.; Yazdani Nezhad, H. (2022). A Review on Biomedical Application of Polysaccharide-Based Hydrogels with a Focus on Drug Delivery Systems, *Polymers*, Vol. 14, Issue 24, pp. 1–26. doi:10.3390/polym14245432
- [6] Cao, Z.; Bai, X.; Wang, C.; Ren, L.; Ma, D. (2021). A simple polysaccharide based injectable hydrogel compositing nano-hydroxyapatite for bone tissue engineering, *Materials Letters*, Vol. 293, pp. 129755. doi:10.1016/j.matlet.2021.129755
- [7] Yuan, Y.; Shen, S.; Fan, D. (2021). A physicochemical double cross-linked multifunctional hydrogel for dynamic burn wound healing: shape adaptability, injectable self-healing property and enhanced adhesion, *Biomaterials*, Vol. 276, Issue November 2020, pp. 120838. doi:10.1016/j.biomaterials.2021.120838
- [8] Lee, S.; Choi, J.; Youn, J.; Lee, Y.; Kim, W.; Choe, S.; Song, J.; Reis, R. L.; Khang, G. (2021). Development and evaluation of gellan gum/silk fibroin/chondroitin sulfate ternary injectable hydrogel for cartilage tissue engineering, *Biomolecules*, Vol. 11, Issue 8, pp. 1–17. doi:10.3390/biom11081184
- [9] Nishi, K. K.; Jayakrishnan, A. (2007). Self-gelling primaquine-gum Arabic conjugate: An injectable controlled delivery system for primaquine, *Biomacromolecules*, Vol. 8, Issue 1, pp. 84–90. doi:10.1021/bm060612x
- [10] Poudel, H.; RanguMagar, A. B.; Singh, P.; Oluremi, A.; Ali, N.; Watanabe, F.; Batta-Mpouma, J.; Kim, J. W.; Ghosh, A.; Ghosh, A. (2023). Guar-Based Injectable Hydrogel for Drug Delivery and In Vitro Bone Cell Growth, *Bioengineering*, Vol. 10, Issue 9, pp. 1088.

- doi:10.3390/bioengineering10091088
- [11] Karmakar, P. Das; Velu, K.; Vineeth Kumar, C. M.; Pal, A. (2024). Advances in injectable hydrogel: Design, functional regulation, and biomedical applications, *Polymers for Advanced Technologies*, Vol. 35, Issue 1, pp. e6193. doi:10.1002/pat.6193
- [12] Wei, Z.; Zhao, J.; Chen, Y. M.; Zhang, P.; Zhang, Q. (2016). Self-healing polysaccharide-based hydrogels as injectable carriers for neural stem cells, *Scientific Reports*, Vol. 6, Issue 1, pp. 37841. doi:10.1038/srep37841
- [13] Liu, Y.; Teng, J.; Huang, R.; Zhao, W.; Yang, D.; Ma, Y.; Wei, H.; Chen, H.; Zhang, J.; Chen, J. (2024). Injectable plant-derived polysaccharide hydrogels with intrinsic antioxidant bioactivity accelerate wound healing by promoting epithelialization and angiogenesis, *International Journal of Biological Macromolecules*, Vol. 266, pp. 131170. doi:10.1016/j.ijbiomac.2024.131170
- [14] Raczuk, E.; Dmochowska, B.; Samaszko-Fiertek, J.; Madaj, J. (2022). Different Schiff Bases—Structure, Importance and Classification, *Molecules*, Vol. 27, Issue 3, pp. 787. doi:10.3390/molecules27030787
- [15] Mo, C.; Xiang, L.; Chen, Y. (2021). Advances in Injectable and Self-healing Polysaccharide Hydrogel Based on the Schiff Base Reaction, *Macromolecular Rapid Communications*, Vol. 42, Issue 10, pp. 2100025. doi:10.1002/marc.202100025
- [16] Nair, S.; Remya, N. S.; Remya, S.; Nair, P. D. (2011). A biodegradable in situ injectable hydrogel based on chitosan and oxidized hyaluronic acid for tissue engineering applications, *Carbohydrate Polymers*, Vol. 85, Issue 4, pp. 838–844. doi:10.1016/j.carbpol.2011.04.004
- [17] Wang, W.; Shi, D.; Zhang, Y.; Li, W.; Li, F.; Feng, H.; Ma, L.; Yang, C.; Peng, Z.; Song, G.; Zeng, H.; Xie, L. (2023). An injectable hydrogel based on hyaluronic acid prepared by Schiff base for long-term controlled drug release, *International Journal of Biological Macromolecules*, Vol. 245, pp. 125341. doi:10.1016/j.ijbiomac.2023.125341
- [18] Ding, C.; Tian, M.; Feng, R.; Dang, Y.; Zhang, M. (2020). Novel Self-Healing Hydrogel with Injectable, pH-Responsive, Strain-Sensitive, Promoting Wound-Healing, and Hemostatic Properties Based on Collagen and Chitosan, *ACS Biomaterials Science and Engineering*, Vol. 6, Issue 7, pp. 3855–3867. doi:10.1021/acsbiomaterials.0c00588
- [19] Ma, J.; Du, C.; Zhang, Y.; Zhan, J.; Lai, Y.; Zhao, M. (2023). Important application value of injectable hydrogels loaded with omeprazole Schiff base complex in the treatment of pancreatitis, *Open Chemistry*, Vol. 21, Issue 1, pp. 1–7. doi:10.1515/chem-2023-0147
- [20] Shi, H.; Ma, D.; Wu, D.; Qiu, X.; Yang, S.; Wang, Y.; Xiao, L.; Ji, X.; Zhang, W.; Han, S.; Huo, P.; Dong, J.; Kong, X.; Guan, X.; Zhang, D. (2024). A pHresponsive, injectable and self-healing chitosan-coumarin hydrogel based on

- Schiff base and hydrogen bonds, *International Journal of Biological Macromolecules*, Vol. 255, pp. 128122. doi:10.1016/j.ijbiomac.2023.128122
- [21] Li, D.; Tohti, M.; Fu, Y.; Zhang, Y.; Xiong, Z.; Li, J.; Guo, Y.-F. (2024). Aldehyde group pendant-grafted pectin-based injectable hydrogel, *International Journal of Biological Macromolecules*, Vol. 264, pp. 130453. doi:10.1016/j.ijbiomac.2024.130453
- [22] Teng, J.; Zhao, W.; Zhang, S.; Yang, D.; Liu, Y.; Huang, R.; Ma, Y.; Jiang, L.; Wei, H.; Zhang, J.; Chen, J. (2024). Injectable nanoparticle-crosslinked xyloglucan/ε-poly--lysine composite hydrogel with hemostatic, antimicrobial, and angiogenic properties for infected wound healing, *Carbohydrate Polymers*, Vol. 336, pp. 122102. doi:10.1016/j.carbpol.2024.122102
- [23] Hisham, F.; Maziati Akmal, M. H.; Ahmad, F.; Ahmad, K.; Samat, N. (2024). Biopolymer chitosan: Potential sources, extraction methods, and emerging applications, *Ain Shams Engineering Journal*, Vol. 15, Issue 2, pp. 102424. doi:10.1016/j.asej.2023.102424
- [24] Yadav, M.; Kaushik, B.; Rao, G. K.; Srivastava, C. M.; Vaya, D. (2023). Advances and challenges in the use of chitosan and its derivatives in biomedical fields: A review, *Carbohydrate Polymer Technologies and Applications*, Vol. 5, Issue May, pp. 100323. doi:10.1016/j.carpta.2023.100323
- [25] Abourehab, M. A. S.; Pramanik, S.; Abdelgawad, M. A.; Abualsoud, B. M.; Kadi, A.; Ansari, M. J.; Deepak, A. (2022). Recent Advances of Chitosan Formulations in Biomedical Applications, *International Journal of Molecular Sciences*, Vol. 23, Issue 18, pp. 10975. doi:10.3390/ijms231810975
- [26] Ul-Islam, M.; Alabbosh, K. F.; Manan, S.; Khan, S.; Ahmad, F.; Ullah, M. W. (2023). Chitosan-based nanostructured biomaterials: Synthesis, properties, and biomedical applications, *Advanced Industrial and Engineering Polymer Research*, Vol. Issue 1, pp. 79-99. doi:10.1016/j.aiepr.2023.07.002
- [27] Jayakumar, R.; Prabaharan, M.; Sudheesh Kumar, P. T.; Nair, S. V.; Tamura, H. (2011). Biomaterials based on chitin and chitosan in wound dressing applications, *Biotechnology Advances*, Vol. 29, Issue 3, pp. 322–337. doi:10.1016/j.biotechadv.2011.01.005
- [28] Shariatinia, Z. (2018). Carboxymethyl chitosan: Properties and biomedical applications, *International Journal of Biological Macromolecules*, Vol. 120, pp. 1406–1419. doi:10.1016/j.ijbiomac.2018.09.131
- [29] Sonika, S.; Dhiman, S.; Singh, T. G.; Arora, G.; Arora, S. (2020). Review article moringa gum: A comprehensive review on its physicochemical and functional properties, *Plant Archives*, Vol. 20, pp. 3794–3805
- [30] Kaushik, A.; Yadav, S.; Mudgal, P.; Pahwa, R.; Kumar, T.; Ahuja, M. (2023). Propyl modification of Moringa gum for drug delivery applications, *Polymer Bulletin*, Vol. 81, Issue 3, pp. 2643–2670. doi:10.1007/s00289-023-04840-3
- [31] Singh, B.; Singh, J.; Sharma, V.; Sharma, P.; Kumar, R. (2023).

- Functionalization of bioactive moringa gum for designing hydrogel wound dressings, *Hybrid Advances*, Vol. 4, Issue September, pp. 100096. doi:10.1016/j.hybadv.2023.100096
- [32] Badwaik, H. R.; Hoque, A. Al; Kumari, L.; Sakure, K.; Baghel, M.; Giri, T. K. (2020). Moringa gum and its modified form as a potential green polymer used in biomedical field, *Carbohydrate Polymers*, Vol. 249, pp. 116893. doi:10.1016/j.carbpol.2020.116893
- [33] Ranote, S.; Musioł, M.; Kowalczuk, M.; Joshi, V.; Chauhan, G. S.; Kumar, R.; Chauhan, S.; Kumar, K. (2022). Functionalized Moringa oleifera Gum as pH-Responsive Nanogel for Doxorubicin Delivery: Synthesis, Kinetic Modelling and In Vitro Cytotoxicity Study, *Polymers*, Vol. 14, Issue 21, pp. 4697. doi:10.3390/polym14214697
- [34] Ahmad, S.; Manzoor, K.; Purwar, R.; Ikram, S. (2020). Morphological and Swelling Potential Evaluation of Moringa oleifera Gum/Poly(vinyl alcohol) Hydrogels as a Superabsorbent, *ACS Omega*, Vol. 5, Issue 29, pp. 17955–17961. doi:10.1021/acsomega.0c01023
- [35] Moreno-Trejo, M. B.; Sánchez-Domínguez, M. (2016). Mesquite gum as a novel reducing and stabilizing agent for modified tollens synthesis of highly concentrated ag nanoparticles, *Materials*, Vol. 9, Issue 10, pp. 817. doi:10.3390/ma9100817
- [36] Mudgil, D.; Barak, S. (2020). Mesquite gum (Prosopis gum): Structure, properties & Samp; applications A review, *International Journal of Biological Macromolecules*, Vol. 159, pp. 1094–1102. doi:10.1016/j.ijbiomac.2020.05.153
- [37] Rodríguez-Rodríguez, R.; Espinosa-Andrews, H.; Morales-Hernández, N.; Lobato-Calleros, C.; Vernon-Carter, E. J. (2019). Mesquite gum/chitosan insoluble complexes: relationship between the water state and viscoelastic properties, *Journal of Dispersion Science and Technology*, Vol. 40, Issue 9, pp. 1345–1352. doi:10.1080/01932691.2018.1513848
- [38] Tibebu, A.; Haile, G.; Kebede, A. (2018). Review On Medicinal Value And Other Application Of Neem Tree: Senior Seminar On Animal Health, *Biomedicine and Nursing*, Vol. 4, Issue 1, pp. 62–69. doi:10.7537/marsbnj040118.10
- [39] Mankotia, P.; Choudhary, S.; Sharma, K.; Kumar, V.; Kaur Bhatia, J.; Parmar, A.; Sharma, S.; Sharma, V. (2020). Neem gum based pH responsive hydrogel matrix: A new pharmaceutical excipient for the sustained release of anticancer drug, *International Journal of Biological Macromolecules*, Vol. 142, pp. 742–755. doi:10.1016/j.ijbiomac.2019.10.015
- [40] Nasrine, A.; Narayana, S.; Gulzar Ahmed, M.; Sultana, R.; Noushida, N.; Raunak Salian, T.; Almuqbil, M.; Almadani, M. E.; Alshehri, A.; Alghamdi, A.; Alshehri, S.; Mohammed Basheeruddin Asdaq, S. (2023). Neem (Azadirachta Indica) and silk fibroin associated hydrogel: Boon for wound healing treatment

- regimen, Saudi Pharmaceutical Journal, Vol. 31, Issue 10, pp. 101749. doi:10.1016/j.jsps.2023.101749
- [41] Nagpal, M.; Aggarwal, G.; Jain, U. K.; Madan, J. (2017). Extraction of gum from Abelmoschus Esculentus: Physicochemical peculiarity and antioxidant prepatent, *Asian Journal of Pharmaceutical and Clinical Research*, Vol. 10, Issue 9, pp. 174–179. doi:10.22159/ajpcr.2017.v10i9.19260
- [42] Chaudhari, S.; Dhuppad, U. (2023). Extraction and Characterization of Okra and Almond Gum as a Pharmaceutical Aid, *International Journal Of Drug Delivery Technology*, Vol. 13, Issue 04, pp. 1503–1508. doi:10.25258/ijddt.13.4.58
- [43] Kamel, H.; Al-kubaisi, S. A.; Al-dosary, M. M.; Al-marsoumi, S. M. H. (2016). Identification of natural gum extracted from Okra Fruits, Vol. 10, Issue September, pp. 254–258
- [44] Puri, A.; Dev, D.; Prasad, D. N.; Hira, S.; Sharma, R. (2019). Modified Okra Gum with Silica: A Novel Superdisintegrant for Fast Disintegrating Tablet, *Journal of Drug Delivery and Therapeutics*, Vol. 9, Issue 3, pp. 206–211. doi:10.22270/jddt.v9i3-s.3002
- [45] Rajalakshmi, M.; Sangeetha, S. (2023). Okra Mucilage- Method Of Extraction And A Novel Strategy For Pharmaceutical Drug Delivery System, *Journal of Pharmaceutical Negative Results*, Vol. 14, Issue 2, pp. 2473–2481. doi:10.47750/pnr.2023.14.S02.291
- [46] Raj, V.; Shim, J.; Lee, J. (2020). Grafting modification of okra mucilage: Recent findings, applications, and future directions, Vol. 246, Issue May, pp. 116653. doi:10.1016/j.carbpol.2020.116653
- [47] Basharat, M.; Noreen, S.; Ghumman, S. A.; Anwar, F.; Ijaz, B.; Batool, T.; Batool, F.; Aslam, A.; Munawar, K. S.; Aslam, S. (2024). Development and Evaluation of Ph-Sensitive Acrylic Acid Grafted Abelmoschus Esculentus Hydrogel as a Promising Carrier for Pantoprazole Sodium, *Abelmoschus Esculentus*. doi:10.2139/ssrn.4693466
- [48] Okunlola, A.; Odeniyi, M. A.; Arhewoh, M. I. (2020). Microsphere formulations of ambroxol hydrochloride: influence of Okra (Abelmoschus esculentus) mucilage as a sustained release polymer, *Progress in Biomaterials*, Vol. 9, Issue 1–2, pp. 65–80. doi:10.1007/s40204-020-00132-5
- [49] Ghumman, S. A.; Bashir, S.; Noreen, S.; Khan, A. M.; Riffat, S.; Abbas, M. (2018). Polymeric microspheres of okra mucilage and alginate for the controlled release of oxcarbazepine: In vitro & wamp; in vivo evaluation, *International Journal of Biological Macromolecules*, Vol. 111, pp. 1156–1165. doi:10.1016/j.ijbiomac.2018.01.058
- [50] Maryam, S.; Barkat, K.; Khalid, I.; Mehmood, Y.; Syed, M. A.; Malik, N. S.; Aslam, M. (2022). Polymeric blends of okra gum/gelatin prepared by aqueous polymerization technique: their characterization and toxicological evaluation,

- Polymer Bulletin, Vol. 79, Issue 7, pp. 5339–5363. doi:10.1007/s00289-021-03561-9
- [51] Patra, S.; Bala, N. N.; Nandi, G. (2020). Synthesis, characterization and fabrication of sodium carboxymethyl-okra-gum-grafted-polymethacrylamide into sustained release tablet matrix, *International Journal of Biological Macromolecules*, Vol. 164, pp. 3885–3900. doi:10.1016/j.ijbiomac.2020.09.025
- [52] Bharskar, G. R. (2020). A review on hydrogel, *American Journal of Pharmtech Research*, Vol. 8, Issue 3, pp. 41-61. doi:10.20959/wjpps20207-16602
- [53] Fan, F.; Saha, S.; Hanjaya-Putra, D. (2021). Biomimetic Hydrogels to Promote Wound Healing, *Frontiers in Bioengineering and Biotechnology*, Vol. 20, Issue 9, pp. 718377. doi:10.3389/fbioe.2021.718377
- [54] Firlar, I.; Altunbek, M.; McCarthy, C.; Ramalingam, M.; Camci-Unal, G. (2022). Functional Hydrogels for Treatment of Chronic Wounds, *Gels*, Vol. 8, Issue 2, pp. 127. doi:10.3390/gels8020127
- [55] Liang, Y.; He, J.; Guo, B. (2021). Functional Hydrogels as Wound Dressing to Enhance Wound Healing, *ACS Nano*, Vol. 15, Issue 8, pp. 12687–12722. doi:10.1021/acsnaIssue1c04206
- [56] Huang, X.; Hu, B.; Zhang, X.; Fan, P.; Chen, Z.; Wang, S. (2024). Recent advances in the application of clay-containing hydrogels for hemostasis and wound healing, *Expert Opinion on Drug Delivery*, Vol. 21, Issue 3, pp. 457–477. doi:10.1080/17425247.2024.2329641
- [57] Ahmad, S.; Ahmad, M.; Manzoor, K.; Purwar, R.; Ikram, S. (2019). A review on latest innovations in natural gums based hydrogels: Preparations & Camp; applications, *International Journal of Biological Macromolecules*, Vol. 136, pp. 870–890. doi:10.1016/j.ijbiomac.2019.06.113
- [58] Mittal, H.; Al Alili, A.; Alhassan, S. M.; Naushad, M. (2022). Advances in the role of natural gums-based hydrogels in water purification, desalination and atmospheric-water harvesting, *International Journal of Biological Macromolecules*, Vol. 222, pp. 2888–2921. doi:10.1016/j.ijbiomac.2022.10.067
- [59] Hamdani, A. M.; Wani, I. A.; Bhat, N. A. (2019). Sources, structure, properties and health benefits of plant gums: A review, *International Journal of Biological Macromolecules*, Vol. 135, pp. 46–61. doi:10.1016/j.ijbiomac.2019.05.103
- [60] Ahmad, S.; Ahmad, M.; Manzoor, K.; Purwar, R.; Ikram, S. (2019). A review on latest innovations in natural gums based hydrogels: Preparations & applications, *International Journal of Biological Macromolecules*, Vol. 136, pp. 870–890. doi:10.1016/j.ijbiomac.2019.06.113
- [61] Barak, S.; Mudgil, D.; Taneja, S. (2020). Exudate gums: chemistry, properties and food applications a review, *Journal of the Science of Food and Agriculture*, Vol. 100, Issue 7, pp. 2828–2835. doi:10.1002/jsfa.10302

- [62] Prajapati, V. D.; Jani, G. K.; Moradiya, N. G.; Randeria, N. P. (2013). Pharmaceutical applications of various natural gums, mucilages and their modified forms, *Carbohydrate Polymers*, Vol. 92, Issue 2, pp. 1685–1699. doi:10.1016/j.carbpol.2012.11.021
- [63] Koyyada, A.; Orsu, P. (2021). Natural gum polysaccharides as efficient tissue engineering and drug delivery biopolymers, *Journal of Drug Delivery Science and Technology*, Vol. 63, pp. 102431. doi:10.1016/j.jddst.2021.102431
- [64] Salehi, F. (2020). Edible Coating of Fruits and Vegetables Using Natural Gums: A Review, *International Journal of Fruit Science*, Vol. 20, Issue sup2, pp. S570–S589. doi:10.1080/15538362.2020.1746730
- [65] Deshmukh, A. S.; Aminabhavi, T. M. (2014). Pharmaceutical Applications of Various Natural Gums, *Polysaccharides*, Springer International Publishing, Cham, pp. 1–30. doi:10.1007/978-3-319-03751-6 4-1
- [66] Ghani, A.; Zare, E. N.; Makvandi, P.; Rabiee, N. (2024). Antioxidant, antibacterial and biodegradable hydrogel films from carboxymethyl tragacanth gum and clove extract: Potential for wound dressings application, *Carbohydrate Polymer Technologies and Applications*, Vol. 7, Issue January, pp. 100428. doi:10.1016/j.carpta.2024.100428
- [67] Koneru, A.; Dharmalingam, K.; Anandalakshmi, R. (2020). Cellulose based nanocomposite hydrogel films consisting of sodium carboxymethylcellulose—grapefruit seed extract nanoparticles for potential wound healing applications, *International Journal of Biological Macromolecules*, Vol. 148, pp. 833–842. doi:10.1016/j.ijbiomac.2020.01.018
- [68] Mahajan, P.; Nangare, S.; Patil, A.; Jain, P.; Zawar, L. (2024). Chia (Salvia hispanica L.) seed mucilage (a heteropolysaccharide) based antimicrobial hydrogel scaffold for wound healing: In vitro-in-vivo characterization, *Carbohydrate Polymer Technologies and Applications*, Vol. 7, Issue January, pp. 100432. doi:10.1016/j.carpta.2024.100432
- [69] Babaluei, M.; Mojarab, Y.; Mottaghitalab, F.; Saeb, M. R.; Farokhi, M. (2024). Conductive hydrogels based on tragacanth and silk fibroin containing dopamine functionalized carboxyl-capped aniline pentamer: Merging hemostasis, antibacterial, and anti-oxidant properties into a multifunctional hydrogel for burn wound healing, *International Journal of Biological Macromolecules*, Vol. 261, Issue P2, pp. 129932. doi:10.1016/j.ijbiomac.2024.129932
- [70] Sharma, D.; Singh, B. (2024). Designing aloe vera-sterculia gum based copolymeric hydrogel dressings for drug delivery, *Hybrid Advances*, Vol. 5, Issue November 2023, pp. 100142. doi:10.1016/j.hybadv.2024.100142
- [71] Li, N.; Liu, C.; Chen, W. (2019). Facile Access to Guar Gum Based Supramolecular Hydrogels with Rapid Self-Healing Ability and Multistimuli Responsive Gel-Sol Transitions, *Journal of Agricultural and Food Chemistry*, Vol. 67, Issue 2, pp. 746–752. doi:10.1021/acs.jafc.8b05130

- [72] Palem, R. R.; Shimoga, G.; Rao, K. S. V. K.; Lee, S. H.; Kang, T. J. (2020). Guar gum graft polymer-based silver nanocomposite hydrogels: synthesis, characterization and its biomedical applications, *Journal of Polymer Research*, Vol. 27, Issue 3. doi:10.1007/s10965-020-2026-8
- [73] Singh, B.; Dhiman, A. (2016). Design of Acacia Gum-Carbopol-Cross-Linked-Polyvinylimidazole Hydrogel Wound Dressings for Antibiotic/Anesthetic Drug Delivery, *Industrial and Engineering Chemistry Research*, Vol. 55, Issue 34, pp. 9176–9188. doi:10.1021/acs.iecr.6b01963
- [74] Zhu, J.; Tang, C.; Zhang, M.; Zhang, M.; Fu, L. (2024). Sulfated zwitterionic poly(sulfobetaine methacrylate)/κ-Capacarragan double network hydrogel wound dressing for skin wound repair, European Polymer Journal, Vol. 207, pp. 112809. doi:10.1016/j.eurpolymj.2024.112809
- [75] Xu, Z.; Li, Z.; Jiang, S.; Bratlie, K. M. (2018). Chemically Modified Gellan Gum Hydrogels with Tunable Properties for Use as Tissue Engineering Scaffolds, *ACS Omega*, Vol. 3, Issue 6, pp. 6998–7007. doi:10.1021/acsomega.8b00683
- [76] Dehghan-Niri, M.; Vasheghani-Farahani, E.; Baghaban Eslaminejad, M.; Tavakol, M.; Bagheri, F. (2020). Physicomechanical, rheological and in vitro cytocompatibility properties of the electron beam irradiated blend hydrogels of tyramine conjugated gum tragacanth and poly (vinyl alcohol), *Materials Science and Engineering C*, Vol. 114, Issue May, pp. 111073. doi:10.1016/j.msec.2020.111073
- [77] El-sayed, N. S.; Hashem, A. H.; Khattab, T. A.; Kamel, S. (2023). New antibacterial hydrogels based on sodium alginate, *International Journal of Biological Macromolecules*, Vol. 248, Issue July, pp. 125872. doi:10.1016/j.ijbiomac.2023.125872
- [78] Rodrigues, J. P.; da Costa Silva, J. R.; Ferreira, B. A.; Veloso, L. I.; Quirino, L. S.; Rosa, R. R.; Barbosa, M. C.; Rodrigues, C. M.; Gaspari, P. B. F.; Beletti, M. E.; Goulart, L. R.; Corrêa, N. C. R. (2024). Development of collagenous scaffolds for wound healing: characterization and in vivo analysis, *Journal of Materials Science: Materials in Medicine*, Vol. 35, Issue 12. doi:10.1007/s10856-023-06774-8
- [79] García-García, A.; Pérez-Álvarez, L.; Ruiz-Rubio, L.; Larrea-Sebal, A.; Martin, C.; Vilas-Vilela, J. L. (2024). Extrusion-Based 3D Printing of Photocrosslinkable Chitosan Inks, Gels, Vol. 10, Issue 2, pp. 126. doi:10.3390/gels10020126
- [80] Ramírez-alba, M. D.; Molins-martínez, M.; García-torres, J.; Romanini, M.; Macovez, R.; Maria, M. P.; Alem, C. (2024). pH and electrically responsive hydrogels with adhesive property, Vol. 196, Issue 38, pp. 105841. doi:10.1016/j.reactfunctpolym.2024.105841
- [81] Singh, B.; Sharma, S.; Dhiman, A. (2017). Acacia gum polysaccharide based hydrogel wound dressings: Synthesis, characterization, drug delivery and

- biomedical properties, *Carbohydrate Polymers*, Vol. 165, pp. 294–303. doi:10.1016/j.carbpol.2017.02.039
- [82] Palem, R. R.; Shimoga, G.; Kang, T. J.; Lee, S.-H. (2020). Fabrication of multifunctional Guar gum-silver nanocomposite hydrogels for biomedical and environmental applications, *International Journal of Biological Macromolecules*, Vol. 159, pp. 474–486. doi:10.1016/j.ijbiomac.2020.05.041
- [83] Deka, R.; Sarma, S.; Patar, P.; Gogoi, P.; Sarmah, J. K. (2020). Highly stable silver nanoparticles containing guar gum modified dual network hydrogel for catalytic and biomedical applications, *Carbohydrate Polymers*, Vol. 248, pp. 116786. doi:10.1016/j.carbpol.2020.116786
- [84] Palem, R. R.; Shimoga, G.; Rao, K. S. V. K.; Lee, S.-H.; Kang, T. J. (2020). Guar gum graft polymer-based silver nanocomposite hydrogels: synthesis, characterization and its biomedical applications, *Journal of Polymer Research*, Vol. 27, Issue 3, pp. 68. doi:10.1007/s10965-020-2026-8
- [85] Sarika, P. R.; Cinthya, K.; Jayakrishnan, A.; Anilkumar, P. R.; James, N. R. (2014). Modified gum arabic cross-linked gelatin scaffold for biomedical applications, *Materials Science and Engineering: C*, Vol. 43, pp. 272–279. doi:10.1016/j.msec.2014.06.042
- [86] Dalei, G.; Das, S.; Das, S. P. (2019). Non-thermal plasma assisted surface nanotextured carboxymethyl guar gum/chitosan hydrogels for biomedical applications, *RSC Advances*, Vol. 9, Issue 3, pp. 1705–1716. doi:10.1039/C8RA09161G
- [87] Lopéz-Martínez, E. E.; Claudio-Rizo, J. A.; Caldera-Villalobos, M.; Becerra-Rodríguez, J. J.; Cabrera-Munguía, D. A.; Cano-Salazar, L. F.; Betancourt-Galindo, R. (2022). Hydrogels for Biomedicine Based on Semi-Interpenetrating Polymeric Networks of Collagen/Guar Gum: Applications in Biomedical Field and Biocompatibility, *Macromolecular Research*, Vol. 30, Issue 6, pp. 384–390. doi:10.1007/s13233-022-0048-2
- [88] Singh, B.; Sharma, V.; Rohit; Sen, H. (2023). Fabrication of acacia gum grafted copolymeric network hydrogel for biomedical applications, *Bioactive Carbohydrates and Dietary Fibre*, Vol. 29, pp. 100353. doi:10.1016/j.bcdf.2023.100353
- [89] Rao, K. M.; Kumar, A.; Krishna Rao, K. S. V.; Haider, A.; Han, S. S. (2018). Biodegradable Tragacanth Gum Based Silver Nanocomposite Hydrogels and Their Antibacterial Evaluation, *Journal of Polymers and the Environment*, Vol. 26, Issue 2, pp. 778–788. doi:10.1007/s10924-017-0989-2
- [90] Sagbas, S.; Sahiner, N. (2018). Modifiable natural gum based microgel capsules as sustainable drug delivery systems, *Carbohydrate Polymers*, Vol. 200, pp. 128–136. doi:10.1016/j.carbpol.2018.07.085
- [91] Saruchi; Kaith, B. S.; Jindal, R.; Kapur, G. S. (2014). Synthesis of Gum tragacanth and acrylic acid based hydrogel: its evaluation for controlled release

- of antiulcerative drug pantoprazole sodium, *Journal of the Chinese Advanced Materials Society*, Vol. 2, Issue 2, pp. 110–117. doi:10.1080/22243682.2014.911114
- [92] Singh, B.; Rohit. (2022). Tailoring and evaluating poly(vinyl sulfonic acid)-sterculia gum network hydrogel for biomedical applications, *Materialia*, Vol. 25, pp. 101524. doi:10.1016/j.mtla.2022.101524
- [93] Sani Mamman, I.; Teo, Y. Y.; Misran, M. (2021). Synthesis, characterization and rheological study of Arabic gum-grafted-poly (methacrylic acid) hydrogels, *Polymer Bulletin*, Vol. 78, Issue 6, pp. 3399–3423. doi:10.1007/s00289-020-03267-4
- [94] Gutierrez-Reyes, J. E.; Caldera-Villalobos, M.; Claudio-Rizo, J. A.; Cabrera-Munguía, D. A.; Becerra-Rodriguez, J. J.; Soriano-Corral, F.; Herrera-Guerrero, A. (2023). Smart collagen/xanthan gum-based hydrogels with antibacterial effect, drug release capacity and excellent performance in vitro bioactivity for wound healing application, *Biomedical Materials*, Vol. 18, Issue 3, pp. 035011. doi:10.1088/1748-605X/acc99c
- [95] Qi, Y.; Zhang, S.; He, Y.; Ou, S.; Yang, Y.; Qu, Y.; Li, J.; Lian, W.; Li, G.; Tian, J.; Xu, C. (2022). A cell adhesion-promoting multi-network 3D printing bio-ink based on natural polysaccharide hydrogel, *Frontiers in Bioengineering and Biotechnology*, Vol. 10. doi:10.3389/fbioe.2022.1070566
- [96] Pak, S.; Chen, F. (2023). Functional Enhancement of Guar Gum-Based Hydrogel by Polydopamine and Nanocellulose, *Foods*, Vol. 12, Issue 6, pp. 1304. doi:10.3390/foods12061304
- [97] Singh, B.; Singh, B. (2018). Modification of sterculia gum polysaccharide via network formation by radiation induced crosslinking polymerization for biomedical applications, *International Journal of Biological Macromolecules*, Vol. 116, pp. 91–99. doi:10.1016/j.ijbiomac.2018.05.032
- [98] Gupta, V. K.; Sood, S.; Agarwal, S.; Saini, A. K.; Pathania, D. (2018). Antioxidant activity and controlled drug delivery potential of tragacanth gumcl- poly (lactic acid-co-itaconic acid) hydrogel, *International Journal of Biological Macromolecules*, Vol. 107, pp. 2534–2543. doi:10.1016/j.ijbiomac.2017.10.138
- [99] Bashir, S.; Teo, Y. Y.; Ramesh, S.; Ramesh, K. (2018). Synthesis and characterization of karaya gum-g- poly (acrylic acid) hydrogels and in vitro release of hydrophobic quercetin, *Polymer*, Vol. 147, pp. 108–120. doi:10.1016/j.polymer.2018.05.071
- [100] Sultan, M.; Mohamed, O. A.; El-Masry, H. M.; Taha, G. (2023). Fabrication and evaluation of antimicrobial cellulose/Arabic gum hydrogels as potential drug delivery vehicle, *International Journal of Biological Macromolecules*, Vol. 242, pp. 125083. doi:10.1016/j.ijbiomac.2023.125083
- [101] Ghauri, Z. H.; Islam, A.; Qadir, M. A.; Gull, N.; Haider, B.; Khan, R. U.; Riaz,

- T. (2021). Development and evaluation of pH-sensitive biodegradable ternary blended hydrogel films (chitosan/guar gum/PVP) for drug delivery application, *Scientific Reports*, Vol. 11, Issue 1, pp. 21255. doi:10.1038/s41598-021-00452-x
- [102] Piola, B.; Sabbatini, M.; Gino, S.; Invernizzi, M.; Renò, F. (2022). 3D Bioprinting of Gelatin–Xanthan Gum Composite Hydrogels for Growth of Human Skin Cells, *International Journal of Molecular Sciences*, Vol. 23, Issue 1, pp. 539. doi:10.3390/ijms23010539
- [103] Singh, B.; Sharma, V.; Pal, L. (2011). Formation of sterculia polysaccharide networks by gamma rays induced graft copolymerization for biomedical applications, *Carbohydrate Polymers*, Vol. 86, Issue 3, pp. 1371–1380. doi:10.1016/j.carbpol.2011.06.041
- [104] Sharma, V.; Singh, B.; Sharma, P. (2023). Development of almond gum based copolymeric hydrogels for use in effectual colon-drug delivery, *Journal of Drug Delivery Science and Technology*, Vol. 84, pp. 104470. doi:10.1016/j.jddst.2023.104470
- [105] Singh, B.; Dhiman, A.; Kumar, S. (2023). Polysaccharide gum based network hydrogels for controlled drug delivery of ceftriaxone: Synthesis, characterization and biomedical evaluations, *Results in Chemistry*, Vol. 5, pp. 100695. doi:10.1016/j.rechem.2022.100695
- [106] Mankotia, P.; Sharma, K.; Sharma, V.; Mishra, Y. K.; Kumar, V. (2023). Curcumin-loaded Butea monosperma gum-based hydrogel: A new excipient for controlled drug delivery and anti-bacterial applications, *International Journal of Biological Macromolecules*, Vol. 242, pp. 124703. doi:10.1016/j.ijbiomac.2023.124703
- [107] Sharma, D.; Sharma, A.; Bala, R.; Singh, B. (2024). Investigations on physiochemical and biomedical properties of Aloe vera Sterculia gum copolymeric dressings impregnated with antibiotic-anesthetic drugs to enhance wound healing, *International Journal of Biological Macromolecules*, Vol. 267, pp. 131363. doi:10.1016/j.ijbiomac.2024.131363
- [108] Rahmani, S.; Olad, A.; Rahmani, Z. (2023). Preparation of self-healable nanocomposite hydrogel based on Gum Arabic/gelatin and graphene oxide: study of drug delivery behavior, *Polymer Bulletin*, Vol. 80, Issue 4, pp. 4117–4138. doi:10.1007/s00289-022-04247-6
- [109] Singh, B.; Varshney, L.; Sharma, V. (2014). Design of sterile mucoadhesive hydrogels for use in drug delivery: Effect of radiation on network structure, *Colloids and Surfaces B: Biointerfaces*, Vol. 121, pp. 230–237. doi:10.1016/j.colsurfb.2014.06.020
- [110] Ullah, H.; Ihsan, J.; Mohamed, R. M. K.; Khan, M. A.; Ghani, M.; Rauf, N.; Ullah, S.; Javed, A.; Farooq, M. (2023). Bionanocomposite scaffolds based on MnS-nanorods loaded acacia-Senegal-gum hydrogels: Fabrication, characterization and biological evaluation, *Bioactive Carbohydrates and*

- Dietary Fibre, Vol. 30, pp. 100368. doi:10.1016/j.bcdf.2023.100368
- [111] Ibrahim, S. M.; Yin, T. Y.; Misran, M. (2020). Arabic Gum Grafted PEGDMA Hydrogels: Synthesis, Physico-Chemical Characterization and In-vitro Release of Hydrophobic Drug, *Macromolecular Research*, Vol. 28, Issue S1, pp. 1220–1231. doi:10.1007/s13233-020-8166-1
- [112] Nagaraja, K.; Rao, K. M.; Reddy, G. V.; Rao, K. S. V. K. (2021). Tragacanth gum-based multifunctional hydrogels and green synthesis of their silver nanocomposites for drug delivery and inactivation of multidrug resistant bacteria, *International Journal of Biological Macromolecules*, Vol. 174, pp. 502–511. doi:10.1016/j.ijbiomac.2021.01.203
- [113] HaqAsif, A.; Karnakar, R. R.; Sreeharsha, N.; Gite, V. V.; Borane, N.; Al-Dhubiab, B. E.; Kaliyadan, F.; Rasool, T.; Nanjappa, S. H.; Meravanige, G. (2021). pH and Salt Responsive Hydrogel based on Guar Gum as a Renewable Material for Delivery of Curcumin: A Natural Anti-Cancer Drug, *Journal of Polymers and the Environment*, Vol. 29, Issue 6, pp. 1978–1989. doi:10.1007/s10924-020-01934-1
- [114] Jahanban-Esfahlan, R.; Soleimani, K.; Derakhshankhah, H.; Haghshenas, B.; Rezaei, A.; Massoumi, B.; Farnudiyan-Habibi, A.; Samadian, H.; Jaymand, M. (2021). Multi-stimuli-responsive magnetic hydrogel based on Tragacanth gum as a de novo nanosystem for targeted chemo/hyperthermia treatment of cancer, *Journal of Materials Research*, Vol. 36, Issue 4, pp. 858–869. doi:10.1557/s43578-021-00137-1
- [115] Nagaraja, K.; Rao, K. M.; Rao, K. S. V. K.; Han, S. S. (2022). Dual responsive tamarind gum-co-poly(N-isopropyl acrylamide-co-ethylene glycol vinyl ether) hydrogel: A promising device for colon specific anti-cancer drug delivery, *Colloids and Surfaces A: Physicochemical and Engineering Aspects*, Vol. 641, pp. 128456. doi:10.1016/j.colsurfa.2022.128456
- [116] Singh, B.; Singh, J.; Rajneesh. (2021). Application of tragacanth gum and alginate in hydrogel wound dressing's formation using gamma radiation, *Carbohydrate Polymer Technologies and Applications*, Vol. 2, pp. 100058. doi:10.1016/j.carpta.2021.100058
- [117] Dalei, G.; Das, S.; Das, S. P. (2021). Low-pressure nitrogen and ammonia plasma treatment on carboxymethyl guar gum/PVA hydrogels: impact on drug delivery, biocompatibility and biodegradability, *International Journal of Polymeric Materials and Polymeric Biomaterials*, Vol. 70, Issue 2, pp. 75–89. doi:10.1080/00914037.2019.1695204
- [118] Anwar, M.; Pervaiz, F.; Shoukat, H.; Noreen, S.; Shabbir, K.; Majeed, A.; Ijaz, S. (2021). Formulation and evaluation of interpenetrating network of xanthan gum and polyvinylpyrrolidone as a hydrophilic matrix for controlled drug delivery system, *Polymer Bulletin*, Vol. 78, Issue 1, pp. 59–80. doi:10.1007/s00289-019-03092-4
- [119] Pandit, A. H.; Mazumdar, N.; Imtiyaz, K.; Rizvi, M. M. A.; Ahmad, S. (2019).

- Periodate-Modified Gum Arabic Cross-linked PVA Hydrogels: A Promising Approach toward Photoprotection and Sustained Delivery of Folic Acid, *ACS Omega*, Vol. 4, Issue 14, pp. 16026–16036. doi:10.1021/acsomega.9b02137
- [120] Farooq, A.; Farooq, A.; Jabeen, S.; Islam, A.; Gull, N.; Khan, R. U.; Shifa ul Haq, H. M.; Mehmood, A.; Hussain, N.; Bilal, M. (2022). Designing Kappa-carrageenan/guar gum/polyvinyl alcohol-based pH-responsive silane-crosslinked hydrogels for controlled release of cephradine, *Journal of Drug Delivery Science and Technology*, Vol. 67, pp. 102969. doi:10.1016/j.jddst.2021.102969
- [121] Rana, V. S.; Sharma, N. (2024). In vitro release dynamics of doxorubicin hydrochloride & gentamicin sulphate through nanoparticle embedded sterculia gum/gelatin self crosslinked hydrogel system, *Journal of Drug Delivery Science and Technology*, Vol. 95, pp. 105602. doi:10.1016/j.jddst.2024.105602
- [122] Dehghan-Niri, M.; Vasheghani-Farahani, E.; Baghaban Eslaminejad, M.; Tavakol, M.; Bagheri, F. (2020). Physicomechanical, rheological and in vitro cytocompatibility properties of the electron beam irradiated blend hydrogels of tyramine conjugated gum tragacanth and poly (vinyl alcohol), *Materials Science and Engineering: C*, Vol. 114, pp. 111073. doi:10.1016/j.msec.2020.111073
- [123] Ghosh, S. K.; Das, A.; Basu, A.; Halder, A.; Das, S.; Basu, S.; Abdullah, M. F.; Mukherjee, A.; Kundu, S. (2018). Semi-interpenetrating hydrogels from carboxymethyl guar gum and gelatin for ciprofloxacin sustained release, *International Journal of Biological Macromolecules*, Vol. 120, pp. 1823–1833. doi:10.1016/j.ijbiomac.2018.09.212
- [124] Jena, S. R.; Dalei, G.; Das, S.; Nayak, J.; Pradhan, M.; Samanta, L. (2022). Harnessing the potential of dialdehyde alginate-xanthan gum hydrogels as niche bioscaffolds for tissue engineering, *International Journal of Biological Macromolecules*, Vol. 207, pp. 493–506. doi:10.1016/j.ijbiomac.2022.03.024
- [125] Baljit Singh; Rajneesh; Baldev Singh; Kumar, A.; Aery, S. (2019). Polysaccharides Sterculia Gum/Psyllium Based Hydrogel Dressings for Drug Delivery Applications, *Polymer Science, Series A*, Vol. 61, Issue 6, pp. 865–874. doi:10.1134/S0965545X19060105
- [126] Thakur, N.; Singh, B. (2024). Evaluating physiochemical characteristics of tragacanth gum-gelatin network hydrogels designed through graft copolymerization technique, *International Journal of Biological Macromolecules*, Vol. 266, pp. 131082. doi:10.1016/j.ijbiomac.2024.131082
- [127] Bachra, Y.; Grouli, A.; Damiri, F.; Zhu, X. X.; Talbi, M.; Berrada, M. (2022). Synthesis, Characterization, and Swelling Properties of a New Highly Absorbent Hydrogel Based on Carboxymethyl Guar Gum Reinforced with Bentonite and Silica Particles for Disposable Hygiene Products, *ACS Omega*, Vol. 7, Issue 43, pp. 39002–39018. doi:10.1021/acsomega.2c04744

- [128] Singh, B.; Dhiman, A. (2016). Design of Acacia Gum—Carbopol—Cross-Linked-Polyvinylimidazole Hydrogel Wound Dressings for Antibiotic/Anesthetic Drug Delivery, *Industrial & Engineering Chemistry Research*, Vol. 55, Issue 34, pp. 9176–9188. doi:10.1021/acs.iecr.6b01963
- [129] Singh, B.; Sharma, V.; Ram, K.; Kumar, S.; Sharma, P.; Rohit. (2022). Impregnating graphene oxide into polyvinylsulphonic acid–sterculia gum hydrogels to modulate antibiotic drug vancomycin interactions for controlled drug delivery applications, *Diamond and Related Materials*, Vol. 130, pp. 109483. doi:10.1016/j.diamond.2022.109483
- [130] Singh, B.; Kumar, A.; Rohit. (2021). Gamma radiation formation of sterculia gum-alginate-carbopol hydrogel dressing by grafting method for use in brain drug delivery, *Chemical Physics Letters*, Vol. 779, pp. 138875. doi:10.1016/j.cplett.2021.138875
- [131] Dave, P. N.; Macwan, P. M.; Kamaliya, B. (2023). Preparation and Enhancing Properties of pH-Sensitive Hydrogel in Light of Gum Ghatti- cl -poly(acrylic acid)/ o -MWCNT for Sodium Diclofenac Drug Release, *Macromolecular Chemistry and Physics*, Vol. 224, Issue 12, pp. 2300038. doi:10.1002/macp.202300038
- [132] Kim, H. J.; Kummara, M. R.; Rao, K. S. V. K.; Han, S. S. (2023). Bioactive phosphate cross-linked guar gum-based hydrogels with enhanced mineralization ability for application in bone tissue engineering, *Ceramics International*, Vol. 49, Issue 23, pp. 39029–39038. doi:10.1016/j.ceramint.2023.09.240
- [133] Sami, A. J.; Khalid, M.; Jamil, T.; Aftab, S.; Mangat, S. A.; Shakoori, A. R.; Iqbal, S. (2018). Formulation of novel chitosan guargum based hydrogels for sustained drug release of paracetamol, *International Journal of Biological Macromolecules*, Vol. 108, pp. 324–332. doi:10.1016/j.ijbiomac.2017.12.008
- [134] Pourjalili, N.; Bagheri Marandi, G.; Kurdtabar, M.; Rezanejade Bardajee, G. (2022). Synthesis and characterization of double network hydrogel based on gellan-gum for drug delivery, *Journal of Macromolecular Science, Part A*, Vol. 59, Issue 8, pp. 537–549. doi:10.1080/10601325.2022.2092411
- [135] Nagaraja, K.; Krishna Rao, K. S. V.; Zo, S.; Soo Han, S.; Rao, K. M. (2021). Synthesis of Novel Tamarind Gum-co-poly(acrylamidoglycolic acid)-Based pH Responsive Semi-IPN Hydrogels and Their Ag Nanocomposites for Controlled Release of Chemotherapeutics and Inactivation of Multi-Drug-Resistant Bacteria, *Gels*, Vol. 7, Issue 4, pp. 237. doi:10.3390/gels7040237
- [136] Ramani, J.; Alle, M.; Sharma, G.; Reddy, K. V. N. S.; Park, Y.; Rao, K. S. V. K.; Kim, J.-C. (2022). Guar gum-g-poly(N-acryloyl-L-phenyl alanine) based pH responsive smart hydrogels for in-vitro anticancer drug delivery, *Soft Materials*, Vol. 20, Issue 3, pp. 329–343. doi:10.1080/1539445X.2022.2041033
- [137] Călina, I.; Demeter, M.; Scărișoreanu, A.; Micutz, M. (2021). Development of Novel Superabsorbent Hybrid Hydrogels by E-Beam Crosslinking, *Gels*, Vol.

- 7, Issue 4, pp. 189. doi:10.3390/gels7040189
- [138] Tiwari, A.; Grailer, J. J.; Pilla, S.; Steeber, D. A.; Gong, S. (2009). Biodegradable hydrogels based on novel photopolymerizable guar gummethacrylate macromonomers for in situ fabrication of tissue engineering scaffolds, *Acta Biomaterialia*, Vol. 5, Issue 9, pp. 3441–3452. doi:10.1016/j.actbio.2009.06.001
- [139] Ngwabebhoh, F. A.; Zandraa, O.; Patwa, R.; Saha, N.; Capáková, Z.; Saha, P. (2021). Self-crosslinked chitosan/dialdehyde xanthan gum blended hypromellose hydrogel for the controlled delivery of ampicillin, minocycline and rifampicin, *International Journal of Biological Macromolecules*, Vol. 167, pp. 1468–1478. doi:10.1016/j.ijbiomac.2020.11.100
- [140] Tavakol, M.; Dehshiri, S.; Vasheghani-Farahani, E. (2016). Electron beam irradiation crosslinked hydrogels based on tyramine conjugated gum tragacanth, *Carbohydrate Polymers*, Vol. 152, pp. 504–509. doi:10.1016/j.carbpol.2016.07.044
- [141] Huang, Y.; Yu, H.; Xiao, C. (2007). pH-sensitive cationic guar gum/poly (acrylic acid) polyelectrolyte hydrogels: Swelling and in vitro drug release, *Carbohydrate Polymers*, Vol. 69, Issue 4, pp. 774–783. doi:10.1016/j.carbpol.2007.02.016
- [142] Pervaiz, F.; Tanveer, W.; Shoukat, H.; Rehman, S. (2023). Formulation and evaluation of polyethylene glycol/Xanthan gum-co-poly (Acrylic acid) interpenetrating network for controlled release of venlafaxine, *Polymer Bulletin*, Vol. 80, Issue 1, pp. 469–493. doi:10.1007/s00289-022-04098-1
- [143] Sharma, K.; Kumar, V.; Chaudhary, B.; Kaith, B. S.; Kalia, S.; Swart, H. C. (2016). Application of biodegradable superabsorbent hydrogel composite based on Gum ghatti-co-poly(acrylic acid-aniline) for controlled drug delivery, *Polymer Degradation and Stability*, Vol. 124, pp. 101–111. doi:10.1016/j.polymdegradstab.2015.12.021
- [144] Singh, B.; Sharma, V. (2014). Influence of polymer network parameters of tragacanth gum-based pH responsive hydrogels on drug delivery, *Carbohydrate Polymers*, Vol. 101, pp. 928–940. doi:10.1016/j.carbpol.2013.10.022
- [145] Sethi, S.; Kaith, B. S.; Kaur, M.; Sharma, N.; Khullar, S. (2019). Study of a cross-linked hydrogel of Karaya gum and Starch as a controlled drug delivery system, *Journal of Biomaterials Science, Polymer Edition*, Vol. 30, Issue 18, pp.1687–1708. doi:10.1080/09205063.2019.1659710
- [146] Irantash, S.; Gholipour-Kanani, A.; Najmoddin, N.; Varsei, M. (2024). A Hybrid Structure based on Silk Fibroin/PVA Nanofibers and Alginate/Gum Tragacanth Hydrogel Embedded with Cardamom Extract, *Scientific Reports*, Vol. 14, Issue 1. doi:10.21203/rs.3.rs-4045523/v1
- [147] Sharma, A. K.; Kaith, B. S.; Shanker, U.; Gupta, B. (2020). γ-radiation induced synthesis of antibacterial silver nanocomposite scaffolds derived from natural

- gum Boswellia serrata, *Journal of Drug Delivery Science and Technology*, Vol. 56, pp. 101550. doi:10.1016/j.jddst.2020.101550
- [148] Dai, L.; Nadeau, B.; An, X.; Cheng, D.; Long, Z.; Ni, Y. (2016). Silver nanoparticles-containing dual-function hydrogels based on a guar gum-sodium borohydride system, *Scientific Reports*, Vol. 6, Issue 1, pp. 36497. doi:10.1038/srep36497
- [149] George, M.; Abraham, T. E. (2007). pH sensitive alginate—guar gum hydrogel for the controlled delivery of protein drugs, *International Journal of Pharmaceutics*, Vol. 335, Nos. 1–2, pp. 123–129. doi:10.1016/j.ijpharm.2006.11.009
- [150] Kajjari, P. B.; Manjeshwar, L. S.; Aminabhavi, T. M. (2011). Novel Interpenetrating Polymer Network Hydrogel Microspheres of Chitosan and Poly(acrylamide)- grafted -Guar Gum for Controlled Release of Ciprofloxacin, *Industrial & Engineering Chemistry Research*, Vol. 50, Issue 23, pp. 13280– 13287. doi:10.1021/ie2012856
- [151] He, Y.; Zhao, W.; Dong, Z.; Ji, Y.; Li, M.; Hao, Y.; Zhang, D.; Yuan, C.; Deng, J.; Zhao, P.; Zhou, Q. (2021). A biodegradable antibacterial alginate/carboxymethyl chitosan/Kangfuxin sponges for promoting blood coagulation and full-thickness wound healing, *International Journal of Biological Macromolecules*, Vol. 167, pp. 182–192. doi:10.1016/j.ijbiomac.2020.11.168
- [152] Gao, Y.; Wang, H.; Niu, X. (2024). A hydrogen-bonded curdlan-chitosan/polyvinyl alcohol edible dual functional hydrogel bandage against MRSA promotes wound healing, *International Journal of Biological Macromolecules*, Vol. 259, Issue P2, pp. 129351. doi:10.1016/j.ijbiomac.2024.129351
- [153] Heydari, M.; Alvandi, H.; Jaymand, M.; Dolatyari, H.; Hosseinzadeh, L.; Rahmatabadi, S. soheil; Arkan, E. (2024). A two-layer nanofiber-Tragacanth hydrogel composite containing Lavender extract and Mupirocin as a wound dressing, *Polymer Bulletin*, Vol. 81, Issue 1, pp. 373–389. doi:10.1007/s00289-022-04655-8
- [154] Li, M.; Li, H.; Li, X.; Zhu, H.; Xu, Z.; Liu, L.; Ma, J.; Zhang, M. (2017). A Bioinspired Alginate-Gum Arabic Hydrogel with Micro-/Nanoscale Structures for Controlled Drug Release in Chronic Wound Healing, *ACS Applied Materials and Interfaces*, Vol. 9, Issue 27, pp. 22160–22175. doi:10.1021/acsami.7b04428
- [155] Sharma, P.; Sharma, S.; Soleimani, M. Z.; Paiva-Santos, A. C.; Nejaddehbashi, F.; Kumar, A.; Makvandi, P.; Xu, Y. (2024). Accelerated in-vivo infected dermal wound healing with antimicrobial Bio-nanocomposite hydrogel, *Alexandria Engineering Journal*, Vol. 88, Issue October 2023, pp. 230–244. doi:10.1016/j.aej.2023.12.059
- [156] Jahan, I.; Ganesan, V.; Sahu, M.; Nandave, M.; Sen, S. (2024). Adhesivity-

- tuned bioactive gelatin/gellan hybrid gels drive efficient wound healing, *International Journal of Biological Macromolecules*, Vol. 254, Issue P2, pp. 127735. doi:10.1016/j.ijbiomac.2023.127735
- [157] Nakipoglu, M.; Özkabadayı, Y.; Karahan, S.; Tezcaner, A. (2024). Bilayer wound dressing composed of asymmetric polycaprolactone membrane and chitosan-carrageenan hydrogel incorporating storax balsam, *International Journal of Biological Macromolecules*, Vol. 254, Issue November 2023 pp. 128020. doi:10.1016/j.ijbiomac.2023.128020
- [158] Song, Y.; Hu, Q.; Liu, S.; Wang, Y.; Zhang, H.; Chen, J.; Yao, G. (2024). Electrospinning/3D printing drug-loaded antibacterial polycaprolactone nanofiber/sodium alginate-gelatin hydrogel bilayer scaffold for skin wound repair, *International Journal of Biological Macromolecules*, pp. 129705. doi:10.1016/j.ijbiomac.2024.129705
- [159] Das, I. J.; Bal, T. (2024). Evaluation of Opuntia-carrageenan superporous hydrogel (OPM-CRG SPH) as an effective biomaterial for drug release and tissue scaffold, *International Journal of Biological Macromolecules*, Vol. 256, Issue P2, pp. 128503. doi:10.1016/j.ijbiomac.2023.128503
- [160] Ghorbani, M.; Ramezani, S.; Rashidi, M. R. (2021). Fabrication of honey-loaded ethylcellulose/gum tragacanth nanofibers as an effective antibacterial wound dressing, *Colloids and Surfaces A: Physicochemical and Engineering Aspects*, Vol. 621, Issue February, pp. 126615. doi:10.1016/j.colsurfa.2021.126615
- [161] Adel, I. M.; ElMeligy, M. F.; Amer, M. S.; Elkasabgy, N. A. (2024). Gellan gum-based bi-polymeric hydrogel scaffolds loaded with Rosuvastatin calcium: A useful tool for tendon tissue regeneration, *European Journal of Pharmaceutical Sciences*, Vol. 192, Issue November 2023, pp. 106659. doi:10.1016/j.ejps.2023.106659
- [162] Cerqueira, M. T.; Da Silva, L. P.; Santos, T. C.; Pirraco, R. P.; Correlo, V. M.; Reis, R. L.; Marques, A. P. (2014). Gellan gum-hyaluronic acid spongy-like hydrogels and cells from adipose tissue synergize promoting neoskin vascularization, *ACS Applied Materials and Interfaces*, Vol. 6, Issue 22, pp. 19668–19679. doi:10.1021/am504520j
- [163] He, S.; Liu, Z.; Wu, X.; Liu, J.; Fang, H.; Shao, W. (2024). Novel flexible hydrogels based on carboxymethyl guar gum and polyacrylic acid for ultrahighly sensitive and reliable strain and pressure sensors, *Carbohydrate Polymers*, Vol. 324, Issue July 2023, pp. 121515. doi:10.1016/j.carbpol.2023.121515
- [164] Zeng, Q.; Qian, Y.; Huang, Y.; Ding, F.; Qi, X.; Shen, J. (2021). Polydopamine nanoparticle-dotted food gum hydrogel with excellent antibacterial activity and rapid shape adaptability for accelerated bacteria-infected wound healing, *Bioactive Materials*, Vol. 6, Issue 9, pp. 2647–2657. doi:10.1016/j.bioactmat.2021.01.035

- [165] Davydova, G. A.; Chaikov, L. L.; Melnik, N. N.; Gainutdinov, R. V.; Selezneva, I. I.; Perevedentseva, E. V.; Mahamadiev, M. T.; Proskurin, V. A.; Yakovsky, D. S.; Mohan, A. G.; Rau, J. V. (2024). Polysaccharide Composite Alginate–Pectin Hydrogels as a Basis for Developing Wound Healing Materials, *Polymers*, Vol. 16, Issue 2, pp. 287. doi:10.3390/polym16020287
- [166] Diniz, F. R.; Maia, R. C. A. P.; Rannier, L.; Andrade, L. N.; Chaud, M. V.; da Silva, C. F.; Corrêa, C. B.; de Albuquerque Junior, R. L. C.; da Costa, L. P.; Shin, S. R.; Hassan, S.; Sanchez-Lopez, E.; Souto, E. B.; Severino, P. (2020). Silver nanoparticles-composing alginate/gelatine hydrogel improves wound healing in vivo, *Nanomaterials*, Vol. 10, Issue 2, pp. 390. doi:10.3390/nano10020390
- [167] Huang, T.; Zhang, Y.; Zhao, L.; Ren, Y.; Wang, K.; Zhang, N.; Zhang, X.; Wang, J.; Tu, Q. (2024). Sodium hyaluronate hydrogel for wound healing and human health monitoring based on deep eutectic solvent, *International Journal of Biological Macromolecules*, Vol. 257, Issue P2, pp. 128801. doi:10.1016/j.ijbiomac.2023.128801
- [168] Zhang, X.; Kang, X.; Jin, L.; Bai, J.; Liu, W.; Wang, Z. (2018). Stimulation of wound healing using bioinspired hydrogels with basic fibroblast growth factor (bFGF), *International Journal of Nanomedicine*, Vol. 13, pp. 3897–3906. doi:10.2147/IJN.S168998
- [169] Sun, L.; Huang, Y.; Bian, Z.; Petrosino, J.; Fan, Z.; Wang, Y.; Park, K. H.; Yue, T.; Schmidt, M.; Galster, S.; Ma, J.; Zhu, H.; Zhang, M. (2016). Sundew-Inspired Adhesive Hydrogels Combined with Adipose-Derived Stem Cells for Wound Healing, ACS Applied Materials and Interfaces, Vol. 8, Issue 3, pp. 2423–2434. doi:10.1021/acsami.5b11811
- [170] Shi, W.; Zhang, D.; Han, L.; Shao, W.; Liu, Q.; Song, B.; Yan, G.; Tang, R.; Yang, X. (2024). Supramolecular chitin-based hydrogels with self-adapting and fast-degradation properties for enhancing wound healing, *Carbohydrate Polymers*, Vol. 323, Issue June 2023, pp. 121374. doi:10.1016/j.carbpol.2023.121374
- [171] Iqbal, D. N.; Tariq, M.; Khan, S. M.; Gull, N.; Sagar Iqbal, S.; Aziz, A.; Nazir, A.; Iqbal, M. (2020). Synthesis and characterization of chitosan and guar gum based ternary blends with polyvinyl alcohol, *International Journal of Biological Macromolecules*, Vol. 143, pp. 546–554. doi:10.1016/j.ijbiomac.2019.12.043
- [172] Srivastava, N.; Roy Choudhury, A. (2024). Thermo-reversible self-assembled novel gellan gum hydrogels containing amino acid biogelators with antibacterial activity, *Carbohydrate Polymers*, Vol. 324, Issue June 2023, pp. 121462. doi:10.1016/j.carbpol.2023.121462
- [173] Sher, M.; Shah, L. A.; Ara, L.; Ullah, R.; Khan, M.; Yoo, H. M.; Fu, J. (2024). Xanthan gum toughen ionically conductive hydrogels for flexible and artificial epidermis sensors with multifunctionality and self-healability, *Sensors and Actuators A: Physical*, Vol. 370, pp. 115199. doi:10.1016/j.sna.2024.115199

- [174] Muktar, M. Z.; Ismail, W. I. W.; Razak, S. I. A.; Razali, M. H.; Amin, K. A. M. (2018). Accelerated wound healing of physically cross linked Gellan Gum-Virgin Coconut Oil hydrogel containing Manuka Honey, ASM Science Journal, Vol. 11, Issue Special Issue 1, pp. 166–182
- [175] Keykhaee, M.; Rahimifard, M.; Najafi, A.; Baeeri, M.; Abdollahi, M.; Mottaghitalab, F.; Farokhi, M.; Khoobi, M. (2023). Alginate/gum arabic-based biomimetic hydrogel enriched with immobilized nerve growth factor and carnosine improves diabetic wound regeneration, *Carbohydrate Polymers*, Vol. 321, Issue July, pp. 121179. doi:10.1016/j.carbpol.2023.121179
- [176] Singh, H.; Yadav, I.; Sheikh, W. M.; Dan, A.; Darban, Z.; Shah, S. A.; Mishra, N. C.; Shahabuddin, S.; Hassan, S.; Bashir, S. M.; Dhanka, M. (2023). Dual cross-linked gellan gum/gelatin-based multifunctional nanocomposite hydrogel scaffold for full-thickness wound healing, *International Journal of Biological Macromolecules*, Vol. 251, Issue July, pp. 126349. doi:10.1016/j.ijbiomac.2023.126349
- [177] Shawan, M. M. A. K.; Islam, N.; Aziz, S.; Khatun, N.; Sarker, S. R.; Hossain, M.; Hossan, T.; Morshed, M.; Sarkar, M.; Shakil, S.; Rahman, N.; Begum, M. H. A.; Hasan, M. A. (2019). Fabrication of Xanthan gum: Gelatin (Xnt:Gel) Hybrid Composite Hydrogels for Evaluating Skin Wound Healing Efficacy, Modern Applied Science, Vol. 13, Issue 3, pp. 101. doi:10.5539/mas.v13n3p101
- [178] Synytsya, A.; Poučková, P.; Zadinová, M.; Troshchynska, Y.; Štětina, J.; Synytsya, A.; Saloň, I.; Král, V. (2020). Hydrogels based on low-methoxyl amidated citrus pectin and flaxseed gum formulated with tripeptide glycyl-Lhistidyl-L-lysine improve the healing of experimental cutting wounds in rats, *International Journal of Biological Macromolecules*, Vol. 165, pp. 3156–3168. doi:10.1016/j.ijbiomac.2020.09.251
- [179] Mahmood, H.; Khan, I. U.; Asif, M.; Khan, R. U.; Asghar, S.; Khalid, I.; Khalid, S. H.; Irfan, M.; Rehman, F.; Shahzad, Y.; Yousaf, A. M.; Younus, A.; Niazi, Z. R.; Asim, M. (2021). In vitro and in vivo evaluation of gellan gum hydrogel films: Assessing the co impact of therapeutic oils and ofloxacin on wound healing, *International Journal of Biological Macromolecules*, Vol. 166, pp. 483–495. doi:10.1016/j.ijbiomac.2020.10.206
- [180] Deng, Y.; Yang, X.; Zhang, X.; Cao, H.; Mao, L.; Yuan, M.; Liao, W. (2020). Novel fenugreek gum-cellulose composite hydrogel with wound healing synergism: Facile preparation, characterization and wound healing activity evaluation, *International Journal of Biological Macromolecules*, Vol. 160, pp. 1242–1251. doi:10.1016/j.ijbiomac.2020.05.220
- [181] Kar, A. K.; Singh, A.; Dhiman, N.; Purohit, M. P.; Jagdale, P.; Kamthan, M.; Singh, D.; Kumar, M.; Ghosh, D.; Patnaik, S. (2019). Polymer-assisted in situ synthesis of silver nanoparticles with epigallocatechin gallate (EGCG) impregnated wound patch potentiate controlled inflammatory responses for brisk wound healing, *International Journal of Nanomedicine*, Vol. 14, pp. 9837–9854. doi:10.2147/IJN.S228462

- [182] Deng, Y.; Chen, J.; Huang, J.; Yang, X.; Zhang, X.; Yuan, S.; Liao, W. (2020). Preparation and characterization of cellulose/flaxseed gum composite hydrogel and its hemostatic and wound healing functions evaluation, *Cellulose*, Vol. 27, Issue 7, pp. 3971–3988. doi:10.1007/s10570-020-03055-3
- [183] Li, W.; Jian, X.; Zou, Y.; Wu, L.; Huang, H.; Li, H.; Hu, D.; Yu, B. (2021). The Fabrication of a Gellan Gum-Based Hydrogel Loaded With Magnesium Ions for the Synergistic Promotion of Skin Wound Healing, *Frontiers in Bioengineering and Biotechnology*, Vol. 9, Issue September, pp. 1–13. doi:10.3389/fbioe.2021.709679
- [184] Alves, A.; Miguel, S. P.; Araujo, A. R. T. S.; Jes, D. (2020). Xanthan Gum Konjac Glucomannan Blend Hydrogel, *Polymers*, Vol. 12, Issue 99, pp. 1–15. doi: 10.3390/polym12010099
- [185] Lu, S.; Bian, S.; Jia, Y.; Guo, Y.; Xiao, H.; Zhang, M.; Liu, K.; Huang, L.; Chen, L.; Ni, Y.; Wu, H. (2024). Catechol-functionalised dialdehyde cellulose-containing hydrogels with tissue adhesion, sensing and haemostatic properties for wound healing, *Cellulose*, Vol. 31, Issue 4, pp. 2355–2377. doi:10.1007/s10570-024-05762-7
- [186] Piskunova, A.; Khomutov, N.; Di Martino, A.; Piskunov, M. (2024). Deposition of hydrogel particle impacting on smooth glass and porous nanofiber mat, *International Communications in Heat and Mass Transfer*, Vol. 152, pp. 107278. doi:10.1016/j.icheatmasstransfer.2024.107278
- [187] Martínez-ramírez, J.; Toldos-torres, M.; Benayas, E.; Villar-gómez, N.; Fernández-méndez, L.; Espinosa, F. M.; García, R.; Veintemillas-verdaguer, S.; Morales, P.; Serrano, M. C. (2024). Hybrid hydrogels support neural cell culture development under magnetic actuation at high frequency, Vol. 176, pp. 156-172. doi:10.1016/j.actbio.2024.01.030
- [188] Chelu, M.; Calderon Moreno, J.; Atkinson, I.; Pandele Cusu, J.; Rusu, A.; Bratan, V.; Aricov, L.; Anastasescu, M.; Seciu-Grama, A.-M.; Musuc, A. M. (2022). Green synthesis of bioinspired chitosan-ZnO-based polysaccharide gums hydrogels with propolis extract as novel functional natural biomaterials, *International Journal of Biological Macromolecules*, Vol. 211, pp. 410–424. doi:10.1016/j.ijbiomac.2022.05.070
- [189] Farooq, M.; Ihsan, J.; M.K. Mohamed, R.; Khan, M. A.; Rehman, T. U.; Ullah, H.; Ghani, M.; Saeed, S.; Siddiq, M. (2022). Highly biocompatible formulations based on Arabic gum Nano composite hydrogels: Fabrication, characterization, and biological investigation, *International Journal of Biological Macromolecules*, Vol. 209, pp. 59–69. doi:10.1016/j.ijbiomac.2022.03.162
- [190] Abdullaev, S. S.; Althomali, R. H.; Abdu Musad Saleh, E.; Robertovich, M. R.; Sapaev, I. B.; Romero-Parra, R. M.; Alsaab, H. O.; Gatea, M. A.; Fenjan, M. N. (2023). Synthesis of novel antibacterial and biocompatible polymer nanocomposite based on polysaccharide gum hydrogels, *Scientific Reports*, Vol. 13, Issue 1, pp. 16800. doi:10.1038/s41598-023-42146-6

- [191] Manda, M. G.; da Silva, L. P.; Cerqueira, M. T.; Pereira, D. R.; Oliveira, M. B.; Mano, J. F.; Marques, A. P.; Oliveira, J. M.; Correlo, V. M.; Reis, R. L. (2018). Gellan gum-hydroxyapatite composite spongy-like hydrogels for bone tissue engineering, *Journal of Biomedical Materials Research Part A*, Vol. 106, Issue 2, pp. 479–490. doi:10.1002/jbm.a.36248
- [192] Li, M.; Li, H.; Li, X.; Zhu, H.; Xu, Z.; Liu, L.; Ma, J.; Zhang, M. (2017). A Bioinspired Alginate-Gum Arabic Hydrogel with Micro-/Nanoscale Structures for Controlled Drug Release in Chronic Wound Healing, *ACS Applied Materials & Interfaces*, Vol. 9, Issue 27, pp. 22160–22175. doi:10.1021/acsami.7b04428
- [193] Haghbin, M.; Malekshah, R. E.; Sobhani, M.; Izadi, Z.; Haghshenas, B.; Ghasemi, M.; Kalani, B. S.; Samadian, H. (2023). Fabrication and characterization of Persian gum-based hydrogel loaded with gentamicin-loaded natural zeolite: An in vitro and in silico study, *International Journal of Biological Macromolecules*, Vol. 235, pp. 123766. doi:10.1016/j.ijbiomac.2023.123766
- [194] Sun, X.; Liang, Y.; Ye, L.; Liang, H. (2021). An extremely tough and ionic conductive natural-polymer-based double network hydrogel, *Journal of Materials Chemistry B*, Vol. 9, Issue 37, pp. 7751–7759. doi:10.1039/D1TB01458G
- [195] Bernal-Chávez, S. A.; Alcalá-Alcalá, S.; Almarhoon, Z. M.; Turgumbayeva, A.; Gürer, E. S.; De Los Dolores Campos-Echeverria, M.; Cortés, H.; Romero-Montero, A.; Del Prado-Audelo, M. L.; Sharifi-Rad, J.; Leyva-Gómez, G. (2023). Novel ultra-stretchable and self-healing crosslinked poly (ethylene oxide)-cationic guar gum hydrogel, *Journal of Biological Engineering*, Vol. 17, Issue 1, pp. 64. doi:10.1186/s13036-023-00376-2
- [196] Adedeji, O. E.; Choi, J.-Y.; Park, G. E.; Kang, H. J.; Aminu, M. O.; Min, J. H.; Chinma, C. E.; Moon, K.-D.; Jung, Y. H. (2022). Formulation and characterization of an interpenetrating network hydrogel of locust bean gum and cellulose microfibrils for 3D printing, Innovative Food Science & Emerging Technologies, Vol. 80, pp. 103086. doi:10.1016/j.ifset.2022.103086
- [197] Khan, M. U. A.; Iqbal, I.; Ansari, M. N. M.; Razak, S. I. A.; Raza, M. A.; Sajjad, A.; Jabeen, F.; Riduan Mohamad, M.; Jusoh, N. (2021). Development of Antibacterial, Degradable and pH-Responsive Chitosan/Guar Gum/Polyvinyl Alcohol Blended Hydrogels for Wound Dressing, *Molecules*, Vol. 26, Issue 19, pp. 5937. doi:10.3390/molecules26195937
- [198] Bernal-Chávez, S. A.; Alcalá-Alcalá, S.; Tapia-Guerrero, Y. S.; Magaña, J. J.; Del Prado-Audelo, M. L.; Leyva-Gómez, G. (2022). Cross-linked polyvinyl alcohol-xanthan gum hydrogel fabricated by freeze/thaw technique for potential application in soft tissue engineering, *RSC Advances*, Vol. 12, Issue 34, pp. 21713–21724. doi:10.1039/D2RA02295H
- [199] Hanna, D. H.; Saad, G. R. (2019). Encapsulation of ciprofloxacin within modified xanthan gum- chitosan based hydrogel for drug delivery, *Bioorganic Chemistry*, Vol. 84, pp. 115–124. doi:10.1016/j.bioorg.2018.11.036

- [200] Choopani, L.; Aliabadi, H. A. M.; Ganjali, F.; Kashtiaray, A.; Eivazzadeh-Keihan, R.; Maleki, A.; Salimibani, M.; Karimi, A. H.; Salehpour, N.; Mahdavi, M. (2024). Fabrication of a magnetic nanocomposite based on natural hydrogel: Pectin, tragacanth gum, silk fibroin, and integrated graphitic carbon nitride for hyperthermia and biological features, *Carbohydrate Polymer Technologies and Applications*, Vol. 7, pp. 100495. doi:10.1016/j.carpta.2024.100495
- [201] Fathollahipour, S.; Maziarfar, S.; Tavakoli, J. (2013). Characterization and evaluation of acacia gum loaded PVA hybrid wound dressing, 2013 20th Iranian Conference on Biomedical Engineering (ICBME), IEEE, pp. 149–154. doi:10.1109/ICBME.2013.6782209
- [202] Ghosh, D.; Basak, M.; Deka, D.; Das, G. (2023). Quinoxaline-probe embedded injectable fluorogenic hydrogels: Comparative detection of mesitylene in guar gum and i-carrageenan hydrogels, *International Journal of Biological Macromolecules*, Vol. 229, pp. 615–623. doi:10.1016/j.ijbiomac.2022.12.310
- [203] Oliveira Cardoso, V. M. de; Stringhetti Ferreira Cury, B.; Evangelista, R. C.; Daflon Gremião, M. P. (2017). Development and characterization of crosslinked gellan gum and retrograded starch blend hydrogels for drug delivery applications, *Journal of the Mechanical Behavior of Biomedical Materials*, Vol. 65, pp. 317–333. doi:10.1016/j.jmbbm.2016.08.005
- [204] Al-Musawi, M. H.; Rashidi, M.; Mohammadzadeh, V.; Albukhaty, S.; Mahmoudi, E.; Ghorbani, M. (2023). Development of a Novel Scaffold Based on Basil Seed Gum/Chitosan Hydrogel Containing Quercetin-Loaded Zein Microshphere for Bone Tissue Engineering, *Journal of Polymers and the Environment*, Vol. 31, Issue 11, pp. 4738–4751. doi:10.1007/s10924-023-02913-y
- [205] Deng, Y.; Huang, M.; Sun, D.; Hou, Y.; Li, Y.; Dong, T.; Wang, X.; Zhang, L.; Yang, W. (2018). Dual Physically Cross-Linked κ-Carrageenan-Based Double Network Hydrogels with Superior Self-Healing Performance for Biomedical Application, *ACS Applied Materials & Interfaces*, Vol. 10, Issue 43, pp. 37544–37554. doi:10.1021/acsami.8b15385
- [206] Wu, Y.; Liang, Y.; Liu, Y.; Hao, Y.; Tao, N.; Li, J.; Sun, X.; Zhou, M.; Liu, Y.-N. (2021). A Bi 2 S 3 -embedded gellan gum hydrogel for localized tumor photothermal/antiangiogenic therapy, *Journal of Materials Chemistry B*, Vol. 9, Issue 14, pp. 3224–3234. doi:10.1039/D1TB00257K
- [207] Jalababu, R.; Satya Veni, S.; Reddy, K. V. N. S. (2019). Development, characterization, swelling, and network parameters of amino acid grafted guar gum based pH responsive polymeric hydrogels, *International Journal of Polymer Analysis and Characterization*, Vol. 24, Issue 4, pp. 304–312. doi:10.1080/1023666X.2019.1594058
- [208] Kang, M.; Oderinde, O.; Liu, S.; Huang, Q.; Ma, W.; Yao, F.; Fu, G. (2019). Characterization of Xanthan gum-based hydrogel with Fe3+ ions coordination and its reversible sol-gel conversion, *Carbohydrate Polymers*, Vol. 203, pp. 139–147. doi:10.1016/j.carbpol.2018.09.044

- [209] Mali, K. K.; Ghorpade, V. S.; Dias, R. J.; Dhawale, S. C. (2023). Synthesis and characterization of citric acid crosslinked carboxymethyl tamarind gumpolyvinyl alcohol hydrogel films, *International Journal of Biological Macromolecules*, Vol. 236, pp. 123969. doi:10.1016/j.ijbiomac.2023.123969
- [210] Slavutsky, A. M.; Bertuzzi, M. A. (2019). Formulation and characterization of hydrogel based on pectin and brea gum, *International Journal of Biological Macromolecules*, Vol. 123, pp. 784–791. doi:10.1016/j.ijbiomac.2018.11.038
- [211] Salazar Salas, B. M.; Grijalva Bustamante, G. A.; Fernández Quiroz, D.; Castillo Ortega, M. M.; Encinas, J. C.; Herrera Franco, P. J.; del Castillo Castro, T. (2022). Nanocomposite hydrogels of gellan gum and polypyrrole for electrostimulated ibuprofen release application, *Reactive and Functional Polymers*, Vol. 176, pp. 105296. doi:10.1016/j.reactfunctpolym.2022.105296
- [212] Fernández-Ferreiro, A.; González Barcia, M.; Gil-Martínez, M.; Vieites-Prado, A.; Lema, I.; Argibay, B.; Blanco Méndez, J.; Lamas, M. J.; Otero-Espinar, F. J. (2015). In vitro and in vivo ocular safety and eye surface permanence determination by direct and Magnetic Resonance Imaging of ion-sensitive hydrogels based on gellan gum and kappa-carrageenan, *European Journal of Pharmaceutics and Biopharmaceutics*, Vol. 94, pp. 342–351. doi:10.1016/j.ejpb.2015.06.003
- [213] Reddy, O. S.; Subha, M.; Jithendra, T.; Madhavi, C.; Rao, K. C. (2021). Fabrication and characterization of smart karaya gum/sodium alginate semi-IPN microbeads for controlled release of D-penicillamine drug, *Polymers and Polymer Composites*, Vol. 29, Issue 3, pp. 163–175. doi:10.1177/0967391120904477
- [214] Oh, G. W.; Kim, S. C.; Cho, K. J.; Ko, S. C.; Lee, J. M.; Yim, M. J.; Kim, K. W.; Kim, H. S.; Kim, J. Y.; Lee, D. S.; Heo, S. Y.; Kim, Y. M.; Jung, W. K. (2024). Poly(vinyl alcohol)/chitosan hydrogel incorporating chitooligosaccharide-gentisic acid conjugate with antioxidant and antibacterial properties as a potential wound dressing, *International Journal of Biological Macromolecules*, Vol. 255, Issue November 2023, pp. 128047. doi:10.1016/j.ijbiomac.2023.128047
- [215] Hua, D.; Gao, S.; Zhang, M.; Ma, W.; Huang, C. (2020). A novel xanthan gumbased conductive hydrogel with excellent mechanical, biocompatible, and self-healing performances, *Carbohydrate Polymers*, Vol. 247, Issue July, pp. 116743. doi:10.1016/j.carbpol.2020.116743
- [216] Shahriari-Khalaji, M.; Sattar, M.; Cao, R.; Zhu, M. (2023). Angiogenesis, hemocompatibility and bactericidal effect of bioactive natural polymer-based bilayer adhesive skin substitute for infected burned wound healing, *Bioactive Materials*, Vol. 29, Issue July, pp. 177–195. doi:10.1016/j.bioactmat.2023.07.008
- [217] Lu, S.; Wu, H.; Ge, S.; Huang, L.; Chen, L.; Connor, C.; Guo, Z.; Jiang, Y.; Xu,
   B. Bin; Peng, W. (2024). A Cellulose/Chitosan Dual Cross-Linked Multifunctional and Resilient Hydrogel for Emergent Open Wound

- Management, *Advanced Healthcare Materials*, Vol. 13, Issue 13. doi:10.1002/adhm.202304676
- [218] Matar, G. H.; Kaymazlar, E.; Andac, M.; Andac, O. (2023). Novel Binary Blended Hydrogel Films (Chitosan-Vanillin Schiff Base/Locust Bean Gum and Fe(III), Cu(II) & Description (Complexes): Synthesis, Characterization, Conductivity, and Antibacterial Activity, *Journal of Polymers and the Environment*, Vol. 31, Issue 8, pp. 3509–3521. doi:10.1007/s10924-023-02822-0
- [219] Sahraro, M.; Barikani, M.; Daemi, H.; Baei, P. (2021). Anti-fatigue, highly resilient photocrosslinkable gellan gum hydrogels reinforced by flexible nanoparticulate polyurethane multi-crosslinkers, *International Journal of Biological Macromolecules*, Vol. 183, pp. 831–838. doi:10.1016/j.ijbiomac.2021.04.144
- [220] Ling, Q.; Liu, W.; Liu, J.; Zhao, L.; Ren, Z.; Gu, H. (2022). Highly Sensitive and Robust Polysaccharide-Based Composite Hydrogel Sensor Integrated with Underwater Repeatable Self-Adhesion and Rapid Self-Healing for Human Motion Detection, *ACS Applied Materials & Interfaces*, Vol. 14, Issue 21, pp. 24741–24754. doi:10.1021/acsami.2c01785
- [221] Rao, K. M.; Narayanan, K. B.; Uthappa, U. T.; Park, P.-H.; Choi, I.; Han, S. S. (2022). Tissue Adhesive, Self-Healing, Biocompatible, Hemostasis, and Antibacterial Properties of Fungal-Derived Carboxymethyl Chitosan-Polydopamine Hydrogels, *Pharmaceutics*, Vol. 14, Issue 5, pp. 1028. doi:10.3390/pharmaceutics14051028
- [222] Chen, C.; Zhou, P.; Huang, C.; Zeng, R.; Yang, L.; Han, Z.; Qu, Y.; Zhang, C. (2021). Photothermal-promoted multi-functional dual network polysaccharide hydrogel adhesive for infected and susceptible wound healing, *Carbohydrate Polymers*, Vol. 273, pp. 118557. doi:10.1016/j.carbpol.2021.118557
- [223] Yerra, P.; Migliario, M.; Gino, S.; Sabbatini, M.; Bignotto, M.; Invernizzi, M.; Renò, F. (2024). Polydopamine Blending Increases Human Cell Proliferation in Gelatin–Xanthan Gum 3D-Printed Hydrogel, *Gels*, Vol. 10, Issue 2, pp. 145. doi:10.3390/gels10020145
- [224] Xie, C.; Liu, G.; Wang, L.; Yang, Q.; Liao, F.; Yang, X.; Xiao, B.; Duan, L. (2024). Synthesis and Properties of Injectable Hydrogel for Tissue Filling, *Pharmaceutics*, Vol. 16, Issue 3, pp. 430. doi:10.3390/pharmaceutics16030430
- [225] Yu, C.; Xu, J.; Heidari, G.; Jiang, H.; Shi, Y.; Wu, A.; Makvandi, P.; Neisiany, R. E.; Zare, E. N.; Shao, M.; Hu, L. (2024). Injectable hydrogels based on biopolymers for the treatment of ocular diseases, *International Journal of Biological Macromolecules*, Vol. 269, pp. 132086. doi:10.1016/j.ijbiomac.2024.132086
- [226] Li, A.; Ma, B.; Hua, S.; Ping, R.; Ding, L.; Tian, B.; Zhang, X. (2024). Chitosan-based injectable hydrogel with multifunction for wound healing: A critical review, *Carbohydrate Polymers*, Vol. 333, pp. 121952.

- doi:10.1016/j.carbpol.2024.121952
- [227] Yu, X.; Cheng, C.; Peng, X.; Zhang, K.; Yu, X. (2022). A self-healing and injectable oxidized quaternized guar gum/carboxymethyl chitosan hydrogel with efficient hemostatic and antibacterial properties for wound dressing, *Colloids and Surfaces B: Biointerfaces*, Vol. 209, Issue P1, pp. 112207. doi:10.1016/j.colsurfb.2021.112207
- [228] Oliveira, I. M.; Gonçalves, C.; Shin, M. E.; Lee, S.; Reis, R. L.; Khang, G.; Oliveira, J. M. (2020). Anti-inflammatory properties of injectable betamethasone-loaded tyramine-modified gellan gum/silk fibroin hydrogels, *Biomolecules*, Vol. 10, Issue 10, pp. 1–17. doi:10.3390/biom10101456
- [229] He, D.; Li, H. (2020). Bifunctional Cx43 Mimic Peptide Grafted Hyaluronic Acid Hydrogels Inhibited Tumor Recurrence and Stimulated Wound Healing for Postsurgical Tumor Treatment, *Advanced Functional Materials*, Vol. 30, Issue 51, pp. 1–20. doi:10.1002/adfm.202004709
- [230] Zong, H.; Wang, B.; Li, G.; Yan, S.; Zhang, K.; Shou, Y.; Yin, J. (2020). Biodegradable High-Strength Hydrogels with Injectable Performance Based on Poly(1 -Glutamic Acid) and Gellan Gum, *ACS Biomaterials Science and Engineering*, Vol. 6, Issue 8, pp. 4702–4713. doi:10.1021/acsbiomaterials.0c00915
- [231] Lee, S. J.; Nah, H.; Heo, D. N.; Kim, K. H.; Seok, J. M.; Heo, M.; Moon, H. J.; Lee, D.; Lee, J. S.; An, S. Y.; Hwang, Y. S.; Ko, W. K.; Kim, S. J.; Sohn, S.; Park, S. A.; Park, S. Y.; Kwon, I. K. (2020). Induction of osteogenic differentiation in a rat calvarial bone defect model using an In situ forming graphene oxide incorporated glycol chitosan/oxidized hyaluronic acid injectable hydrogel, *Carbon*, Vol. 168, pp. 264–277. doi:10.1016/j.carbon.2020.05.022
- [232] Ren, Y.; Zhang, D.; He, Y.; Chang, R.; Guo, S.; Ma, S.; Yao, M.; Guan, F. (2021). Injectable and antioxidative ht/qga hydrogel for potential application in wound healing, *Gels*, Vol. 7, Issue 4. doi:10.3390/gels7040204
- [233] Yavari Maroufi, L.; Ghorbani, M. (2021). Injectable chitosan-quince seed gum hydrogels encapsulated with curcumin loaded-halloysite nanotubes designed for tissue engineering application, *International Journal of Biological Macromolecules*, Vol. 177, pp. 485–494. doi:10.1016/j.ijbiomac.2021.02.113
- [234] Pan, Y.; Zhao, Y.; Kuang, R.; Liu, H.; Sun, D.; Mao, T.; Jiang, K.; Yang, X.; Watanabe, N.; Mayo, K. H.; Lin, Q.; Li, J. (2020). Injectable hydrogel-loaded nano-hydroxyapatite that improves bone regeneration and alveolar ridge promotion, *Materials Science and Engineering C*, Vol. 116, Issue May, pp. 111158. doi:10.1016/j.msec.2020.111158
- [235] Pandit, A. H.; Nisar, S.; Imtiyaz, K.; Nadeem, M.; Mazumdar, N.; Rizvi, M. M. A.; Ahmad, S. (2021). Injectable, Self-Healing, and Biocompatible N,O-Carboxymethyl Chitosan/Multialdehyde Guar Gum Hydrogels for Sustained Anticancer Drug Delivery, *Biomacromolecules*, Vol. 22, Issue 9, pp. 3731–3745. doi:10.1021/acs.biomac.1c00537

- [236] Balitaan, J. N. I.; Hsiao, C. Der; Yeh, J. M.; Santiago, K. S. (2020). Innovation inspired by nature: Biocompatible self-healing injectable hydrogels based on modified-β-chitin for wound healing, *International Journal of Biological Macromolecules*, Vol. 162, pp. 723–736. doi:10.1016/j.ijbiomac.2020.06.129
- [237] Yang, P.; Ju, Y.; Liu, X.; Li, Z.; Liu, H.; Yang, M.; Chen, X.; Lei, L.; Fang, B. (2023). Natural self-healing injectable hydrogels loaded with exosomes and berberine for infected wound healing, *Materials Today Bio*, Vol. 23, Issue August, pp. 100875. doi:10.1016/j.mtbio.2023.100875
- [238] Ding, C.; Yang, Q.; Tian, M.; Guo, C.; Deng, F.; Dang, Y.; Zhang, M. (2020). Novel collagen-based hydrogels with injectable, self-healing, wound-healing properties via a dynamic crosslinking interaction, *Polymer International*, Vol. 69, Issue 9, pp. 858–866. doi:10.1002/pi.6027
- [239] Zhao, L.; Niu, L.; Liang, H.; Tan, H.; Liu, C.; Zhu, F. (2017). PH and Glucose Dual-Responsive Injectable Hydrogels with Insulin and Fibroblasts as Bioactive Dressings for Diabetic Wound Healing, *ACS Applied Materials and Interfaces*, Vol. 9, Issue 43, pp. 37563–37574. doi:10.1021/acsami.7b09395
- [240] Li, Z.; Zhao, Y.; Liu, H.; Ren, M.; Wang, Z.; Wang, X.; Liu, H.; Feng, Y.; Lin, Q.; Wang, C.; Wang, J. (2021). pH-responsive hydrogel loaded with insulin as a bioactive dressing for enhancing diabetic wound healing, *Materials and Design*, Vol. 210, pp. 110104. doi:10.1016/j.matdes.2021.110104
- [241] Nezhad-Mokhtari, P.; Ghorbani, M.; Abdyazdani, N. (2021). Reinforcement of hydrogel scaffold using oxidized-guar gum incorporated with curcumin-loaded zein nanoparticles to improve biological performance, *International Journal of Biological Macromolecules*, Vol. 167, pp. 59–65. doi:10.1016/j.ijbiomac.2020.11.103
- [242] Zhang, R.; Tao, Y.; Xu, Q.; Liu, N.; Chen, P.; Zhou, Y.; Bai, Z. (2020). Rheological and ion-conductive properties of injectable and self-healing hydrogels based on xanthan gum and silk fibroin, *International Journal of Biological Macromolecules*, Vol. 144, pp. 473–482. doi:10.1016/j.ijbiomac.2019.12.132
- [243] Basu, S.; Pacelli, S.; Paul, A. (2020). Self-healing DNA-based injectable hydrogels with reversible covalent linkages for controlled drug delivery, *Acta Biomaterialia*, Vol. 105, pp. 159–169. doi:10.1016/j.actbio.2020.01.021
- [244] Yuan, M.; Xu, S.; Zhou, Y.; Chen, Y.; Song, J.; Ma, S.; He, Y.; Mao, H.; Kong, D.; Gu, Z. (2023). A facile bioorthogonal chemistry-based reversible to irreversible strategy to surmount the dilemma between injectability and stability of hyaluronic acid hydrogels, *Carbohydrate Polymers*, Vol. 317, Issue June, pp. 121103. doi:10.1016/j.carbpol.2023.121103
- [245] Li, J.; Su, J.; Liang, J.; Zhang, K.; Xie, M.; Cai, B.; Li, J. (2024). A hyaluronic acid / chitosan composite functionalized hydrogel based on enzyme-catalyzed and Schiff base reaction for promoting wound healing, *International Journal of Biological Macromolecules*, Vol. 255, Issue May 2023, pp. 128284.

- doi:10.1016/j.ijbiomac.2023.128284
- [246] Luo, J.; Sun, F.; Rao, P.; Zhu, T.; Liu, Y.; Du, J.; Chen, S.; Jin, X.; Jin, J.; Chai, Y. (2023). A poly (glycerol-sebacate-acrylate) nanosphere enhanced injectable hydrogel for wound treatment, *Frontiers in Bioengineering and Biotechnology*, Vol. 10, Issue January, pp. 1–12. doi:10.3389/fbioe.2022.1091122
- [247] Ma, W.; Yang, M.; Wu, C.; Wang, S.; Du, M. (2023). Bioinspired self-healing injectable nanocomposite hydrogels based on oxidized dextran and gelatin for growth-factor-free bone regeneration, *International Journal of Biological Macromolecules*, Vol. 251, Issue July, pp. 126145. doi:10.1016/j.ijbiomac.2023.126145
- [248] Bai, Q.; Gao, Q.; Hu, F.; Zheng, C.; Chen, W.; Sun, N.; Liu, J.; Zhang, Y.; Wu, X.; Lu, T. (2023). Chitosan and hyaluronic-based hydrogels could promote the infected wound healing, *International Journal of Biological Macromolecules*, Vol. 232, Issue October 2022, pp. 123271. doi:10.1016/j.ijbiomac.2023.123271
- [249] Gu, H.; Li, H.; Wei, L.; Lu, J.; Wei, Q. (2023). Collagen-based injectable and self-healing hydrogel with multifunction for regenerative repairment of infected wounds, *Regenerative Biomaterials*, Vol. 10, Issue March. doi:10.1093/rb/rbad018
- [250] Wang, R.; Liu, L.; He, X.; Xia, Z.; Zhao, Z.; Xi, Z.; Yu, J.; Wang, J. (2023). Dynamic Crosslinked Injectable Mussel-Inspired Hydrogels with Adhesive, Self-Healing, and Biodegradation Properties, *Polymers*, Vol. 15, Issue 8. doi:10.3390/polym15081876
- [251] Wu, Y.; Xu, W.; Li, J.; Zhong, Z.; Huang, L.; Li, S.; Tan, H. (2024). Influence of tannic acid post-treatment on the degradation and drug release behavior of Schiff base crosslinked konjac glucomannan/chitosan hydrogel, *European Polymer Journal*, Vol. 202, Issue November 2023, pp. 112592. doi:10.1016/j.eurpolymj.2023.112592
- [252] Lin, X.; Lv, J.; Wang, D.; Liu, K. (2023). Injectable adhesive carboxymethyl chitosan-based hydrogels with self-mending and antimicrobial features for the potential management of periodontal diseases, *RSC Advances*, Vol. 13, Issue 18, pp. 11903–11911. doi:10.1039/d3ra00904a
- [253] Wei, H.; Yu, S.; Zhang, Y.; Zhang, H.; Ma, Y.; Xu, M.; An, P.; Zhou, Y.; Halila, S.; Wei, Y.; Chen, J. (2023). Injectable chitosan/xyloglucan composite hydrogel with mechanical adaptivity and endogenous bioactivity for skin repair, *Carbohydrate Polymers*, Vol. 313, Issue September 2022, pp. 120904. doi:10.1016/j.carbpol.2023.120904
- [254] Tan, Y.; Ma, L.; Chen, X.; Ran, Y.; Tong, Q.; Tang, L.; Li, X. (2022). Injectable hyaluronic acid/hydroxyapatite composite hydrogels as cell carriers for bone repair, *International Journal of Biological Macromolecules*, Vol. 216, Issue July, pp. 547–557. doi:10.1016/j.ijbiomac.2022.07.009
- [255] Shen, J.; Jiao, W.; Chen, Z.; Wang, C.; Song, X.; Ma, L.; Tang, Z.; Yan, W.;

- Xie, H.; Yuan, B.; Wang, C.; Dai, J.; Sun, Y.; Du, L.; Jin, Y. (2023). Injectable multifunctional chitosan/dextran-based hydrogel accelerates wound healing in combined radiation and burn injury, *Carbohydrate Polymers*, Vol. 316, Issue March, pp. 121024. doi:10.1016/j.carbpol.2023.121024
- [256] Li, C.; Jiang, T.; Zhou, C.; Jiang, A.; Lu, C.; Yang, G.; Nie, J.; Wang, F.; Yang, X.; Chen, Z. (2023). Injectable self-healing chitosan-based POSS-PEG hybrid hydrogel as wound dressing to promote diabetic wound healing, *Carbohydrate Polymers*, Vol. 299, Issue October 2022, pp. 120198. doi:10.1016/j.carbpol.2022.120198
- [257] Ren, H.; Zhang, Z.; Cheng, X.; Zou, Z.; Chen, X.; He, C. (2023). Injectable, self-healing hydrogel adhesives with firm tissue adhesion and on-demand biodegradation for sutureless wound closure, *Science Advances*, Vol. 9, Issue 33. doi:10.1126/sciadv.adh4327
- [258] Nie, L.; Wei, Q.; Sun, M.; Ding, P.; Wang, L.; Sun, Y.; Ding, X.; Okoro, O. V.; Jiang, G.; Shavandi, A. (2023). Injectable, self-healing, transparent, and antibacterial hydrogels based on chitosan and dextran for wound dressings, *International Journal of Biological Macromolecules*, Vol. 233, Issue November 2022, pp. 123494. doi:10.1016/j.ijbiomac.2023.123494
- [259] Sun, A.; Hu, D.; He, X.; Ji, X.; Li, T.; Wei, X.; Qian, Z. (2022). Mussel-inspired hydrogel with injectable self-healing and antibacterial properties promotes wound healing in burn wound infection, *NPG Asia Materials*, Vol. 14, Issue 1, pp. 86. doi:10.1038/s41427-022-00434-z
- [260] Ruan, T.; Fu, C.; Lin, C.; Chou, K.; Lin, Y. (2023). Biomaterials Nanocontroller-mediated dissolving hydrogel that can sustainably release cold-mimetic menthol to induce adipocyte browning for treating obesity and its related metabolic disorders, *Biomaterials*, Vol. 297, Issue April, pp. 122120. doi:10.1016/j.biomaterials.2023.122120
- [261] Cui, P.; Pan, P.; Qin, L.; Wang, X.; Chen, X.; Deng, Y. (2023). Bioactive Materials Nanoengineered hydrogels as 3D biomimetic extracellular matrix with injectable and sustained delivery capability for cartilage regeneration, *Bioactive Materials*, Vol. 19, Issue March 2022, pp. 487–498. doi:10.1016/j.bioactmat.2022.03.032
- [262] Li, L.; Xiang, F.; Wang, F.; Liu, Y. (2024). Preparation and antitumor study of intelligent injectable hydrogel: Carboxymethyl chitosan aldehyde gum Arabic composite graphene oxide hydrogel, Vol. 259, Issue December 2023, pp. 129429. doi:10.1016/j.ijbiomac.2024.129429
- [263] Zhang, L.; Luo, B.; An, Z.; Zheng, P.; Liu, Y.; Zhao, H.; Zhang, Z.; Gao, T.; Cao, Y.; Zhang, Y.; Pei, R. (2023). MMP-Responsive Nanoparticle-Loaded, Injectable, Adhesive, Self-Healing Hydrogel Wound Dressing Based on Dynamic Covalent Bonds, *Biomacromolecules*, Vol. 24, Issue 12, pp. 5769–5779, doi:10.1021/acs.biomac.3c00773
- [264] Mohabatpour, F.; Yazdanpanah, Z.; Papagerakis, S.; Chen, X.; Papagerakis, P.

- (2022). Self-Crosslinkable Oxidized Alginate-Carboxymethyl Chitosan Hydrogels as an Injectable Cell Carrier for In Vitro Dental Enamel Regeneration, *Journal of Functional Biomaterials*, Vol. 13, Issue 2, pp. 71. doi:10.3390/jfb13020071
- [265] Sarmah, D.; Ahmad, M.; Sarkar, A.; Mandal, M.; Sankaranarayanan, K.; Karak, N. (2023). Self-cross-linked starch / chitosan hydrogel as a biocompatible vehicle for controlled release of drug, *International Journal of Biological Macromolecules*, Vol. 237, Issue March, pp. 124206. doi:10.1016/j.ijbiomac.2023.124206
- [266] Hosseini, S.; Eslahi, N.; Jahanmardi, R. (2023). Self-healing nanocomposite hydrogels based on chitosan / modified polyethylene glycol / graphene, *Materials Today Communications*, Vol. 37, Issue October, pp. 107417. doi:10.1016/j.mtcomm.2023.107417
- [267] Zhao, Z.; Gao, J.; Cai, W.; Li, J.; Kong, Y.; Zhou, M. (2023). Synthesis of oxidized carboxymethyl cellulose / chitosan hydrogels doped with graphene oxide for pH- and NIR-responsive drug delivery, *European Polymer Journal*, Vol. 199, Issue August, pp. 112437. doi:10.1016/j.eurpolymj.2023.112437
- [268] Pacelli, S.; Paolicelli, P.; Dreesen, I.; Kobayashi, S.; Vitalone, A.; Casadei, M. A. (2015). Injectable and photocross-linkable gels based on gellan gum methacrylate: A new tool for biomedical application, *International Journal of Biological Macromolecules*, Vol. 72, pp. 1335–1342. doi:10.1016/j.ijbiomac.2014.10.046
- [269] Pacelli, S.; Paolicelli, P.; Moretti, G.; Petralito, S.; Di Giacomo, S.; Vitalone, A.; Casadei, M. A. (2016). Gellan gum methacrylate and laponite as an innovative nanocomposite hydrogel for biomedical applications, *European Polymer Journal*, Vol. 77, pp. 114–123. doi:10.1016/j.eurpolymj.2016.02.007
- [270] Qu, Y.; He, S.; Luo, S.; Zhao, J.; Liang, R.; Liao, C.; Zheng, L. (2023). Photocrosslinkable, Injectable Locust Bean Gum Hydrogel Induces Chondrogenic Differentiation of Stem Cells for Cartilage Regeneration, *Advanced Healthcare Materials*, Vol. 12, Issue 18. doi:10.1002/adhm.202203079
- [271] Zong, H.; Wang, B.; Li, G.; Yan, S.; Zhang, K.; Shou, Y.; Yin, J. (2020). Biodegradable High-Strength Hydrogels with Injectable Performance Based on Poly( <scp>|</scp> -Glutamic Acid) and Gellan Gum, ACS Biomaterials Science & Engineering, Vol. 6, Issue 8, pp. 4702–4713. doi:10.1021/acsbiomaterials.0c00915
- [272] Pandit, A. H.; Mazumdar, N.; Imtiyaz, K.; Alam Rizvi, M. M.; Ahmad, S. (2020). Self-Healing and Injectable Hydrogels for Anticancer Drug Delivery: A Study with Multialdehyde Gum Arabic and Succinic Anhydride Chitosan, *ACS Applied Bio Materials*, Vol. 3, Issue 12, pp. 8460–8470. doi:10.1021/acsabm.0c00835
- [273] Ren, B.; Chen, X.; Du, S.; Ma, Y.; Chen, H.; Yuan, G.; Li, J.; Xiong, D.; Tan,

- H.; Ling, Z.; Chen, Y.; Hu, X.; Niu, X. (2018). Injectable polysaccharide hydrogel embedded with hydroxyapatite and calcium carbonate for drug delivery and bone tissue engineering, *International Journal of Biological Macromolecules*, Vol. 118, pp. 1257–1266. doi:10.1016/j.ijbiomac.2018.06.200
- [274] Pandit, A. H.; Nisar, S.; Imtiyaz, K.; Nadeem, M.; Mazumdar, N.; Rizvi, M. M. A.; Ahmad, S. (2021). Injectable, Self-Healing, and Biocompatible N, O-Carboxymethyl Chitosan/Multialdehyde Guar Gum Hydrogels for Sustained Anticancer Drug Delivery, *Biomacromolecules*, Vol. 22, Issue 9, pp. 3731–3745. doi:10.1021/acs.biomac.1c00537
- [275] Chen, M.; Tan, H.; Xu, W.; Wang, Z.; Zhang, J.; Li, S.; Zhou, T.; Li, J.; Niu, X. (2022). A self-healing, magnetic and injectable biopolymer hydrogel generated by dual cross-linking for drug delivery and bone repair, *Acta Biomaterialia*, Vol. 153, pp. 159–177. doi:10.1016/j.actbio.2022.09.036
- [276] Kim, Y.; Hu, Y.; Jeong, J.; Jung, S. (2022). Injectable, self-healable and adhesive hydrogels using oxidized Succinoglycan/chitosan for pH-responsive drug delivery, *Carbohydrate Polymers*, Vol. 284, pp. 119195. doi:10.1016/j.carbpol.2022.119195
- [277] Tan, W.; Long, T.; Wan, Y.; Li, B.; Xu, Z.; Zhao, L.; Mu, C.; Ge, L.; Li, D. (2023). Dual-drug loaded polysaccharide-based self-healing hydrogels with multifunctionality for promoting diabetic wound healing, *Carbohydrate Polymers*, Vol. 312, pp. 120824. doi:10.1016/j.carbpol.2023.120824
- [278] Huang, J.; Deng, Y.; Ren, J.; Chen, G.; Wang, G.; Wang, F.; Wu, X. (2018). Novel in situ forming hydrogel based on xanthan and chitosan re-gelifying in liquids for local drug delivery, *Carbohydrate Polymers*, Vol. 186, pp. 54–63. doi:10.1016/j.carbpol.2018.01.025
- [279] Chen, M.; Zhai, X.; Pan, Y.; Tan, H. (2021). Covalent and environment-responsive biopolymer hydrogel for drug delivery and wound healing, *Journal of Macromolecular Science*, *Part A*, Vol. 58, 11, pp. 736–747. doi:10.1080/10601325.2021.1929316
- [280] Balitaan, J. N. I.; Hsiao, C.-D.; Yeh, J.-M.; Santiago, K. S. (2020). Innovation inspired by nature: Biocompatible self-healing injectable hydrogels based on modified-β-chitin for wound healing, *International Journal of Biological Macromolecules*, Vol. 162, pp. 723–736. doi:10.1016/j.ijbiomac.2020.06.129
- [281] Babo, P. S.; Pires, R. L.; Santos, L.; Franco, A.; Rodrigues, F.; Leonor, I.; Reis, R. L.; Gomes, M. E. (2017). Platelet Lysate-Loaded Photocrosslinkable Hyaluronic Acid Hydrogels for Periodontal Endogenous Regenerative Technology, *ACS Biomaterials Science and Engineering*, Vol. 3, Issue 7, pp. 1359–1369. doi:10.1021/acsbiomaterials.6b00508
- [282] Shah, S. A.; Sohail, M.; Minhas, M. U.; Khan, S.; Hussain, Z.; Mahmood, A.; Kousar, M.; Thu, H. E.; Abbasi, M.; Kashif, M. ur R. (2021). Curcumin-laden hyaluronic acid-co-Pullulan-based biomaterials as a potential platform to

- synergistically enhance the diabetic wound repair, *International Journal of Biological Macromolecules*, Vol. 185, Issue June, pp. 350–368. doi:10.1016/j.ijbiomac.2021.06.119
- [283] Zheng, Y.; Liang, Y.; Zhang, D.; Sun, X.; Liang, L.; Li, J.; Liu, Y. N. (2018). Gelatin-Based Hydrogels Blended with Gellan as an Injectable Wound Dressing, *ACS Omega*, Vol. 3, Issue 5, pp. 4766–4775. doi:10.1021/acsomega.8b00308
- [284] Kocak, F. Z.; Yar, M.; Rehman, I. U. (2022). Hydroxyapatite-Integrated, Heparin-and Glycerol-Functionalized Chitosan-Based Injectable Hydrogels with Improved Mechanical and Proangiogenic Performance, *International Journal of Molecular Sciences*, Vol. 23, Issue 10. doi:10.3390/ijms23105370
- [285] Shah, S. A.; Sohail, M.; Khan, S. A.; Kousar, M. (2021). Improved drug delivery and accelerated diabetic wound healing by chondroitin sulfate grafted alginate-based thermoreversible hydrogels, *Materials Science and Engineering C*, Vol. 126, Issue April, pp. 112169. doi:10.1016/j.msec.2021.112169
- [286] Kouhi, M.; Varshosaz, J.; Hashemibeni, B.; Sarmadi, A. (2020). Injectable gellan gum/lignocellulose nanofibrils hydrogels enriched with melatonin loaded forsterite nanoparticles for cartilage tissue engineering: Fabrication, characterization and cell culture studies, *Materials Science and Engineering C*, Vol. 115, Issue May, pp. 111114. doi:10.1016/j.msec.2020.111114
- [287] Kocak, F. Z.; Talari, A. C. S.; Yar, M.; Rehman, I. U. (2020). In-situ forming ph and thermosensitive injectable hydrogels to stimulate angiogenesis: Potential candidates for fast bone regeneration applications, *International Journal of Molecular Sciences*, Vol. 21, Issue 5. doi:10.3390/ijms21051633
- [288] Zhou, J.; Liu, W.; Zhao, X.; Xian, Y.; Wu, W.; Zhang, X.; Zhao, N.; Xu, F. J.; Wang, C. (2021). Natural Melanin/Alginate Hydrogels Achieve Cardiac Repair through ROS Scavenging and Macrophage Polarization, *Advanced Science*, Vol. 8, Issue 20, pp. 1–14. doi:10.1002/advs.202100505
- [289] Xu, L.; Bai, X.; Yang, J.; Li, J.; Xing, J.; Yuan, H.; Xie, J.; Li, J. (2020). Preparation and characterisation of a gellan gum-based hydrogel enabling osteogenesis and inhibiting Enterococcus faecalis, *International Journal of Biological Macromolecules*, Vol. 165, pp. 2964–2973. doi:10.1016/j.ijbiomac.2020.10.083
- [290] Ng, J. Y.; Zhu, X.; Mukherjee, D.; Zhang, C.; Hong, S.; Kumar, Y.; Gokhale, R.; Ee, P. L. R. (2021). Pristine Gellan Gum-Collagen Interpenetrating Network Hydrogels as Mechanically Enhanced Anti-inflammatory Biologic Wound Dressings for Burn Wound Therapy, *ACS Applied Bio Materials*, Vol. 4, Issue 2, pp. 1470–1482. doi:10.1021/acsabm.0c01363
- [291] Li, S.; Wang, L.; Zheng, W.; Yang, G.; Jiang, X. (2020). Rapid Fabrication of Self-Healing, Conductive, and Injectable Gel as Dressings for Healing Wounds in Stretchable Parts of the Body, *Advanced Functional Materials*, Vol. 30, Issue 31. doi:10.1002/adfm.202002370

- [292] Xie, C.; Zhang, Q.; Li, Z.; Ge, S.; Ma, B. (2022). Sustained and Microenvironment-Accelerated Release of Minocycline from Alginate Injectable Hydrogel for Bacteria-Infected Wound Healing, *Polymers*, Vol. 14, Issue 9, pp. 1816. doi:10.3390/polym14091816
- [293] Zhang, Q.; Yan, Y.; Li, Z.; Du, J.; Zhang, K.; Zhang, L.; Wang, T.; Bianco, A.; Ge, S.; Ma, B. (2024). A uniform-unsaturated crosslinking strategy to construct injectable alginate hydrogel, *International Journal of Biological Macromolecules*, Vol. 254, Issue P2, pp. 127726. doi:10.1016/j.ijbiomac.2023.127726
- [294] Chijcheapaza-flores, H.; Tabary, N.; Chai, F.; Maton, M.; Staelens, J.; Neut, C.; Martel, B.; Blanchemain, N.; Garcia-fernandez, M. J. (2023). Foot Ulcer Infections
- [295] Li, N.; Liu, C.; Chen, W. (2019). Facile Access to Guar Gum Based Supramolecular Hydrogels with Rapid Self-Healing Ability and Multistimuli Responsive Gel-Sol Transitions, *Journal of Agricultural and Food Chemistry*, Vol. 67, Issue 2, pp. 746–752. doi:10.1021/acs.jafc.8b05130
- [296] Kim, S. in; Jeon, G. Y.; Kim, S. E.; Choe, S. H.; Kim, S. J.; Seo, J. S.; Kang, T. W.; Song, J. E.; Khang, G. (2022). Injectable Hydrogel Based on Gellan Gum/Silk Sericin for Application as a Retinal Pigment Epithelium Cell Carrier, ACS Omega, Vol. 7, Issue 45, pp. 41331–41340. doi:10.1021/acsomega.2c05113
- [297] Wang, Y.; Yang, M.; Zhao, Z. (2023). Facile fabrication of self-healing, injectable and antimicrobial cationic guar gum hydrogel dressings driven by hydrogen bonds, *Carbohydrate Polymers*, Vol. 310, pp. 120723. doi:10.1016/j.carbpol.2023.120723
- [298] Xu, L.; Bai, X.; Yang, J.; Li, J.; Xing, J.; Yuan, H.; Xie, J.; Li, J. (2020). Preparation and characterisation of a gellan gum-based hydrogel enabling osteogenesis and inhibiting Enterococcus faecalis, *International Journal of Biological Macromolecules*, Vol. 165, pp. 2964–2973. doi:10.1016/j.ijbiomac.2020.10.083
- [299] Shah, S. A.; Sohail, M.; Khan, S. A.; Kousar, M. (2021). Improved drug delivery and accelerated diabetic wound healing by chondroitin sulfate grafted alginate-based thermoreversible hydrogels, *Materials Science and Engineering: C*, Vol. 126, pp. 112169. doi:10.1016/j.msec.2021.112169
- [300] Chegini, S. P.; Varshosaz, J.; Sadeghi, H. M.; Dehghani, A.; Minaiyan, M. (2020). Shear sensitive injectable hydrogels of cross-linked tragacanthic acid for ocular drug delivery: Rheological and biological evaluation, *International Journal of Biological Macromolecules*, Vol. 165, pp. 2789–2804. doi:10.1016/j.ijbiomac.2020.10.164
- [301] Dai, L.; Cheng, T.; Wang, Y.; Lu, H.; Nie, S.; He, H.; Duan, C.; Ni, Y. (2019). Injectable all-polysaccharide self-assembling hydrogel: a promising scaffold for localized therapeutic proteins, *Cellulose*, Vol. 26, Issue 11, pp. 6891–6901.

- [302] Liang, Y.; Xu, H.; Li, Z.; Zhangji, A.; Guo, B. (2022). Bioinspired Injectable Self-Healing Hydrogel Sealant with Fault-Tolerant and Repeated Thermo-Responsive Adhesion for Sutureless Post-Wound-Closure and Wound Healing, *Nano-Micro Letters*, Vol. 14, Issue 1, pp. 185. doi:10.1007/s40820-022-00928-z
- [303] Guo, H.; Huang, S.; Yang, X.; Wu, J.; Kirk, T. B.; Xu, J.; Xu, A.; Xue, W. (2021). Injectable and Self-Healing Hydrogels with Double-Dynamic Bond Tunable Mechanical, Gel-Sol Transition and Drug Delivery Properties for Promoting Periodontium Regeneration in Periodontitis, *ACS Applied Materials and Interfaces*, Vol. 13, Issue 51, pp. 61638–61652. doi:10.1021/acsami.1c18701
- [304] Chen, M.; Tan, H.; Xu, W.; Wang, Z.; Zhang, J.; Li, S.; Zhou, T.; li, J.; Niu, X. (2022). A self-healing, magnetic and injectable biopolymer hydrogel generated by dual cross-linking for drug delivery and bone repair, *Acta Biomaterialia*, Vol. 153, pp. 159–177. doi:10.1016/j.actbio.2022.09.036
- [305] Tang, L.; Zhang, Z.; Lei, S.; Zhou, J.; Liu, Y.; Yu, X.; Wang, J.; Wan, D.; Shi, J.; Wang, S. (2023). A temperature and pH dual-responsive injectable self-healing hydrogel prepared by chitosan oligosaccharide and aldehyde hyaluronic acid for promoting diabetic foot ulcer healing, *International Journal of Biological Macromolecules*, Vol. 253, Issue P6, pp. 127213. doi:10.1016/j.ijbiomac.2023.127213
- [306] Ma, W.; Dong, W.; Zhao, S.; Du, T.; Wang, Y.; Yao, J.; Liu, Z.; Sun, D.; Zhang, M. (2021). An injectable adhesive antibacterial hydrogel wound dressing for infected skin wounds, *Materials Science and Engineering C*, Vol. 134, Issue September 2021, pp. 112584. doi:10.1016/j.msec.2021.112584
- [307] Li, C.; Liu, Y.; Weng, T.; Yang, M.; Wang, X.; Chai, W. (2023). Fabrication of Injectable Kartogenin-Conjugated Composite Hydrogel with a Sustained Drug Release for Cartilage Repair, *Pharmaceutics*, Vol. 15, Issue 7. doi:10.3390/pharmaceutics15071949
- [308] Han, W.; Chen, C.; Yang, K.; Wang, H.; Xia, H.; Zhao, Y.; Teng, Y.; Feng, G.; Chen, Y. M. (2023). Hyaluronic acid and chitosan-based injectable and self-healing hydrogel with inherent antibacterial and antioxidant bioactivities, *International Journal of Biological Macromolecules*, Vol. 227, Issue December 2022, pp. 373–383. doi:10.1016/j.ijbiomac.2022.12.037
- [309] Mondal, P.; Chatterjee, K. (2022). Injectable and self-healing double network polysaccharide hydrogel as a minimally-invasive delivery platform, *Carbohydrate Polymers*, Vol. 291, Issue April, pp. 119585. doi:10.1016/j.carbpol.2022.119585
- [310] Shi, T.; Niu, D.; You, J.; Li, S.; Li, G.; Ren, K.; Yan, S.; Xu, G.; Yin, J. (2023). Injectable macro-porous chitosan/polyethylene glycol-silicotungstic acid double-network hydrogels based on "smashed gels recombination" strategy for

- cartilage tissue engineering, *International Journal of Biological Macromolecules*, Vol. 233, Issue October 2022, pp.123542. doi:10.1016/j.ijbiomac.2023.123541
- [311] Zhou, Y.; Li, M.; Gao, W.; Li, X.; Long, L.; Hou, X.; Zhao, J. (2023). Microstructure-united heterogeneous sodium alginate doped injectable hydrogel for stable hemostasis in dynamic mechanical environments, *International Journal of Biological Macromolecules*, Vol. 248, Issue July, pp. 125877. doi:10.1016/j.ijbiomac.2023.125877
- [312] Ting, L.; Mei, Y.; Aziz, Y.; Wei, W.; Yi, X.; He, Y.; Li, J.; Li, H.; Miyatake, H.; Ito, Y. (2024). Tough, self-healing and injectable dynamic nanocomposite hydrogel based on gelatin and sodium alginate, *Carbohydrate Polymers*, Vol. 330, Issue January, pp. 121812. doi:10.1016/j.carbpol.2024.121812
- [313] Guo, H.; Huang, S.; Yang, X.; Wu, J.; Kirk, T. B.; Xu, J.; Xu, A.; Xue, W. (2021). Injectable and Self-Healing Hydrogels with Double-Dynamic Bond Tunable Mechanical, Gel-Sol Transition and Drug Delivery Properties for Promoting Periodontium Regeneration in Periodontitis, *ACS Applied Materials & Interfaces*, Vol. 13, Issue 51, pp. 61638–61652. doi:10.1021/acsami.1c18701
- [314] Zhang, Z.; Song, Q.; Jin, Y.; Feng, Y.; Li, J.; Zhang, K. (2023). Advances in Schiff Base and Its Coating on Metal Biomaterials—A Review, *Metals*, Vol. 13, Issue 2, pp. 386. doi:10.3390/met13020386
- [315] Zhao, X.; Yang, Y.; Yu, J.; Ding, R.; Pei, D.; Zhang, Y.; He, G.; Cheng, Y.; Li, A. (2022). Injectable hydrogels with high drug loading through B–N coordination and ROS-triggered drug release for efficient treatment of chronic periodontitis in diabetic rats, *Biomaterials*, Vol. 282, Issue January, pp. 121387. doi:10.1016/j.biomaterials.2022.121387
- [316] Deng, Y.; Ren, J.; Chen, G.; Li, G.; Wu, X.; Wang, G.; Gu, G.; Li, J. (2017). Injectable in situ cross-linking chitosan-hyaluronic acid based hydrogels for abdominal tissue regeneration, *Scientific Reports*, Vol. 7, Issue 1, pp. 1–13. doi:10.1038/s41598-017-02962-z
- [317] Xuan, H.; Wu, S.; Fei, S.; Li, B.; Yang, Y.; Yuan, H. (2021). Injectable nanofiber-polysaccharide self-healing hydrogels for wound healing, *Materials Science and Engineering C*, Vol. 128, Issue June, pp. 112264. doi:10.1016/j.msec.2021.112264
- [318] Zhao, Y.; Li, R.; Liu, Y.; Song, L.; Gao, Z.; Li, Z.; Peng, X.; Wang, P. (2023). An injectable, self-healable, antibacterial, and pro-healing oxidized pullulan polysaccharide/carboxymethyl chitosan hydrogel for early protection of open abdominal wounds, *International Journal of Biological Macromolecules*, Vol. 250, Issue August, pp. 126282. doi:10.1016/j.ijbiomac.2023.126282
- [319] Li, S.; Mao, W.; Xia, L.; Wu, X.; Guo, Y.; Wang, J.; Huang, J.; Xiang, H.; Jin, L.; Fu, H.; Shou, Q. (2023). An injectable, self-healing and degradable hydrogel scaffold as a functional biocompatible material for tissue engineering applications, *Journal of Materials Science*, Vol. 58, Issue 15, pp. 6710–6726.

- doi:10.1007/s10853-023-08393-8
- [320] Bazghaleh, A. A.; Dogolsar, M. A.; Barzin, J. (2022). Development of an injectable self-healing hydrogel based on N-succinyl chitosan/ oxidized pectin for biomedical applications, *Journal of Polymer Research*, Vol. 29, Issue 5, pp. 165. doi:10.1007/s10965-022-02983-x
- [321] Hegazy, H. A.; Moon, H. H.; Lee, D.; Bhang, S. H.; Kim, Y.-C.; Song, C.; Kim, J. (2023). Preparation of polyaspartamide-based adhesive hydrogels via Schiff base reaction with aldehyde-functionalized dextran, *Materials Advances*, Vol. 4, Issue 8, pp. 1989–1997. doi:10.1039/D3MA00032J
- [322] Kim, S. W.; Kim, D. Y.; Roh, H. H.; Kim, H. S.; Lee, J. W.; Lee, K. Y. (2019). Three-Dimensional Bioprinting of Cell-Laden Constructs Using Polysaccharide-Based Self-Healing Hydrogels, *Biomacromolecules*, Vol. 20, Issue 5, pp. 1860–1866. doi:10.1021/acs.biomac.8b01589
- [323] Li, Z.; Liu, L.; Chen, Y. (2020). Dual dynamically crosslinked thermosensitive hydrogel with self-fixing as a postoperative anti-adhesion barrier, *Acta Biomaterialia*, Vol. 110, pp. 119–128. doi:10.1016/j.actbio.2020.04.034
- [324] Wang, H.; Zhu, D.; Paul, A.; Cai, L.; Enejder, A.; Yang, F.; Heilshorn, S. C. (2017). Covalently Adaptable Elastin-Like Protein-Hyaluronic Acid (ELP-HA) Hybrid Hydrogels with Secondary Thermoresponsive Crosslinking for Injectable Stem Cell Delivery, *Advanced Functional Materials*, Vol. 27, Issue 28. doi:10.1002/adfm.201605609
- [325] Wang, S.; Nawale, G. N.; Oommen, O. P.; Hilborn, J.; Varghese, O. P. (2019). Influence of ions to modulate hydrazone and oxime reaction kinetics to obtain dynamically cross-linked hyaluronic acid hydrogels, *Polymer Chemistry*, Vol. 10, Issue 31, pp. 4322–4327. doi:10.1039/C9PY00862D
- [326] Zhu, D.; Wang, H.; Trinh, P.; Heilshorn, S. C.; Yang, F. (2017). Elastin-like protein-hyaluronic acid (ELP-HA) hydrogels with decoupled mechanical and biochemical cues for cartilage regeneration, *Biomaterials*, Vol. 127, pp. 132–140. doi:10.1016/j.biomaterials.2017.02.010
- [327] Wang, L. L.; Highley, C. B.; Yeh, Y.; Galarraga, J. H.; Uman, S.; Burdick, J. A. (2018). Three-dimensional extrusion bioprinting of single- and double-network hydrogels containing dynamic covalent crosslinks, *Journal of Biomedical Materials Research Part A*, Vol. 106, Issue 4, pp. 865–875. doi:10.1002/jbm.a.36323
- [328] Chen, F.; Ni, Y.; Liu, B.; Zhou, T.; Yu, C.; Su, Y.; Zhu, X.; Yu, X.; Zhou, Y. (2017). Self-crosslinking and injectable hyaluronic acid/RGD-functionalized pectin hydrogel for cartilage tissue engineering, *Carbohydrate Polymers*, Vol. 166, pp. 31–44. doi:10.1016/j.carbpol.2017.02.059
- [329] Li, Z.; Zhou, F.; Li, Z.; Lin, S.; Chen, L.; Liu, L.; Chen, Y. (2018). Hydrogel Cross-Linked with Dynamic Covalent Bonding and Micellization for Promoting Burn Wound Healing, ACS Applied Materials & Interfaces, Vol. 10, Issue 30,

- pp. 25194–25202. doi:10.1021/acsami.8b08165
- [330] Lou, J.; Liu, F.; Lindsay, C. D.; Chaudhuri, O.; Heilshorn, S. C.; Xia, Y. (2018). Dynamic Hyaluronan Hydrogels with Temporally Modulated High Injectability and Stability Using a Biocompatible Catalyst, *Advanced Materials*, Vol. 30, Issue 22. doi:10.1002/adma.201705215
- [331] Janarthanan, G.; Shin, H. S.; Kim, I.-G.; Ji, P.; Chung, E.-J.; Lee, C.; Noh, I. (2020). Self-crosslinking hyaluronic acid–carboxymethylcellulose hydrogel enhances multilayered 3D-printed construct shape integrity and mechanical stability for soft tissue engineering, *Biofabrication*, Vol. 12, Issue 4, pp. 045026. doi:10.1088/1758-5090/aba2f7
- [332] Paidikondala, M.; Wang, S.; Hilborn, J.; Larsson, S.; Varghese, O. P. (2019). Impact of Hydrogel Cross-Linking Chemistry on the in Vitro and in Vivo Bioactivity of Recombinant Human Bone Morphogenetic Protein-2, *ACS Applied Bio Materials*, Vol. 2, Issue 5, pp. 2006–2012. doi:10.1021/acsabm.9b00060
- [333] Samanta, S.; Rangasami, V. K.; Sarlus, H.; Samal, J. R. K.; Evans, A. D.; Parihar, V. S.; Varghese, O. P.; Harris, R. A.; Oommen, O. P. (2022). Interpenetrating gallol functionalized tissue adhesive hyaluronic acid hydrogel polarizes macrophages to an immunosuppressive phenotype, *Acta Biomaterialia*, Vol. 142, pp. 36–48. doi:10.1016/j.actbio.2022.01.048
- [334] Dalei, G.; Das, S.; Ranjan Jena, S.; Jena, D.; Nayak, J.; Samanta, L. (2023). In situ crosslinked dialdehyde guar gum-chitosan Schiff-base hydrogels for dual drug release in colorectal cancer therapy, *Chemical Engineering Science*, Vol. 269, pp. 118482. doi:10.1016/j.ces.2023.118482
- [335] Zhang, X.; Pan, Y.; Li, S.; Xing, L.; Du, S.; Yuan, G.; Li, J.; Zhou, T.; Xiong, D.; Tan, H.; Ling, Z.; Chen, Y.; Hu, X.; Niu, X. (2020). Doubly crosslinked biodegradable hydrogels based on gellan gum and chitosan for drug delivery and wound dressing, *International Journal of Biological Macromolecules*, Vol. 164, pp. 2204–2214. doi:10.1016/j.ijbiomac.2020.08.093
- [336] Bashiri, G.; Shojaosadati, S. A.; Abdollahi, M. (2021). Synthesis and characterization of Schiff base containing bovine serum albumin-gum arabic aldehyde hybrid nanogels via inverse miniemulsion for delivery of anticancer drug, *International Journal of Biological Macromolecules*, Vol. 170, pp. 222–231. doi:10.1016/j.ijbiomac.2020.12.150
- [337] Dr Nisha Sharma; Ganesh Kumar. (2022). Facile functionalization cum fabrication of novel fenugreek gum /chitosan based self-crosslinked hydrogel networks through Schiff base formation: Characterization & Swelling kinetic studies, *Journal of Advanced Applied Scientific Research*, Vol. 4, Issue 6. doi:10.46947/joaasr462022265
- [338] Maiti, S.; Khillar, P. S.; Mishra, D.; Nambiraj, N. A.; Jaiswal, A. K. (2021). Physical and self-crosslinking mechanism and characterization of chitosangelatin-oxidized guar gum hydrogel, *Polymer Testing*, Vol. 97, pp. 107155.

- doi:10.1016/j.polymertesting.2021.107155
- [339] El-Sayed, N. S.; Hashem, A. H.; Kamel, S. (2022). Preparation and characterization of Gum Arabic Schiff's bases based on 9-aminoacridine with in vitro evaluation of their antimicrobial and antitumor potentiality, *Carbohydrate Polymers*, Vol. 277, pp. 118823. doi:10.1016/j.carbpol.2021.118823
- [340] Li, S.; Pei, M.; Wan, T.; Yang, H.; Gu, S.; Tao, Y.; Liu, X.; Zhou, Y.; Xu, W.; Xiao, P. (2020). Self-healing hyaluronic acid hydrogels based on dynamic Schiff base linkages as biomaterials, *Carbohydrate Polymers*, Vol. 250, pp. 116922. doi:10.1016/j.carbpol.2020.116922
- [341] Wang, L.; Li, M.; Li, X.; Liu, J.; Mao, Y.; Tang, K. (2020). A Biomimetic Hybrid Hydrogel Based on the Interactions between Amino Hydroxyapatite and Gelatin/Gellan Gum, *Macromolecular Materials and Engineering*, Vol. 305, Issue 9. doi:10.1002/mame.202000188
- [342] Wang, Y.; Tong, L.; Zheng, Y.; Pang, S.; Sha, J.; Li, L.; Zhao, G. (2019). Hydrogels with self-healing ability, excellent mechanical properties and biocompatibility prepared from oxidized gum arabic, *European Polymer Journal*, Vol. 117, pp. 363–371. doi:10.1016/j.eurpolymj.2019.05.033
- [343] Aghajanzadeh, M. S.; Imani, R.; Nazarpak, M. H. (2023). In situ forming aldehyde-modified xanthan/gelatin hydrogel for tissue engineering applications: synthesis, characterization, and optimization, *Journal of Materials Science*, Vol. 58, Issue 35, pp. 14187–14206. doi:10.1007/s10853-023-08878-6
- [344] do N. Ferreira, C. R.; de L. Ramos, E. L.; Araujo, L. F. S.; da S. Sousa, L. M.; Feitosa, J. P. A.; Cunha, A. F.; Oliveira, M. B.; Mano, J. F.; da S. Maciel, J. (2021). Synthesis and characterization of scaffolds produced under mild conditions based on oxidized cashew gums and carboxyethyl chitosan, *International Journal of Biological Macromolecules*, Vol. 176, pp. 26–36. doi:10.1016/j.ijbiomac.2021.01.178
- [345] Sarmah, D.; Rather, M. A.; Sarkar, A.; Mandal, M.; Sankaranarayanan, K.; Karak, N. (2023). Self-cross-linked starch/chitosan hydrogel as a biocompatible vehicle for controlled release of drug, *International Journal of Biological Macromolecules*, Vol. 237, pp. 124206. doi:10.1016/j.ijbiomac.2023.124206
- [346] Zhang, Z.; Bu, J.; Li, B.; Xuan, H.; Jin, Y.; Yuan, H. (2022). Dynamic Double Cross-Linked Self-Healing Polysaccharide Hydrogel Wound Dressing Based on Schiff Base and Thiol-Alkynone Reactions, *International Journal of Molecular Sciences*, Vol. 23, Issue 22, pp. 13817. doi:10.3390/ijms232213817
- [347] Ding, P.; Okoro, O. V.; Sun, Y.; Wang, L.; Wei, X.; Liu, S.; Deng, Y.; Fan, L.; Jiang, G.; Wang, L.; Shavandi, A.; Nie, L. (2022). Graphene oxide-reinforced alginate/gelatin hydrogel via Schiff-base bond and thiol-Michael addition for bone regeneration, *Materials Today Communications*, Vol. 33, pp. 104904. doi:10.1016/j.mtcomm.2022.104904

- [348] Draye, J.-P.; Delaey, B.; Van de Voorde, A.; Van Den Bulcke, A.; Bogdanov, B.; Schacht, E. (1998). In vitro release characteristics of bioactive molecules from dextran dialdehyde cross-linked gelatin hydrogel films, *Biomaterials*, Vol. 19, Issue 1–3, pp. 99–107. doi:10.1016/S0142-9612(97)00164-6
- [349] Yin, H.; Song, P.; Chen, X.; Huang, Q.; Huang, H. (2022). A self-healing hydrogel based on oxidized microcrystalline cellulose and carboxymethyl chitosan as wound dressing material, *International Journal of Biological Macromolecules*, Vol. 221, pp. 1606–1617. doi:10.1016/j.ijbiomac.2022.09.060
- [350] Nezhad-Mokhtari, P.; Ghorbani, M.; Abdyazdani, N. (2021). Reinforcement of hydrogel scaffold using oxidized-guar gum incorporated with curcumin-loaded zein nanoparticles to improve biological performance, *International Journal of Biological Macromolecules*, Vol. 167, pp. 59–65. doi:10.1016/j.ijbiomac.2020.11.103
- [351] Yan, M.; Hu, S.-Y.; Wang, Z.-G.; Hong, R.; Peng, X.; Kuzmanović, M.; Yang, M.; Dai, R.; Wang, Y.; Gou, J.; Li, K.; Xu, J.-Z.; Li, Z.-M. (2024). Antibacterial, Fatigue-Resistant, and Self-Healing Dressing from Natural-Based Composite Hydrogels for Infected Wound Healing, *Biomacromolecules*, Vol. 25, Issue 4, pp. 2438–2448. doi:10.1021/acs.biomac.3c01385
- [352] Yu, H.; Lu, J.; Xiao, C. (2007). Preparation and Properties of Novel Hydrogels from Oxidized Konjac Glucomannan Cross-Linked Chitosan for in vitro Drug Delivery, *Macromolecular Bioscience*, Vol. 7, Nos. 9–10, pp. 1100–1111. doi:10.1002/mabi.200700035
- [353] Liang, Y.; Liu, W.; Han, B.; Yang, C.; Ma, Q.; Song, F.; Bi, Q. (2011). An in situ formed biodegradable hydrogel for reconstruction of the corneal endothelium, *Colloids and Surfaces B: Biointerfaces*, Vol. 82, Issue 1, pp. 1–7. doi:10.1016/j.colsurfb.2010.07.043
- [354] Su, H.; Zhang, W.; Wu, Y.; Han, X.; Liu, G.; Jia, Q.; Shan, S. (2018). Schiff base-containing dextran nanogel as pH-sensitive drug delivery system of doxorubicin: Synthesis and characterization, *Journal of Biomaterials Applications*, Vol. 33, Issue 2, pp. 170–181. doi:10.1177/0885328218783969
- [355] Yu, G.; Niu, C.; Liu, J.; Wu, J.; Jin, Z.; Wang, Y.; Zhao, K. (2023). Preparation and Properties of Self-Cross-Linking Hydrogels Based on Chitosan Derivatives and Oxidized Sodium Alginate, *ACS Omega*, Vol. 8, Issue 22, pp. 19752–19766. doi:10.1021/acsomega.3c01401
- [356] Li, N.-N.; Fu, C.-P.; Zhang, L.-M. (2014). Using casein and oxidized hyaluronic acid to form biocompatible composite hydrogels for controlled drug release, *Materials Science and Engineering: C*, Vol. 36, pp. 287–293. doi:10.1016/j.msec.2013.12.025
- [357] Xie, M.; Zeng, Y.; Wu, H.; Wang, S.; Zhao, J. (2022). Multifunctional carboxymethyl chitosan/oxidized dextran/sodium alginate hydrogels as dressing for hemostasis and closure of infected wounds, *International Journal*

- of Biological Macromolecules, Vol. 219, pp. 1337–1350. doi:10.1016/j.ijbiomac.2022.08.166
- [358] Maciel, J. S.; Azevedo, S.; Correia, C. R.; Costa, A. M. S.; Costa, R. R.; Magalhães, F. A.; de Sousa Monteiro, A. A.; Costa, J. F. G.; de Paula, R. C. M.; Feitosa, J. P. A.; Mano, J. F. (2019). Oxidized Cashew Gum Scaffolds for Tissue Engineering, *Macromolecular Materials and Engineering*, Vol. 304, Issue 3. doi:10.1002/mame.201800574
- [359] Mourad, R.; El Mogy, S. A.; Darwesh, O.; Abdel-Hakim, A. (2024). In-vitro evaluation of antimicrobial and anti-inflammatory efficacy of the gelatin-β-cyclodextrin hydrogels as biodegradable carriers for rutin, *ChemistrySelect*, Vol. 9, Issue 4. doi:10.1002/slct.202303705
- [360] Sharma, S.; Jain, P.; Tiwari, S. (2020). Dynamic imine bond based chitosan smart hydrogel with magnified mechanical strength for controlled drug delivery, *International Journal of Biological Macromolecules*, Vol. 160, pp. 489–495. doi:10.1016/j.ijbiomac.2020.05.221
- [361] Zhao, F.; Liu, Y.; Song, T.; Zhang, B.; Li, D.; Xiao, Y.; Zhang, X. (2022). A chitosan-based multifunctional hydrogel containing in situ rapidly bioreduced silver nanoparticles for accelerating infected wound healing, *Journal of Materials Chemistry B*, Vol. 10, Issue 13, pp. 2135–2147. doi:10.1039/D1TB02850B
- [362] Zhao, L.; Ke, T.; Ling, Q.; Liu, J.; Li, Z.; Gu, H. (2021). Multifunctional Ionic Conductive Double-Network Hydrogel as a Long-Term Flexible Strain Sensor, *ACS Applied Polymer Materials*, Vol. 3, Issue 11, pp. 5494–5508. doi:10.1021/acsapm.1c00805
- [363] Hu, C.; Long, L.; Cao, J.; Zhang, S.; Wang, Y. (2021). Dual-crosslinked mussel-inspired smart hydrogels with enhanced antibacterial and angiogenic properties for chronic infected diabetic wound treatment via pH-responsive quick cargo release, *Chemical Engineering Journal*, Vol. 411, pp. 128564. doi:10.1016/j.cej.2021.128564
- [364] Zhao, H.; Zhang, Y.; Zhou, C.; Zhang, C.; Liu, B. (2023). Engineering pH responsive carboxyethyl chitosan and oxidized pectin -based hydrogels with self-healing, biodegradable and antibacterial properties for wound healing, *International Journal of Biological Macromolecules*, Vol. 253, pp. 127364. doi:10.1016/j.ijbiomac.2023.127364
- [365] Chen, Z.; Zhao, J.; Wu, H.; Wang, H.; Lu, X.; Shahbazi, M.-A.; Wang, S. (2023). A triple-network carboxymethyl chitosan-based hydrogel for hemostasis of incompressible bleeding on wet wound surfaces, *Carbohydrate Polymers*, Vol. 303, pp. 120434. doi:10.1016/j.carbpol.2022.120434
- [366] Li, M.; Dong, Y.; Wang, M.; Lu, X.; Li, X.; Yu, J.; Ding, B. (2023). Hydrogel/nanofibrous membrane composites with enhanced water retention, stretchability and self-healing capability for wound healing, *Composites Part B: Engineering*, Vol. 257, pp. 110672. doi:10.1016/j.compositesb.2023.110672

- [367] Yang, Y.; Xu, H.; Li, M.; Li, Z.; Zhang, H.; Guo, B.; Zhang, J. (2022). Antibacterial Conductive UV-Blocking Adhesion Hydrogel Dressing with Mild On-Demand Removability Accelerated Drug-Resistant Bacteria-Infected Wound Healing, ACS Applied Materials & Interfaces, Vol. 14, Issue 37, pp. 41726–41741. doi:10.1021/acsami.2c10490
- [368] Hu, Y.; Liu, N.; Chen, K.; Liu, M.; Wang, F.; Liu, P.; Zhang, Y.; Zhang, T.; Xiao, X. (2022). Resilient and Self-Healing Hyaluronic Acid/Chitosan Hydrogel With Ion Conductivity, Low Water Loss, and Freeze-Tolerance for Flexible and Wearable Strain Sensor, *Frontiers in Bioengineering and Biotechnology*, Vol. 10. doi:10.3389/fbioe.2022.837750
- [369] Li, Z.; Li, B.; Li, X.; Lin, Z.; Chen, L.; Chen, H.; Jin, Y.; Zhang, T.; Xia, H.; Lu, Y.; Zhang, Y. (2021). Ultrafast in-situ forming halloysite nanotube-doped chitosan/oxidized dextran hydrogels for hemostasis and wound repair, *Carbohydrate Polymers*, Vol. 267, pp. 118155. doi:10.1016/j.carbpol.2021.118155
- [370] Pasaribu, S. P.; Kaban, J.; Ginting, M.; Silalahi, J. (2019). Preparation of In Situ Cross-Linked N-Maleoyl Chitosan-Oxidized Sodium Alginate Hydrogels for Drug Delivery Applications, *Open Access Macedonian Journal of Medical Sciences*, Vol. 7, Issue 21, pp. 3546–3553. doi:10.3889/oamjms.2019.850
- [371] Feng, C.; Xi, J.; Gao, Q.; Cheng, S.; Shen, M. (2023). Guar Gum-based multifunctional hydrogels with high sensitivity and negligible hysteresis for wearable electronics, *Colloids and Surfaces A: Physicochemical and Engineering Aspects*, Vol. 677, pp. 132409. doi:10.1016/j.colsurfa.2023.132409
- [372] El-Araby, A.; Janati, W.; Ullah, R.; Ercisli, S.; Errachidi, F. (2024). Chitosan, chitosan derivatives, and chitosan-based nanocomposites: eco-friendly materials for advanced applications (a review), *Frontiers in Chemistry*, Vol. 11. doi:10.3389/fchem.2023.1327426
- [373] Suryani, S.; Chaerunisaa, A.; Joni, I. M.; Ruslin, R.; Aspadiah, V.; Anton, A.; Sartinah, A.; Ramadhan, L. O. A. (2024). The Chemical Modification to Improve Solubility of Chitosan and Its Derivatives Application, Preparation Method, Toxicity as a Nanoparticles, Nanotechnology, Science and Applications, Vol. 17,pp. 41–57. doi:10.2147/NSA.S450026
- [374] Affes, S.; Aranaz, I.; Acosta, N.; Heras, Á.; Nasri, M.; Maalej, H. (2024). Physicochemical and biological properties of chitosan derivatives with varying molecular weight produced by chemical depolymerization, *Biomass Conversion and Biorefinery*, Vol. 14, Issue 3, pp. 4111–4121. doi:10.1007/s13399-022-02662-3
- [375] Ruiz, G. A. M.; Corrales, H. F. Z. (2017). Chitosan, Chitosan Derivatives and their Biomedical Applications, *Biological Activities and Application of Marine Polysaccharides*, InTech. doi:10.5772/66527
- [376] Fan, P.; Fan, H.; Wang, S. (2024). From emerging modalities to advanced

- applications of hydrogel piezoelectrics based on chitosan, gelatin and related biological macromolecules: A review, *International Journal of Biological Macromolecules*, Vol. 262, pp. 129691. doi:10.1016/j.ijbiomac.2024.129691
- [377] Pellis, A.; Guebitz, G. M.; Nyanhongo, G. S. (2022). Chitosan: Sources, Processing and Modification Techniques, *Gels*, Vol. 8, Issue 7, pp. 393. doi:10.3390/gels8070393
- [378] Guo, Y.; Qiao, D.; Zhao, S.; Liu, P.; Xie, F.; Zhang, B. (2024). Biofunctional chitosan—biopolymer composites for biomedical applications, *Materials Science and Engineering: R: Reports*, Vol. 159, pp. 100775. doi:10.1016/j.mser.2024.100775
- [379] Ojeda-Hernández, D. D.; Canales-Aguirre, A. A.; Matias-Guiu, J.; Gomez-Pinedo, U.; Mateos-Díaz, J. C. (2020). Potential of Chitosan and Its Derivatives for Biomedical Applications in the Central Nervous System, *Frontiers in Bioengineering and Biotechnology*, Vol. 8. doi:10.3389/fbioe.2020.00389
- [380] Rasool, A.; Rizwan, M.; Islam, A.; Abdullah, H.; Shafqat, S. S.; Azeem, M. K.; Rasheed, T.; Bilal, M. (2024). Chitosan-Based Smart Polymeric Hydrogels and Their Prospective Applications in Biomedicine, *Starch Stärke*, Vol. 76, Nos. 1–2. doi:10.1002/star.202100150
- [381] Vaidya, G.; Pramanik, S.; Kadi, A.; Rayshan, A. R.; Abualsoud, B. M.; Ansari, M. J.; Masood, R.; Michaelson, J. (2024). Injecting hope: chitosan hydrogels as bone regeneration innovators, *Journal of Biomaterials Science, Polymer Edition*, Vol. 35, Issue 5, pp. 756–797. doi:10.1080/09205063.2024.2304952
- [382] Almajidi, Y. Q.; Ponnusankar, S.; Chaitanya, M. V. N. L.; Marisetti, A. L.; Hsu, C.-Y.; Dhiaa, A. M.; Saadh, M. J.; Pal, Y.; Thabit, R.; Adhab, A. H.; Alsaikhan, F.; Narmani, A.; Farhood, B. (2024). Chitosan-based nanofibrous scaffolds for biomedical and pharmaceutical applications: A comprehensive review, *International Journal of Biological Macromolecules*, Vol. 264, pp. 130683. doi:10.1016/j.ijbiomac.2024.130683
- [383] Xu, K.; Zhang, Q.; Zhu, D.; Jiang, Z. (2024). Hydrogels in Gene Delivery Techniques for Regenerative Medicine and Tissue Engineering, *Macromolecular Bioscience*, Vol. 24, Issue 6. doi:10.1002/mabi.202300577
- [384] Haider, A.; Khan, S.; Iqbal, D. N.; Shrahili, M.; Haider, S.; Mohammad, K.; Mohammad, A.; Rizwan, M.; Kanwal, Q.; Mustafa, G. (2024). Advances in chitosan-based drug delivery systems: A comprehensive review for therapeutic applications, *European Polymer Journal*, Vol. 210, pp. 112983. doi:10.1016/j.eurpolymj.2024.112983
- [385] Ho, T. T.; Tran, H. A.; Doan, V. K.; Maitz, J.; Li, Z.; Wise, S. G.; Lim, K. S.; Rnjak-Kovacina, J. (2024). Natural Polymer-Based Materials for Wound Healing Applications, *Advanced NanoBiomed Research*, Vol. 4, Issue 5. doi:10.1002/anbr.202300131
- [386] Zhou, Q.; Lan, W.; Xie, J. (2024). Phenolic acid-chitosan derivatives: An

- effective strategy to cope with food preservation problems, *International Journal of Biological Macromolecules*, Vol. 254, pp. 127917. doi:10.1016/j.ijbiomac.2023.127917
- [387] Jin, J.; Luo, B.; Xuan, S.; Shen, P.; Jin, P.; Wu, Z.; Zheng, Y. (2024). Degradable chitosan-based bioplastic packaging: Design, preparation and applications, *International Journal of Biological Macromolecules*, Vol. 266, pp. 131253. doi:10.1016/j.ijbiomac.2024.131253
- [388] Kaczorowska, M. A.; Bożejewicz, D. (2024). The Application of Chitosan-Based Adsorbents for the Removal of Hazardous Pollutants from Aqueous Solutions—A Review, *Sustainability*, Vol. 16, Issue 7, pp. 2615. doi:10.3390/su16072615
- [389] Wang, L.; Zhang, X.; Yang, K.; Fu, Y. V.; Xu, T.; Li, S.; Zhang, D.; Wang, L.; Lee, C. (2020). A Novel Double-Crosslinking-Double-Network Design for Injectable Hydrogels with Enhanced Tissue Adhesion and Antibacterial Capability for Wound Treatment, *Advanced Functional Materials*, Vol. 30, Issue 1. doi:10.1002/adfm.201904156
- [390] Zheng, Z.; Bian, S.; Li, Z.; Zhang, Z.; Liu, Y.; Zhai, X.; Pan, H.; Zhao, X. (2020). Catechol modified quaternized chitosan enhanced wet adhesive and antibacterial properties of injectable thermo-sensitive hydrogel for wound healing, *Carbohydrate Polymers*, Vol. 249, Issue August, pp. 116826. doi:10.1016/j.carbpol.2020.116826
- [391] Babaluei, M.; Mojarab, Y.; Mottaghitalab, F.; Farokhi, M. (2023). Injectable hydrogel based on silk fibroin/carboxymethyl cellulose/agarose containing polydopamine functionalized graphene oxide with conductivity, hemostasis, antibacterial, and anti-oxidant properties for full-thickness burn healing, *International Journal of Biological Macromolecules*, Vol. 249, Issue July, pp. 126051. doi:10.1016/j.ijbiomac.2023.126051
- [392] Cui, L.; Li, J.; Guan, S.; Zhang, K.; Zhang, K.; Li, J. (2022). Injectable multifunctional CMC/HA-DA hydrogel for repairing skin injury, *Materials Today Bio*, Vol. 14, Issue March, pp. 100257. doi:10.1016/j.mtbio.2022.100257
- [393] Zhou, T.; Zhou, H.; Wang, F.; Zhang, P.; Shang, J.; Shi, L. (2024). An injectable carboxymethyl chitosan hydrogel scaffold formed via coordination bond for antibacterial and osteogenesis in osteomyelitis, *Carbohydrate Polymers*, Vol. 324, Issue July 2023, pp. 121466. doi:10.1016/j.carbpol.2023.121466
- [394] Xu, J.; Chen, T. Y.; Tai, C. H.; Hsu, S. hui. (2023). Bioactive self-healing hydrogel based on tannic acid modified gold nano-crosslinker as an injectable brain implant for treating Parkinson's disease, *Biomaterials Research*, Vol. 27, Issue 1. doi:10.1186/s40824-023-00347-0
- [395] Qian, Z.; Zhao, N.; Xu, S.; Yuan, W. (2024). In situ injectable thermoresponsive nanocomposite hydrogel based on hydroxypropyl chitosan for precise synergistic calcium-overload, photodynamic and photothermal tumor therapy, *Carbohydrate Polymers*, Vol. 324, Issue September 2023, pp. 121487.

- doi:10.1016/j.carbpol.2023.121487
- [396] Hu, K.; Jia, E.; Zhang, Q.; Zheng, W.; Sun, R.; Qian, M.; Tan, Y.; Hu, W. (2023). Injectable carboxymethyl chitosan-genipin hydrogels encapsulating tea tree oil for wound healing, *Carbohydrate Polymers*, Vol. 301, pp. 120348. doi:10.1016/j.carbpol.2022.120348
- [397] Yang, Y.; Feng, G.; Wang, J.; Zhang, R.; Zhong, S.; Wang, J.; Cui, X. (2023). Injectable chitosan-based self-healing supramolecular hydrogels with temperature and pH dual-responsivenesses, *International Journal of Biological Macromolecules*, Vol. 227, Issue July 2022, pp. 1038–1047. doi:10.1016/j.ijbiomac.2022.11.279
- [398] Nie, M.; Kong, B.; Chen, G.; Xie, Y.; Zhao, Y.; Sun, L. (2022). Bioactive Materials MSCs-laden injectable self-healing hydrogel for systemic sclerosis treatment, *Bioactive Materials*, Vol. 17, Issue August 2021, pp. 369–378. doi:10.1016/j.bioactmat.2022.01.006
- [399] Koshani, R.; Heidari, M.; Ataie, Z.; Wang, Y. (2024). Multifunctional self-healing hydrogels via nanoengineering of colloidal and polymeric cellulose, *International Journal of Biological Macromolecules*, Vol. 259, Issue P1, pp. 129181. doi:10.1016/j.ijbiomac.2023.129181
- [400] Wang, Y.; Zhao, J.; Wang, X.; Zhang, R.; Liang, F. (2023). Mussel-mimetic chitosan based injectable hydrogel with fast-crosslinking and water-resistance as tissue adhesive, *International Journal of Adhesion and Adhesives*, Vol. 124, Issue April, doi: 10.1186/s40824-023-00347-0
- [401] Zhou, Y.; Zhai, Z.; Yao, Y.; Stant, J. C.; Landrum, S. L.; Bortner, J.; Frazier, C. E.; Edgar, K. J. (2023). Oxidized hydroxypropyl cellulose / carboxymethyl chitosan hydrogels permit pH-responsive, targeted drug release, *Carbohydrate Polymers*, Vol. 300, Issue July 2022, pp. 120213. doi:10.1016/j.carbpol.2022.120213
- [402] Chanmontri, M.; Swilem, A. E.; Mutch, A. L.; Gr, L.; Suwantong, O. (2023). Physicochemical and in vitro biological evaluation of an injectable self-healing quaternized chitosan / oxidized pectin hydrogel for potential use as a wound dressing material, *International Journal of Biological Macromolecules*, Vol. 242, Issue February, pp. 124984. doi:10.1016/j.ijbiomac.2023.124984
- [403] Chang, R.; Zhao, D.; Zhang, C.; Liu, K.; He, Y.; Guan, F.; Yao, M. (2023). PMN-incorporated multifunctional chitosan hydrogel for postoperative synergistic photothermal melanoma therapy and skin regeneration, *International Journal of Biological Macromolecules*, Vol. 253, Issue P4, pp. 126854. doi:10.1016/j.ijbiomac.2023.126854
- [404] Huang, F.; Chen, J.; Mao, X.; Tang, S. (2023). Preparation and biological properties of Schiff-base hydrogels crosslinked by benzaldehyde substituted agarose oligosaccharides, *Reactive and Functional Polymers*, Vol. 193, Issue September, pp. 105745. doi:10.1016/j.reactfunctpolym.2023.105745

- [405] Bazghaleh, A. A. (2023). Preparation and characterization of oxidized pectin / N succinyl chitosan / graphene oxide hydrogels, *Cellulose*, Vol. 30, Issue 4, pp. 2165–2179. doi:10.1007/s10570-022-05015-5
- [406] Shi, H.; Hu, C.; Li, A.; Lin, X.; Deng, M.; Jiang, B.; Xiao, B. (2023). Preparation of carboxymethylchitosan based rapid self-healing injectable hydrogels, *Journal of Polymer Research*, Vol. 30, Issue 9, pp. 342. doi:10.1007/s10965-023-03705-7
- [407] Huang, L.; Wang, W.; Xian, Y.; Liu, L.; Fan, J.; Liu, H.; Zheng, Z.; Wu, D. (2023). Materials Today Bio Rapidly in situ forming an injectable Chitosan / PEG hydrogel for intervertebral disc repair, *Materials Today Bio*, Vol. 22, Issue June, pp. 100752. doi:10.1016/j.mtbio.2023.100752
- [408] Xu, S.; Qian, Z.; Zhao, N.; Yuan, W. (2024). Journal of Colloid And Interface Science Thermoresponsive injectable self-healing hydrogel containing polydopamine-coated Fe / Mo-doped TiO 2 nanoparticles for efficient synergistic sonodynamic-chemodynamic-photothermal-chemo therapy, *Journal of Colloid And Interface Science*, Vol. 654, Issue PB, pp. 1431–1446. doi:10.1016/j.jcis.2023.10.145
- [409] Yang, Y.; Nan, W.; Zhang, R.; Shen, S.; Wu, M.; Zhong, S.; Zhang, Y.; Cui, X. (2024). Fabrication of carboxymethyl cellulose-based thermo-sensitive hydrogels and inhibition of corneal neovascularization, *International Journal of Biological Macromolecules*, Vol. 261, Issue P2, pp. 129933. doi:10.1016/j.ijbiomac.2024.129933
- [410] Li, X.; Xing, D.; Bai, Y.; Du, Y.; Lang, S.; Li, K.; Xiang, J.; Liu, G.; Liu, S. (2024). Injectable hydrogel with antimicrobial and anti-inflammatory properties for postoperative tumor wound care, *Biomedical Materials (Bristol)*, Vol. 19, Issue 2, pp. 025028. doi:10.1088/1748-605X/ad2408
- [411] Lv, X.; Liu, Y.; Song, S.; Tong, C.; Shi, X.; Zhao, Y.; Zhang, J.; Hou, M. (2019). Influence of chitosan oligosaccharide on the gelling and wound healing properties of injectable hydrogels based on carboxymethyl chitosan/alginate polyelectrolyte complexes, *Carbohydrate Polymers*, Vol. 205, pp. 312–321. doi:10.1016/j.carbpol.2018.10.067
- [412] Perumalsamy, H.; Balusamy, S. R.; Sukweenadhi, J.; Nag, S.; MubarakAli, D.; El-Agamy Farh, M.; Vijay, H.; Rahimi, S. (2024). A comprehensive review on Moringa oleifera nanoparticles: importance of polyphenols in nanoparticle synthesis, nanoparticle efficacy and their applications, *Journal of Nanobiotechnology*, Vol. 22, Issue 1, pp. 71. doi:10.1186/s12951-024-02332-8
- [413] Singh, B.; Sharma, V.; Rajneesh; Kumar, A.; Rohit; Mohan, M.; Kumar, R.; Kumari, A.; Sharma, P.; Ram, K. (2022). Development of dietary fibers moringa-sterculia gum hydrogel for drug delivery applications, *Food Hydrocolloids for Health*, Vol. 2, pp. 100095. doi:10.1016/j.fhfh.2022.100095
- [414] Kumari, L.; Baghel, M.; Panda, S.; Sakure, K.; Giri, T. K.; Badwaik, H. (2021). Chemistry, Biological Activities, and Uses of Moringa Gum, 1–24.

- doi:10.1007/978-3-030-76523-1 10-1
- [415] Gupta, S.; Kachhwaha, S.; Kothari, S.; Bohra, M. K.; Jain, R. (2020). Surface Morphology and Physicochemical Characterization of Thermostable Moringa Gum: A Potential Pharmaceutical Excipient, *ACS Omega*, Vol. 5, Issue 45, pp. 29189–29198. doi:10.1021/acsomega.0c03966
- [416] Ahmad, S.; Manzoor, K.; Purwar, R.; Ikram, S. (2020). Morphological and Swelling Potential Evaluation of Moringa oleifera Gum/Poly(vinyl alcohol) Hydrogels as a Superabsorbent, *ACS Omega*, Vol. 5, Issue 29, pp. 17955–17961. doi:10.1021/acsomega.0c01023
- [417] Singh, B.; Kumar, A. (2018). Network formation of Moringa oleifera gum by radiation induced crosslinking: Evaluation of drug delivery, network parameters and biomedical properties, *International Journal of Biological Macromolecules*, Vol. 108, pp. 477–488. doi:10.1016/j.ijbiomac.2017.12.041
- [418] Nangia, S.; Katyal, D.; Warkar, S. G. (2023). Thermodynamics, kinetics and isotherm studies on the removal of anionic Azo-dye (Congo red) using synthesized Chitosan/ Moringa oleifera gum hydrogel composites, *Separation Science and Technology*, Vol. 58, Issue 1, pp. 13–28. doi:10.1080/01496395.2022.2104731
- [419] Singh, B.; Sharma, V.; Kumar, R. and A. (2021). Designing moringa gumsterculia gum-polyacrylamide hydrogel wound dressings for drug delivery applications, *Carbohydrate Polymer Technologies and Applications*, Vol. 2, pp. 100062. doi:10.1016/j.carpta.2021.100062
- [420] Singh, B.; Kumar, A. (2018). Hydrogel formation by radiation induced crosslinked copolymerization of acrylamide onto moringa gum for use in drug delivery applications, *Carbohydrate Polymers*, Vol. 200, pp. 262–270. doi:10.1016/j.carbpol.2018.08.018
- [421] Singh, B.; Kumar, A. (2018). Radiation-induced graft copolymerization of N-vinyl imidazole onto moringa gum polysaccharide for making hydrogels for biomedical applications, *International Journal of Biological Macromolecules*, Vol. 120, pp. 1369–1378. doi:10.1016/j.ijbiomac.2018.09.148
- [422] Singh, B.; Kumar, A. (2021). Development of dietary fibre moringa gum and polyvinylpyrrolidone based hydrogels for drug delivery application, *Food Hydrocolloids for Health*, Vol. 1, pp. 100008. doi:10.1016/j.fhfh.2021.100008
- [423] Singh, B.; Sharma, A.; Thakur, N.; Kumar, R. (2023). Developing dietary fiber moringa gum based ciprofloxacin encapsulated hydrogel wound dressings for better wound care, *Food Hydrocolloids for Health*, Vol. 3, pp. 100128. doi:10.1016/j.fhfh.2023.100128
- [424] Singh, B.; Kumar, A. (2020). Graft and crosslinked polymerization of polysaccharide gum to form hydrogel wound dressings for drug delivery applications, *Carbohydrate Research*, Vol. 489, pp. 107949. doi:10.1016/j.carres.2020.107949

- [425] Singh, B.; Sharma, V.; Mohan, M.; Rohit; Sharma, P.; Ram, K. (2023). Design of ciprofloxacin impregnated dietary fiber psyllium-moringa gum-alginate network hydrogels via green approach for use in gastro-retentive drug delivery system, *Bioactive Carbohydrates and Dietary Fibre*, Vol. 29, pp. 100345. doi:10.1016/j.bcdf.2022.100345
- [426] Ranote, S.; Musioł, M.; Kowalczuk, M.; Joshi, V.; Chauhan, G. S.; Kumar, R.; Chauhan, S.; Kumar, K. (2022). Functionalized Moringa oleifera Gum as pH-Responsive Nanogel for Doxorubicin Delivery: Synthesis, Kinetic Modelling and In Vitro Cytotoxicity Study, *Polymers*, Vol. 14, Issue 21, pp. 4697. doi:10.3390/polym14214697
- [427] Roy, D.; Bal, T.; Swain, S. (2020). Fabrication and evaluation of pH-sensitive biocompatible microwave irradiated moringa barkgum-carrageenan (MOG-CRG-IPN) interpenetrating isotropic polymeric network for controlled delivery of pharmaceuticals, *Sustainable Chemistry and Pharmacy*, Vol. 18, pp. 100325. doi:10.1016/j.scp.2020.100325
- [428] Mayuri, T.; Shukla, R. N.; Balaji, J. (2022). Biobased Food Packaging Materials: Sustainable Alternative to Conventional Petrochemical Packaging Materials: A Review, *Asian Journal of Dairy and Food Research*, Vol. 42, No 2, pp. 137-143. doi:10.18805/ajdfr.DR-1841
- [429] de Souza, E. L.; Lundgren, G. A.; de Oliveira, K. Á. R.; Berger, L. R. R.; Magnani, M. (2019). An Analysis of the Published Literature on the Effects of Edible Coatings Formed by Polysaccharides and Essential Oils on Postharvest Microbial Control and Overall Quality of Fruit, *Comprehensive Reviews in Food Science and Food Safety*, Vol. 18, Issue 6, pp. 1947–1967. doi:10.1111/1541-4337.12498
- [430] Giustra, M.; Cerri, F.; Anadol, Y.; Salvioni, L.; Antonelli Abella, T.; Prosperi, D.; Galli, P.; Colombo, M. (2022). Eco-luxury: Making sustainable drugs and cosmetics with Prosopis cineraria natural extracts, *Frontiers in Sustainability*, Vol. 3. doi:10.3389/frsus.2022.1047218
- [431] Goh, K. K. T.; Kumar, R.; Wong, S. (2014). Functionality of Non-Starch Polysaccharides (NSPs), *Functional Foods and Dietary Supplements*, Wiley, pp. 187–225. doi:10.1002/9781118227800.ch8
- [432] Dr. S. Arunkumar; P. Bharathvaaj; R.K. Mathubalan; S. Logesh. (2024). A Review on Composite Materials Reinforcing with Organic/ Natural Materials, *International Research Journal on Advanced Engineering and Management (IRJAEM)*, Vol. 2, Issue 03, pp. 538–544. doi:10.47392/IRJAEM.2024.0074
- [433] Reddy, I. V. S.; Neelima, P. (2022). Neem (Azadirachta indica): A Review on Medicinal Kalpavriksha, *International Journal of Economic Plants*, Vol. 9, Issue 1, pp. 059–063. doi:10.23910/2/2021.0437d
- [434] Sarkar, S.; Singh, R. P.; Bhattacharya, G. (2021). Exploring the role of Azadirachta indica (neem) and its active compounds in the regulation of biological pathways: an update on molecular approach, *3 Biotech*, Vol. 11, Issue

- 4, pp. 178. doi:10.1007/s13205-021-02745-4
- [435] Islas, J. F.; Acosta, E.; G-Buentello, Z.; Delgado-Gallegos, J. L.; Moreno-Treviño, M. G.; Escalante, B.; Moreno-Cuevas, J. E. (2020). An overview of Neem (Azadirachta indica) and its potential impact on health, *Journal of Functional Foods*, Vol. 74, pp. 104171. doi:10.1016/j.jff.2020.104171
- [436] Martínez-Romero, A.; Ortega-Sánchez, J. L.; Hernández-González, S. I.; Olivas- Calderón, E. H.; Alba-Romero, J. J. (2016). Application of neem tree in agriculture, industry, medicine, and environment: a review, *African Journal of Traditional, Complementary and Alternative Medicines*, Vol. 13, Issue 2, pp. 191. doi:10.4314/ajtcam.v13i2.23
- [437] Wylie, M. R.; Merrell, D. S. (2022). The Antimicrobial Potential of the Neem Tree Azadirachta indica, *Frontiers in Pharmacology*, Vol. 13. doi:10.3389/fphar.2022.891535
- [438] Devi, S.; Paul, J. P. (2015). World Journal of Pharmaceutical research FREEZE DRYING, *World Journal Of Pharmaceutical Research*, Vol. 4, Issue 6, pp. 96–111. doi:10.20959/wjpr202213-25748
- [439] Korde, S. A.; Thombre, P. B.; Dipake, S. S.; Sangshetti, J. N.; Rajbhoj, A. S.; Gaikwad, S. T. (2023). Neem gum (Azadirachta indicia) facilitated green synthesis of TiO2 and ZrO2 nanoparticles as antimicrobial agents, *Inorganic Chemistry Communications*, Vol. 153, pp. 110777. doi:10.1016/j.inoche.2023.110777
- [440] Malviya, R.; Sharma, P. K.; Dubey, S. K. (2018). Microwave Controlled the Green Synthesis of Acrylamide Graft Copolymers of Azadirachita indica Gum for the Wastewater Management, *Current Applied Polymer Science*, Vol. 2, Issue 2, pp. 130–149. doi:10.2174/2452271602666180517093813
- [441] Malviya, R.; Sharma, P. K.; Dubey, S. K. (2019). Microwave-assisted preparation of biodegradable, hemocompatible, and antimicrobial neem gumgrafted poly (acrylamide) hydrogel using (3)2 factorial design, *Emergent Materials*, Vol. 2, Issue 1, pp. 95–112. doi:10.1007/s42247-019-00022-y
- [442] Mankotia, P.; Choudhary, S.; Sharma, K.; Kumar, V.; Kaur Bhatia, J.; Parmar, A.; Sharma, S.; Sharma, V. (2020). Neem gum based pH responsive hydrogel matrix: A new pharmaceutical excipient for the sustained release of anticancer drug, *International Journal of Biological Macromolecules*, Vol. 142, pp. 742–755. doi:10.1016/j.ijbiomac.2019.10.015
- [443] Singh, B.; Ram, K. (2023). Exploring neem gum in designing hydrogel dressings by covalent and supra-molecular interactions for better wound healing, *Results in Surfaces and Interfaces*, Vol. 13, pp. 100161. doi:10.1016/j.rsurfi.2023.100161
- [444] Malviya, R.; Sharma, P. K.; Dubey, S. K. (2018). Stability facilitation of nanoparticles prepared by ultrasound assisted solvent-antisolvent method: Effect of neem gum, acrylamide grafted neem gum and carboxymethylated

- neem gum over size, morphology and drug release, *Materials Science and Engineering: C*, Vol. 91, pp. 772–784. doi:10.1016/j.msec.2018.06.013
- [445] Bhagwat, D. A.; Kolekar, V. R.; Nadaf, S. J.; Choudhari, P. B.; More, H. N.; Killedar, S. G. (2020). Acrylamide grafted neem (Azadirachta indica) gum polymer: Screening and exploration as a drug release retardant for tablet formulation, *Carbohydrate Polymers*, Vol. 229, pp. 115357. doi:10.1016/j.carbpol.2019.115357
- [446] Singh, B.; Ram, K.; Singh, B. (2022). Development and characterization of azadirachta indica gum-poly(2-hydroxyethyl methacrylate) crosslinked copolymeric hydrogels for drug delivery applications, *Chemical Physics Letters*, Vol. 792, pp. 139401. doi:10.1016/j.cplett.2022.139401
- [447] Singh, B.; Mohan, M.; Singh, B. (2020). Synthesis and characterization of the azadirachta indica gum-polyacrylamide interpenetrating network for biomedical applications, *Carbohydrate Polymer Technologies and Applications*, Vol. 1, pp. 100017. doi:10.1016/j.carpta.2020.100017
- [448] Singh, B.; Kumar, R.; Kumar, S.; Thakur, N.; Ram, K. (2023). Design of polysaccharide gum based network copolymeric hydrogels for drug delivery and wound dressing applications, *Medicine in Novel Technology and Devices*, Vol. 20, pp. 100262. doi:10.1016/j.medntd.2023.100262
- [449] Patil, T.; Pawar, A.; Korake, S.; Patil, R.; Pawar, A.; Kamble, R. (2022). Green synthesis of polyacrylamide grafted Neem Gum for gastro retentive floating drug delivery of Ciprofloxacin Hydrochloride: In vitro and in vivo evaluation, *Journal of Drug Delivery Science and Technology*, Vol. 72, pp. 103417. doi:10.1016/j.jddst.2022.103417
- [450] Singh, B.; Singh, B. (2020). Graft copolymerization of polyvinylpyrollidone onto Azadirachta indica gum polysaccharide in the presence of crosslinker to develop hydrogels for drug delivery applications, *International Journal of Biological Macromolecules*, Vol. 159, pp. 264–275. doi:10.1016/j.ijbiomac.2020.05.091
- [451] Singh, B.; Singh, B. (2021). Design of dietary fiber azadiracta indica gum based hydrogels for use in drug delivery, *Food Hydrocolloids for Health*, Vol. 1, pp. 100011. doi:10.1016/j.fhfh.2021.100011
- [452] Singh, B.; Sharma, V.; Ram, K. (2023). Design of moxifloxacin encapsulated network hydrogel wound dressings: Evaluation of polymer-drug, polymer-blood, and polymer-bio membrane interactions, *Polymer Engineering & Science*, Vol. 63, Issue 1, pp. 78–90. doi:10.1002/pen.26187
- [453] Sharma, S.; Bal, T. (2023). Exploring and Characterizing the drug Release Potential of Novel Tissue Compatible Amphiphilic Graft Copolymer of Polyvinyl Acetate Grafted Neem Gum (NG-g-PVAc), *Journal of Polymers and the Environment*, Vol. 31, Issue 6, pp. 2364–2379. doi:10.1007/s10924-023-02765-6

- [454] Rajput, K.; Tawade, S.; Nangare, S.; Shirsath, N.; Bari, S.; Zawar, L. (2022). Formulation, optimization, and in-vitro-ex-vivo evaluation of dual-crosslinked zinc pectinate-neem gum-interpenetrating polymer network mediated lansoprazole loaded floating microbeads, *International Journal of Biological Macromolecules*, Vol. 222, pp. 915–926. doi:10.1016/j.ijbiomac.2022.09.216
- [455] Choudary, R.; Chopra, D. S.; Singh, D.; Singh, N. (2023). Sustained Release of Azadirachta indica Extract from Stimuli Responsive Bacterial Cellulose— Carbapol Hydrogel for Chronic Burn Wound Management, *Biomedical Materials & Devices*. doi:10.1007/s44174-023-00129-1
- [456] Zhu, X.; Xu, R.; Wang, H.; Chen, J.; Tu, Z. (2020). Structural Properties, Bioactivities, and Applications of Polysaccharides from Okra [ Abelmoschus esculentus (L.) Moench]: A Review, *Journal of Agricultural and Food Chemistry*, Vol. 68, Issue 48, pp. 14091–14103. doi:10.1021/acs.jafc.0c04475
- [457] Dantas, T. L.; Alonso Buriti, F. C.; Florentino, E. R. (2021). Okra (Abelmoschus esculentus L.) as a Potential Functional Food Source of Mucilage and Bioactive Compounds with Technological Applications and Health Benefits, *Plants*, Vol. 10, Issue 8, pp. 1683. doi:10.3390/plants10081683
- [458] Kesharwani, T.; Garg, M.; Sadhu, S. D. (2023). Extraction, structural properties, and applications of okra gum, *Natural Gums*, Elsevier, pp. 277–303. doi:10.1016/B978-0-323-99468-2.00009-7
- [459] Aziz, N. S.; Sofian-Seng, N.-S.; Yusop, S. M.; Kasim, K. F.; Mohd Razali, N. S. (2018). Functionality of Okra Gum as a Novel Carbohydrate-based Fat Replacer in Ice Cream, *Food Science and Technology Research*, Vol. 24, Issue 3, pp. 519–530. doi:10.3136/fstr.24.519
- [460] Agregán, R.; Pateiro, M.; Bohrer, B. M.; Shariati, M. A.; Nawaz, A.; Gohari, G.; Lorenzo, J. M. (2023). Biological activity and development of functional foods fortified with okra ( Abelmoschus esculentus ), *Critical Reviews in Food Science and Nutrition*, Vol. 63, Issue 23, pp. 6018–6033. doi:10.1080/10408398.2022.2026874
- [461] Hussain, A.; Qureshi, F.; Abbas, N.; Arshad, M.; Ali, E. (2017). An Evaluation of the Binding Strength of Okra Gum and the Drug Release Characteristics of Tablets Prepared from It, *Pharmaceutics*, Vol. 9, Issue 4, pp. 20. doi:10.3390/pharmaceutics9020020
- [462] Zaharuddin, N. D.; Noordin, M. I.; Kadivar, A. (2014). The Use of Hibiscus esculentus (Okra) Gum in Sustaining the Release of Propranolol Hydrochloride in a Solid Oral Dosage Form, *BioMed Research International*, Vol. 2014, pp. 1–8. doi:10.1155/2014/735891
- [463] Singh, A.; Kaith, B. S.; Mehra, R.; Balram; Sardul, V.; Bhatti, M. S. (2023). Okra-psyllium based green synthesis of eco-friendly bio-adsorbent for efficient removal of uranium and crystal violet dye from aqueous media: statistical optimization using response surface methodology, *Zeitschrift Für Physikalische Chemie*, Vol. 237, Issue 9, pp. 1287–1309. doi:10.1515/zpch-2023-0250

- [464] Deka, R.; Sarmah, J. K.; Baruah, S.; Dutta, R. R. (2023). An okra polysaccharide (Abelmoschus esculentus) reinforced green hydrogel based on guar gum and poly-vinyl alcohol double network for controlled release of nanocurcumin, *International Journal of Biological Macromolecules*, Vol. 234, pp. 123618. doi:10.1016/j.ijbiomac.2023.123618
- [465] Chokboribal, J.; Vipavin, A.; Sirinjullapong, A.; Suchaiya, V.; Lahpun, N. (2023). Xanthan gum/carrageenan-based hydrogel pads with okra fruit mucilage powder for cosmeceutical and medical applications, *Suranaree Journal of Science and Technology*, Vol. 30, Issue 2. doi:10.55766/sujst-2023-02-e01536
- [466] Ma, Y.; Liu, K.; Lao, L.; Li, X.; Zhang, Z.; Lu, S.; Li, Y.; Li, Z. (2022). A stretchable, self-healing, okra polysaccharide-based hydrogel for fast-response and ultra-sensitive strain sensors, *International Journal of Biological Macromolecules*, Vol. 205, pp. 491–499. doi:10.1016/j.ijbiomac.2022.02.065
- [467] Saleem, A.; Rehman, R.; Hussain, S.; Salem, M. A.; Ali, F.; Shah, S. A. A.; Younas, U.; El-Bahy, S. M.; El-Bahy, Z. M.; Iqbal, M. (2023). Biodegradable and hemocompatible alginate/okra hydrogel films with promising stability and biological attributes, *International Journal of Biological Macromolecules*, Vol. 245, pp. 125532. doi:10.1016/j.ijbiomac.2023.125532
- [468] Choudhary, V.; Sharma, S.; Shukla, P. K.; Malik, A. (2023). Biocompatible stimuli responsive hydrogels of okra mucilage with acrylic acid for controlled release phytochemicals of Calendula officinalis: In vitro assay, *Materials Today: Proceedings*. doi:10.1016/j.matpr.2023.03.701
- [469] Fazli, S.; Hezari, S.; Olad, A. (2024). Preparation of hydrogels based on okra pods/chia seeds mucilage for drug delivery application, *Polymer Bulletin*, Vol. 81, Issue 13, pp. 11539–11562. doi:10.1007/s00289-024-05221-0
- [470] Zhang, M.; Chen, G.; Lei, M.; Lei, J.; Li, D.; Zheng, H. (2021). A pH-sensitive oxidized-dextran based double drug-loaded hydrogel with high antibacterial properties, *International Journal of Biological Macromolecules*, Vol. 182, pp. 385–393. doi:10.1016/j.ijbiomac.2021.03.169
- [471] Cheng, F.; Wu, Y.; Li, H.; Yan, T.; Wei, X.; Wu, G.; He, J.; Huang, Y. (2019). Biodegradable N, O-carboxymethyl chitosan/oxidized regenerated cellulose composite gauze as a barrier for preventing postoperative adhesion, *Carbohydrate Polymers*, Vol. 207, pp. 180–190. doi:10.1016/j.carbpol.2018.10.077
- [472] Santos, M. B.; dos Santos, C. H. C.; de Carvalho, M. G.; de Carvalho, C. W. P.; Garcia-Rojas, E. E. (2019). Physicochemical, thermal and rheological properties of synthesized carboxymethyl tara gum (Caesalpinia spinosa), *International Journal of Biological Macromolecules*, Vol. 134, pp. 595–603. doi:10.1016/j.ijbiomac.2019.05.025
- [473] Liu, C.; Wu, J.; Gan, D.; Li, Z.; Shen, J.; Tang, P.; Luo, S.; Li, P.; Lu, X.; Zheng, W. (2020). The characteristics of mussel-inspired nHA/OSA injectable hydrogel and repaired bone defect in rabbit, *Journal of Biomedical Materials*

- Research Part B Applied Biomaterials, Vol. 108, Issue 5, pp. 1814–1825. doi:10.1002/jbm.b.34524
- [474] Sadeghi-Abandansari, H.; Pakian, S.; Nabid, M. R.; Ebrahimi, M.; Rezalotfi, A. (2021). Local co-delivery of 5-fluorouracil and curcumin using Schiff's base cross-linked injectable hydrogels for colorectal cancer combination therapy, *European Polymer Journal*, Vol. 157, Issue July, pp. 110646. doi:10.1016/j.eurpolymj.2021.110646
- [475] Su, W. Y.; Chen, K. H.; Chen, Y. C.; Lee, Y. H.; Tseng, C. L.; Lin, F. H. (2011). An injectable oxidated hyaluronic acid/adipic acid dihydrazide hydrogel as a vitreous substitute, *Journal of Biomaterials Science, Polymer Edition*, Vol. 22, Issue 13, pp. 1777–1797. doi:10.1163/092050610X522729
- [476] Pandit, A. H.; Mazumdar, N.; Imtiyaz, K.; Alam Rizvi, M. M.; Ahmad, S. (2020). Self-Healing and Injectable Hydrogels for Anticancer Drug Delivery: A Study with Multialdehyde Gum Arabic and Succinic Anhydride Chitosan, *ACS Applied Bio Materials*, Vol. 3, Issue 12, pp. 8460–8470. doi:10.1021/acsabm.0c00835
- [477] Lucas de Lima, E.; Fittipaldi Vasconcelos, N.; da Silva Maciel, J.; Karine Andrade, F.; Silveira Vieira, R.; Andrade Feitosa, J. P. (2020). Injectable hydrogel based on dialdehyde galactomannan and N-succinyl chitosan: a suitable platform for cell culture, *Journal of Materials Science: Materials in Medicine*, Vol. 31, Issue 1, pp. 5. doi:10.1007/s10856-019-6343-6
- [478] Yan, S.; Wang, T.; Li, X.; Jian, Y.; Zhang, K.; Li, G.; Yin, J. (2017). Fabrication of injectable hydrogels based on poly(l-glutamic acid) and chitosan, *RSC Advances*, Vol. 7, Issue 28, pp. 17005–17019. doi:10.1039/c7ra01864a
- [479] Wang, X.; Yang, Z.; Meng, Z.; Sun, S. K. (2022). Transforming Commercial Copper Sulfide into Injectable Hydrogels for Local Photothermal Therapy, *Gels*, Vol. 8, Issue 5, pp. 1–15. doi:10.3390/gels8050319
- [480] Chiesa, E.; Genta, I.; Dorati, R.; Modena, T.; Conti, B. (2019). Poly(gamma-glutamic acid) based thermosetting hydrogels for injection: Rheology and functional parameters evaluation, *Reactive and Functional Polymers*, Vol. 140, Issue March, pp. 93–102. doi:10.1016/j.reactfunctpolym.2019.03.021
- [481] Ketabat, F.; Karkhaneh, A.; Mehdinavaz Aghdam, R.; Hossein Ahmadi Tafti, S. (2017). Injectable conductive collagen/alginate/polypyrrole hydrogels as a biocompatible system for biomedical applications, *Journal of Biomaterials Science, Polymer Edition*, Vol. 28, Issue 8, pp. 794–805. doi:10.1080/09205063.2017.1302314
- [482] Qu, J.; Zhao, X.; Ma, P. X.; Guo, B. (2017). pH-responsive self-healing injectable hydrogel based on N-carboxyethyl chitosan for hepatocellular carcinoma therapy, *Acta Biomaterialia*, Vol. 58, pp. 168–180. doi:10.1016/j.actbio.2017.06.001
- [483] Qu, J.; Zhao, X.; Liang, Y.; Zhang, T.; Ma, P. X.; Guo, B. (2018). Antibacterial

- adhesive injectable hydrogels with rapid self-healing, extensibility and compressibility as wound dressing for joints skin wound healing, *Biomaterials*, Vol. 183, Issue July, pp. 185–199. doi:10.1016/j.biomaterials.2018.08.044
- [484] Grewal, P.; Mundlia, J.; Ahuja, M. (2019). Thiol modified Moringa gum A potential bioadhesive polymer, *Carbohydrate Polymers*, Vol. 209, pp. 400–408. doi:10.1016/j.carbpol.2018.12.100
- [485] Liang, Y.; Zhao, X.; Ma, P. X.; Guo, B.; Du, Y.; Han, X. (2019). pH-responsive injectable hydrogels with mucosal adhesiveness based on chitosan-grafted-dihydrocaffeic acid and oxidized pullulan for localized drug delivery, *Journal of Colloid and Interface Science*, Vol. 536, pp. 224–234. doi:10.1016/j.jcis.2018.10.056
- [486] Ma, L.; Tan, Y.; Chen, X.; Ran, Y.; Tong, Q.; Tang, L.; Su, W.; Wang, X.; Li, X. (2022). Injectable oxidized alginate/carboxylmethyl chitosan hydrogels functionalized with nanoparticles for wound repair, *Carbohydrate Polymers*, Vol. 293, Issue May, pp. 119733. doi:10.1016/j.carbpol.2022.119733
- [487] Yan, Y.; Guan, S.; Wang, S.; Xu, J.; Sun, C. (2022). Synthesis and characterization of protocatechuic acid grafted carboxymethyl chitosan with oxidized sodium alginate hydrogel through the Schiff's base reaction, *International Journal of Biological Macromolecules*, Vol. 222, Issue PB, pp. 2581–2593. doi:10.1016/j.ijbiomac.2022.10.041
- [488] Koley, R.; Kasilingam, R.; Sahoo, S.; Chattopadhyay, S.; Bhowmick, A. K. (2019). Synthesis and Characterization of Phenol Furfural Resin from Moringa Oleifera Gum and Biophenol and Its Application in Styrene Butadiene Rubber, *Industrial and Engineering Chemistry Research*, Vol. 58, Issue 40, pp. 18519–18532. doi:10.1021/acs.iecr.9b03684
- [489] Wei, X.; Cui, C.; Fan, C.; Wu, T.; Li, Y.; Zhang, X.; Wang, K.; Pang, Y.; Yao, P.; Yang, J. (2022). Injectable hydrogel based on dodecyl-modified N-carboxyethyl chitosan/oxidized konjac glucomannan effectively prevents bleeding and postoperative adhesions after partial hepatectomy, *International Journal of Biological Macromolecules*, Vol. 199, Issue December 2021, pp. 401–412. doi:10.1016/j.ijbiomac.2021.12.193
- [490] Balitaan, J. N. I.; Hsiao, C.-D.; Yeh, J.-M.; Santiago, K. S. (2020). Innovation inspired by nature: Biocompatible self-healing injectable hydrogels based on modified-β-chitin for wound healing, *International Journal of Biological Macromolecules*, Vol. 162, pp. 723–736. doi:10.1016/j.ijbiomac.2020.06.129
- [491] Li, S.; Pei, M.; Wan, T.; Yang, H.; Gu, S.; Tao, Y.; Liu, X.; Zhou, Y.; Xu, W.; Xiao, P. (2020). Self-healing hyaluronic acid hydrogels based on dynamic Schiff base linkages as biomaterials, *Carbohydrate Polymers*, Vol. 250, Issue August, pp. 116922. doi:10.1016/j.carbpol.2020.116922
- [492] Singh, B.; Kumar, A. (2021). Development of dietary fibre moringa gum and polyvinylpyrrolidone based hydrogels for drug delivery application, *Food Hydrocolloids for Health*, Vol. 1, Issue November 2020, pp. 100008.

- doi:10.1016/j.fhfh.2021.100008
- [493] Grewal, P.; Mundlia, J.; Ahuja, M. (2019). Thiol modified Moringa gum A potential bioadhesive polymer, *Carbohydrate Polymers*, Vol. 209, Issue January, pp. 400–408. doi:10.1016/j.carbpol.2018.12.100
- [494] Guan, S.; Zhang, K.; Cui, L.; Liang, J.; Li, J.; Guan, F. (2021). Injectable gelatin/oxidized dextran hydrogel loaded with apocynin for skin tissue regeneration, *Materials Science and Engineering C*, Vol. 133, Issue December 2021, pp. 112604. doi:10.1016/j.msec.2021.112604
- [495] Singh, B.; Sharma, V.; Rajneesh; Kumar, A.; Rohit; Mohan, M.; Kumar, R.; Kumari, A.; Sharma, P.; Ram, K. (2022). Development of dietary fibers moringa-sterculia gum hydrogel for drug delivery applications, *Food Hydrocolloids for Health*, Vol. 2, Issue September. doi:10.1016/j.fhfh.2022.100095
- [496] Wu, X.; He, C.; Wu, Y.; Chen, X. (2016). Synergistic therapeutic effects of Schiff's base cross-linked injectable hydrogels for local co-delivery of metformin and 5-fluorouracil in a mouse colon carcinoma model, *Biomaterials*, Vol. 75, pp.148–162. doi:10.1016/j.biomaterials.2015.10.016
- [497] Li, D. qiang; Wang, S. ya; Meng, Y. jie; Li, J. fang; Li, J. (2020). An injectable, self-healing hydrogel system from oxidized pectin/chitosan/γ-Fe2O3, *International Journal of Biological Macromolecules*, Vol. 164, pp. 4566–4574. doi:10.1016/j.ijbiomac.2020.09.072
- [498] Liu, J.; Qi, C.; Tao, K.; Zhang, J.; Zhang, J.; Xu, L.; Jiang, X.; Zhang, Y.; Huang, L.; Li, Q.; Xie, H.; Gao, J.; Shuai, X.; Wang, G.; Wang, Z.; Wang, L. (2016). Sericin/Dextran Injectable Hydrogel as an Optically Trackable Drug Delivery System for Malignant Melanoma Treatment, *ACS Applied Materials and Interfaces*, Vol. 8, Issue 10, pp. 6411–6422. doi:10.1021/acsami.6b00959
- [499] Aghajanzadeh, M. S.; Imani, R.; Nazarpak, M. H. (2023). In situ forming aldehyde-modified xanthan/gelatin hydrogel for tissue engineering applications: synthesis, characterization, and optimization, *Journal of Materials Science*, Vol. 58, Issue 35, pp. 14187–14206. doi:10.1007/s10853-023-08878-6
- [500] Zhang, X.; Zhan, X.; Cheng, H.; Dong, Z.; Hu, C.; Liu, C.; Liang, J.; Chen, Y.; Fan, Y.; Zhang, X. (2024). Cartilage-like protein-polysaccharide hybrid hydrogel for enhancing chondrogenic differentiation of bone marrow mesenchymal stem cells, *Collagen and Leather*, Vol. 6, Issue 1, pp. 6–17. doi:10.1186/s42825-023-00146-2
- [501] Mourya, V. .; N. Inamdara; Ashutosh Tiwari, N. (2010). Carboxymethyl Chitosan And Its Applications, *Advanced Materials Letters*, Vol. 1, Issue 1, pp. 11–33. doi:10.5185/amlett.2010.3108
- [502] Wang, S.; Liu, Y.; Sun, Q.; Zeng, B.; Liu, C.; Gong, L.; Wu, H.; Chen, L.; Jin, M.; Guo, J.; Gao, Z.; Huang, W. (2023). Triple Cross-linked Dynamic

- Responsive Hydrogel Loaded with Selenium Nanoparticles for Modulating the Inflammatory Microenvironment via PI3K/Akt/NF-κB and MAPK Signaling Pathways, *Advanced Science*, Vol. 10, Issue 31. doi:10.1002/advs.202303167
- [503] Kumar, J.; Purwar, R. (2024). Self-Healing, Biocompatible Injectable Hydrogel Based on Multialdehyde Moringa oleifera Gum and Carboxymethyl Chitosan: A Suitable Platform for Drug Delivery in Wound Healing Application, ChemistrySelect, Vol. 9, Issue 9. doi:10.1002/slct.202400309
- [504] Yin, H.; Song, P.; Chen, X.; Huang, Q.; Huang, H. (2022). A self-healing hydrogel based on oxidized microcrystalline cellulose and carboxymethyl chitosan as wound dressing material, *International Journal of Biological Macromolecules*, Vol. 221, Issue September, pp. 1606–1617. doi:10.1016/j.ijbiomac.2022.09.060
- [505] Kumar, J.; Purwar, R. (2024). Biodegradable, biocompatible, and self-healing, injectable hydrogel based on oxidized Azadirachta indica gum and carboxymethyl chitosan through dynamic imine-linkage for biomedical application, *Iranian Polymer Journal*. doi:10.1007/s13726-024-01386-7
- [506] Chen, H.; Cheng, J.; Ran, L.; Yu, K.; Lu, B.; Lan, G.; Dai, F.; Lu, F. (2018). An injectable self-healing hydrogel with adhesive and antibacterial properties effectively promotes wound healing, *Carbohydrate Polymers*, Vol. 201, pp. 522–531. doi:10.1016/j.carbpol.2018.08.090
- [507] Singh, B.; Singh, B. (2020). Graft copolymerization of polyvinylpyrollidone onto Azadirachta indica gum polysaccharide in the presence of crosslinker to develop hydrogels for drug delivery applications, *International Journal of Biological Macromolecules*, Vol. 159, pp. 264–275. doi:10.1016/j.ijbiomac.2020.05.091
- [508] Manna, P. J.; Mitra, T.; Pramanik, N.; Kavitha, V.; Gnanamani, A.; Kundu, P. P. (2015). Potential use of curcumin loaded carboxymethylated guar gum grafted gelatin film for biomedical applications, *International Journal of Biological Macromolecules*, Vol. 75, pp. 437–446. doi:10.1016/j.ijbiomac.2015.01.047
- [509] Daoub, R. M. A.; Elmubarak, A. H.; Misran, M.; Hassan, E. A.; Osman, M. E. (2018). Characterization and functional properties of some natural Acacia gums, *Journal of the Saudi Society of Agricultural Sciences*, Vol. 17, Issue 3, pp. 241–249. doi:10.1016/j.jssas.2016.05.002
- [510] Li, S.; Pei, M.; Wan, T.; Yang, H.; Gu, S.; Tao, Y.; Liu, X.; Zhou, Y.; Xu, W.; Xiao, P. (2020). Self-healing hyaluronic acid hydrogels based on dynamic Schiff base linkages as biomaterials, *Carbohydrate Polymers*, Vol. 250, Issue August, pp. 116922. doi:10.1016/j.carbpol.2020.116922
- [511] Mohamed, N. A.; El-Ghany, N. A. A. (2016). Swelling behavior of cross-linked terephthaloyl thiourea carboxymethyl chitosan hydrogels, *Cellulose Chemistry and Technology*, Vol. 50, Nos. 3–4, pp. 463–471

- [512] Chen, Y.-C.; Ho, H.-O.; Liu, D.-Z.; Siow, W.-S.; Sheu, M.-T. (2015). Swelling/Floating Capability and Drug Release Characterizations of Gastroretentive Drug Delivery System Based on a Combination of Hydroxyethyl Cellulose and Sodium Carboxymethyl Cellulose, *PLOS ONE*, Vol. 10, Issue 1, pp. e0116914. doi:10.1371/journal.pone.0116914
- [513] Arora, G.; Malik, K.; Singh, I.; Arora, S.; Rana, V. (2011). Formulation and evaluation of controlled release matrix mucoadhesive tablets of domperidone using Salvia plebeian gum, *Journal of Advanced Pharmaceutical Technology & Research*, Vol. 2, Issue 3, pp. 163. doi:10.4103/2231-4040.85534
- [514] Sharma, P. K.; Taneja, S.; Singh, Y. (2018). Hydrazone-Linkage-Based Self-Healing and Injectable Xanthan–Poly(ethylene glycol) Hydrogels for Controlled Drug Release and 3D Cell Culture, *ACS Applied Materials & Interfaces*, Vol. 10, Issue 37, pp. 30936–30945. doi:10.1021/acsami.8b07310
- [515] Yeh, Y.; Tsai, Y.; Wu, C.; Tu, L.; Bai, M.; Yeh, Y. (2022). The Role of Aldehyde-Functionalized Crosslinkers on the Property of Chitosan Hydrogels, *Macromolecular Bioscience*, Vol. 22, Issue 10. doi:10.1002/mabi.202200366
- [516] Li, J.; Su, J.; Liang, J.; Zhang, K.; Xie, M.; Cai, B.; Li, J. (2024). A hyaluronic acid / chitosan composite functionalized hydrogel based on enzyme-catalyzed and Schiff base reaction for promoting wound healing, *International Journal of Biological Macromolecules*, Vol. 255, pp. 128284. doi:10.1016/j.ijbiomac.2023.128284
- [517] Efstathiou, S.; Wemyss, A. M.; Patias, G.; Al-Shok, L.; Grypioti, M.; Coursari, D.; Ma, C.; Atkins, C. J.; Shegiwal, A.; Wan, C.; Haddleton, D. M. (2021). Self-healing and mechanical performance of dynamic glycol chitosan hydrogel nanocomposites, *Journal of Materials Chemistry B*, Vol. 9, Issue 3, pp. 809–823. doi:10.1039/d0tb02390f
- [518] Xue, X.; Liang, K.; Huang, W.; Yang, H.; Jiang, L.; Jiang, Q.; Jiang, T.; Lin, B.; Chen, Y.; Jiang, B.; Komarneni, S. (2022). Molecular Engineering of Injectable, Fast Self-Repairing Hydrogels with Tunable Gelation Time: Characterization by Diffusing Wave Spectroscopy, *Macromolecules*, Vol. 55, Issue 15, pp. 6474–6486. doi:10.1021/acs.macromol.2c00899
- [519] Zhang, F.; Zhang, S.; Lin, R.; Cui, S.; Jing, X.; Coseri, S. (2023). Injectable multifunctional carboxymethyl chitosan/hyaluronic acid hydrogel for drug delivery systems, *International Journal of Biological Macromolecules*, Vol. 249, Issue April, pp. 125801. doi:10.1016/j.ijbiomac.2023.125801
- [520] Chiesa, E.; Genta, I.; Dorati, R.; Modena, T.; Conti, B. (2019). Poly(gamma-glutamic acid) based thermosetting hydrogels for injection: Rheology and functional parameters evaluation, *Reactive and Functional Polymers*, Vol. 140, pp. 93–102. doi:10.1016/j.reactfunctpolym.2019.03.021
- [521] Bertsch, P.; Diba, M.; Mooney, D. J.; Leeuwenburgh, S. C. G. (2023). Self-Healing Injectable Hydrogels for Tissue Regeneration, *Chemical Reviews*, Vol. 123, Issue 2, 834–873. doi:10.1021/acs.chemrev.2c00179

- [522] Ganji, F.; Abdekhodaie, M. J.; Ramazani, A. S.A. (2007). Gelation time and degradation rate of chitosan-based injectable hydrogel, *Journal of Sol-Gel Science and Technology*, Vol. 42, pp 47-53. doi.org/10.1007/s10971-006-9007-1
- [523] Aftab, M.; Javed, F.; Haider, S.; Khan, R.; Khan, S. U.; Alam, K.; Amir, A.; Ullah, F.; Ali S.N. (2024). Design and Characterization of Chitosan-Based Smart Injectable Hydrogel for Improved Sustained Release of Antinarcotics, *pharmaceuticals*, Vol. 17, pp749, doi: 10.3390/ph17060749.
- [524] Zehra, F.K.; Yar, M.; Rehman, I. U., (2024). In vitro degradation, swelling, and bioactivity performances of in situ forming injectable chitosan-matrixed hydrogels for bone regeneration and drug delivery, *Biotechnology and Bioengineering*, Vol. 121, pp. 2767-2779, doi.org/10.1002/bit.28755.

#### LIST OF PUBLICATIONS AND THEIR PROOFS

#### **Journal articles from thesis work:**

- **1. Jitendra Kumar**<sup>1</sup> and Roli Purwar\*, Self-Healing, Biocompatible Injectable Hydrogel Based on Multialdehyde Moringa oleifera Gum and Carboxymethyl Chitosan: A Suitable Platform for Drug Delivery in Wound Healing Application, (2024), Chemistry Select, 9(9), e202400309, DOI: 10.1002/slct.202400309
- **2. Jitendra Kumar¹** and Roli Purwar\*, Injectable mesquite gum and carboxymethyl chitosan hydrogel using Schiff base crosslinks: a versatile platform for drug delivery in wound care, (2024), Macromolecular Research, 32, 1237–1254, DOI: 10.1007/s13233-024-00300-7
- **3. Jitendra Kumar**<sup>1</sup> and Roli Purwar\*, Biodegradable, Biocompatible, and Self-healing, Injectable Hydrogel Based on Oxidized *Azadirachta indica* Gum and Carboxymethyl Chitosan via Dynamic Imine-Linkage for Biomedical Application, (2024), Iranian Polymer Journal, 34, 465-483, DOI: https://doi.org/10.1007/s13726-024-01386-7
- **4. Jitendra Kumar**<sup>1</sup> and Roli Purwar\*, A Schiff Base Hydrogel of Oxidized Okra Gum and Carboxymethylated Chitosan: A Biocompatible and Biodegradable Injectable System for Drug Delivery in Wound Care, (2024), Colloid and Polymer Science, 302 (12), 1923–1938, DOI: 10.1007/s00396-024-05316-0

#### Journal articles during Ph.D. tenure:

Mehul Verma, **Jitendra Kumar**, Abhinav Ayush Pradhan, Nilotpal Majumder, Sourabh Ghosh, Roli Purwar, Assessing rheological properties of oxidized Moringa oleifera gum and carboxymethyl chitosan - based self - healing hydrogel for additive manufacturing applications, (2024), Polymer Engineering and Science, 64(10), 5229-5238, DOI: 10.1002/pen.26915

#### **Conference Proceedings:**

- 1. Jitendra Kumar and Roli Purwar\* Poster presentation, Natural Gum Based Injectable Hydrogel: A Roadmap on Emerging Biomaterial for Regenerative Medicine, 1st International Conference on "Recent Trends in Chemical Sciences & Sustainable Energy" (RTCSSE-2023), held on 24th -25th March 2023, organized by Department of Applied Sciences, National Institute of Technology Delhi and Department of Chemistry Swami Shraddhanand College, University of Delhi.
- **2. Jitendra Kumar** and Roli Purwar\* Oral presentation, An introduction to a promising biomaterial for regenerative medicine: natural gum-based injectable hydrogel, International Conference on recent advances in biofuels and biomaterials (ICRABB-2023), held on 13th-14th October 2023, organized by Dr. B.R. Ambedkar National Institute of Technology, Jalandhar (Punjab), India.
- **3. Jitendra Kumar** and Roli Purwar\* Poster presentation, Moringa oleifera gum-clacrylic acid/polyethylene glycol-based hydrogel: Future scope for wound healing

application, 17th International Conference on Polymer Science and Technology SPSI-MACRO-2023 held on 10th – 13th December, 2023, organized by IIT Guwahati, India.

#### PROOF OF PUBLICATION

#### **Proof of Journal articles from thesis work:**



#### ARTICLE



# Injectable mesquite gum and carboxymethyl chitosan hydrogel using schiff base crosslinks: a versatile platform for drug delivery in wound care

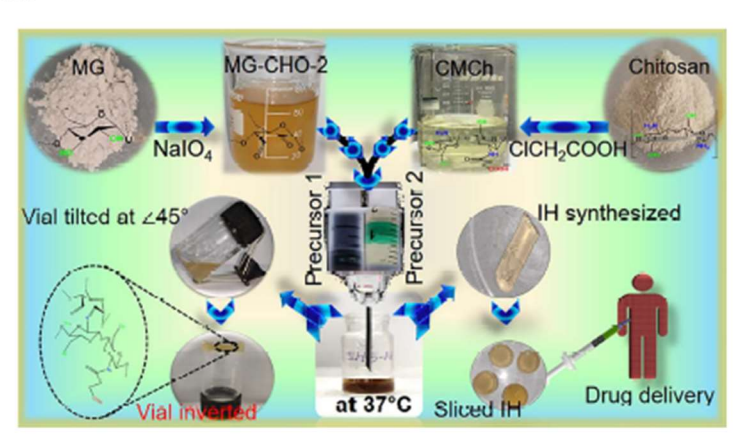
Jitendra Kumar<sup>1</sup> · Roli Purwar<sup>1</sup>

Received: 22 May 2024 / Revised: 10 July 2024 / Accepted: 15 July 2024 □ The Author(s), under exclusive licence to The Polymer Society of Korea 2024

#### **Abstract**

The novel injectable hydrogel (IH) is developed at 37 °C using the dynamic imine bond between mesquite gum with multialdehyde groups (MG-CHO) and carboxymethyl chitosan (CMCh). The investigation consists of determining the ideal concentration of an oxidizing agent to maximize the amount of aldehydes in mesquite gum. Then, the oxidized mesquite gum with the optimized aldehyde content (47.6%) determines the minimum gelation time (7 to 2 min.). Structural characterization is conducted through Fourier transform infrared spectroscopy (FT-IR) and proton nuclear magnetic resonance spectroscopy (<sup>1</sup>H-NMR). The scanning electron microscopy (pore size = 14 to 34 µm) and rheometer examine surface morphology and rheological properties. The swelling ratio in phosphate buffer saline (PBS) at varying pH levels (5.5, 7.4, and 8.5) is measured for both dry and gel forms, revealing a decrease in the swelling ratio with increasing pH (5.5 to 7.4), followed by an increase at pH 8.5. Ciprofloxacin HCl is employed as a model drug for release experiments, and drug release behavior is compared in PBS at pH 5.5, 7.4, and 8.5, using the Korsemeyer–Peppas model to determine the release mechanism. Biocompatibility of injectable hydrogels is assessed regarding in vitro cytotoxicity using L-929 fibroblast cell lines and hemolysis assay. Additionally, the antibacterial study is analyzed using gram-positive and gram-negative bacteria. Furthermore, the hydrolytic biodegradability of IHs in phosphate buffer saline at pH 7.4 is evaluated.

#### **Graphical abstract**



Synthesis of self-healing, biocompatible, and biodegradable injectable hydrogel using mesquite gum and carboxymethyl chitosan crosslinked through Schiff base mechanism utilized for drug delivery application

Extended author information available on the last page of the article

Published online: 09 August 2024



#### ORIGINAL RESEARCH



# Biodegradable, biocompatible, and self-healing, injectable hydrogel based on oxidized *Azadirachta indica* gum and carboxymethyl chitosan through dynamic imine-linkage for biomedical application

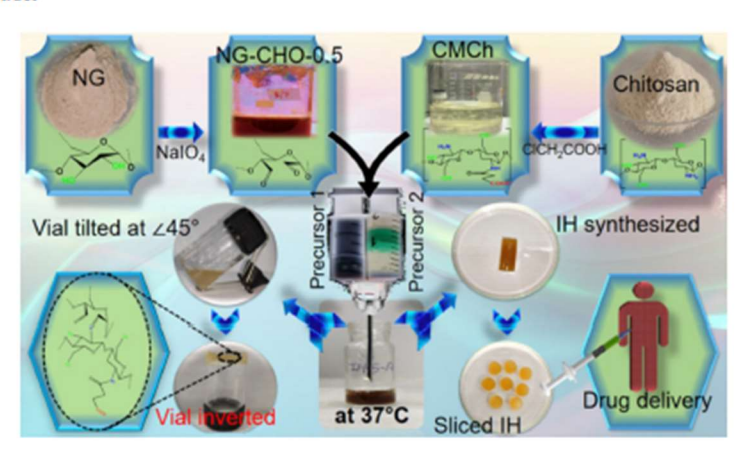
Jitendra Kumar¹ · Roli Purwar¹⊙

Received: 22 May 2024 / Accepted: 14 July 2024 © Iran Polymer and Petrochemical Institute 2024

#### Abstract

At physiological temperature (37 °C), neem gum (NG) containing multialdehyde groups (NG-CHO) and carboxymethyl chitosan (CMCh) were combined to formulate an injectable hydrogel through the utilization of dynamic imine linkages. The investigation comprises determining the ideal oxidizing agent concentration to maximize the amount of aldehydes in neem gum. The best-oxidized neem gum determined the minimum gelation time (3 min). The injectable hydrogel's syringeability (~99%), porosity (47–71%), self-healing ability, and gel content (58–76%) were evaluated. Characterization techniques, including FTIR and <sup>1</sup>H NMR, confirmed the synthesis, and FESEM showed the morphology of the injectable hydrogel (pore size ~80 to 120 µm). Rheometry technique was used for quantitative analysis of shear-thinning behavior and self-healing ability. The swelling ratio was assessed for dry and gel forms of injectable hydrogels in phosphate buffer saline (PBS) at pH 5.5, 7.4, and 8.5. The swelling ratio decreased as the pH increased (5.5–7.4) and then increased at pH 8.5 for all synthesized injectable hydrogels (IHs) in dry and gel forms. For the release assay, an antibiotic model drug, ciprofloxacin HCl (Cipro), was loaded in situ, and the drug release behavior of dry and gel forms of injectable hydrogel was compared within all pH ranges. The drug release kinetics were estimated using the Korsmeyer–Peppas model. Cytotoxicity evaluation using L-929 fibroblast cell lines, antibacterial assay, and hydrolytic degradability (20–65%) in phosphate buffer saline at pH 7.4 was also conducted.

#### Graphical Abstract



Keywords Carboxymethyl chitosan · Neem gum · Injectable hydrogel · Self-healing · Schiff base

Extended author information available on the last page of the article

Published online: 13 September 2024





#### RESEARCH



# A Schiff base hydrogel of oxidized okra gum and carboxymethylated chitosan: a biocompatible and biodegradable injectable system for drug delivery in wound care

Jitendra Kumar<sup>1</sup> · Roli Purwar<sup>1</sup>

Received: 9 July 2024 / Revised: 12 August 2024 / Accepted: 26 August 2024

© The Author(s), under exclusive licence to Springer-Verlag GmbH Germany, part of Springer Nature 2024

#### Abstract

For the first time, functionalized okra gum with multi-aldehyde groups (OG-CHO) and carboxymethyl chitosan (CMCh) is used to create injectable hydrogels (IHs) via Schiff base reaction at 37 °C. Gelation time is optimized based on the ratio of aldehyde groups of OG-CHO to amine groups of CMCh ( $9\pm3$  to  $2\pm1$  min). Physical characteristics such as gel content ( $84\pm2$ ) and porosity ( $66\pm3$ ) are assessed. The syringeability, injectability, and self-healing properties are evaluated qualitatively using a pherometer. Structural analysis is carried out by FT-IR and <sup>1</sup>H-NMR spectroscopy, while surface morphology and pore size ( $80\pm5$  µm) are examined via SEM. The swelling ratio is studied in the gel state of the IH in phosphate buffer saline (PBS) at varying pH levels of 5.5, 7.4, and 8.5, revealing a decrease in swelling ratio with increasing pH from 5.5 to 7.4 ( $75\pm24$  to  $635\pm20\%$ ), followed by an increase in swelling at pH 8.5 ( $724\pm18.5\%$ ). Ciprofloxacin is employed as a model drug for release assays, and drug release behavior in gel forms of IH across different wound pH ranges is evaluated. The swelling and drug release behavior is described using the Korsmeyer–Peppas model, which shows non-Fickian diffusion. Furthermore, biocompatibility (cell viability > 90%), antibacterial assay, and in vitro degradation ( $\sim98\%$ ) are also assessed.

Keywords Carboxymethyl chitosan · Okra gum · Injectable hydrogel · Self-healing · Schiff base · Drug delivery

#### Introduction

Recent advancements in drug delivery have been propelled by the quest for safer, more patient-friendly, and effective treatment methods. Among the innovative materials making waves in this field are hydrogels. These hydrogels offer precise control over the release kinetics of various therapeutic agents, including proteins, peptides, and small molecules, by encapsulating and delivering them [1]. Injectable hydrogels, in particular, provide a less invasive means of localized drug administration, offering advantages such as reduced systemic side effects and improved patient compliance [2]. Natural polymers, especially polysaccharides, have gained popularity in hydrogel formulation due to their biocompatibility, biodegradability, and ability to interact with biological systems [3]. Examples of these natural polymers include Moringa oleifera gum [4], chitosan [5], Acacia gum [6], and carrageenan gum [7]. Schiff base crosslinking, formed by the reaction between a primary amine and an aldehyde, offers several benefits for the design of injectable hydrogels, including mild reaction conditions, controlled crosslinking, and the potential for customizable mechanical and drug release properties [8]. These Schiff-based injectable hydrogels present a promising option for drug delivery, exhibiting strong stability and the ability to respond to external stimuli dynamically [9].

Carboxymethyl chitosan, a water-soluble chitosan derivative, was used in various biomedical applications and is a popular material for synthesizing injectable hydrogel via Schiff base reaction [9]. Another biopolymer, okra gum (OG), or lady's finger gum, is a natural polysaccharide extracted from the pods of the okra plant (Abelmoschus esculentus) [10]. The chemical structure of okra gum comprises a complex polysaccharide matrix that includes rhamnose, galactose, and glucose as its primary constituents

Published online: 12 September 2024



Discipline of Polymer Science and Chemical Technology, Department of Applied Chemistry, Delhi Technological University, Delhi, India

#### **Proof of Journal Article during Ph. D tenure:**

teceived: 12 June 2024 Revised: 25 July 2024 Accepted: 26 July 2024

DOI: 10.1002/pen.26915

#### RESEARCH ARTICLE



### Assessing rheological properties of oxidized Moringa oleifera gum and carboxymethyl chitosan-based self-healing hydrogel for additive manufacturing applications

Mehul Verma | Jitendra Kumar | Abhinav Ayush Pradhan | Nilotpal Majumder | Sourabh Ghosh | Roli Purwar 10

<sup>1</sup>Discipline of Polymer Science and Chemical Technology, Department of Applied Chemistry, Delhi Technological University, Delhi, India

<sup>2</sup>Department of Textile and Fibre Engineering, Indian Institute of Technology, New Delhi, Delhi, India

Roli Purwar, Discipline of Polymer Science and Chemical Technology, Department of Applied Chemistry, Delhi Technological University, Delhi, India Email: roli.purwar@dtu.ac.in

#### Funding information

Delhi Technological University

Rheology plays a vital role in pneumatic three-dimensional (3D) printing of hydrogels. This study investigates the rheological behavior of a novel self-healing hydrogel (O-MOG/CMCh) formed by a Schiff base crosslinking reaction between oxidized Moringa oleifera gum (O-MOG), a biodegradable antimicrobial polysaccharide, and carboxymethyl chitosan (CMCh), a water-soluble biocompatible chitosan derivative. Three hydrogel formulations were designed using 5% w/v of CMCh with varied concentrations of O-MOG (3% w/v, 4% w/v, and 5% w/v) and evaluated through rheology analyses, including frequency sweeps, amplitude sweeps, oscillatory thixotropy, and gelation kinetics. These tests revealed that the material has shear thinning, self-healing properties, a high linear viscoelastic region (LVE), and gel formation times (tgel) of 3.23-4.57 min. The hydrogel synthesized with 5% w/v of O-MOG composition exhibited the best characteristics for printability based on rheological assessments, and this composition was used for further printing assessment, where bi-layered  $4 \times 4$  and  $2 \times 2$  grids were successfully printed using 22 G (0.41 mm) and 23 G (0.34 mm) syringes. All the constructs had a printability index value of  $1 \pm 0.13$  and spreading ratios <6.5, demonstrating the feasibility of employing the synthesized hydrogel as an acellular matrix via additive manufacturing.

#### Highlights

- · Self-healing hydrogel was prepared by mixing the precursors through a
- · Rheology was examined using standard tests for printability assessment.
- · 3D printability was achieved using two different gauze syringes.
- · Printability parameters were recorded and analyzed for the constructs.

#### KEYWORDS

3D printability, additive manufacturing, carboxymethyl chitosan, Moringa oleifera gum, rheology, Schiff base

Polym Eng Sci. 2024;64:5229-5238.

wileyonlinelibrary.com/journal/pen

© 2024 Society of Plastics Engineers. 5229

#### **Proof of Conference Proceedings:**





डा बी आर अम्बेडकर राष्ट्रीय प्रौदयोगिकी संस्थान जालंधर Dr B R AMBEDKAR NATIONAL INSTITUTE OF TECHNOLOGY, JALANDHAR (PUNJAB), INDIA

## INTERNATIONAL CONFERENCE

ON RECENT ADVANCES IN BIOFUELS AND BIOMATERIALS (ICRABB-2023) October 13-14, 2023

CERTIFICATE

This is to certify that Mr Jiteudra Kumar , Delhi technological University has presented a paper entitled "An introduction to a promising biomaterial for regenerative medicine: natural gum based injectable involvagel" authored with Jiteudra Kumar and Roli Purwar in International Conference on "RECENT ADVANCES IN BIOFICELS AND BIOMATERIALS (ICRABB -2023)" held during October 13-14, 2023 in Department of Chemical Engineering, Dr B R Ambedkar National Institute of Technology, Jalandhar, Punjab (INDIA).

Organizing Secretary

May Prof. M. K. Jha Organizing Chairman



# DELIECH \* DELIECH

#### DELHI TECHNOLOGICAL UNIVERSITY

# (Formerly Delhi College of Engineering) Shahbad Daulatpur, Main Bawana Road, Delhi-110042

## **PLAGIARISM VERIFICATION**

Title of the thesis: Studies on natural gum-based injectable hydrogel for wound healing applications

Total pages: 318 Name of the Scholar: Jitendra Kumar

Supervisor: Prof Roli Purwar

Department of Applied Chemistry

This is to certify that the above thesis was scanned for similarity detection. The process and outcome are given below:

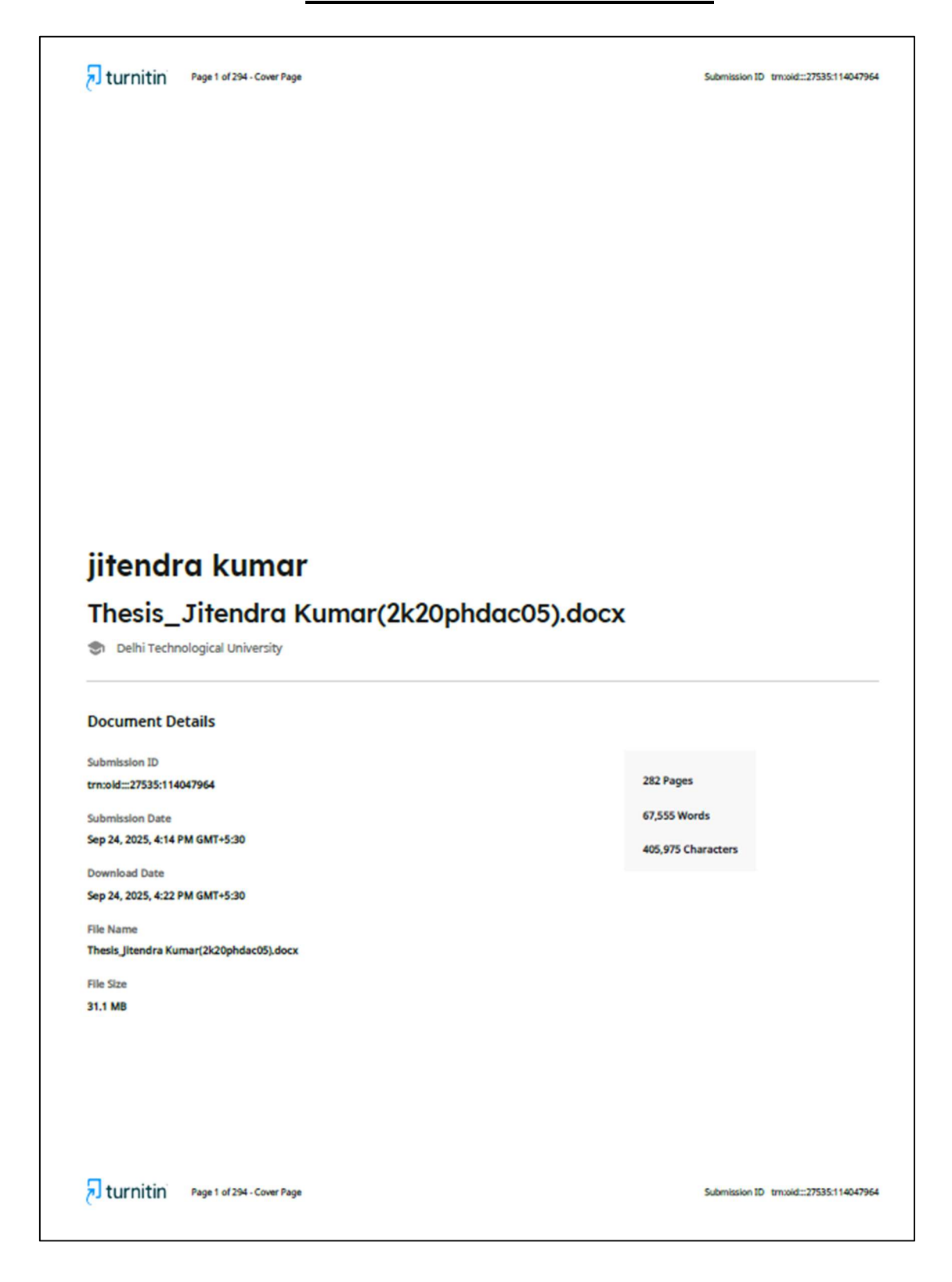
Software used: **Turnitin** Similarity Index: **10 %**, Total Word Count: **72,969** 

Date: 08.10.2025

**Candidate's Signature** 

**Signature of Supervisor** 

## PROOF OF PLAGIARISM REPORT



## 10% Overall Similarity

The combined total of all matches, including overlapping sources, for each database.

#### Filtered from the Report

- ► Bibliography
- ► Small Matches (less than 10 words)

#### **Exclusions**

► 4 Excluded Sources

#### Match Groups

365Not Cited or Quoted 10%

Matches with neither in-text citation nor quotation marks

2 Missing Quotations 0%

Matches that are still very similar to source material

0 Missing Citation 0%
 Matches that have quotation marks, but no in-text citation

\* 0 Cited and Quoted 0% Matches with in-text citation present, but no quotation marks

#### **Top Sources**

4% Internet sources

8% Publications

3% \_\_ Submitted works (Student Papers)

#### **Integrity Flags**

#### 0 Integrity Flags for Review

No suspicious text manipulations found.

Our system's algorithms look deeply at a document for any inconsistencies that would set it apart from a normal submission. If we notice something strange, we flag it for you to review.

A Flag is not necessarily an indicator of a problem. However, we'd recommend you focus your attention there for further review.

turnitin Page 2 of 294 - Integrity Overview

Submission ID trnxoid:::27535:114047964

#### **Curriculum Vitae**



# PERSONAL INFORMATION

#### Mr. Jitendra Kumar

Date of Birth: 05th May 1991

U-302, Prem Nagar, II, Kirari Suleman Nagar, Delhi-110086

itendrakumar6234437@gmail.com
 itendrakumar6234437@gmail.com

#### **SPECIALIZATION**

Biopolymer, Polymer chemistry, Polymer Characterization, Medicinal chemistry, Wound healing, 3D printing

#### PROFILE SUMMARY

Polymer and material science professional with 7+ years of combined research and industrial experience in polymer testing, characterization, hydrogel, and injectable hydrogel development. Skilled in handling advanced instruments (DSC, TGA, Rheometer, FT-IR, UTM, Electrospinning, etc.) and well-versed in BIS, ISO, ASTM standards. Published 5 SCIE-indexed research articles on injectable hydrogels for biomedical and 3D printing applications. Adept at solving client product issues, preparing technical documentation, and contributing to ISO/IEC 17025:2017 audits. Seeking to leverage expertise in a dynamic role within the chemical, polymer, biomedical industry, and green chemistry.

#### EDUCATION QUALIFICATIONS

2020 – 2025 Doctor of Philosophy, Chemistry

Delhi Technological University (Formerly DCE), Delhi, India

Thesis title: Studies on Natural gum-based injectable hydrogel for wound

healing application.

Supervisor: Prof. Roli Purwar

Course Work Subjects: Research methodology, Research and Publication Ethics,

Polymer chemistry, and Green Polymers

Total CGPA of 7.77 on a scale of 10 with First Division.

2014 - 2016 Master of Science, Polymer Science

Mohanlal Sukhadiya University, Udaipur, Rajasthan, India

Secured 66.95 % in total with First Division.

2011 - 2014 Bachelor of Science (Hons.), Polymer Science

Bhaskaracharya College of Applied Sciences, University of Delhi, Delhi, India.

Secured 64.05 % in total with First Division.

#### WORK EXPERIENCE

May 2014 – June 2014

#### **Quality Inspector**

Polymer article manufacturing industry, Mayapuri industrial area, Delhi, India

May 2017- July 2020

#### Polymer technician

Narang Metallurgical and Spectro Services Delhi, India-110055

2020-2024

#### Teaching assistant

Conducted and supervised practical lab sessions for B.Tech, M.tech, and Ph.D. students in polymer science and engineering at Delhi Technological University, Delhi, India

2025

#### Peer Reviewer

Journal of Polymer & Innovation, Springer Journal of Polymer & Environment, Springer Journal of Biomedical Devices, Springer

#### **AWARDS**

September 2025

#### Research Excellence Award

Recipient of Research and Innovation Excellence Award (Commendable Research) by Delhi Technological University, Delhi, India for 4 published research article in SCIE journals.

•

#### **PUBLICATIONS**

February 2024

Jitendra Kumar and Roli Purwar, Self-Healing, Biocompatible Injectable Hydrogel Based on Multialdehyde Moringa oleifera Gum and Carboxymethyl Chitosan: A Suitable Platform for Drug Delivery in Wound Healing Application, (2024), Chemistry Select, 9(9), e202400309 DOI: 10.1002/slct.202400309, (I.F. = 2) (SCIE)

August 2024

• **Jitendra Kumar** and Roli Purwar, Injectable mesquite gum and carboxymethyl chitosan hydrogel using Schiff base crosslinks: a versatile platform for drug delivery in wound care, (2024), Macromolecular Research, 32, 1237–1254, DOI: 10.1007/s13233-024-00300-7, (I.F. = 3.4) (SCIE)

August 2024

• Mehul Verma, Jitendra Kumar, Abhinav Ayush Pradhan, Nilotpal Majumder, Sourabh Ghosh, Roli Purwar, Assessing rheological properties of oxidized Moringa oleifera gum and carboxymethyl chitosan-based self-healing hydrogel for additive manufacturing applications, (2024), Polymer Engineering and Science, 64(10), 5229-5238, DOI: 10.1002/pen.26915, (I.F. = 3.2) (SCIE)

September 2024

• **Jitendra Kumar** and Roli Purwar, Biodegradable, Biocompatible, and Selfhealing, Injectable Hydrogel Based on Oxidized Azadirachta indica Gum and Carboxymethyl Chitosan via Dynamic Imine-Linkage for Biomedical Application, (2024), Iranian Polymer Journal, DOI: doi.org/10.1007/s13726-024-01386-7, (I.F. = 2.8) (SCIE)

September 2024

Jitendra Kumar and Roli Purwar, A Schiff Base Hydrogel of Oxidized Okra Gum

and Carboxymethylated Chitosan: A Biocompatible and Biodegradable Injectable System for Drug Delivery in Wound Care, (2024), Colloid and Polymer Science, 302 (12), 1923–1938, DOI: 10.1007/s00396-024-05316-0, I.F -2.2 (I.F. = 2.3) (SCIE)

#### WORKSHOPS

- Participated in workshop on "Accelerators/Incubation Incubation-Opportunities for Students & Faculties-Early Stage Entrepreneurs" held on 19<sup>th</sup> June 2021, organized at Delhi Technological University, New Delhi, India.
- Participated in workshop on "Beyond Industry 4.0: Industry and Environment", held from 25<sup>th</sup> to 29<sup>st</sup> July 2022, organized by University School of Chemical Technology, Guru Gobind Singh Indrasprastha University, New Delhi, India.
- Participated in INUP-i2, 6<sup>th</sup> user awareness workshop on "Fabrication and characterization facility for nanotechnology" held on 4<sup>th</sup>-5<sup>th</sup> March 2023, organized by Indian institute of technology Delhi, Delhi, India.
- Participated in workshop on "Intellectual Property (IP) Awareness Programme (2 times)" organized by IPR cell, Delhi Technological University, Delhi, India.
- Participated in five days annual information literacy workshop "E-Resources:
   A Gateway for Research", 7<sup>th</sup> Edition (2023,) held from 25<sup>th</sup> -29<sup>th</sup> September 2023, organized by central library, Delhi Technological University, New Delhi, India.
- Participated in INUP-i2, 7<sup>th</sup> user awareness workshop on "Fabrication and characterization facility for nanotechnology" held on 11<sup>th</sup>-12<sup>th</sup> March 2023, organized by Indian institute of technology Delhi, Delhi, India.
- Participated in one day online session on "Distillation Columns"-An Industry Perspective, held on 24<sup>th</sup> February 2022, organized by Department of Applied Chemistry, Delhi Technological University, Delhi, India.
- Participated in one day national workshop on "Ascertaining A skill Centre For Glass and Glazing (SSCGG-2023)", held on 11<sup>th</sup> August 2023, organized by Department of Applied Physics, Delhi Technological University, Delhi, India.
- Participated in workshop on "Research and Publication Ethics" held on 28<sup>th</sup>
  January 2022, organized by University School of Management and
  Entrepreneurship, Delhi Technological University, New Delhi, India
- Participated in training workshop on "Safety From Hazards: Fire, Chemical, Biological and Natural Disasters" held on 11<sup>th</sup> June 2025, organized by Shriram Institute of Industrial Research, Delhi, India at India International Centre, New Delhi, India.
- Participated in one week (15<sup>th</sup> to 21<sup>st</sup> October 2022) training workshop on "Analytical Advances in Studying Molecules" under the aegis of DST-

# TRAINING WORKSHOPS

Synergistic Training Programme Utilizing the Scientific and Technological Infrastructure (STUTI), organized by Department of Chemistry BITS Pilani, Pilani Campus, in association with Sophisticated Analytical Instrument Facility (SAIF) Panjab University, Chandigarh (PMU), India.

- Participated in a one-week (5<sup>th</sup> to 9<sup>th</sup> May 2018) training workshop on "Tailor Made training Programme on Plastics Testing & Identification" at Central Institute of Plastic Engineering & Technology (CIPET), Lucknow, Uttar Pradesh, India.
- Poster presentation, 1st International Conference on "Recent Trends in Chemical Sciences & Sustainable Energy" (RTCSSE-2023), held on 24th -25th March 2023, organized by Department of Applied Sciences, National Institute of Technology Delhi and Department of Chemistry, Swami Shraddhanand College, University of Delhi, India.
- Oral presentation in International Conference on recent advances in biofuels and biomaterials (ICRABB-2023), held on 13<sup>th</sup>-14<sup>th</sup> October 2023, organized by Dr. B.R. Ambedkar National Institute of Technology, Jalandhar (Punjab), India

#### **CONFERENCES**

- Poster presentation in 17<sup>th</sup> International Conference on Polymer Science and Technology (SPSI-MACRO-2023) held on 10<sup>th</sup> – 13<sup>th</sup> December, 2023, organized by IIT Guwahati, India.
- Participated in International Conference on "Chemical & Allied Science and Their Applications", held on 20<sup>th</sup> January 2023, organized by Department of Applied Chemistry, Delhi Technological University, Delhi, India.

#### **SEMINARS**

- Attended one day industry Academia seminar on "Petrochemicals in Today's World", held on 21<sup>st</sup> April 2023, organized by Just Polymer Solutions and Pluss advanced technologies and Department of Applied Chemistry, Delhi Technological University, New Delhi, India
- Attended one day national seminar on "Implementation of NEP-2020 in special reference to Innovation & Entrepreneurship", held on 24<sup>th</sup> February 2023, organized by Institution's Innovation Council and Department of Applied Physics, Delhi Technological University, New Delhi, India
- Attended one day national seminar on "National Science Day (NSD-2023), held on 28<sup>th</sup> February 2023, organized by Human Resource Development Centre and Institution's Innovation Council and Department of Applied Physics, Delhi Technological University, New Delhi, India
- Attended one day webinar on "Become a smart Researcher: Essential Tips to Navigate Springer Nature Platforms", held on 15<sup>th</sup> July 2025, organized by Springer Nature.
- Attended one day webinar on "Inspiring Research & Innovation", held on 1<sup>st</sup> March 2024, organized by IEEE and Delhi Technological University, New Delhi, India

 Attended one day national seminar on "Characterization of Polymeric Materials by Thermal and Rheological Analytical Techniques", held on 16<sup>th</sup> June 2023, organized at Indian Institute of Technology, Delhi in association with Department of Textile and Fibre Engineering, IIT Delhi, India.

# PERSONAL SKILLS

MOTHER TONGUE

Hindi

LANGUAGE PROFICIENCY English, Hindi

# WORK EXPERIENCES

#### Hands-on Experience with instruments (In Industry) Rubber and Plastic

- Density apparatus
- Melt flow indexer,
- Universal testing machine (Plastic and rubber)
- ATR FT-IR
- Hardness tester (Shore A and Shore D)
- Compression test apparatus (Rubber)
- Injection Molding Machine
- Compression Molding Machine
- pH meter

#### **Paint**

- Scratch hardness tester
- Flash point apparatus
- Humidity chamber
- Ford cup flow apparatus
- Bend test apparatus
- Gloss value apparatus
- Salt-spray chamber Additionally, apart from instrument knowledge

#### Hands-on Experience with Instruments (In Academics)

- Two-roll mill
- Extruder
- UV-Visible spectrophotometer (Perkin Almer)
- Differential Scanning Calorimeter (Perkin Almer)
- Thermogravimetric analyzer (Perkin Almer)
- Rheometer (Anton Paar)
- Fluorescence microscope
- Electrospinning machine
- Ball mill apparatus

#### Additional skills gained in industry

- For plastic and rubber testing Material Identification of plastics by conventional techniques. Identification of rubber by chemical analysis (IS: 3400 part 22), Elongation at break (IS: 3400 Part 1), Resistance to accelerated aging (IS: 3400 Part 4), Ash Content (IS: 3400 Part 22 Cl A).
- For paint and varnishes testing (IS: 101) Density of paint, Water Content, Pigment

content, volatile and non-volatile content, Resistance to humidity, consistency by ford cup method, drying time, Finish of paint, color and fineness of grind.

- To check performance qualification of the polymer products
- Prepare reports for operational and performance qualification.
- Inspection of the Finished Product and maintain DHR (Device History Record)
- Solve clients' issues related to final goods made from plastic and rubber.
- Preparing protocol and report for the testing.
- Experienced technical Audit twice by ISO 17025:2017.

#### SOFTWARE KNOWLEDGE

- Certificate course on Fundamental knowledge of computer (6 months)
- Origin
- Chemdraw
- Image J
- Mendeley

#### REFERENCES

- Prof. Roli Purwar
- Professor
- Delhi Technological University (D.T.U), Delhi, India
- roli.purwar@dtu.ac.in
- +91-9711114165
- Prof. Anil Kumar
- Professor
- Delhi Technological University (D.T.U), Delhi, India
- asl213@gmail.com
- #91-9818293031

#### DECLARATION

I hereby declare that all the details furnished in the CV above are true to the best of my knowledge.

Place: New Delhi, India

Jitendra Kumar